

**Beneficiation of Goan ore rejects to get pure iron oxide
and utilisation of the iron oxide to synthesize ferrites,
high-tech magnetic materials**

A THESIS
SUBMITTED TO THE
GOA UNIVERSITY
FOR THE DEGREE OF
DOCTOR OF PHILOSOPHY

IN
CHEMISTRY

BY

VIDHYADATTA M. S. VERENKAR



546.62
VER/Ben

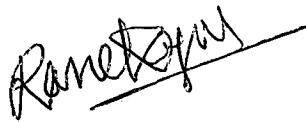
T-139

DEPARTMENT OF CHEMISTRY
GOA UNIVERSITY
TALEGAO PLATEAU
GOA-403206

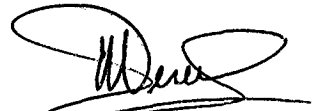
OCTOBER 1997

STATEMENT

I hereby state that this thesis for the Ph.D. degree on “ Beneficia-
tion of Goan ore rejects to get pure iron oxide and utilisation of the
iron oxide to synthesize ferrites, high-tech magnetic materials” is my
original work and that it has not previously formed the basis for the
award of any degree, diploma, associateship and fellowship or any
other similar title to the best of my knowledge and information.



Dr.K.S. Rane
(Research Guide)



Vidhyadatta M. S. Verenkar
(candidate)

70.....

MY MOTHER

CERTIFICATE

As required under the University ordinance, I certify that the thesis entitled "Beneficiation of Goan ore rejects to get pure iron oxide and utilisation of the iron oxide to synthesize ferrites, high-tech magnetic materials" submitted by

Mr. Vidhyadatta M. S. Verenkar for the award of Doctor of Philosophy in Chemistry is a record of research done by the candidate during the period of study under my guidance and that it has not previously formed the basis for the award to the candidate of any degree, diploma, associateship, fellowship or other similar titles.



Rane K S

Date 20 October 1997

Dr. K. S. Rane,
Research Guide,
Department of Chemistry,
Goa University.

ACKNOWLEDGMENTS

I wish to express my deep sense of gratitude to Dr K. S. Rane , Reader in Inorganic chemistry, for his inspiring and valuable guidance during the course of this work.

It is with great pleasure, I express my thanks to,

Vice chancellor, Goa University, for the encouragement,

Present and former Head, Department of Chemistry, Goa University for extending necessary facilities,

Prof. J. A. Lodya, South Africa and Prof. H. Watanabe, Japan for their generous help in taking Mossbauer spectra and SEM Micrographs, respectively,

Dr. S. R. Sawant, Department of Physics, Shivaji University, Kolhapur, for extending the laboratory facilities and Mr.Nandkishor Choudhary for helping me in carrying out the experiments,

Dr. Arun Umarji, IISc., Bangalore for TG/DTA traces,

Mr. S. Tripathi, Director, FDA, Panaji-Goa for extending the laboratory facilities and Ms.Valery for helping me in carrying out the experiments,

Mr. Angelo Pimenta, Principal , and staff of Govt. Multipurpose Higher Secondary, Margao-Goa for their full co-operation,

My all research colleagues especially Sajo, Kamlesh, Teotone, Purnakala, Tushar, Deepa, Shridhar, Hinde, Rajesh, Sachin, Ratnakar, Dr. Ganpat and P. Y. Sawant for their encouragement, constructive suggestion and help,

Dr. Gaurish Naik, Head, USIC, Goa University, for his help in instrumental set up along with Mr. Jaiprakash Kamat,

Dr. Budkule, Dr.Salkar, Dr. Srinivasan, Dr. B.D.Desai, Dr. B.D.Gupta and
Other teaching and non teaching staff of chemistry department,

Supriya Gawas for patiently typing my thesis.

I am proud of my wife Sunita who gave me constant encouragement as well as moral support. So also the source of continuous help and encouragement from my father-in-law, Shivaji and brother -in-laws Sanjay and Sandeep Desai besides my Mother-in-law and sister-in-laws.

I am also thankful to my cousins and finally to my parents, my brothers, Ganaraj and Vijayanand and my sister Mita for their moral support.

CONTENTS

CHAPTER I

1.	GENERAL INTRODUCTION	1
	Applications of iron oxides	
	National and international scenario of ferrites	
	Iron oxide sources for ferrites manufacture	
	Iron ores in Goa and India	
	Iron ore rejects and iron ore fines, Blue dust	
	Ferrite grade iron oxide from iron ore fines(India)	
	India and world ferrite market	
	utilization of iron ores and ore rejects	
1.1	Upgradation of Iron ores	8
1.1.1	Physical beneficiation	8
	Goan facilities to beneficiate iron ores	
	Jigging of Barsuan Iron ores (India)	
	Floataion beneficiation of Goan ore	
	Flocculation studies on Donimalai(India) ore	
	Selective oil agglomeration of Nigerian ore	
	Flocculation of hematite ore fines of India	
1.1.2	Chemical beneficiation	10
	Four zones of iron ore horizon of Goa	
	Dissolution characteristics of ore -a subterranean	

	Solution activity - mechanism for blue dust formation-	
	pH and dissolution relation	
	Enhancement of the dissolution using complexing agents, chelating agents.	
	a) Redox dissolution: hydrazine	12
	Clue for chemical beneficiation	
	Reaction of hydrazine with $\text{Fe}_2\text{O}_3/\text{Fe}_3\text{O}_4$	
	Reductive dissolution of MnO_2 by hydrazine	
	Selective extraction of cobalt from nickel laterite using $\text{N}_2\text{H}_4 \cdot \text{H}_2\text{SO}_4$	
1.2	Iron oxides	13
1.3	Ferrites	14
	Applications of ferrites	
1.3.1	Historical developments	15
	Load stone or magnetite.	
	First synthesis of ferrite, MFe_2O_4 spinel	
1.3.2	Crystal structure of spinel ferrites	16
	a) Normal spinel ferrites	17
	b) Inverse spinel ferrites	19
	c) Random spinel ferrites	19
1.3.3	Cation distribution in spinels	20
1.3.4	Properties of ferrites	21
	Extrinsic and intrinsic properties	

a) Electrical properties	21
i. Resistivity	21
ii. Dielectric behaviour	22
b) Magnetic properties	22
i. Saturation magnetization	22
ii. Permeability	23
iii. Hysteresis	23
Soft and hard ferrites	
iv. Susceptibility	24
1.3.5 Synthesis of Ferrites	24
a) Ceramic technique: Solid state technique	24
b) Mechanism of solid state reaction	25
case A: Counter diffusion	26
case B: Preferential diffusion of anions	26
case C: Preferential diffusion of iron	26
c) Conventional ceramic technique	28
d) Precursor technique	29
i. Hydroxide precursors	30
ii. Carboxylate precursors	31
iii. Hydrazinate precursors	32
Combustion process	
e) Wet chemical method	35
Spray reactions	

	Freeze drying	
	hydrothermal oxidation	
	f) Other methods	36
	Explosion method	
	Supercritical drying	
	Anodic dissolution	
	Hot isostatic pressing	
1.4	Historical and structural background of Gamma iron oxide, $\gamma\text{-Fe}_2\text{O}_3$	38
1.4.1	A brief review of Fe-O system	38
1.4.2	Gamma ferric oxide	40
	Oxidation of Fe_3O_4 to $\gamma\text{-Fe}_2\text{O}_3$	
	Importance of water vapour in Fe_3O_4 oxidation	
	Similarity in LiFe_5O_8 and HFe_5O_8	
	Hydrogen iron oxide phase	
	Crystalline arrangement of $\gamma\text{-Fe}_2\text{O}_3$	
1.5	Importance of $\gamma\text{-Fe}_2\text{O}_3$ in ferrite synthesis	47
	Superior reactivity of $\gamma\text{-Fe}_2\text{O}_3$ to $\alpha\text{-Fe}_2\text{O}_3$	
1.6	Aim, scope, methodology and work plan	51
1.6.1	Aim	51
1.6.2	Scope	52
1.6.3	Methodology	54

CHAPTER II

2.	METHODS OF PREPARATION AND CHARACTERIZATION	61
2.1	Methods of preparation of precursors and oxides	61
2.1.1	Preparation of precursors	62
	a) Iron hydroxides and iron oxyhydroxides	62
	b) Iron (II) carboxylato - hydrazinate	62
2.1.2	Preparation of oxides of iron	62
2.1.3	Preparation of magnesium ferrite, $MgFe_2O_4$	62
	a) Preheating	62
	b) Sintering	63
	i. Presintering	63
	ii. Final sintering	63
2.2	Methods of characterization of precursors and oxides	64
2.2.1	Chemical analysis	64
	a) Analysis of metal content	64
	b) C,H,N analysis	64
	c) Hydrazine estimation	64
2.2.2	Infra red analysis	64
2.2.3	Density	66
2.2.4	Thermal analysis	66
	a) Isothermal studies	66
	b) Thermogravimetric analysis(TGA)	67
	c) Differential thermal analysis (DTA)	67

d) Electrothermal analysis (ETA)	67
2.2.5 Decomposition of precursors	68
a) Decomposition in different atmosphere	68
b) Autocatalytic decomposition	69
2.2.6 X-ray diffraction analysis	69
2.2.7 Magnetic characterization of ferrites	69
a) Alternating current (ac) hysteresis loop tracer	70
b) A.C. susceptibility	71
c) Initial permeability	72
2.2.8 Mossbauer spectroscopy	73
2.2.9 Microstructure	73
2.2.10 Electrical characteristics of iron oxides and ferrites	74
a) Conductivity of γ -Fe ₂ O ₃ in different atmospheres	74
b) Resistivity of magnesium ferrite in air	74
2.2.11 Dielectric constant	74

CHAPTER III

3. SYNTHESIS OF γ -Fe ₂ O ₃	76
3.1 Literature survey on γ -Fe ₂ O ₃ preparation	77
Part- I: Studies on synthesis, characterization and decomposition of iron oxyhydroxides	88
3.2 Experimental: Preparation, characterization and thermal decomposition	89

3.2.1	Chemical beneficiation of iron ore reject	89
	a) Direct precipitation of $\text{Fe}(\text{OH})_3$ from acid extract of the ore	89
	b) Preparation of ferric nitrate and ferrous chloride, from $\text{Fe}(\text{OH})_3$ of ore rejects.	90
3.2.2	Synthesis of iron oxyhydroxides: From ferric nitrate and ferrous chloride prepared from $\text{Fe}(\text{OH})_3$ of iron ore	91
	a) γ - FeOOH	91
	b) α - FeOOH	92
	c) Amorphous FeOOH	92
3.2.3	Hydrazination of iron hydroxide and iron oxyhydroxides	92
	a) Equilibration method	92
3.2.4	Characterization	93
	a) Chemical analysis	93
	b) Infrared analysis	94
	c) Density measurements	94
	d) X-ray diffraction	94
	e) magnetic characterization	95
	f) Mössbauer studies	95
3.2.5	Thermal analysis and decomposition	95
	a) TG and isothermal	95
	b) Thermal decomposition of iron hydroxide /oxyhydroxides	95
	i Air decomposition	98

ii N ₂	98
iii N ₂ +H ₂ O + air	98
iv N ₂ + MeOH	98
v N ₂ + IPA	99
vi N ₂ + cyclohexane	99
c) Autocatalytic decomposition of iron hydroxides/ oxyhydroxides	
3.2.6 Hydrazine equilibration studies of iron oxyhydroxides by electrical conductivity measurements	
a) Variation of electrical conductivity on hydrazination as a function of time	
3.3 Results and discussions	101
3.3.1 Fixation of chemical formulas	101
a) Chemical formulas of iron oxyhydroxides	101
i Chemical analysis	101
ii Infrared analysis	102
iii Pycnometric density	102
iv TG and total mass loss	102
b) Hydrazine equilibration of hydroxide/ oxyhydroxides	103
i Equilibration in 80% and 99-100% hydrazine hydrate	103
ii Hydrazine estimation	105
iii Variation of d.c. electrical conductivity during hydrazination as a function of time	107

c) Analysis of the thermal products of iron oxyhydroxides and hydrazinated iron oxyhydroxides	110
i X-ray diffraction analysis	110
ii IR. Analysis	112
iii Magnetic characterisation	114
iv Mössbauer spectroscopy	116
d) Decomposition of Fe(OH) ₃ and hydrazinated Fe(OH) ₃ of iron ore	121
e) Mechanism of γ -Fe ₂ O ₃ formation	121
3.3.2 Conclusions	125
Part II: Synthesis of γ -Fe ₂ O ₃ from iron(II) carboxylato-hydrazinates	127
3.4 Experimental :Preparation, characterization and decomposition	130
3.4.1 Synthesis of iron (II) carboxylato-hydrazinates	130
a) Solution method	131
i Ferrous fumarato-hydrazinate(FFH)	131
ii Ferrous succinato-hydrazinate(FSH)	132
iii Ferrous malonato- hydrazinate (FMH)	132
iv Ferrous maleato- hydrazinate (FEH)	132
v Ferrous malato- hydrazinate (FLH)	132
b) Equilibration method	133
i Ferrous tatrato- hydrazinate (FTH)	133
3.4.2 Characterisation	133
a) Chemical analysis	133

i	Hydrazine estimation	133
ii	C,H,N analysis	133
iii	Iron content	134
b)	Infra red analysis	134
c)	Density measurements	134
3.4.3	Thermal decomposition studies	134
a)	Thermogravimetric analysis(TGA) and Differential thermal analysis (DTA)	134
b)	Isothermal weight loss studies	134
c)	Autocatalytic decomposition	135
3.4.4	Phase identification and magnetic studies on the thermal products	135
a)	X-ray diffraction	135
b)	Magnetic characterization	135
3.4.5	Microstructure analysis	136
3.5	Results and discussions	136
a)	Fixation of chemical formulas of iron (II) carboxylato- hydrazinates	136
i	Infra red analysis	136
ii	Chemical analysis	140
iii	Total weight loss studies	140
iv	Pycnometric studies	143

b) Formation of γ -Fe ₂ O ₃ from iron (II) carboxylato- hydrazinate	144
i Thermal analysis and hydrazine estimation of thermal products	144
ii X-ray characterization	154
iii IR analysis	156
C) Magnetic characterization and microstructural analysis	156
3.6 Conclusions	158

CHAPTER IV

4. STUDY OF FERRITES	161
4.1 Introduction	161
4.2 Experimental: Preparation and characterization	168
4.2.1 Preparation of ferrites: ceramic technique	168
a) Preheating of raw meal	169
b) High temperature heating of preheated samples	169
i Pellet formation	169
c) Final sintering	170
i pellet/torroid formation	170
d) coding of MgFe ₂ O ₄	171
4.2.2 Characterization	171
a) X-ray diffraction studies	171
b) Infra red analysis	171

c) Magnetic characterization	174
i Saturation magnetization	174
ii A.C. Susceptibility	175
iii Initial permeability	175
d) Electrical characteristics	176
i Resistivity	176
ii Dielectric constant	176
4.3 Results and discussion	177
a) Phase identification by XRD	177
b) Infra red analysis	184
c) Magnetic characterization	188
i Saturation magnetization	188
ii A.C. Susceptibility	193
iii Initial permeability	194
d) Electrical properties	202
i Resistivity	202
ii Dielectric constant	210

CHAPTER V

5	IMPORTANCE OF WATER IN STABILISING γ -Fe ₂ O ₃	215
5.1	Introduction	215
5.2	Experimental: Preparation and characterization	219
5.2.1	Preparation of γ -Fe ₂ O ₃	219

	FFHA, FSHA, FMHA, FTHA, FEHA and FLHA	
	γ -FHA and γ -FHHA	
5.2.2	Standard γ -Fe ₂ O ₃	219
5.2.3	Characterization	220
	a) X-ray diffraction	220
	b) Infra red analysis	220
	c) Magnetic characteristics	220
5.2.4	Thermal analysis	220
	TG/DTA/DSC	
5.2.5	Direct current electrical conductivity in air, N ₂ and N ₂ /H ₂ O atmosphere	220
5.3	Results and discussions	222
5.3.1	Direct current (dc) electrical conductivity of γ -Fe ₂ O ₃ in air, N ₂ and in air after equilibrating in water vapours	222
5.3.1.a	Hysteresis behaviour of conductivity	222
	FFHA, FSHA, FMHA, FTHA, FEHA and FLHA	
	Standard γ -Fe ₂ O ₃	
	Arrhenius plot	
	γ -FHA and γ -FHHA	
	γ -FHA	
	i Electro-thermal analysis	233
	ii Study of electrical conductivity of γ -FHA	236
5.4	General Conclusions	239

LIST OF FIGURES

CHAPTER I

- 1.1 Crystal structure of spinel ferrites showing tetrahedral and octahedral co-ordination
- 1.2 Diffusion mechanism in ferrites
- 1.3 A bird's view of the planned work

CHAPTER II

- 2.1 Flow chart of preparation of ferrites

CHAPTER III

- 3.1 Assembly for controlled atmospheric decomposition
- 3.2 Hydrazine estimation set up
- 3.3 Variations in electrical conductivity of iron oxyhydroxides in hydrazine atmosphere as a function of time A) γ -FeOOH
B) amorphous FeOOH and C) α -FeOOH
- 3.4 Infra red spectra of the end products of iron oxyhydroxides decomposed in different atmospheres

Auto cat, N₂/MeOH, N₂/IPA N₂/cyclohexane

γ -FeOOH	γF_8	γF_1	γF_2	γF_{12}
α -FeOOH	NF ₆	NF ₄	NF ₅	NF ₁₀
Amp. FeOOH	AM ₅	AF ₂	AF ₃	AM ₇

- 3.5 Saturation magnetization, σ_s , in emu/g of decomposed end products of iron oxyhydroxides and their hydrazinated complexes
- 3.6a) Mössbauer spectra of 1) amorphous FeOOH and 2) amorphous FeOOH decomposed autocatalytically
- 3.6 b) Mössbauer spectra of decomposed end products of amorphous FeOOH at 300°C in 1) dry N₂ + MeOH atmosphere and 2) dry N₂ + IPA atmosphere
- 3.6 c) Mössbauer spectra of decomposed end products of amorphous FeOOH at 300°C in 1) N₂ + H₂O + air atmosphere and 2) dry N₂ atmosphere
- 3.7 a) Infra red spectra of 1) FFH and 2) FSH
- 3.7 b) Infra red spectra of 1) FEH and 2) FLH
- 3.7 c) Infra red spectra of 1)FMH and 2)FTH
- 3.7 d) Infra red spectra of the end products of iron(II) carboxylato hydrazinates
- 3.8 a) TG/DTA traces of 1) FFH and 2) FSH
- 3.8 b) TG/DTA traces of 1) FMH and 2) FTH
- 3.8 c) TG/DTA traces of 1) FEH and 2) FLH
- 3.9 XRD patterns of the autocatalytically decomposed end products of Iron(II) carboxylato-hydrazinates
- 3.10 SEM micrographs of the autocatalytically decomposed end products of iron (II) carboxylato-hydrazinates

CHAPTER IV

- 4.1a) XRD patterns of MgFe_2O_4 (Mg=MG) ferrites 1) MgFFHA
2) MgFSHA 3) MgFMHA and 4) MgFTHA
- 4.1b) XRD patterns of MgFe_2O_4 ferrite 1) MgyFA 2) Mg α FA
3) MgAmpFA and 4) MgHEM
- 4.2 Infra red spectra of MgFe_2O_4 ferrites 1) MgFFHA 2) MgFSHA
3) MgFMHA 4) MgFTHA 5) MgyFA 6) Mg α FA 7) MgAmpFA and
8) MgHEM
- 4.3a) Temperature dependence of low field a.c. susceptibility of
 MgFe_2O_4 ferrites 1) Mg α FA 2) MgFSHA and 3) MgHEM
- 4.3 b) Temperature dependence of low field a.c. susceptibility of
 MgFe_2O_4 ferrites 1) MgFFHA 2) MgFMHA and 3) MgFTHA
- 4.3 c) Temperature dependence of low field a.c. susceptibility of
 MgFe_2O_4 ferrites 1) MgAmpFA and 2) MgyFA
- 4.4a) Temperature variation of initial permeability of MgFe_2O_4 ferrites
1) MgFTHA 2) MgFMHA and 3) MgFFHA
- 4.4b) Temperature variation of initial permeability of MgFe_2O_4 ferrites
1) MgyFA 2) MgAmpFA 3) MgHEM and 4) Mg α FA
- 4.5 a) Plot of $\text{Log } \rho$ versus $10^3/T$ of MgFe_2O_4 ferrites 1) Mg α FA
2) MgFFHA and 3) MgFSHA

- 4.5 b) Plot of $\text{Log } \rho$ versus $10^3/T$ of MgFe_2O_4 ferrites 1) MgAmpFA
2) MgyFA and 3) MgHEM
- 4.5 c) Plot of $\text{Log } \rho$ versus $10^3/T$ of MgFe_2O_4 ferrites 1) MgFTHA and
MgFMHA
- 4.6 a) Variation of dielectric constant with temperature of MgFe_2O_4
ferrites 1) MgFFHA 2) MgFSHA 3) MgFMHA and 4) MgFTHA
- 4.6 b) Variation of dielectric constant with temperature of MgFe_2O_4
ferrites 1) MgyFA 2) Mg α FA 3) MgAmpFA and 4) MgHEM

CHAPTER V

- 5.1 Temperature variation of conductivity of $\gamma\text{-Fe}_2\text{O}_3$ synthesised
from ferrous tartrato-hydrazinate (FTHA), in a) air b) Second
run in air and c) in air after moisture equilibration $\sim 200^\circ\text{C}$.
- 5.2 Temperature variation of conductivity and DTA/TG traces of
standard $\gamma\text{-Fe}_2\text{O}_3$
- 5.2a) DTA/TG traces of $\gamma\text{-Fe}_2\text{O}_3$, RT- 600°C and conductivity behaviour
of $\gamma\text{-Fe}_2\text{O}_3$ transformation to $\alpha\text{-Fe}_2\text{O}_3$
- 5.2 b) $\text{Log } \sigma$ v/s $1/T$ plot of standard $\gamma\text{-Fe}_2\text{O}_3$ upto 350°C during heating
and cooling in air
- 5.2 c) $\text{Log } \sigma$ v/s $1/T$ plot of standard $\gamma\text{-Fe}_2\text{O}_3$ in air after flushing in N_2
 $\sim 350^\circ\text{C}$ and equilibration $\sim 200^\circ\text{C}$
- 5.3 DSC traces of standard $\gamma\text{-Fe}_2\text{O}_3$

- 5.4 Temperature variation of conductivity of $\gamma\text{-Fe}_2\text{O}_3$ synthesised from $\gamma\text{-FeOOH}$ a) in air and b) in air after moisture equilibration $\sim 200^\circ\text{C}$.
- 5.5 Temperature variation of conductivity of $\gamma\text{-Fe}_2\text{O}_3$ synthesised by hydrazine method from $\gamma\text{-FeOOH}$ autocatalytically, a) in air and b) in air after moisture equilibration $\sim 200^\circ\text{C}$

LIST OF TABLES

CHAPTER I

- 1.1 Future utilisation of iron oxide raw materials for ferrite production.
- 1.2 Estimated world ferrite production for 1990 in metric tonnes year

CHAPTER III

- 3.1 Chemical analysis, density, IR, total weight loss of iron oxyhydroxides
- 3.2 Chemical analysis of iron oxyhydroxides on hydrazine equilibration in 80% $N_2H_4.H_2O$
- 3.3 XRD data of iron oxides obtained by decomposition of iron oxyhydroxides in different atmospheres
- 3.4 Chemical analysis, density, IR and total weight loss of iron(II) carboxylato-hydrazinates
- 3.5 Isothermal weight loss and TG/DTA analysis of iron (II) carboxylato hydrazinates

CHAPTER IV

- 4.1 a) XRD data of $MgFe_2O_4$ ferrites 1) MgFFHA and 2) MgFSHA

- 4.1 b) XRD data of $MgFe_2O_4$ ferrites 1) MgFM11A and 2) MgFT11A
- 4.1 c) XRD data of $MgFe_2O_4$ ferrites 1)MgyFA and 2) MG α FA
- 4.1d) XRD data of $MgFe_2O_4$ ferrites 1) MgAmpFA and 2) MgHEM
- 4.2 Data on lattice parameter, bond length(R_A and R_B) and site radii (r_A and r_B) for magnesium ferrite
- 4.3 X-ray density, Physical(actual) density and porosity data for magnesium ferrites
- 4.4 Data on saturation magnetisation (σ_s), $4\pi M_s$ and magnetone number (n_B) for magnesium ferrites.
- 4.5 Data on curie temperatures by different methods for magnesium ferrites.
- 4.6 Data on activation energy and curie temperature for magnesium ferrites.

CHAPTER I

General Introduction

General Introduction

Iron oxides, hematite ($\alpha\text{-Fe}_2\text{O}_3$), magnetite (Fe_3O_4) and maghemite ($\gamma\text{-Fe}_2\text{O}_3$), have wide industrial applications other than in steel industry. These oxides find use as pigments in paint industry, catalysts in chemical industry and magnetic recording media in electronic industry. Iron oxides in combination with other metal oxides are special high-tech materials of interesting magnetic properties and are called ferrites.

Gamma ferric oxide, $\gamma\text{-Fe}_2\text{O}_3$ (Maghemite), a ferrimagnetic material, finds use as a magnetic tape material in recording media. Its spinel structure makes it superior to $\alpha\text{-Fe}_2\text{O}_3$ (Hematite) in oxidative dehydrogenation of hydrocarbons [1-6] and several other catalytic reactions. The catalytic activity of $\gamma\text{-Fe}_2\text{O}_3$ is more or less similar to the other spinel ferrites used for such reactions. In the synthesis of industrially important magnetic materials such as ferrites (both soft and hard)

$\alpha\text{-Fe}_2\text{O}_3$ is a main raw material, however, it has now been observed [7] that, in the preparation of Zinc and Barium ferrites, the rate of spinelization can be speeded up with the raw material containing a larger percentage of $\gamma\text{-Fe}_2\text{O}_3$ in it and even the ferritization reaction can be brought down at lower temperatures. Magnetite, Fe_3O_4 , as a starting material in the synthesis of Barium ferrite [8] also found to increase the ferritization reaction at lower temperatures. Here, the starting material, Fe_3O_4 , during the synthesis first transforms into an active $\gamma\text{-Fe}_2\text{O}_3$ and then reacts with the other constituent, barium, yielding the ferrites easily. Magnetic performance parameters and resistivity values of Nickel-Zinc ferrites have also found to be enhanced [9] when $\gamma\text{-Fe}_2\text{O}_3$ was used as a precursor in the synthesis.

Magnetic materials find a place in day to day used products such as communication equipments, data processing devices, automobiles, electronic goods, and home appliances. The applications of ferrites, magnetic oxide materials, in telecommunication and other microwave devices are widely known and a number of technical reports, special articles and proceedings of international conferences on ferrites are available [10-20].

The ever expanding electronic industry is expected to consume more ferrites (both soft and hard) for various applications in years to come. A casual look in the world's estimated ferrites production projected [21], in the year 1989, indicates [Table1.1] the world scenario about ferrites. The estimated total world ferrites production in metric tonnes per year (MTPY), in year 1990, 1995 and 2000, is respectively, 516000, 665500 and 974000 MTPY.

TABLE 1.1 Future utilisation of iron oxide raw materials for ferrite production[21]

Year	1990	1995	2000
Estimated total world ferrite production in MTPY	516,000	665,500	974,000
Total ferric oxide consumption in MTPY			
Hard ferrites (x0.87)	318,000	420,000	550,000
Soft ferrites (x0.70)	105,000	130,000	155,000
Sub total ferric oxide	423,000	550,000	705,000

Iron oxide Source	Year 1990	Year 1995	Year 2000
1. *Upgraded Magnetite	*5%	*5%	*5%
2. *Upgraded Hematite	*30%	*50%	*65%
3. *Oil free Mill Scale	*15%	*10%	*10%
4. *Fluidized bed regenerated granules	*50%	*35%	*20%
*Subtotal 1-4 (MTPY)	127,000	192,000	282,500
5. Spray roasted ferric oxide, high content of impurities	20%	15%	10%
6. Spray roasted ferric oxide, medium content of impurities	70%	65%	60%
7. Spray roasted ferric oxide, little impurities (~200 ppm SiO ₂)	10%	20%	30%
Subtotal 5-7 (MTPY)	275,000	330,000	387,000
8. *Sulfate processed medium impurity	*16%	*16%	*16%
9. *Sulfate processed little impurities	*80%	*80%	*80%
10. *Carbonyl	*4%	*4%	*4%
*Subtotal 8-10 (MTPY)	21,000	27,500	36,000

[Ref 21]

In ferrites, iron oxide is the main constituent and the other divalent ions are added in minor quantities to obtain a spinel of particular stoichiometry and properties.

Considering such a huge ferrites production, by the turn of this century, the iron oxide requirement for the manufacture of ferrites is also expected to increase. The iron oxide consumption in year 1990 was 423,000 MTPY which is expected to increase to 705,000 MTPY, by year 2000. And, iron oxide sources for such ferrites synthesis are mainly, (1) upgraded magnetite, (2) upgraded hematite, (3) oil free mill scale, (4) fluidized bed regenerated granules, (5) spray roasted ferric oxide (high content of impurities), (6) spray roasted ferric oxide (medium content of impurities), (7) spray roasted ferric oxide (little impurities), (8) sulphate processed medium impurities, (9) sulphate processed little impurities and (10) carbonyl. From table 1.1 it can be seen clearly that the upgraded hematite source for iron oxide is going to be of importance by the turn of this century (year 2000) in meeting the huge global ferrites demand of ~ 974000 MTPY.

To meet this huge ferrite demand of ~ 974,000 MTPY, by the turn of this century, about 705,000 MTPY ferrite grade iron oxide is required, which can be met mainly by the upgradation of hematite ore.

A comparative figure of ferrites production [21] of year 1979 and 1989 of various countries [Table 1.2] indicates a grim picture about India's ferrites production capacity. India with its 9000 MTPY production in the year 1979 showed no change in its production capacity in the year 1989. The tonnage remained the same. Japan, on the other hand, increased its production of ferrites from 130,000

TABLE 1.2 Estimated world ferrite production for 1990 in metric tonnes per year

Metric tons per year estimated world ferrite production 1990				
	Hard ferrites		Soft ferrites	
Country	Estimate 1979-ICF3	Estimate 1989-ICF5	Estimate 1979-ICF3	Estimate 1989-ICF5
Canada	4,000	4,000	3,000	300
U S A	85,000	75,000	45,000	10,000
Mexico	3,500	2,500	2,000	400
Venezuela	2,500	1,000	1,500	200
Brasil	15,000	10,000	5,000	3,000
Argentina	3,000	1,500	2,000	500
Chile	600	600	400	200
Scand.	1,500	100	2,000	300
G Britain	10,000	6,000	7,500	6,000
Spain	3,000	2,500	2,000	1,000
France	13,500	13,500	0,000	0000
Germany	12,500	12,500	0,000	0,000
Italy	20,000	10,000	1,000	200
Holland	2,500	200	3,500	500
Yugoslav.	1,600	1,600	1,000	1000
Bulgaria	1,200	1,500	600	800
Rumania	1,500	1,500	600	800
Hungary	1,500	1,500	1,500	1,000
CSSR	3,000	2,500	2,000	2,000
Poland	4,000	2,000	3,000	1,000
G. D. R.	16,000	12,000	8,000	7,000
U. S. S. R.	30,000	30,000	15,000	15,000
Egypt	1,500	1,000	1,000	200
Algeria	1,000	1,000	1,000	200
S. Africa	1,000	1,000	500	200
China	20,000	25,000	15,000	12,000
Japan	65,000	140,000	50,000	40,000
India	6,000	6,000	3,000	3,000
Indonesia	2,500	2,500	1,200	1,200
Singapore	-	6,000	-	500
Thailand	-	3,000	-	-
Malaysia	-	-	-	1,000
Phillipinas	1,500	1,500	1,000	500
Australia	1,200	1,000	600	500
Turkey	1,000	1,000	500	100
Israel	600	600	300	200
Iran	1,500	1,000	1,000	500
S. Korea	6,000	20,000	4,000	12,000
N. Korea	2,000	500	1,500	200
Taiwan	6,000	20,000	4,000	14,000
World ferrite production	302,200	431,100	200,700	159,500

[Ref 21]

MTPY in the year 1979 to 180,000 MTPY in the year 1989. The table clearly indicates how the other countries have increased their production capacity in 10 years time.

India, with its poor ferrites manufacturing capacity, thus, has to depend on imported ferrites materials for its ever expanding electronic industry. India is depending on import of iron oxide of ferrites grade for the manufacture of ferrites (both soft and hard). Infact, the annual demand for the iron oxide in 1977 was 25 metric tonnes (MT) and was met through import [22]. The scenario in 1989 was not much different than that in 1977, as the imports of ferric oxide were still continued (Business India, 11-24th July 1988), not only for recording medium but also as a raw material for the manufacture of ferrites.

India has begun in a small way to upgrade iron ore fines (Blue dust) and a pilot plant of capacity ~ 50,000 tonnes/year is already set up (The Economics Times, Bombay, India, 27th August 1990) and, a 10,000 tonnes capacity plant for ultra pure iron oxide of ferrites grade is also mooted.

India is one of the few countries which have rich iron sources. And, considering the global demand of ferrites in years to come and the huge iron oxide requirement needed for such ferrites production, the beneficiation of hematite ore can be considered best suitable for India to be active in ferrite industry. In his key note address, Dr. B.B.Ghate (Bell lab, USA) during the 5th International conference on Ferrites (ICF-5,1989), Bombay, India, made it clear [23] that there was ample opportunity for entrepreneurs, scientists and technologists trained in ferrites and related disciplines to contribute to the economic growth of India and to the world

ferrite market. Prof. P.S.Deodhar (chairman, ICF-5) in his inaugural address also made emphasis on iron oxide sources for ferrites industry.

The present reserves of iron ore in India [24] is about 15265 million tonnes (mt) which will last for another 250 years with the present rate of mining of ~ 60 mt per year. And Goa, a tiny state of India, was blessed with such rich iron source. But because of rampant high grade iron ore export, since 1950, amounting to about 300 mt, Goa now has an estimated reserves of ~ 400 mt and is expected to last for another 20 - 25 years at the present rate of production of 15 -17 mt per year. Indian iron ore mining industry is mostly export oriented and Goa's contribution to such an export is almost 30 % of the total. So far the iron ore industry in Goa is remained 100 % export oriented.

Considering the high grade exploitation during the last 50 years in India, there is a huge pile up of low grade iron ores and rejects going as a waste. In Goa, there is an estimated 900 -1000 mt of such low grade iron ore rejects, tailings which are being dumped around the mining area.

Intense mechanical mining carried out all over in India to meet the projected annual export figure and domestic use, has resulted into another huge waste, that is the iron ore fines of very high quality: BLUE DUST.

Iron ore fines, blue dust and the iron ore rejects together are creating environmental problems in and around the mining areas. The high grade iron ore fines and fairly good grade iron ore rejects going as dump, are national wastes.

Although, Indian iron ore industry, at present, puts emphasis on very high grade iron ore for export and domestic consumption in steel industry, the fairly

good grade ores that are being kept as rejects now require upgradation by suitable beneficiation processes. Also, the iron ore fines of high quality need to be utilised adequately. Intense activities are going on in this direction all over the world [25].

A modest beginning can be made to tap our rich iron oxide sources, especially the fairly high grade iron ore rejects and iron ore fines, to make them useful in obtaining ferrite grade iron oxides. And, this was the theme of our research programme and the present thesis deals with these aspects of beneficiation of Goan ore rejects to get pure iron oxide and utilisation of the iron oxide to synthesize ferrites, high-tech magnetic materials.

1.1 Upgradation of iron ores

1.1.1 Physical beneficiation

Economically viable beneficiation processes are being adopted for high grade iron sources required for steel industry.

A very low grade iron ore with less than 40% Fe is being processed [26] and a high concentrate of more than 60 % Fe is obtained. As for example, the Lisakovisky deposit in Russia with 40% Fe ore is processed to enrich it to over 62% Fe by adopting a process called magnetic roasting.

Results of various R&D efforts to beneficiate alumina rich Indian iron ore slimes in order to reduce alumina from present 6-10% to less than 2%, so as to make them acceptable for sinter making are critically reviewed by Indian metallurgist [27] who also highlighted the need to develop reagents for hematite gibbsite separation, an important observation ignored, so far, in R&D efforts.

Goan facilities developed for beneficiation of marginal grade ores included crushing, dry screening, washing (wet screening and classification with scrubbing or gravity separation -jigging) and magnetic as well as gravity (spirals) separation, to some extent. Processing low grade ores calls for reduction of deleterious constituents, recovery from slimes and recovery of multiple products involving a combination of concentration steps of different processes [28].

Now, the present problem haunting the geoscientists is the alumina-silica ratio and phosphorous content of the low grade iron ores. The beneficiable ore with its varying silica & alumina characteristics warrant treatment through various beneficiation processes to produce the ore of specified quality. Beneficiation by jigging was found to be most suitable one for such ores.

From the experimental studies done by Wadhvani et al [29] on Barsuan iron ore mines of Rourkela steel plant, it was observed that jigging helps the Fe percentages to go up by 3.1% and the SiO₂ and Al₂O₃ percentages to go down by 1% and 1.6%, respectively. Further, the advanced research work conducted by I.B.M. on the ore samples collected from cyclone under flow of Barsuan iron ore mine of Rourkela steel plant shows the following improvement of the ore qualities by applying high intensity wet magnetic separation [30].

	Fe	SiO ₂	Al ₂ O ₃
Before the process :	58.01%	4.60%	5.60%
After the process :	62.65%	2.21%	3.63%

The flotation beneficiation of low grade iron ore of Goan origin [31] by us-

ing sodium oleate and pine oil is promising one which brings down the Al_2O_3 and SiO_2 percentages and increases iron percentage.

	Fe	SiO_2	Al_2O_3
Before the process:	43%	9%	13.5%
After the process:	68-70%	1.4%	1.1%

Flocculation studies on Donimalai (India) hematitic iron ore fines were carried out [32] using various types of synthetic polymeric flocculants. The effectiveness of selective flocculation was also tried [33,34] in minimizing alumina:silica in artificial mixture of hematite, quartz and alumina using starch as flocculant.

In upgrading Nigerian iron ore, selective oil agglomeration [35] technique was utilised.

Starch and calcium chloride were used to obtain a larger and tougher flocs while studying the setting and filtration characteristics of hematite ore fines of Kemmangundi [36]. This study has potential in water pollution control in iron ore surrounding. Beneficiation of iron by column flotation [37] was also studied by the metallurgist

1.1.2 Chemical beneficiation

The 30 -35 mts thick iron ore horizon in Goa has been divided from surface downwards into the following four zones[38].

1) Laterite or lateritic ore, earthy, rich in goethite, lepidocrocite partly colloidal to cryptocrystalline and often contains a significant amount of hydrated aluminium oxides. 2) Massive ores of hematite with replacement of goethite and scat-

tered grains of remnant magnetite crystals. 3) The third zone is laminated, porous and consists of fragile or 'biscuity' ores with partially leached hematite while the lowest zone, 4) powdery ore consisting of loose and flat hematite rhombs popularly known as 'blue dust'.

Considering the powdery nature of blue dust and the results of leaching experiments on hard hematite ores of Goa and dissolution characteristics of hematite, quartz and amorphous silica, a subterranean solution activity as the sole mechanism [39,40] is proposed for the formation of the blue dust from the original high grade massive banded ore.

A survey of Eh-pH measurements of all types of natural waters [41] showed that the acidity of the waters in the "environment isolated from the atmosphere" may vary widely from strongly acidic to strongly alkaline but usually falls in the reducing atmosphere. The presence of micro-organisms make this water reducing while the acidity or alkalinity comes from its mineral environment. This water ascends from the depth to the surface, in the process leaches, the hard massive hematite dissolving partly the iron and other dissolvable matter, thereby, loosening the hardness and making it to crumble. This process has been taking place in a long period of geological time ultimately forming blue dust layer, after the precipitation of the leached solution flowing down.

Some researchers [42,43] studied the pH of different mine waste and reported a large variation in acidity among different sites ranging from pH 1.5 to above 10. Wong et al [44] reported that the iron tailings were alkaline.

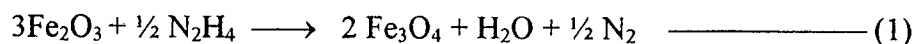
A study of the dissolution phenomenon of hard hematite ore test pieces [45] showed mainly ferric ions in the leached solution of low pH but no traces of these ions in alkaline media. However only 8% of iron is dissolved in pH 2. Absolute solubilities of many important oxides are low [46] and thus it is usual to enhance the solubility through the addition of complexing agents, mainly inorganic and organic anions.

In the study of the interaction of metal hydrous oxides with the chelating agents, a reductive dissolution of hematite and magnetite [47] by aminocarboxylic acid is proposed.

a) Redox dissolution: hydrazine

A redox dissolution seems to be more probable than acidic mechanism and applicable to system like iron oxides where Fe(III) \longrightarrow Fe(II) interconversion may take place. Thus, natural acidic subterranean water in reducing atmosphere may be enhancing the solubility of hematite through the contribution of ferrous ions [48]. These observations may be taken as a clue in chemical beneficiation of iron ore rejects.

Reductive dissolution of hematite and magnetite by amino carboxylic acid, EDTA, is further accelerated by adding a small amounts of hydrazine [47] which helps the redox mechanism. It is well known that hydrazine reacts with ferric oxide [49] according to the equation.



Fe_2O_3 or Fe_3O_4 on heating in a solution of $\text{N}_2\text{H}_4 \cdot 2\text{HCl}$ [50] converts it into $\text{Fe}(\text{N}_2\text{H}_4)_2\text{Cl}_2 \cdot 2\text{H}_2\text{O}$. Reducing property of hydrazine is effectively used in a variety of chemical and metallurgical applications [51]. $\alpha\text{-Fe}_2\text{O}_3$ powders were reduced [52,53] to Fe_3O_4 in an aqueous alkaline solution of hydrazine. It has been demonstrated [54] that the catalytic decomposition of hydrazine sulphate on hydrous ferric oxide in alkaline solution results in the formation of magnetite.

Hydrazine in the presence of carbamate reductively dissolves MnO_2 and this has [55] been explored as a possible way to separate manganese from iron in minerals. Complex ores, especially Nickel laterite types are leached for the selective extraction of cobalt by a reducing agent such as $\text{N}_2\text{H}_4 \cdot \text{H}_2\text{SO}_4$ and hydroxylamine [56].

Chemical beneficiation are being commercially exploited for precious metal extraction but the iron ores are dressed by physical beneficiation techniques followed sometimes by chemical treatments. The high grade iron ores are only being used so far, but the fast deterioration of the natural resources may compell one to go for effective chemical beneficiation of low grade iron ores to obtain value added high-tech material: active iron oxide and ferrites.

1.2 Active iron oxides: $\alpha\text{-Fe}_2\text{O}_3$, Fe_3O_4 and $\gamma\text{-Fe}_2\text{O}_3$

Among iron oxides $\alpha\text{-Fe}_2\text{O}_3$ (Hematite) is being widely exploited in steel industry. High grade hematite ores, after proper beneficiation, have made many countries world leaders in iron metal industry. $\alpha\text{-Fe}_2\text{O}_3$ finds use as pigments in paint industry. Chemical industries use $\alpha\text{-Fe}_2\text{O}_3$ as catalysts in many chemical reactions. High quality $\alpha\text{-Fe}_2\text{O}_3$ is the prime raw material in Ferrites industries.

Magnetic iron oxides, Fe_3O_4 , $\gamma\text{-Fe}_2\text{O}_3$ and mixed metal iron oxides (Ferrites), have been used as device materials in many high tech industries. Infact, the first magnetic material known to man was loadstone or magnetite, Fe_3O_4 . Permanent magnets are made possible from iron oxides. The maghemite, $\gamma\text{-Fe}_2\text{O}_3$ (Gamma ferric oxide), is the prime magnetic material used as a recording medium for applications such as magnetic tapes and other information storage devices like drums and discs [57].

Although $\alpha\text{-Fe}_2\text{O}_3$ is proved industrial catalyst, there are mentions in the literature as regarding the catalytic activities of $\gamma\text{-Fe}_2\text{O}_3$ and ferrites [58-73]. The spinel structure of $\gamma\text{-Fe}_2\text{O}_3$ makes it a superior catalyst to corundum structured $\alpha\text{-Fe}_2\text{O}_3$ in oxidative dehydrogenation of hydrocarbons [58-62]. The catalytic activities of $\gamma\text{-Fe}_2\text{O}_3$ are more or less similar to the spinel ferrites [63] used for such reactions.

1.3 Ferrites

Ferrites are mixed metal oxides of magnetic nature in which iron is the main component. Ferrites possess a wide range of magnetization and find use in radio - receivers, radio transmitters, carrier telepathy, televisions, microwave equipments, high power high frequency transformers (power ferrites), small motors and generators, tape recorders, inverters, converters, novelties, toys etc. These applications of ferrites are due to their high electrical resistivity and permittivity coupled with lower eddy current losses which make them superior to metals and alloys used for such purposes.

1.3.1. Historical development

The first magnetic material known to man was loadstone or magnetite. The chemical formula for the loadstone is Fe_3O_4 (ie. $\text{FeO}\cdot\text{Fe}_2\text{O}_3$) and is in the form of double oxides of iron.

The measurement of saturation magnetization of magnetite was first made by DU Bois in 1890 [74]. Pierre Weiss [75] then studied the magnetic properties of Fe_3O_4 and found its saturation magnetization and curie temperature.

Hilpert [76] first synthetically prepared many ferrites and suggested the basic formula for ferrites as MFe_2O_4 , where M is a divalent metal ion. The preparation of ferrites by solid state reaction has been explained by many researchers [77-79]. The strong foundation for improved properties of ferrites at high frequencies was laid down by Snoek [80] by establishing the importance of accurate oxygen content and homogeneous product.

Some researchers [81,82] have studied the ferrites and reported the structure of ferrite to be spinel type. Barth and Posnjak [83] carried out X-ray analysis of ferrites. They found that it is necessary to assume that the divalent and trivalent metal ions interchange positions in crystals. Thus, they discovered inverted spinel structure which is required for the existence of the ferromagnetic properties in the ferrites. The most extensive and systematic study of artificial ferrite was made by Snoek [84] at Philips laboratories in Holland to meet the commercial demand.

Verwey et al [85-87] reported that the electrical conductivity of ferrites is mainly due to hopping of electrons through the crystal lattice. They carried out X-ray studies on a number of oxides having spinel structure and concluded that Mn,

Co, Mg, Cu and Ni ferrites, which were magnetic had an inverted spinel structure whereas, Zn and Cd ferrites which were non-magnetic had a normal spinel structure.

Neel [88] first introduced the fundamental basic theory of ferrimagnetism. Applying the molecular field theory to ferrites, he introduced the concept of magnetic sub-lattices. Yafet and Kittel [89] extended Neel's theory of magnetic sub-lattices in ferrites by postulating a triangular or canted arrangement of these sub-lattices. The experimental evidence for Neel's theory was given by other researchers [90,91].

In order to explain a.c. conductivity in ferrites, Koops [92] proposed a model to explain the dielectric dispersion. Gilleo [93] proposed a formula to correlate the observed curie temperature, magnetization and cation distribution. Smart [94] and Gorter [95] worked independently and correlated the cation distribution found by microwave resonance and magnetization.

1.3.2 Crystal structure of spinel ferrites .

In general ferrites show four different types of crystal structures.

- 1] Ferros spinel structure.
- 2] Hexagonal structure.
- 3] Garnet structure.
- 4] Perovskite structure.

These groups would cover most of the technologically important oxide magnetic materials.

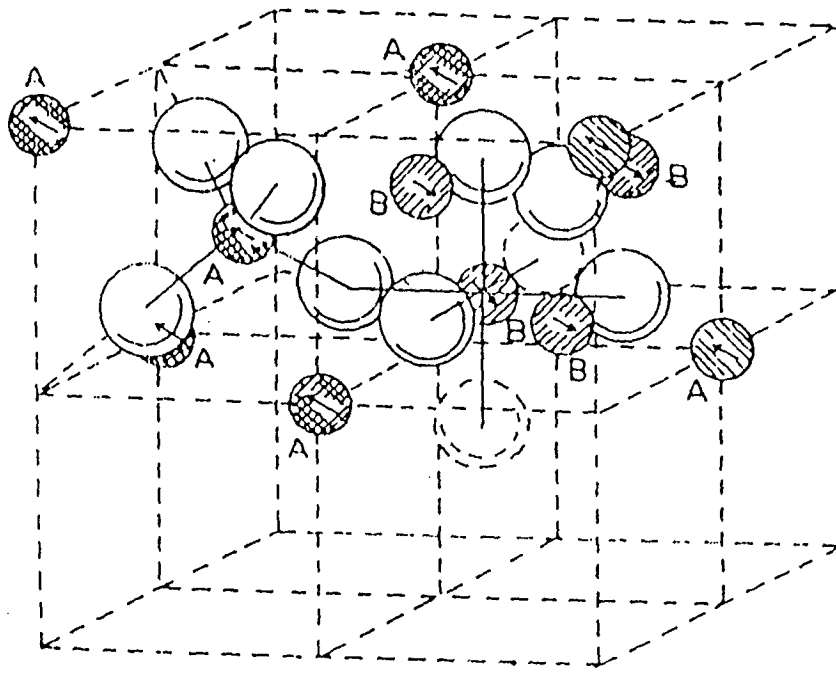
Spinel has a cubic, face centered crystal structure with space group $Fd\bar{3}m$ [96] as shown in figure 1.1. The unit cell contains 8 formula units of MFe_2O_4 . Hence the unit cell has formula $M^{2+}_8 Fe^{3+}_{16} O^{2-}_{32}$. The 32 oxygen ions form two kinds of interstitial sites: tetrahedral or A sites (four oxygen neighbours) and octahedral or B-sites (six oxygen neighbours) per unit cell. In all there are 64 tetrahedral and 32 octahedral sites. Out of these, 8 tetrahedral and 16 octahedral sites are occupied by cations in the ferrites.

In an ideal close packed structure of oxygen anions, lattice can incorporate in tetrahedral sites the metal ions with a radius $r_{tetra} < 0.30 \text{ \AA}$ and in octahedral sites ions with radius $r_{octa} < 0.55 \text{ \AA}$. To accommodate cations such as Mg^{2+} ($r_{octa} = 0.78 \text{ \AA}$), the lattice needs to be expanded. The tetrahedral sites (r_A) and octahedral sites (r_B) are enlarged in the same ratio and distance between tetrahedral site (0,0,0) and oxygen site is $3/8$ and $U_{ideal} = 3/8$. The incorporation of divalent metal ions in tetrahedral sites induces a larger expansion of tetrahedral sites. Therefore U_{obs} is always larger than U_{ideal} .

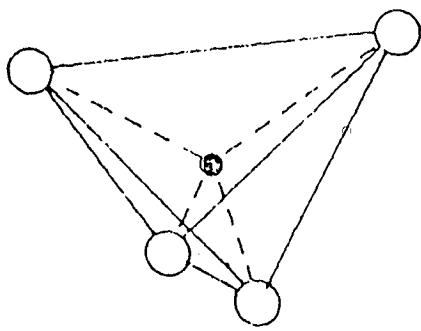
The mode of occupancy of the available A and B sites by the metal ions is very important factor which governs the intrinsic properties of the ferrite material. On the basis of cation distribution Barth and Posnjak [83] have classified spinels into three groups.

a) Normal spinel ferrites

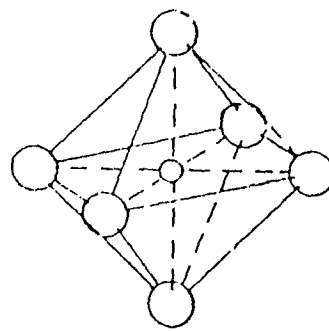
In normal spinel ferrites, all the divalent metal ions occupy A-sites and all the trivalent iron ions occupy B-sites. The structural formula for such a ferrite is given as,



THE SPINEL STRUCTURE

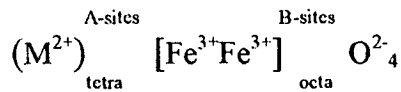


(a) Tetrahedral A site



(b) Octahedral B site

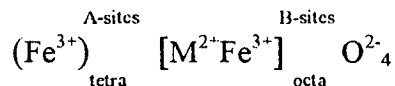
FIG. 1.1 Crystal structure of spinel ferrites showing tetrahedral and octahedral co-ordination



Ferrites like, $ZnFe_2O_4$ and $CdFe_2O_4$ etc., have this type of structure and are non-magnetic.

b) Inverse spinel ferrites

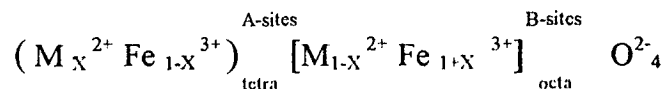
In the inverse spinel ferrites, all the eight divalent metal ions (M^{2+}) occupy B-sites and eight (Fe^{3+}) ions occupy A-sites, whereas, the remaining eight (Fe^{3+}) ions occupy B-sites. The structural formula for such a ferrite is given as,



Ferrites like, $NiFe_2O_4$, $CoFe_2O_4$, $MgFe_2O_4$, Fe_3O_4 , $CuFe_2O_4$, have this type of structure and they are magnetic at room temperature.

c) Random Spinel Ferrites

Normal spinel and inverse spinel both represent the extreme cases of ferrite structure. The random spinel ferrites has intermediate structure between normal and inverse spinels. A fraction of divalent and trivalent ions get distributed randomly along A and B-sites depending upon the physico-chemical conditions of preparation and compositional variation. The general cation distribution can be indicated as ,



where 'x' is the co-efficient of normalcy and (1-x) is the coefficient of inversion.

For normal spinel ferrite $x=1$ and for inverse spinel ferrite $x=0$.

The spinel $MnFe_2O_4$ is a random spinel ferrite with coefficient of normalcy 0.8.

1.3.3 Cations distribution

The cation distribution in a spinel is dependent on the factors such as, [i] electro static energy due to repulsion and attraction between the anions and cations [ii] anion polarisation energy [iii] electronic configuration and crystal field stabilisation energy [iv] ordering energy between different ions on the same sublattice resulting in gain of electrostatic energy and, [v] magnetic ordering energy.

The site preference for individual cations are generally expressed in terms of a particular site stabilisation energy. In an ionic crystal, under the influence of the electrostatic field of the anions, the degeneracy of the d-electrons in the transition metal ions is lifted, resulting into crystal field splitting of the d-states and is associated with the stabilisation energy, designated as crystal field stabilisation energy (CFSE).

Maclure [97] and also Dunitz and Orgel [98] calculated theoretically the values of CFSE for various ions. These values explained the site preference by the cations in the spinel to a good approximation. Miller [99] extended CFSE calculations incorporating Madelung constant, as well as, short range energy terms such as, coulomb and valence terms. He calculated set of site preference energies which could predict the ionic distribution in the spinels involving non transitional and

transitional metal ions. The predicted ionic distribution is in good agreement with the experimental.

1.3.4 Properties of ferrites

The properties of ferrites are classified into two categories [1] Intrinsic properties and [ii] Extrinsic properties.

The intrinsic properties of ferrites are saturation magnetization, magnetostriction, anisotropy, permeability and curie temperature, whereas the extrinsic properties are hysteresis, resistivity, dielectric constant etc. The parameters such as porosity, grain size, impurities etc. affect the extrinsic properties. The extrinsic properties are also referred as structure sensitive properties.

a) Electrical properties

i) Resistivity

Basically ferrites are semiconductors by nature. The resistivity of ferrites vary in the range of 10^{-3} ohm-cm to 10^{11} ohm-cm, at room temperature [100]. The resistivity of ferrites decreases with increase in temperature, according to the relation,

$$\rho = \rho_0 \exp^{-\Delta E/RT}$$

where E is the activation energy, K is the Boltzmann constant and T is absolute temperature. The plot of $\log \rho$ Vs $1/T$ is a straight line which helps to determine activation energy. The activation energy ranges from 0.1 eV to 0.5 eV.

The factors responsible for resistivity are [101] the chemical inhomogeneity caused during preparation, the porosity, the grain size, sintering conditions etc.

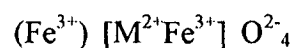
ii) Dielectric behaviour

Ferrites show abnormally high dielectric constant and dispersion of dielectric constant in the frequency range from few Hertz to few MHertz [102,103]. The dielectric parameters of ferrites depend on the preparation technique, grain size and porosity [104]. A dielectric material when subjected to an alternating electric field, the positive and negative charges within the material get displaced with respect to one another and the system acquires an electric dipole moment. The dipole moment per unit volume is called polarization. The dispersion in the dielectric constant has been suggested by Koops [92]. According to him the dielectric constant is inversely proportional to the square root of conductivity. Many researchers [102,105-114] have studied the dielectric properties of ferrites.

b) Magnetic properties

i) Saturation magnetization

Saturation magnetization is one of the intrinsic properties of ferrites and governed by the chemical composition, cation distribution and thermo-physical history. The normal spinels are paramagnetic at room temperature, whereas, the inverse spinels are magnetic at room temperature. The cation distribution of inverse spinel is written as,



The Fe^{3+} ions on A-sites are coupled with their spins antiparallel to those of Fe^{3+} ions on B-sites. Therefore, the net magnetic moment is only due to divalent M^{2+} metallic ions.

The saturation magnetization, of magnesium ferrite, MgFe_2O_4 , [115], Mn Zn ferrite [116] and magnesium ferrite-aluminate [117] has been found to depend on firing schedule of these ferrites.

ii) Permeability

The magnetic permeability is the ratio of magnetic flux density to the magnetic field strength expressed as $\mu = B/H$

The Permeability of the magnetic materials is due to the reversible displacement of domain walls within the material. It is found that the permeability increases with the increase in temperature. The factors affecting permeability are grain size, density, etc.

Okamura et al [118] studied permeability and dielectric constant of various ferrites in the microwave region.

iii) Hysteresis

The lagging of magnetic induction to the magnetizing field is referred to as magnetic hysteresis. The hysteresis study of ferrites helps to find out a valuable information about permeability, saturation magnetization, coercive force etc. Ferrites with low coercive force are called 'soft ferrites' and those with high coercive force are called 'hard ferrites'.

iv) Susceptibility

Alternating Current (a.c.) susceptibility study explores the the existence of multidomains (MD), single domain (SD) and super paramagnetic (SP) particles in the material. For ferrimagnetic materials, the variation of normalized a.c. susceptibility versus temperature have been reported by many workers [119-121]. From these curves the curie temperature and domain structure have been estimated.

Below curie temperature, ferrites have ferrimagnetic nature. Above curie temperature, magnetic transition occurs from ferri magnetic to paramagnetic. The variation of normalized susceptibility (χ_T/χ_{RT}) versus temperature (T) curves show Hopkinson's peak, just below the curie temperature. Bean [122] has reported that for single domain (SD) particles coercive force is large, whereas, it tends to zero for super paramagnetic particles. The a.c. susceptibility studies for mixed ferrites have been carried out by number of researchers to study the effect of temperature and identify multi domain, single domain and, superparamagnetic particles [123].

1.3.5 Synthesis of Ferrites

a) Ceramic technique : Solid State technique

Ferrites have been prepared by many workers by a standard ceramic technique and also by chemical methods. In the conventional ceramic technique $\alpha\text{-Fe}_2\text{O}_3$ is thoroughly mixed with the required divalent metal oxides taken in a stoichiometric amounts. Sometimes, salts such as carbonates, oxalates, nitrates or sulphates of divalent metals are used, which decompose to give reactive metal oxides *in situ*. These divalent oxides then react with $\alpha\text{-Fe}_2\text{O}_3$ more easily. The mixing is usually

carried out in a liquid suspension (water, alcohol, acetone) in steel ball mills. After the slurry is filtered and dried, the dried powder mixture is transferred to ceramic crucible and preheated in air or oxygen.

In order to have better homogenization of the product more grinding is usually done on the preheated products in steel ball mills and then cold pressed into ferrite cores of different shapes and sizes. The second grinding not only reduces the diffusion distances but also decreases grain size of the product as well as the grain size distribution.

Organic binders like Polyvinyl alcohol (PVA) are often added to the preheated samples and then milled and pressed into a core of desired shape and sizes. The pressure applied is generally $5-25 \times 10^6 \text{ kg m}^{-2}$. The pressed material having 50-60 % theoretical density is then fired in air or oxygen atmosphere between 1100-1500 °C, when the solid state reaction between the metal oxides is completed to give a homogeneous ferrite.

The mechanism of formation of ferrite, MFe_2O_4 , by the solid state reaction between MO and Fe_2O_3 has been discussed by several authors [124-131].

b) Mechanism

The mechanism of solid state reactions leading to the formation of ferrite spinels has been discussed on the basis of simple diffusion couple involving divalent metal oxide MO and Fe_2O_3 . In the beginning there is only one phase boundary between the reactants. After the nucleation of the ferrite, this boundary is replaced by two different phase boundaries, one between MO and Ferrite MFe_2O_4 and the other between Fe_2O_3 and MFe_2O_4 . Further progress of the reaction can only take place by

the transport of reactants through the ferrite phase. The three different ways in which this can occur are represented in Fig.1.2 , indicating ionic and electronic fluxes as well as the position of the inert markers, before and after the formation of a ferrite layer.

Case A]. In this mechanism , known as counter diffusion mechanism as suggested by Wagner [125], the cations migrate in opposite directions and the oxygen ions are essentially stationary. Here position of inert marker does not change. The ratio of the amount of ferrite formed on both the sides of the line of marker is 1:3. The reaction between MgO and Fe₂O₃ forming MgFe₂O₄ [132] has been found to undergo through this mechanism.

Case B]. In this case anions take part in the diffusion process. In an extreme case we may have a reaction in which the diffusion of one cation (either Fe²⁺ or M²⁺) is compensated completely by an associated flux of anions. If the diffusion rate of Fe³⁺ ions is greater than that of the divalent metal, the inert marker should displace together with MFe₂O₄ /Fe₂O₃ boundary. A typical example [128] is the reaction between ZnO and Fe₂O₃ to form ZnFe₂O₄.

Case C]. Here the iron diffuses through the ferrite layer in a reduced state of Fe²⁺, as indicated by Paulus [131] and oxygen is transported through the gas phase. Oxygen is evolved at Fe₂O₃/ferrite interface and reabsorbed at the MO/ferrite interface. The inert marker displacement is proportional to the amount of oxygen transported through the proportional phase. Formation of NiFe₂O₄ between NiO and Fe₂O₃ proceeds by this mechanism of preferential diffusion of iron through the ferrite layer in the direction of NiO and, thus, the reaction occurs pre-

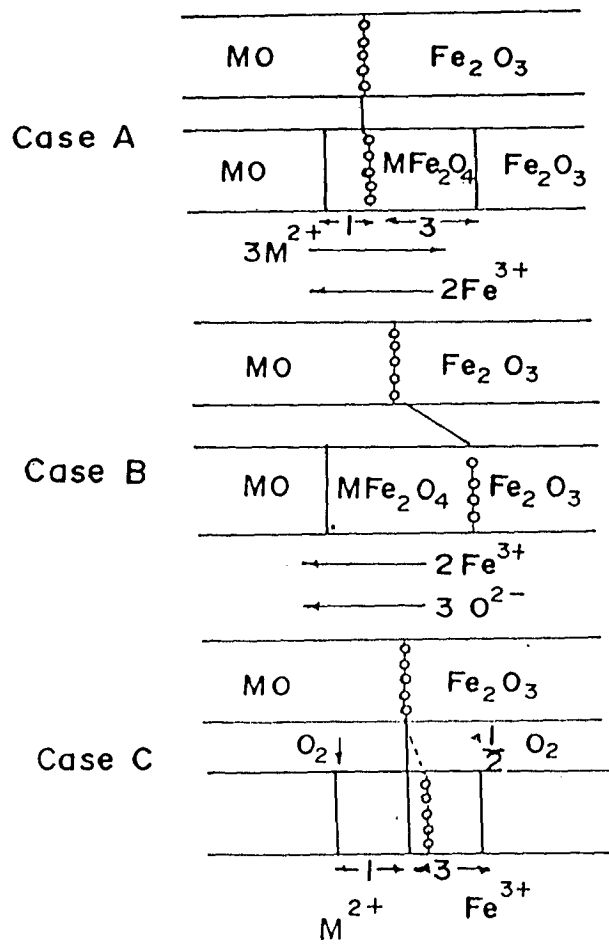
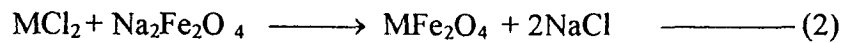


FIG. 1.2 Diffusion mechanism in ferrites

dominantly at the NiO/NiFe₂O₄ interface. Blackman [129] and Reijnen [130] have established the presence of Fe²⁺ ions in the reaction layer.

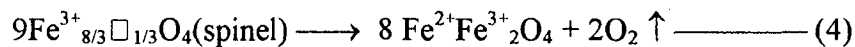
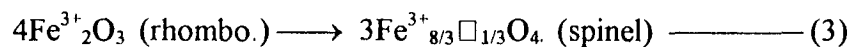
The pioneering work on the preparation of ferrites was carried out by Hilpert, as early as, 1909. Wold [133] has reported the preparation of a number of transition metal ferrites by solid state double decomposition of transition metal chlorides with alkali ferrites.



Since then a number of novel methods have been developed for the preparation of homogeneous, fine-particle, high purity ferrites.

c) Conventional ceramic technique

The method used in the most of the industries for the ferrite manufacture is conventional ceramic method, which requires high temperatures. The raw material generally used in the preparation of ferrites is rhombohedral α -Fe₂O₃ which gets converted to spinel by the following equations [134].



Cation vacancies play an important role in the ferrite sintering kinetics. On increasing the temperature and decreasing the oxygen content, the number of cation vacancies diminish. According to Richards and White [135] pure Fe₂O₃ dissociates to Fe₃O₄ evolving oxygen at 1385°C. But, in the presence of other metal oxides like MgO, dissociation occurs at lower temperatures. They pointed out that first, one

mole of Fe_2O_3 undergoes dissociation at higher temperature to form Fe_3O_4 , which dissolves in MgFe_2O_3 to give a single phase compound.

Ceramic method was used by many researchers [136-142] to prepare ferrites. Economos [136-137] has prepared MnFe_2O_4 and MgFe_2O_4 by solid state reaction between constituent metal oxides. Turk [138] also prepared Ni-Zn ferrite by a similar method. Guiland [139] has shown that reactive oxides formed by the calcination of oxalates, yield high-quality Mn-Zn ferrites, when metals are taken as oxalates, instead of, usual mixture of metal oxides.

Wickham [140] has shown that the solid-state reaction between oxides or carbonates leading to the formation of ferrites can be accomplished rapidly and at low temperatures by adding to the oxide mixtures a suitable quantity of alkali-metal sulphates. Thus, lithium ferrite has been prepared by reacting lithium carbonate and iron oxide mixture in fused Li_2SO_4 , Na_2SO_4 or K_2SO_4 .

Magnesium ferrite was prepared by many researchers using ceramic method [143-151]. The raw material used in the preparation was oxides of iron and magnesium.

d) Precursor technique

A precursor method involves preparation of an easily decomposable compound of metals and mixed metals which yield the desired oxides on heating. The required stoichiometry for oxides can be fixed at the time of precipitation of the constituent elements from solution using suitable precipitants. By this, one can control the impurity level in the oxide systems. These precursors can be decom-

posed to oxides at lower temperatures and then a proper sintering process would give a dense ceramic oxide required in devices.

i) Hydroxide Precursors.

The most widely used reaction is coprecipitation and thermal decomposition of metal and mixed metal hydroxides. O'Bryan et al [152] used this technique for the preparation of Nickel ferrite. Nickel ferrite with highest density (98% theoretical density) having small grain size has been obtained from co-precipitated hydroxide from a mixture of FeSO_4 and NiSO_4 using KOH. Tseung and Goldstein [153] have prepared ultrafine cobalt ferrites by the coprecipitation of metal hydroxides followed by dehydration at 100 °C.

Coprecipitated hydroxides can be converted into ferrites by the sol-gel process [154]. The process consists of forming a concentrated colloidal sol of the hydroxides and then converting this sol into a semirigid gel, finally the gel is dried and calcined to give the ferrite. This method has been applied to the preparation of a wide range of high-density ferrites [155]. Iijima et al [156] synthesised ultrafine magnetic material from FeCl_2 , FeCl_3 and ZnCl_2 treated with NaOH. The heat treatment was given in a flow of nitrogen for an hour which increased the saturation magnetisation.

However, the disadvantage of the coprecipitation methods is segregation and inability to compact easily to high density [157]. Use of slip casting can overcome this problem as recommended by Tseng and Lin [158]. In this slip casting the coprecipitated Ni, Zn, Fe hydroxide precursor was first calcined at 300°C and an aqueous slip of this material was prepared using ammonium citrate as dispersant,

which was then milled and cast in to moulds. This on sintering at 1100°C in air, a ferrite with 98% density, grain size of 1.2 µm was obtained.

Many researchers [147, 150, 159-161] prepared magnesium ferrite by thermal decomposition of coprecipitated hydroxides precursors.

ii) Carboxylate precursors

Preparation of ferrites from oxalate precipitates is preferred, due to the low solubility and low decomposition temperatures of oxalate precursors. Schuele and Deetscreek [162] prepared fine particle nickel ferrite and cobalt ferrite using oxalate precursors. Schuele [163] reported the decomposition of NiFeoxalate at 390°C resulting in the formation of NiFe₂O₄ containing mixture of some amount of iron oxide and nickel oxide. Wickham [164] has found that ferrite powders obtained from oxalate precursors are finely crystalline and free flowing in nature. Stuijts [165] has reported the formation of nickel ferrite at ~ 300°C from the coprecipitated oxalate precursors.

Paris [166] has prepared magnesium ferrite using complexes such as H₄Mg [Fe(C₂O₄)₃]₂, which decompose at ~ 500°C in air giving magnesium ferrite of particle size < 1µm. Glenn Rupard and Gallagher [167] have studied the thermal decomposition of magnesium and iron oxalate coprecipitates and physical mixtures of magnesium and iron oxalates in air and argon and found that the coprecipitate forms the magnesium ferrite more readily than the corresponding physical mixtures of the oxalate, in ceramic technology.

Bassi et al [168] synthesized alkaline earth ferrites by decomposing malonate solid solutions. Gajbhiye and Prasad [169] prepared fine grain, single domain spinel ferrite particles by thermal decomposition of citrate precursor.

iii) Hydrazinate precursors

Patil et al [170,171] prepared novel mixed metal oxalate hydrazinates which give fine-particle ferrites at temperatures as low as 125-165°C. These precursors have been reported to undergo autocatalytic decomposition, that is, once ignited the combustion is self sustained. The surface area of ferrites, MFe_2O_4 (M=Mg, Mn, Co, Zn), prepared from oxalate hydrazinates varies from 22 to 76 m^2g^{-1} . The low temperature synthesis of ferrites is due to the release of energy accompanied in hydrazine oxidation during the decomposition of the complex.

Sharov et al [172] studied the thermal decomposition of many metal oxalates and their complexes with hydrazine in air and argon atmosphere.

Recently, preparation and properties of fine particle of Mg-Mn ferrite by the thermal decomposition of novel hydrazinium metal hydrazine carboxylate precursors have been reported by Patil et al [173]. Thermal analysis of the precursors carried out by them showed that the complexes decomposed exothermically and autocatalytically in the temperature range of 180-220°C, yielding ferrites with an average particle size of 3.5 μm and the surface area of 50 m^2g^{-1} . These fine particles exhibited superparamagnetic behaviour. This solid solution precursor method has also been employed for the preparation of Ni-Zn ferrites [157,174] and Mn-Zn ferrite [175].

In yet another method [176], a mixture of metal nitrates was treated with a hydrazine hydrate in N_2 atmospheres for several days and then heated at 90-100°C to obtain Ni-Zn ferrite fine particles.

Ravindranathan and Patil [177] have observed that the decomposition of hydrazine carboxylate precursors by melt method in a mixture of $NaNO_3$ and KNO_3 yields 70% of the particles of size $1\mu m$ or below as against 20% of such particles obtained by combustion method. They [178] have also achieved almost 99 % of theoretical density for Ni-Zn ferrites prepared by combustion of novel solid solution precursors of the type $(N_2H_5)_3 Zn_{1-x} Ni_x Fe_2 (N_2H_3COO)_9 \cdot 3H_2O$, where $x = 0.2$ to 0.8. The novelty of such precursors is being their low temperature, exothermic gas producing self-sustained decomposition.

Preparation of mixed metal ferrites (MFe_2O_4 , where $M=Mg, Mn, Co, Ni$ and Zn) by combustion of mixed metal sulphite hydrazinate hydrates was studied by Budkuley and Patil [179,180].

Moye, Rane and Kamat Dalal [181] synthesised Ni-Zn ferrites from oxalates and oxalatohydrazinate precursors prepared by solution and under hydrazine method. They observed in their studies that $\gamma-Fe_2O_3$ type phase is formed *in situ* which increased the rate of spinelization.

Sivasankar and Govindarajan synthesized ferrites [182] and cobaltites [183] by thermally decomposing metal hydrazidocarboxylate hydrazinates. They found that the precursors decompose, in a single step, to give MFe_2O_4 ($M=Mn, Co, Ni, Zn$ and Cd) at very low temperature (below 300°C).

Fine particle Ni-Zn ferrites have been prepared [184] by combustion of redox mixtures containing nickel nitrate, zinc nitrate, iron (III) nitrate and oxalic acid dihydrazide [ODH] in the required mole ratio. The ferrites formed had submicrometer size (60-90nm), large surface area (85-108 m²g⁻¹), and achieved >98% of the theoretical density, when heated at 1050⁰C for 3 hours.

Not only fine particle ferrites but also other ceramic powders such as chromites, manganites, cobaltites, aluminas, ceria, titania, zirconia as well as high T_c cuprates have also been synthesized [185] by combustion of redox compounds or mixtures. For preparing such oxides, a mixture of metal nitrate as oxidiser and fuels such as urea (CH₄N₂O), carbonyl dihydrazide (CH₆N₄O), tetra formyl tris-azine (C₄H₁₆N₆O₂), oxalyl dihydrazide (C₂H₆N₄O₂), maleichydrazide (C₄H₄N₂O₂) and malonic dihydrazide have been used. Stoichiometric amount of metal nitrate (oxidiser) and fuel when ignited ~ 350-500⁰C undergo self-propagating, gas producing combustion reaction (smouldering or flaming; temp. 900-1500⁰C) to yield voluminous metal oxides, in less than 5 minutes.

A new chemical route for the preparation of fine ferrite powder is developed by Pramanik and Pathak [186]. The precursors to MFe₂O₄ (M=Ni, Co and Zn) have been prepared by the evaporation of polyvinyl alcohol added to a mixed metal nitrate solution, in the presence and absence of urea. These ignite at low temperatures (250-400⁰C) and the heat liberated through the process is sufficient for the crystallization of the desired ferrite phase. The authors found that the urea added process yields finer, superparamagnetic particles (12-17nm) compared to the process without urea (particle size 25-30nm).

Precipitated salts of metals such as formates, acetates, acetate-pyridine complexes [187], or acetate-ammonia complexes [188] on decomposition give ferrites. However, the ferrites prepared by decomposing the acetate-pyridine complex are quite poorly sintered.

e) Wet chemical method

Preparation of ferrites from solutions of water soluble salts of the corresponding metals fall under wet chemical method category. These methods are reported to yield ferrite powders having molecular level homogeneity, smaller grain size, low porosity and larger surface area [189]. These methods include 1) spray reactions 2) freeze drying and 3) hydrothermal oxidation.

Spray reactions are classified into flame spraying, spray roasting and spray drying. Flame spraying, otherwise known as the atomizing burner technique, was developed by Wenckus [190]. Malinofsky and Babbit [191] were able to prepare nickel ferrite by this method and could densify it to almost 100 % of theoretical density with a very small grain size of $0.8\mu\text{m}$. Zneimer et al [192] prepared Ni-Al-Ga spinel ferrite by putting the nitrate salts of the desired metallic ions in solution with methanol, atomizing the solution with oxygen and burning the atomized spray.

Ruthner et al [193] have utilized spray roasting method for the production of very reactive Fe_2O_3 suitable for preparing ferrites. A wide range of compounds have been produced from spray-dried solutions of mixed sulfates. These show high purity and homogeneity [194,195]. Peshev and Pecheva [196] prepared Lithium ferrite by thermal treatment of spray-dried formates.

According to Schnettler and Johnson [197], ferrites with small grains and of density close to theoretical could be prepared by freeze drying method. Ni-Zn ferrite prepared by this method gave a density of 5.3 gcm^{-3} (99% of the theoretical density) with a grain size of $5 \mu\text{m}$, when sintered between $1000\text{-}1200^\circ\text{C}$. 100 % of theoretical density is achieved using hot isotactic pressing.

In hydrothermal oxidation, ferrites are obtained directly from the solution. The mixture of hydroxides obtained by adding alkali to metal salt solution was heated between $60\text{-}90^\circ\text{C}$ and air was bubbled uniformly into this, which promoted the oxidation reaction, converting the precipitate into ferrite [198]. Takada and Kiyama [199] have prepared manganese zinc ferrite by this method. Akashi et al [200] have used the powders obtained by this method to prepare high density sintered oxides. Sato et al [201] have prepared manganese ferrite, cobalt ferrite and Mn-Co ferrite, directly by coprecipitation in highly alkaline aqueous solutions in few minutes, at temperature below 100°C .

The main parameters for the preparation of ferrite by this technique are the pH value of the solution, the kind of alkali, the reaction temperature, time and the type of metallic ion.

f) Other methods

There are also mentions in the literature of the preparation of ferrites by the thermal decomposition of the heteronuclear μ -oxoacetate of general formula, $[\text{Fe}^{3+}_2 \text{M}^{2+}\text{O}(\text{CH}_3\text{COO})_6(\text{H}_2\text{O})_3].2\text{H}_2\text{O}$, with $\text{M} = \text{Mn}, \text{Fe}, \text{Co}$ or Ni [202,203].

Langbein et al [204,205] prepared the above mentioned complexes of Nickel, Zinc and Manganese by freeze drying method and then decomposed them to get ferrites.

Gao et al [206] prepared ultrafine magnesium ferrite by explosion method. They added excessive urea to the solution of nitrates and after careful drying, heated it in a muffle furnace, which exploded to give ultrafine powder.

A supercritical drying process has been used by many researchers [207-209] to prepare magnesium ferrite powder from a mixture of magnesium acetate tetrahydrate and ferric acetylacetonate, hydrolyzed in a methanolic solvent. The resultant aerogels that obtained after heating the mixture in an autoclave, had small particle sizes in the range of 10 to 20 nm and high surface areas in the range of 50 to 250 $\text{m}^2 \text{g}^{-1}$.

Glaister [210] used a method similar to the one that used by Beer and Planer [211], which is based on bubbling ozone or air through an electrolyte solution containing the metallic ions in the required concentration. The metallic ions are produced by anodic dissolution. Various anodes include Co, Zn, Ni and Mg and cathode is iron. The concentration ratio of each ion is adjusted by the currents passing through the anodes of the metals needed for a particular ferrite formation. The electrolyte is a solution such as sodium sulphate or chloride.

Mn-Zn ferrites prepared by hot isostatic pressing [212,213] could achieve 98 % of theoretical density. Lubl et al [214] have reported a modified hot-pressing technique which enabled fabrication of Mn-Zn ferrite with a homogeneous grain structure, grain size of 0.1 to 1mm and a porosity lower than 0.1%. Buthker and Berben [215] have also prepared dense Mn-Zn ferrite by isostatic hot pressing.

1.4 Historical and Structural Background of Gamma iron oxide, $\gamma\text{-Fe}_2\text{O}_3$

1.4.1 A brief review of Fe-O system

The Fe-O system has been a subject of extensive investigation, over the past several years [216-219]. The data available up to 1957 have been summarized in the literature [217]. The oxides, oxyhydroxides and hydroxides of iron appear in a variety of structures, such as, Fe_{1-x}O , $\alpha\text{-Fe}_2\text{O}_3$, $\beta\text{-Fe}_2\text{O}_3$, $\gamma\text{-Fe}_2\text{O}_3$, $\epsilon\text{-Fe}_2\text{O}_3$, Fe_3O_4 , $\alpha\text{-FeOOH}$, $\gamma\text{-FeOOH}$, $\delta\text{-FeOOH}$, $\beta\text{-FeOOH}$, amorphous FeOOH , $\text{Fe}(\text{OH})_2$ and $\text{Fe}(\text{OH})_3$. The dioxide FeO_2 has recently been reported [220], but the existence of stable FeO_2 still appears doubtful [221].

These oxides, oxyhydroxides and hydroxides are usually prepared by a precipitation method, in which conditions, such as, temperature, pH, concentration, iron-salt used, the presence of foreign ions and their concentration, contribute strongly to structure, crystallinity, particle size & shape, and other physico-chemical properties of the resulting products. $\text{Fe}(\text{OH})_3$ and amorphous FeOOH are amorphous in nature, while the other solid phases are usually crystalline.

The two iron oxides which do not come under iron sesquioxide (Fe_2O_3) category are wüstite, Fe_{1-x}O , and magnetite, Fe_3O_4 .

Magnetite, Fe_3O_4 , is encountered in nature as the magnetic oxide of iron. It can be prepared in the laboratory and has a narrow range of homogeneity [216-218]. Fe_3O_4 has the cubic inverse spinel structure at room temperature, where Fe^{3+}

ions occupy all the A-sites and one-half the B-sites, while the Fe^{2+} ions occupy the other half of the B-sites. It has a low resistivity at room temperature and is ferromagnetic [222-224].

On cooling to -154°C , Fe_3O_4 undergoes a crystallographic transition to an orthorhombic modification [85-86,225-228]. This has been explained by Verwey et al [85-86] as due to the ordering of the octahedral Fe^{2+} and Fe^{3+} ions into perpendicular rows with the associated reduction in crystal symmetry. This transition is commonly referred to as the Verwey transition.

Fe_3O_4 transforms into $\gamma\text{-Fe}_2\text{O}_3$ between $100\text{-}250^{\circ}\text{C}$ [229,230], while the transformation of $\gamma\text{-Fe}_2\text{O}_3 \rightarrow \alpha\text{-Fe}_2\text{O}_3$ starts at 250°C and completes at 500°C .

Iron sesquioxide (Fe_2O_3), exists in several modifications: $\alpha\text{-Fe}_2\text{O}_3$, the most stable form, has a corundum structure [216-218]. A β form (supposedly metastable), possesses cubic bixbyite structure [231-232], and the γ -modification, which has a tetragonal and cubic structure, is metastable at all conditions of temperature and pressure [217,231,233-236]. The structure of $\delta\text{-Fe}_2\text{O}_3$ is not well established, and even its composition is open to doubt (a better description might be $\delta\text{-FeOOH}$) [237-241]. The ϵ form, which has a monoclinic structure, has recently been characterized [242] and a high-pressure form of Fe_2O_3 having a hypothetical perovskite structure has been deduced from shock-wave experiments [243].

1.4.2 Gamma ferric oxide, $\gamma\text{-Fe}_2\text{O}_3$

Gamma ferric oxide was first described by Robbins in 1859 and was first found in nature in 1909 at Iron mountain, Shasta country, California [244]. Since then it has been identified from many other iron ore deposits [245]. Wagner[246] suggested the name, maghemite, for naturally occurring $\gamma\text{-Fe}_2\text{O}_3$. $\gamma\text{-Fe}_2\text{O}_3$ is a wide spread mineral which appears in nature as a colloidal component in many iron-bearing clays[247].

The structure of $\gamma\text{-Fe}_2\text{O}_3$ was originally believed to be the same as that of magnetite with four oxygen ions added to the unit cell of magnetite with a change in the space group[248]. Verwey [249] pointed out that there is insufficient room to fit four additional oxygen ions into the magnetite unit cell. He suggested that $\gamma\text{-Fe}_2\text{O}_3$ is actually a cation deficient spinel with $2\frac{2}{3}$ cations removed from each unit cell.

Colombo et al [250] have investigated the mechanism of the oxidation of magnetite by thermogravimetric, X-ray diffraction and differential thermal analyses and concluded that it is a two stage process involving a solid solution of $\gamma\text{-Fe}_2\text{O}_3$ and Fe_3O_4 , as an intermediate phase giving finally $\gamma\text{-Fe}_2\text{O}_3$.

$\gamma\text{-Fe}_2\text{O}_3$ is, thus, an oxidation product of Fe_3O_4 . On oxidation Fe^{2+} ions present on octahedral sites of Fe_3O_4 with unit cell structure, $(\text{Fe}^{3+})_8[\text{Fe}^{3+}_8\text{Fe}^{2+}_8]\text{O}_{32}$, get oxidise to Fe^{3+} , leaving vacancies on octahedral sites. The $\gamma\text{-Fe}_2\text{O}_3$ thus formed has the unit cell as, $(\text{Fe}^{3+})_8[\text{Fe}^{3+}_{4/3}\square_{8/3}\text{Fe}^{3+}_{12}]\text{O}_{32}$. where () and [] denote tetrahedral and octahedral positions of iron respectively. '□' indicates vacancies and are located

on octahedral sites, [247,249,251]. However, some authors [252-254] also report that the vacancies may also enter both octahedral and tetrahedral sites, simultaneously.

The oxidation of Fe_3O_4 to $\gamma\text{-Fe}_2\text{O}_3$ has been extensively studied by many researchers. Feitknecht et al. [255-256] have studied this reaction by DTA and found that Fe_3O_4 transforms into $\gamma\text{-Fe}_2\text{O}_3$ at 200°C and then $\gamma\text{-Fe}_2\text{O}_3$ into $\alpha\text{-Fe}_2\text{O}_3$, at 600°C in air. They also showed that magnetite particles larger than 5500\AA in diameter are oxidized directly to $\alpha\text{-Fe}_2\text{O}_3$. Ozdemir et al [257] have reported that the ultrafine Fe_3O_4 when exposed to air, quickly oxidises to air. The reports of Fukasawa et al [258,259] also support this. They also reported that Fe (II) ions from Fe_3O_4 oxidise partially in air at 110°C .

According to Kauffman and Hazel [260] coarse Fe_3O_4 oxidises to $\alpha\text{-Fe}_2\text{O}_3$ at room temperature, if kept wet. Elder [261] showed that, while natural magnetite crystals ground in water to a particle size of less than $1\mu\text{m}$ were converted to $\gamma\text{-Fe}_2\text{O}_3$ at 250°C (more than 75% conversion); the large particles, $25\mu\text{m}$ or more, were, on the other hand, converted only to $\alpha\text{-Fe}_2\text{O}_3$, under the same conditions. The effect of the small particle size, Elder attributed to the stabilizing action of water. As an additional demonstration of the effect, he showed that the smaller particles, ground in dry acetone and heated in dry oxygen, produced only $\alpha\text{-Fe}_2\text{O}_3$, whereas in an atmosphere of water vapour and oxygen, they produced pure $\gamma\text{-Fe}_2\text{O}_3$.

David and Welch [262] showed that 'specimens of magnetite which gave gamma ferric oxide on oxidation invariably contained appreciable percentages of water, while specimens prepared under dry conditions oxidized with great difficulty,

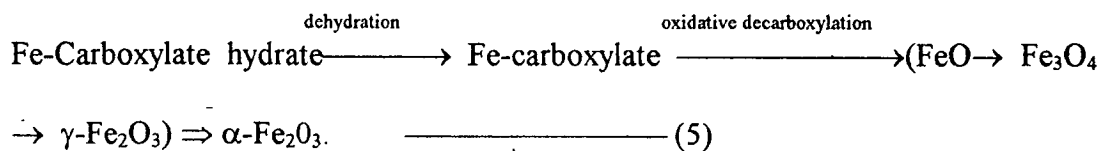
never yielding the gamma oxide'. Further more, they confirmed the findings of Verwey [249] that the gamma ferric oxide itself contained a small amount of water that could not be removed without changing the characteristic structure of the material and transforming it to α -Fe₂O₃.

In magnetite powders prepared synthetically, it is more than likely that the particles contain water either from the solutions in which they were formed or as adsorbed water. However, natural magnetite in the form of bulk samples does not contain water. The oxidation of Fe₃O₄ to γ -Fe₂O₃ is controlled by the particle size (surface area) of Fe₃O₄. The small size of the particles not only help in trapping moisture but also in controlling the rate of oxygen diffusion [263].

Though Fe₃O₄ oxidation yields γ -Fe₂O₃, it is considered that the oxidation process is crucial and water is found to be essential [57,235,261,262,264-271] in stabilizing the metastable phase of iron oxide, γ -Fe₂O₃. In the absence of this water, the oxidation proceeds to thermodynamically more stable oxide of iron, α -Fe₂O₃.

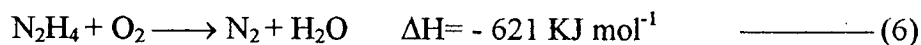
In the preliminary studies done by Rane et al[264] on the thermal decomposition of iron (II) carboxylate, ferrous oxalate dihydrate, FeC₂O₄.2H₂O, it was observed that , under a controlled atmosphere of a known partial pressure of water vapour, γ -Fe₂O₃ is formed. In the absence of this atmosphere, the thermal product is α -Fe₂O₃. This requirement of a known partial pressure of water vapour during the thermal decomposition of the other iron (II) carboxylates: fumarate [272], succinate [273], malonate [274], tartrate [275], maleate [276] and malate [277] to stabilize γ -Fe₂O₃ has also been studied by other groups.

The thermal decomposition of iron (II) carboxylates in general can be represented by the following sequential reactions that take place on heating.



The dehydration is immediately followed by oxidative decomposition. In a controlled atmosphere of water vapour the reaction sequence is arrested, at $\gamma\text{-Fe}_2\text{O}_3$ stage.

The decomposition of ferrous oxalate hydrazinate, $\text{FeC}_2\text{O}_4 \cdot \text{N}_2\text{H}_4$ and $\text{FeC}_2\text{O}_4 \cdot 2\text{N}_2\text{H}_4$ studied by Rane, Moye and Kamat Dalal [278] also confirmed the importance of water vapour in arresting the reaction at $\gamma\text{-Fe}_2\text{O}_3$, as in ferrous oxalate dihydrate. Here the hydrazine liberated on heating iron oxalato-hydrazinates, reacts with atmospheric oxygen, exothermically, releasing enormous energy [279],



The energy thus liberated is sufficient to oxidatively decompose the dehydrazinated carboxylate to $\gamma\text{-Fe}_2\text{O}_3$. The reaction products $\text{N}_2 + \text{H}_2\text{O}$ provide enough water vapour partial pressure to stabilize $\gamma\text{-Fe}_2\text{O}_3$.

The essential requirement of water in stabilizing $\gamma\text{-Fe}_2\text{O}_3$ and the structural similarity of this oxide with that of lithium ferrite, LiFe_5O_8 , $(\text{Fe}^{3+})_8 [\text{Li}^{1+}_4 \text{Fe}^{3+}_{12}] \text{O}_{32}$, allowed the researchers [235,262,265] to assume that the vacancies of $\gamma\text{-Fe}_2\text{O}_3$, $(\text{Fe}^{3+})_8 [\text{Fe}^{3+}_{4/3} \square_{8/3} \text{Fe}^{3+}_{12}] \text{O}_{32}$ are occupied by some 1+ charged species. Since water promotes the stabilization of $\gamma\text{-Fe}_2\text{O}_3$, protons were considered to be incorporated

in the lattice on the octahedral vacant sites. And, a fully protonated $\gamma\text{-Fe}_2\text{O}_3$ is written similar to LiFe_5O_8 as HFe_5O_8 , $(\text{Fe}^{3+})_8 [\text{H}^{1+}_4 \text{Fe}^{3+}_{12}] \text{O}_{32}$.

The gamma ferric oxide stabilized [280] under controlled water vapour decomposition of ferrous oxalate dihydrate was considered to have a composition in between, $(\text{Fe}^{3+})_8 [\text{Fe}^{3+}_{4/3} \square_{8/3} \text{Fe}^{3+}_{12}] \text{O}_{32}$ and $(\text{Fe}^{3+})_8 [\text{H}^{1+}_4 \text{Fe}^{3+}_{12}] \text{O}_{32}$ which may be given as, $(\text{Fe}^{3+})_8 [\text{Fe}^{2+}_x \text{H}^{1+}_{4-2x} \square_x \text{Fe}^{3+}_{12}] \text{O}_{32}$. An extreme case would be $(\text{Fe}^{3+})_8 [\text{Fe}^{2+}_2 \square_2 \text{Fe}^{3+}_{12}] \text{O}_{32}$.

This protonated phase of $\gamma\text{-Fe}_2\text{O}_3$ is called as hydrogen iron oxide $\text{H}_{1-x} \text{Fe}_{5+x/3} \text{O}_8$ [265] or hydrogen doped iron oxide with an upper limit of the presence of proton is put at, $\text{H}_{0.1} \text{Fe}_{5.1/3} \text{O}_8$ [266]. And, it was also considered as hydrogen ferrite type phase by Nikumbh, Rane and Mukhedkar [280], as well as, by Venkataraman and Mukhedkar [281].

The hydrogen iron oxide phase observed by Nikumbh, Rane and Mukhedkar [280] was studied by measuring direct current measurement, on the thermal product of $\text{FeC}_2\text{O}_4 \cdot 2\text{H}_2\text{O}$ under a controlled atmosphere of water vapour that obtained by Rane et al [264]. Arrhenius type of behaviour in logarithm conductivity (σ) Vs $1/T$ plot, upto a temperature, well below the temperature of transformation of $\gamma\text{-Fe}_2\text{O}_3$ to $\alpha\text{-Fe}_2\text{O}_3$, was observed. However, the cooling curve in such measurements did not retrace back the heating path in $\log \sigma$ vs $1/T$ plot, thus, showing a hysteresis behaviour, in the electrical conductivity measurements.

On continuing the measurements during the second heating, the $\log \sigma$ vs $1/T$ plot, did not follow the first heating, however, it did overlap the first cooling and subsequent heating and cooling curves, all of which overlapped the first cooling

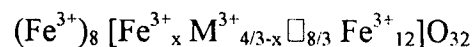
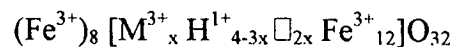
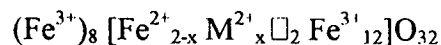
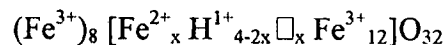
curve. From these studies, it was concluded that the $\gamma\text{-Fe}_2\text{O}_3$ synthesized from ferrous oxalate dihydrate in a controlled atmosphere of water vapour, consists of a phase, at lower temperature, which get lost at higher temperatures

This low temperature phase, once removed, could only be re-introduced when the high temperature phase was exposed to a known water vapour atmosphere or hydrogen atmosphere $\sim 200^\circ\text{C}$. These experimental observations indicated a presence of hydrogen iron oxide or hydrogen ferrite type of phase in $\gamma\text{-Fe}_2\text{O}_3$, at lower temperatures. The high temperature phase is a vacancy ordered, usual $\gamma\text{-Fe}_2\text{O}_3$. The hydrogen iron oxide phase present in $\gamma\text{-Fe}_2\text{O}_3$ is represented by composition as $(\text{Fe}^{3+})_8[\text{Fe}^{2+}_x \text{H}^{1+}_{4-2x} \square_x \text{Fe}^{3+}_{12}]\text{O}_{32}$.

The presence of such hydrogen iron oxide phase, at lower temperature, was also observed in $\gamma\text{-Fe}_2\text{O}_3$ synthesized from other iron (II) carboxylates [272-277], in a controlled atmosphere of water vapour. The low temperature hydrogen iron oxide phase on heating $\sim 200^\circ\text{C}$ loses the protons, H^+ , from the octahedral sites and then transforms into vacancy ordered $\gamma\text{-Fe}_2\text{O}_3$, $(\text{Fe}^{3+})_8[\text{Fe}^{3+}_{4/3} \square_{8/3} \text{Fe}^{3+}_{12}]\text{O}_{32}$. And, this is the reason why hysteresis behaviour was observed in the conductivity studies of $\gamma\text{-Fe}_2\text{O}_3$. On exposure to water vapour, protons were reintroduced into the lattice and the hydrogen iron oxide is reinstated in $\gamma\text{-Fe}_2\text{O}_3$.

The easy removal of protons from the hydrogen iron oxide phase of $\gamma\text{-Fe}_2\text{O}_3$ and then reintroduction of it in the vacancy ordered $\gamma\text{-Fe}_2\text{O}_3$, indicates a reversible process, which can be put into use in oxidative dehydrogenation reaction of hydrocarbons, over $\gamma\text{-Fe}_2\text{O}_3$ catalysts.

In another interesting studies of the effect of divalent M^{2+} and trivalent M^{3+} dopants, on this hydrogen iron oxide phase of $\gamma\text{-Fe}_2\text{O}_3$, Nikumbh, Rane and Mukhedkar [282], observed a negligible hydrogen ferrite type phase in $\gamma\text{-Fe}_2\text{O}_3$, at certain dopant concentrations. Based on such investigation, the following chemical composition were proposed by them,



The introduction of divalent/trivalent cations, thus, modify the concentration of H^+ , indicating that these are the sites into which the divalent and trivalent cations are incorporated.

The literature involving the formation of $\gamma\text{-Fe}_2\text{O}_3$ suggests that water is not only essential in stabilizing $\gamma\text{-Fe}_2\text{O}_3$ but also makes its presence felt as H^+ in the lattice of $\gamma\text{-Fe}_2\text{O}_3$.

The crystalline arrangement of $\gamma\text{-Fe}_2\text{O}_3$ has been studied by different techniques by many researchers [235,254,265,266,283-287]. The structure of $\gamma\text{-Fe}_2\text{O}_3$ can be described as a spinel structure, in which, there exist systematic defects in octahedral cations [288,289]. A description of $\gamma\text{-Fe}_2\text{O}_3$ as a spinel structure requires 1/6 of the octahedral positions to be empty, so that the formula per unit cell is $(\text{Fe}^{3+})_8 [\text{Fe}^{3+}_{13+1/3} \square_{2+2/3}] \text{O}_{32}$, where \square represents an octahedral vacancy.

The arrangement of these vacancies varies from sample to sample and is strongly dependent on the method of preparation; its nature determines the final symmetry of the substance [247].

The idealized crystal structures of the three main varieties of maghemite are as follows.

(1) If the vacancy distribution is totally random, all the octahedral spinel positions are statistically equivalent and the material has an average $Fd3m$ symmetry, the same as in the fully occupied stoichiometric ideal spinel. (2) If the vacancies tend to be placed in some particular positions, the structure changes to primitive cubic belonging to space group $P4_132$, similar to that of lithium ferrite $Fe_8[Li_4Fe_{12}]O_{32}$. (3) Finally, the apparently defect free structure corresponds to the tetragonal $P4_32_12$ space group, with a unit cell three times as large in the C direction as that of spinel, and it is generally admitted that the vacancies are totally ordered.

Consequently, for structure-dependent physical properties, the substance called $\gamma-Fe_2O_3$ has indeed three different phases, two of them optically isotropic and one anisotropic, characterized by a different degree of long range crystal order of the vacancies.

1.5 Importance of $\gamma-Fe_2O_3$ in ferrite synthesis

$\gamma-Fe_2O_3$ is the most widely used recording material in magnetic tapes and disks. Its spinel structure makes it a superior catalyst to $\alpha-Fe_2O_3$ in oxidative dehydrogenation of hydrocarbons [58-63]. The catalytic activity of $\gamma-Fe_2O_3$ is more or

less similar to the spinel ferrites, such as, magnesium and Zinc ferrites, used for such catalytic reactions. The reactivity and oxygen mobility of $\gamma\text{-Fe}_2\text{O}_3$ were investigated in detail in relation to the oxidation of carbon monoxide [290].

Adhyapak et al [291] studied the reactions of ammonium hydrogen fluoride with three oxides of iron, viz, $\alpha\text{-Fe}_2\text{O}_3$, Fe_3O_4 and $\gamma\text{-Fe}_2\text{O}_3$, in the solid state, at room temperature and at slightly higher temperature. They found that the reaction with the $\alpha\text{-Fe}_2\text{O}_3$ was rather sluggish at room temperature, but, was hastened considerably at 80°C . On the other hand, the reaction with Fe_3O_4 was complete in three hours, in the solid state, at room temperature. The reaction with $\gamma\text{-Fe}_2\text{O}_3$ was instantaneous. In all the cases, the product of reaction was $(\text{NH}_4)_3\text{FeF}_6 \cdot 1.5\text{H}_2\text{O}$. Thus, they confirmed that $\gamma\text{-Fe}_2\text{O}_3$ is more reactive than $\alpha\text{-Fe}_2\text{O}_3$.

In hard and soft ferrite synthesis, $\gamma\text{-Fe}_2\text{O}_3$ has been tried [7-9] in place of usual $\alpha\text{-Fe}_2\text{O}_3$, along with the other divalent cations. And, it has been observed [7] that the rate of spinelization can be speeded up with raw material, iron oxide, $\alpha\text{-Fe}_2\text{O}_3$, consisting of larger percentage of $\gamma\text{-Fe}_2\text{O}_3$, in Zinc ferrite and Barium ferrite synthesis and even the ferritization reaction can take place, at lower temperature.

Magnetite, Fe_3O_4 , as a starting material in Barium ferrite preparation [8] increases ferritization reaction at lower temperature. The enhanced reaction is due to the formation of active iron oxide from magnetite during heating process. Magnetic performance parameter and resistivity values of Nickel Zinc ferrites increased [9] when $\gamma\text{-Fe}_2\text{O}_3$ is used as a precursor in the synthesis.

Yamaguchi [292] converted Fe_3O_4 to $\gamma\text{-Fe}_2\text{O}_3$ rich haematite and mixed with other oxides, moulded and sintered to obtain polycrystalline ferrites, useful for video recording heads.

Gillot et al [293], in their kinetic study of low temperature oxidation of titanomagnetites observed that Fe^{2+} ions of B site gets oxidised more rapidly than A site ions. Oxidation of Fe^{2+} ions from B site was found to be associated with lower oxidation energy and higher diffusion coefficient than A site ions. Thus, Fe^{2+} ions in Fe_3O_4 get easily diffused creating site for metal ions to penetrate, during oxidation, which otherwise would have remained vacant or lead to $\gamma\text{-Fe}_2\text{O}_3$ formation. Tzevalov et al [294] during decomposition of NiFe citrate observed Fe_3O_4 as one of the by products. Since, this is an essential intermediate phase, NiFe_2O_4 is formed at lower temperature.

Elwell et al [295] explained the importance of Fe_3O_4 in the ferrite formation. According to him, the intermediate phase during NiFe_2O_4 formation is Fe_3O_4 . Formation of Fe_3O_4 is a must for Nickel ferrite to form, even if the starting material is NiO and $\alpha\text{-Fe}_2\text{O}_3$.

Similar observation is made by Srivastava et al [296]. Barium citrate decomposed to BaCO_3 and Fe citrate to $\alpha\text{-Fe}_2\text{O}_3$, but, the mixture of the two decomposed to form BaO and $\gamma\text{-Fe}_2\text{O}_3$ or Fe_3O_4 or the mixture of the two and not BaO and $\alpha\text{-Fe}_2\text{O}_3$. The decomposed mass yielded Barium ferrite at a temperature of 600°C . Here too $\gamma\text{-Fe}_2\text{O}_3$ or Fe_3O_4 plays an important role in easy ferritisation. This can be understood from the fact that, sintering proceeds with cationic ordering

in ferrites in the initial stages, as revealed from the studies done on (Fe_3O_4 - MnO_3) system, by Voilkovskii et al [297].

The cationic ordering at initial stages means incorporation of the other metal ions in iron oxide and, this can be thought of only, if the iron oxide is in spinel form, $\gamma\text{-Fe}_2\text{O}_3$ or Fe_3O_4 and not rhombohedral $\alpha\text{-Fe}_2\text{O}_3$.

In the synthesis of NiZn ferrite from its oxalate precursor, it was observed by Moye, Rane and Kamat Dalal [181] that, the use of a controlled atmosphere of water vapour during decomposition leads to the formation of $\gamma\text{-Fe}_2\text{O}_3$ type phase, with the other metal ions incorporated in its lattice. Similarly, upon autocatalytic decomposition of hydrazinated complexes, spinel formation is observed. Further heat treatment at higher temperature leads to a better site preference and expected magnetic characteristics are achieved. The ease of spinelization was assumed to be due to the presence of $\gamma\text{-Fe}_2\text{O}_3$ type of phase as an intermediate, during decomposition.

From the forgoing literature survey, it is inferred that spinel ferrites can be easily prepared from $\gamma\text{-Fe}_2\text{O}_3$ or Fe_3O_4 . That is, these spinel oxides when mixed with the divalent oxides, MO, result into spinel ferrite, MFe_2O_4 . Usual ceramic technique of ferrite synthesis is done using $\alpha\text{-Fe}_2\text{O}_3$ of corundum structure. The corundum structured $\alpha\text{-Fe}_2\text{O}_3$ when heated at higher temperature converts to spinel structured Fe_3O_4 as per the equations (3) and (4). And the divalent oxides MO react with the Fe_3O_4 resulting into MFe_2O_4 . The cation vacancies that are created play an important role as divalent ions occupy these vacancies and turn completely

into the ferrite. Hence, the use of $\gamma\text{-Fe}_2\text{O}_3$ (vacancy ordered spinel structure similar to Fe_3O_4) and Fe_3O_4 as a starting material in ferrites synthesis gives a better scope to prepare ferrites.

1.6 Aim, Scope, Methodology and work plan

1.6.1 Aim

Spinel ferrites are usually synthesized by a solid state reaction between corundum $\alpha\text{-Fe}_2\text{O}_3$ and other divalent metal oxides, MO, at elevated temperatures ($>1000^\circ\text{C}$). High temperatures enable $\alpha\text{-Fe}_2\text{O}_3$ to transform it into spinel magnetite, $\text{Fe}^{2+}\text{Fe}^{3+}_2\text{O}_4$ via $\text{Fe}^{3+}_{8/3}\text{O}_{1/3}$ (equation 3 and 4, section 1.3.5.c) and during these transformations the divalent cation (M^{2+}) react with the prevailing spinel phase easily to end up with spinel ferrites phase, $\text{M}^{2+}\text{Fe}^{3+}_2\text{O}_4$. To complete the reaction several hours of heating, at elevated temperatures, are required to get monophasic ferrite of desired stoichiometry. Thus, $\alpha\text{-Fe}_2\text{O}_3$ transform into spinel phase before reacting with the divalent metal ion to complete the spinelization reaction.

There are, however, few mentions in the literature [7-9] about the use of spinel $\gamma\text{-Fe}_2\text{O}_3$ and Fe_3O_4 or $\alpha\text{-Fe}_2\text{O}_3$ containing a large percentage of $\gamma\text{-Fe}_2\text{O}_3$ as a starting material for ferrites synthesis. Use of such starting materials, not only enhances the rate of reaction of spinelization but also allows one to prepare ferrites at lower temperatures, of better characteristics, than the one synthesized by usual method, from $\alpha\text{-Fe}_2\text{O}_3$, as raw material.

In our laboratory [278] these aspects have been preliminarily ascertained. We, therefore, decided to explore further the usefulness of $\gamma\text{-Fe}_2\text{O}_3$ in the synthesis

of ferrites, mainly, MgFe_2O_4 . Hence, as a research programme we undertook a task of synthesizing $\gamma\text{-Fe}_2\text{O}_3$ samples from different precursors to use them in the synthesis of MgFe_2O_4 and compare their characteristics with the ferrites prepared from usual $\alpha\text{-Fe}_2\text{O}_3$.

1.6.2 Scope

We came across the proceeding of 5th International Conference on Ferrites (Bombay, India, 1989) and the invited lectures and research articles appeared in it [23] which gave us national and international scenario [21] of ferrites (section 1.0). In year 1989, estimated ferrite production of India was just 9000 metric tonnes per year as compared to Japan of 180,000 MTPY, the leader in the list of various ferrites manufacturing countries in the world (Table 1.2). And, it is found that ferrites industry has better scope for expansion due to their wide applications in electronic devices.

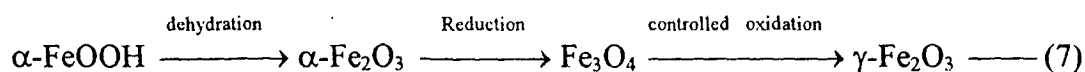
World ferrites demand in the year 2000 is estimated to increase from 665,500 MTPY, in the year 1995 to 974,000 MTPY (Table 1.1). To meet this demand, ferrite grade iron oxide, $\alpha\text{-Fe}_2\text{O}_3$, of about 705,000 MTPY is required, by the turn of this century. The iron oxide needed for ferrites synthesis has to come from mainly upgraded hematite ore and spray roasted pickling solution (Table 1.1). However, the upgraded hematite ore will amount to 65% of the total iron oxide requirement. But, then, the upgraded iron oxide ore will give iron oxide whose trace impurities will be difficult to control. The spray roasted iron pickling solution may, however, be able to give iron oxide of high, medium and little impurities, useful for the manufacture of ferrites of different grades, depending upon the source of pick-

ling solution. This process is energy consuming. Hence, beneficiation process to upgrade iron ore will be adopted world over to meet the global ferrite grade iron oxides requirement.

Both spray roasted and beneficiated iron ore processes give iron oxide of $\alpha\text{-Fe}_2\text{O}_3$ form. Such iron oxide when used in the ferrites synthesis, by ceramic technique, the one with very little impurities (spray roasted) will be the best choice for the manufacture of ferrites of uniform and better characteristics. If impurities are many and varied (as in beneficiated ore), then the ferrites of high quality are difficult to achieve.

Many chemical methods (coprecipitation, precursor techniques, sol gel, freeze drying) although costlier are, hence, adopted for synthesizing ferrites required for high-tech applications, like in power ferrites. Such high quality ferrites requirement runs in several hundred tonnes, rather than million tonnes of ferrites, using $\alpha\text{-Fe}_2\text{O}_3$ synthesized by ceramic technique, required for routine applications.

High quality ferrites synthesis, thus, adopts chemical route. If such methods are costlier and energy consuming, then one can resort to alternate method. As mentioned earlier, the $\gamma\text{-Fe}_2\text{O}_3$ may be tried as a raw material to prepare such ferrites by usual ceramic technique. But, commercial $\gamma\text{-Fe}_2\text{O}_3$ synthesis is a multistep oxidation - reduction process:



And, hence use of such $\gamma\text{-Fe}_2\text{O}_3$ is meaningless in ferrites synthesis as cost will go up. Therefore, some easy method to synthesize $\gamma\text{-Fe}_2\text{O}_3$, if adopted, one can

think about using this for ferrite synthesis of high quality. This was the aim of our present work (section 1.6.1.). However, looking at the world ferrites demand, it is wise to make use of iron ores to synthesize easily $\gamma\text{-Fe}_2\text{O}_3$, by chemical methods. And, this is where the scope of our present work lies.

We have envisaged to make use of iron ores to synthesize $\gamma\text{-Fe}_2\text{O}_3$ easily. But, then, we are making use of low grade iron ore rejects for such purpose. By making use of low grade iron ores to prepare value added materials we may, to some extent, think about preserving our fast deteriorating environment, due to piling up of ore rejects around the mining area. Also, the ore rejects which are going as waste may thus be put in use. This is rather required as rich mineral sources are depleting fast, world over.

1.6.3 Methodology and work plan

Main objective being beneficiation of iron ore rejects to prepare active iron oxide useful in ferrite synthesis, it was decided to first explore various synthetic routes to prepare $\gamma\text{-Fe}_2\text{O}_3$ from different precursors. And, then, make use of these $\gamma\text{-Fe}_2\text{O}_3$ samples to obtain magnesium ferrite, MgFe_2O_4 , by usual ceramic technique. Then characterize the ferrites and compare their characteristics with the ferrites synthesized from $\alpha\text{-Fe}_2\text{O}_3$. After establishing these aspects, iron ore reject of one particular grade was considered to be taken up for study. Idea was to bring the rejects in an acid solution and then precipitate iron into iron hydroxide. And, use this iron hydroxide for $\gamma\text{-Fe}_2\text{O}_3$ synthesis, required for ferrite preparation. A birds view of the planned work is given in FIG.1.3.

Synthesis of ferrites($MgFe_2O_4$)

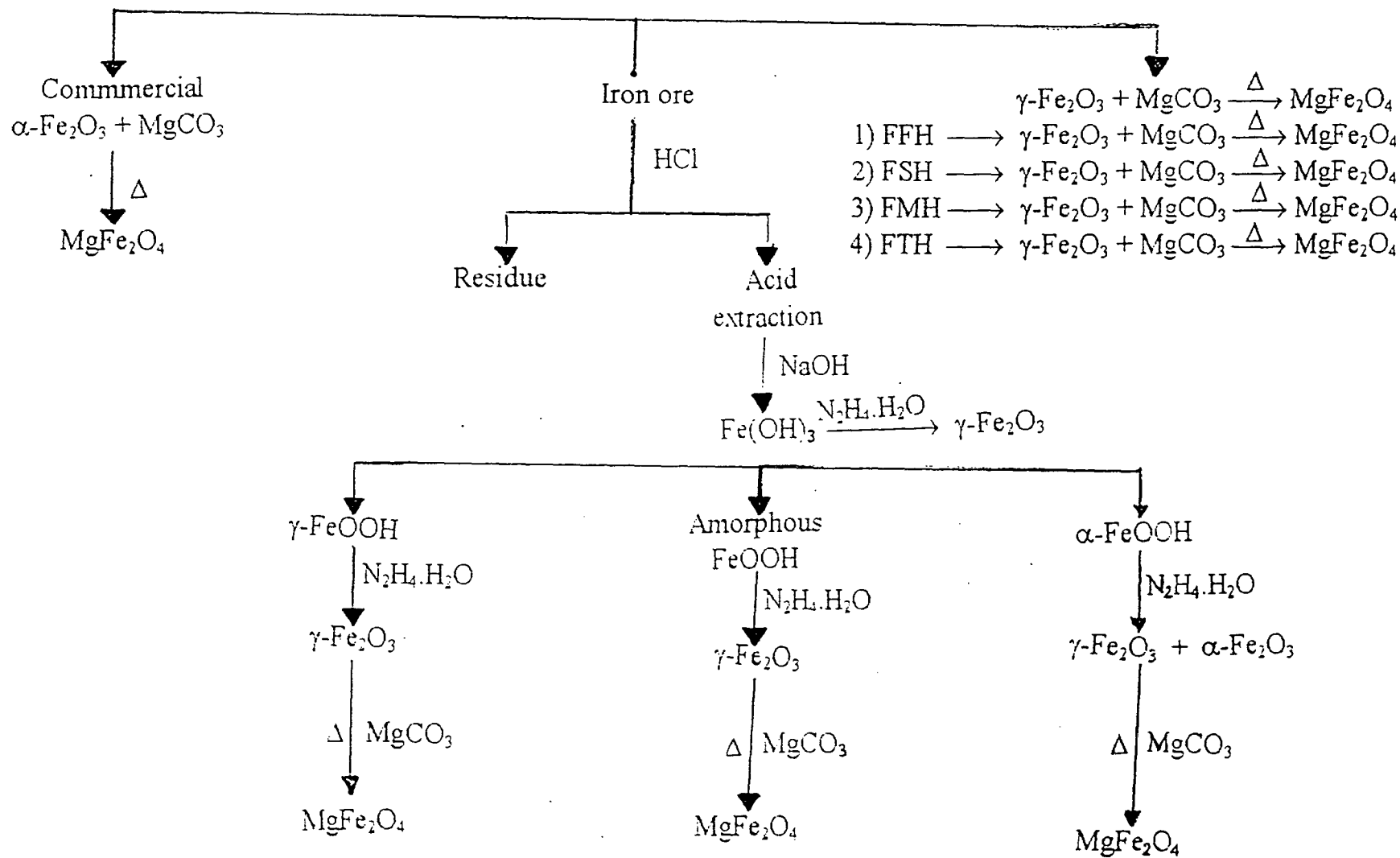


FIG.1.3 A bird's view of the planned work.

Since iron removed from iron ore reject was to be in the form of iron hydroxide, a detailed synthesis of iron hydroxide and iron oxyhydroxides was considered worth taking up in the study.

Thus, work plan was as follows :

- * Prepare iron hydroxide, $\text{Fe}(\text{OH})_3$, from iron ore rejects.
- * Prepare iron oxyhydroxides : $\alpha\text{-FeOOH}$, $\gamma\text{-FeOOH}$ and amorphous FeOOH from $\text{Fe}(\text{OH})_3$.
- * Decompose the iron hydroxide and oxyhydroxides.
- * Prepare MgFe_2O_4 from the thermal products of iron hydroxide and ironoxyhydroxides.
- * Compare the results of the ferrites with the ferrite prepared from commercial $\alpha\text{-Fe}_2\text{O}_3$.

However, excepting $\gamma\text{-FeOOH}$ all the other iron oxyhydroxides and iron hydroxides yield mainly $\alpha\text{-Fe}_2\text{O}_3$, as a thermal product. The $\alpha\text{-Fe}_2\text{O}_3$ was expected to give ferrites of more or less similar characteristics than that normally synthesized from commercial $\alpha\text{-Fe}_2\text{O}_3$. The $\gamma\text{-FeOOH}$, on the other hand, yields $\gamma\text{-Fe}_2\text{O}_3$ and hence the ferrite obtained from such oxide was expected to give superior quality product. It was, therefore, necessary to prepare $\gamma\text{-Fe}_2\text{O}_3$ from these other iron oxyhydroxides, $\alpha\text{-FeOOH}$ and amorphous FeOOH and iron hydroxide from ore.

But, meantime, a novel method to synthesize $\gamma\text{-Fe}_2\text{O}_3$ easily in one step from iron (II) carboxylate, ferrous oxalate dihydrate, $\text{FeC}_2\text{O}_4 \cdot 2\text{H}_2\text{O}$, by hydrazinating and autocatalytic decomposition [278] was developed in our laboratory. Such hydrazine methods were also used by several researchers to obtain easily different oxides

[170-173]. We, therefore planned to prepare hydrazinated iron (II) carboxylates to obtain $\gamma\text{-Fe}_2\text{O}_3$ useful in ferrite synthesis. Therefore, preparation, characterization and decomposition of ferrous fumarato-hydrazinate, ferrous succinato-hydrazinate, ferrous malonato-hydrazinate, ferrous tartrato-hydrazinate, ferrous maleato-hydrazinate and ferrous malato-hydrazinate was taken up in detail in our research programme to ascertain whether $\gamma\text{-Fe}_2\text{O}_3$ can be obtained easily.

And, then, hydrazine being such a novel reagent, we decided to hydrazinate all iron oxyhydroxides and iron hydroxide to see whether $\gamma\text{-Fe}_2\text{O}_3$ can be obtained easily. Based on these above ideas, systematic experimental work was planned and investigations were undertaken. The results of such studies are presented in the thesis and the thesis is organised as follows.

Chapter I --- The subject matter of the research work is introduced in this chapter. After considering the national and international scenario of ferrites, importance of upgradation of iron ore rejects in ferrites manufacture is confirmed. Iron ore sources of India, in general, and, Goa, in particular, are being highlighted here to draw an attention towards a huge iron ore rejects that go as a national waste.

A brief mention about physical and chemical beneficiation processes that have some relevance for using them in obtaining iron oxide of reasonable quality is sketched here.

Important properties of iron oxides and ferrites, their industrial applications, structural and synthetic aspects have been briefly discussed. An emphasis is placed on Fe-O system, especially $\gamma\text{-Fe}_2\text{O}_3$.

Chapter II --- In this chapter methods of preparation of precursors of oxide materials, oxides and their characterization are described, in general.

Chapter III --- This chapter has been divided in two parts: Part I and Part II.

Part I--Synthesis and characterization of iron oxyhydroxides and their hydrazinates have been discussed in this part of the chapter. Thermal decomposition of these iron oxyhydroxides and their hydrazinates are being studied by usual thermal techniques to establish the formation of their products. α -FeOOH and amorphous FeOOH in air $\sim 300^{\circ}\text{C}$ decompose to α -Fe₂O₃ while γ -FeOOH yields mainly γ -Fe₂O₃. In a controlled atmosphere of water vapour in air, α -FeOOH gives $\sim 300^{\circ}\text{C}$ α -Fe₂O₃, but, amorphous FeOOH forms γ -Fe₂O₃. γ -FeOOH, on the other hand, decomposes to γ -Fe₂O₃, with some improved magnetization values, in such a controlled atmosphere of water vapour. These oxyhydroxides are also decomposed in various atmospheres such as dry N₂, dry N₂ + MeOH, dry N₂ + IPA, dry N₂ + Cyclohexane etc.

Hydrazine method gives, in general, γ -Fe₂O₃ of better quality from amorphous FeOOH and γ -FeOOH. However, hydrazinated α -FeOOH gives a mixture of γ -Fe₂O₃ and α -Fe₂O₃.

X-ray and Mossbauer studies done on the products of amorphous FeOOH indicate γ -Fe₂O₃ formation, in all the controlled atmospheres.

Based on these studies, an importance of water in stabilizing γ -Fe₂O₃ is understood and mechanism for the formation of the oxides is proposed.

Part II --- In this part of the chapter, a detailed synthesis and characterization of iron (II) carboxylato-hydrazinates : Ferrous fumarato-hydrazinates, ferrous succi-

nato-hydrazinates, ferrous malonato-hydrazinates, ferrous tartrato-hydrazinates, ferrous maleato-hydrazinate and ferrous malato-hydrazinates, have been described. All the hydrazinate complexes, when ignited with a burning splint, caught fire and a glow is formed which then spreads over whole of the bulk of the sample, thus, autocatalytically decomposing it, in ordinary atmosphere. The products of such decomposition are identified as $\gamma\text{-Fe}_2\text{O}_3$ with X-ray diffraction. Also, a systematic thermal analysis of these complexes have been done by TG/DTA, and isothermal weight loss studies, for getting information about the thermal path of decomposition.

Chapter IV---As the scope of the present investigation was to synthesize $\gamma\text{-Fe}_2\text{O}_3$ easily from iron ores and utilize this for ferrite synthesis, in this chapter, we are presenting our results on the synthesis and characterization of magnesium ferrite, MgFe_2O_4 , prepared from some selected samples of $\gamma\text{-Fe}_2\text{O}_3$, obtained from different precursors, described in chapter III. The result are being compared with ferrites prepared from commercial grade $\alpha\text{-Fe}_2\text{O}_3$. The different techniques used for the characterisation are xrd, ir, ac susceptibility, a c hysteresis loop tracer,

Chapter V ---Although our main objective was to utilize upgraded iron ore rejects for the easy synthesis of $\gamma\text{-Fe}_2\text{O}_3$, it was felt that the importance of water in stabilizing $\gamma\text{-Fe}_2\text{O}_3$ is also required to be studied. The various methods of synthesis that are being undertaken in the present investigation are giving a clear indication of the importance of water in stabilizing $\gamma\text{-Fe}_2\text{O}_3$. If this water introduces protons in $\gamma\text{-Fe}_2\text{O}_3$, then this has to be reflected in the end products as hydrogen iron oxide phase. To substantiate this, we have studied electrical conductivity of $\gamma\text{-Fe}_2\text{O}_3$, synthesized

from various precursors, in different controlled atmosphere and, the result of such studies, on few samples, are compared with the studies done on Std $\gamma\text{-Fe}_2\text{O}_3$ sample. These results are presented in this chapter. There is an indication of H^+ presence in many samples. The chapter is then concluded by summing up all the results obtained in the present investigation.

CHAPTER II

Methods of Preparation and Characterization

Methods of Preparation and Characterization

This chapter deals with a brief review of the methods of preparation of the precursors and the oxide materials followed by the experimental methods involved in the characterization of the precursors, their intermediate products of the decomposition and the final oxide products.

2.1 Methods of Preparation of Precursors and Oxides

A number of novel methods have been developed for the preparation of homogeneous, fine-particle, high-purity oxide materials from precursors. These could be broadly classified under the following three categories.

- (1) Ceramic method
- (2) Precursor method

(3) Wet chemical methods.

All the methods of preparation which fall under these three categories are explained in detail and many examples related to these methods of preparation, with reference to ferrite synthesis are mentioned in section 1.3.5 of chapter 1.

2.1.1 Preparation of precursors

In the present studies precursors for $\gamma\text{-Fe}_2\text{O}_3$ are,

a) Iron hydroxides, iron oxyhydroxides : $\alpha\text{-FeOOH}$, $\gamma\text{-FeOOH}$ and amorphous FeOOH prepared by precipitation method.

b) Iron (II) carboxylato-hydrazinates : Ferrous fumarato-hydrazinate, ferrous succinato-hydrazinate, ferrous malonato-hydrazinate, ferrous tartrato-hydrazinate, ferrous maleato-hydrazinate and ferrous malato-hydrazinate prepared by precipitation method.

2.1.2 Preparation of oxides of iron

Oxides of iron are prepared from the above precursors by thermal decomposition.

2.1.3 Preparation of magnesium ferrite, MgFe_2O_4

The oxides of iron and magnesium carbonate in the required stoichiometry mixed and heat treated as below.

a) Preheating

The mixture of iron oxide and magnesium carbonate after thorough mixing in a nonaqueous medium, acetone, in a agatemortar was preheated in a platinum

crucible to 800°C.

b)

b) Sintering

Sintering is the most important process which controls the extrinsic properties of ferrites. Stuijts [298] has listed the factors which have a dominant effect on sintering. They are particle size, particle size distribution, particle shape, intraparticle porosity, agglomeration, homogeneity in chemical composition, pore size distribution etc. There are two steps of sintering.

(1) Pre-Sintering and (2) Final Sintering.

i Pre-Sintering

The preheated samples are mixed thoroughly by grinding and then cold pressed into pellets. The pellets are then slowly heated to 800°C for 5 hours. During presintering process the raw materials which are partly reacted in preheating process now get better scope to interact closely due to the pelletization.

ii Final sintering

The pre-sintered pellet is ground to a fine powder so as to reduce the particle size and to promote the mixing of any unreacted oxides. The dried powder is then pressed to the required shape using a conventional die applying pressure of several tonnes/inch² from a hydraulic pump. Thus, the pellets and torroids of required size are prepared.

For a good quality ferrites the grain size should be uniform. The pores should be intergranular and discontinuous grains. This can be achieved in the final sintering. The final sintering involves heating the pressed material to high tempera-

ture. The sintering process increases the density and decreases the porosity of the pressed material. A flow chart of preparation of ferrites is shown in Fig 2.1

2.2 Methods of Characterization of Precursors and oxides

2.2.1 Chemical analysis.

a) Analysis of metal content

The percentage of iron in the complexes was determined by the standard potassium dichromate method [299].

b) C, H, N analysis

Carbon and Hydrogen was estimated by the standard techniques.

c) Hydrazine estimation

Hydrazine content of the Iron (II) carboxylato - hydrazinate and hydrazinated oxyhydroxides was analysed titrimetrically using KIO_3 as titrant [299]. About 100mg of the complex was dissolved in a mixture of 15ml of conc. HCl and 10ml of water 5ml of CCl_4 was then added to the solution and it was titrated against 0.025M KIO_3 . From the amount of KIO_3 consumed the hydrazine content was estimated.

2.2.2. Infrared analysis.

Infrared analysis of the precursors and their decomposed products was done on shimadzu FTIR instrument, model 8101A. The pellets used for recording spectra were prepared by mixing 1-2 mg of the sample with a pinch of KBr. The IR spectra in the frequency range of 400 cm^{-1} to 4600 cm^{-1} were recorded at room temperature.

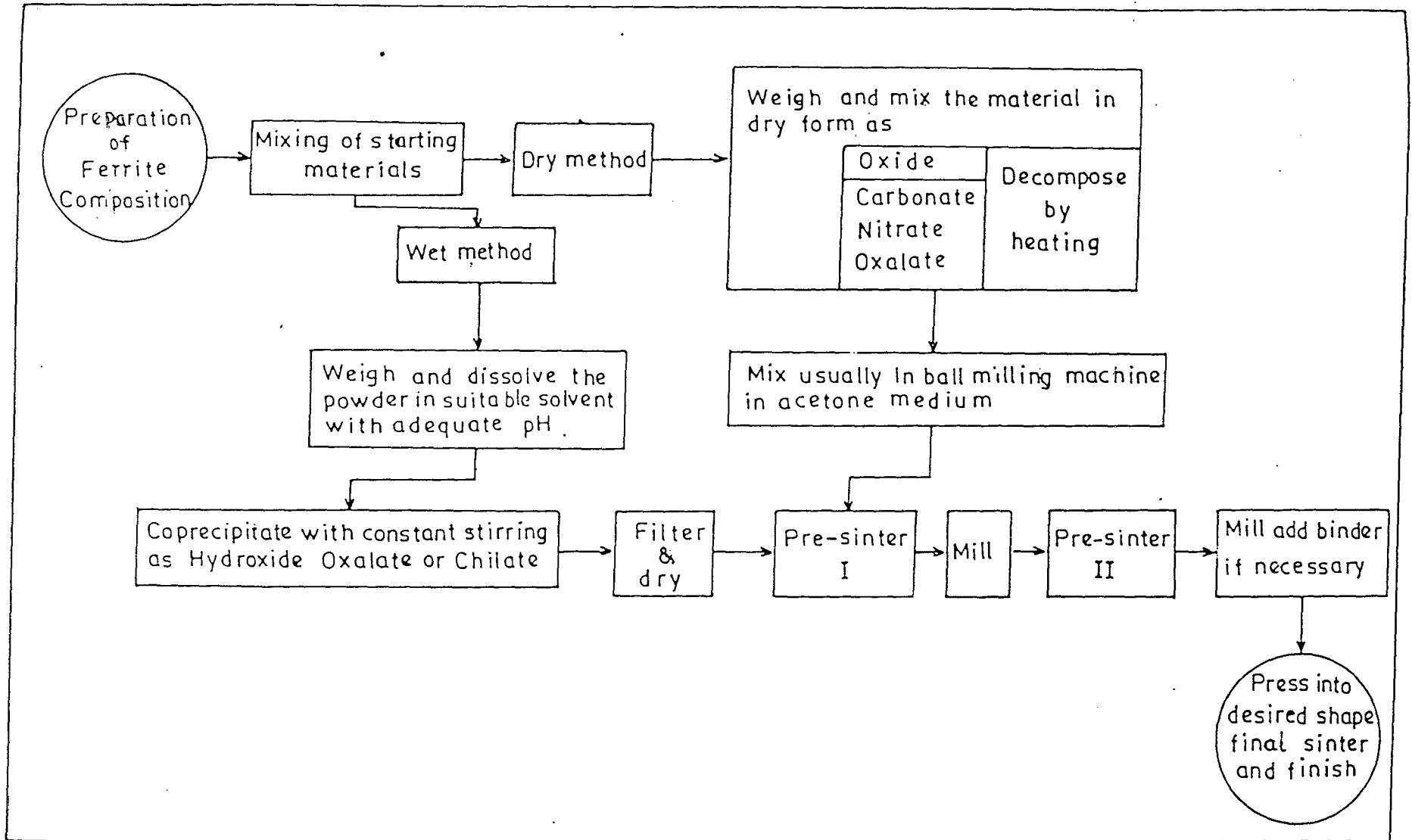


FIG. 2.1 Flow chart of preparation of ferrites

2.2.3. Density Measurements

The Pycnometric densities of the precursors and their decomposed products are measured using CCl_4 as a medium at room temperature by using the expression ,

$$\rho_{\text{sample}} = \frac{\text{weight of the sample}}{(\text{weight of the liquid displaced}) / (\text{Density of the liquid})}$$

2.2.4. Thermal analysis

The changes in the physical as well as chemical properties of a substance can be monitored by the thermal analysis technique. Most commonly used techniques are isothermal weight loss method, thermogravimetry,(TG) differential thermal analysis (DTA), differential scanning calorimetry (DSC) and electro-thermal analysis (ETA).

a) Isothermal weight loss study

The precursors were accurately weighed on mettler balance and placed in platinum crucibles and heated in an oven for 15 minutes, at various temperature ranges. The loss in weight and the percentage of hydrazine at various stages were measured till the precursors show no more weight loss. The total weight loss of the precursor was thus calculated.

b) Thermogravimetric analysis (TGA)

Thermogravimetric analysis deals with the measurement of loss in weight of the sample under investigation as a function of temperature. TG analysis of the precursors was done on STA 1500 instrument in air, as well as, on Rigaku TAS 1000 instrument in N₂ atmosphere. The heating rate employed was 10⁰Cmin⁻¹.

c) Differential thermal analysis.

In differential thermal analysis, the sample and the reference material are simultaneously heated at a controlled heating rate. And, the temperature difference between the two is recorded as a function of furnace temperature. The DTA curves of the precursors were recorded on STA 1500 instrument in air. The heating rate employed was 10⁰C min⁻¹.

d) Electro - thermal analysis (ETA)

The thermal analysis by measurement of electrical resistance [301-302] as a function of temperature, 'Electrothermal analysis' (ETA) was carried out on iron (II) carboxylato-hydrazinates [300,303] and iron oxyhydroxides.

Electrical conductivity (σ) changes accompanying thermal processes of the complexes as a function of temperature (ETA) were measured from home built high temperature conductivity cell [300]. Direct current electrical conductivities were recorded continuously with the rise in temperature. Heating rates were kept at 5-10⁰C per minute. Sample in pellet form, of 15 mm diameter and 2-4 mm thickness, was pressed between platinum disc electrodes, in a special conductivity cell with a

spring action facility to account for any dimensional variations on the pellet during decomposition. A thermo couple close to the pellet, enabled accurate measurement of temperature.

Electrical conductivity measurements were carried out manually during heating when thermal decomposition sets in, in the sample, leading to a final oxide product. And, then during cooling the electrical characteristics measured were of the final oxide. Further measurements during heating and cooling were now exclusively due to the final oxide product of the complexes. The conductivity measuring set up also allows the measurement in different atmospheric control. From these measurements $\log \sigma$ Vs $1/T$ plots were obtained.

2.2.5 Decomposition of the Precursors

a) Thermal decomposition of the precursors in different atmospheres.

To study the thermal decomposition of the precursors in controlled atmospheres like air, dry N_2 , N_2/H_2O /air, dry N_2 + Methanol, dry N_2 + Isopropyl alcohol, dry N_2 + Cyclohexane etc, a temperature controlled tubular furnace was built in our laboratory. For maintaining the required partial pressures of water vapour (H_2O), methanol (MeOH), isopropyl alcohol (IPA) and cyclohexane, a carrier gas, dry nitrogen, was bubbled through these liquids contained in a flask kept at the desired temperature. The carrier gas with the partial pressure of these vapours was made to pass through a preheater before entering the reaction zone containing the sample in a glass tube which can be rotated through $360^\circ C$ for uniform heating of the sample. A pulse of air was also made to enter the reaction zone, whenever re-

quired. The thermal decomposition of all samples was done at a predetermined temperature of 300°C.

b) Autocatalytic decomposition of precursors

The hydrazinated precursors are found to be autocatalytic and thus decomposes autocatalytically. Here the dry samples were spread over a petridish and a burning splint was brought close to the bulk material, when a red glow was observed. This glow then spread all over the bulk thereby completing the decomposition, in an ordinary atmosphere.

2.2.6 X - ray diffraction analysis

X-ray diffraction patterns of the decomposed products of the precursors were obtained by using Philips X-ray diffractometer model PW 1710 with Cu K α radiations and Nickel as a filter, as well as, by using Rigaku D Max II X-ray diffractometer with Cu and Fe targets. The observed d-values of the samples were compared with the reported ones.

2.2.7 Magnetic characterisation.

Magnetic properties are the most fundamental properties of the oxides, especially spinel ferrites. The magnetic properties include saturation magnetization (σ_s), susceptibility (χ), curie temperature (T_c), coercive force (H_c) and permeability (μ) etc.

The saturation magnetization is studied with the help of hysteresis behaviour.

a) Alternating current(AC) hysteresis loop tracer

The saturation magnetization measurements of the samples were carried out using a high field hysteresis loop tracer described by Likhite et al [304] and supplied by M/s Arun electronics, Mumbai, India. The three major parts of this instrument are electromagnet, pick-up coil and balancing and integrating circuits.

The loop tracer consists of an electromagnet working on 50Hz mains frequency. The alternating magnetic field of about 3600 Oersted is produced in an air gap of about 1 cm, in the instrument and a special balancing coil is used to measure the saturation magnetization of the sample in the air gap. Depending upon the magnetic induction in the specimen, pick-up coil produces a field proportional to the magnetic induction of the specimen. A supporting coil produces a signal which is equivalent to the strength of the magnetic field. When the respective signals are supplied to the vertical and horizontal plates of an oscilloscope, it displays a hysteresis loop on the screen.

A digital AC voltmeter which was connected to the output, was made to display peak or RMS value of the signal proportional to the saturation magnetization in millivolts. The calibration of the vertical scale corresponding to the magnetization value was done using pure nickel as a standard substance having magnetization of 53.34 emu/g.

b) A.C.Susceptibility

The domain structure and the curie temperature of the oxide can be obtained by plotting normalized susceptibility (χ_T / χ_{RT}) at various temperature against temperatures, using an a.c.susceptibility method described by Likhite et al [305] and supplied by M/s Arun electronics, Mumbai, India. A.C.susceptibility study can describe the magnetic behaviour of the material that is ferrimagnetic to paramagnetic transition and single domain to superparamagnetic transition.

A.C.Susceptibility measurements of the powdered samples were made in the temperature range from 27 °C to 527 °C using the susceptibility apparatus. The apparatus consists of Helmholtz coil, two pick-up coils, furnace, sample holder and a temperature measuring device.

The Helmholtz coil produces uniform magnetic field. A furnace was fabricated by winding the platinum wire on silica tube to heat the sample. To avoid overheating of coils, a glass jacket with water circulation was used. The furnace was inserted in a glass jacket and was placed at the centre of the pick-up coil. The sample holder was made up of a quartz tube fused at one end. The height of the sample holder was maintained at the centre of the coils. The current to the Helmholtz coil was supplied by an oscillator and a high quality power amplifier.

When the sample was placed in the sample holder, the signal is induced in the double coil which was amplified, rectified and read out on a digital voltmeter. The digital voltmeter was calibrated in terms of magnetic moment. The temperature of the furnace was maintained by a power supply and was measured by using

Platinum- Rhodium thermocouple. The sample was gradually heated and the magnetic moments were recorded at various temperatures. The heating was continued till the signal reduced to zero. From the magnetic moment, normalized susceptibility was calculated and plotted against the temperature.

c) Initial Permeability

Initial permeability, μ_i , is defined as,

$$\mu_i = \frac{B}{H} \text{ or } \mu_i = \frac{dB}{dH}, \quad H \longrightarrow O, B \longrightarrow O$$

But in case of soft magnetic materials

$B = H + 4 \pi M$, where M is intensity of magnetisation and H is the applied field. In most of the magnetic materials, μ_i increases with the temperature upto the curie temperature.

Initial permeability can be measured by (i) The Maxwell bridge, (ii) Resonance circuits and (iii) the standing wave method [306]. In the present investigations we have measured the initial permeability as a function of temperature at 1000 Hz, over a temperature range from 27 to 527°C using MIC 4060 -D LCR meter. The temperature of the furnace was regulated within $\pm 5^\circ\text{C}$ error in the range of measuring temperature.

The initial permeability was calculated from the low field inductance measurements with a torroidal core of 50 turns using the formula,

$$L = 0.0046 \mu_i N^2 h \log d_1/d_2$$

where, L is the inductance in H,

d_1 is the outside diameter of a torroid

d_1 is the outside diameter of a torroid

d_2 is the inside diameter of a torroid

μ_i is the initial permeability of the core

h is the height of the core in inches.

2.2.8 Mössbauer spectroscopy

In Mössbauer spectroscopy the chemical environment of the nucleus has a pronounced effect on the resonant absorption of gamma rays. Extremely small changes are produced in the energy of the gamma rays emitted by a nucleus as a result of the hyperfine interactions between the nucleus and its orbital electrons. These small interactions can be detected in a Mössbauer spectrum. The Mössbauer parameters of greatest interest to a chemist are (a) the isomer shift δ , (b) the quadrupole splitting ΔE_q , and (c) the magnetic hyperfine splitting [307,308].

In the present study the Mössbauer spectra were taken at 27 and -183°C using a constant acceleration spectrometer and a $^{57}\text{Co/Rh}$ source. The isomer shifts are quoted with reference to $\alpha\text{-Fe}$.

2.2.9 Micro - structure

Most of the magnetic properties and characteristics of poly crystalline magnetic materials are microstructure sensitive [309]. For polycrystalline ferrites the microstructure means the porosity, grain structure and phases detectable by micrographic analysis.

SEM - micrographs of a well polished pellet surface of the samples were taken for finding out the average grain size. The average grain size, D_m , was calculated as follows, from SEM photographs [310].

- (1) Drawing a diagonal on the photograph.
- (2) Measuring the maximum unidirectional particle size in the vertical direction against diagonal.
- (3) Averaging the maximum unidirectional particle size.

2.2.10 Electrical characteristics of iron oxides and ferrites.

a) Conductivity of $\gamma\text{-Fe}_2\text{O}_3$ in different atmospheres.

Direct current electrical conductivity, σ , as a function of temperature in air, N_2 and again in air after equilibrating samples with N_2 gas containing water vapours, was measured for $\gamma\text{-Fe}_2\text{O}_3$ synthesized from different precursors, using a home built conductivity cell system described in section 2.2.4.d.

b) Resistivity of MgFe_2O_4 in air

Direct current electrical resistivity, ρ , as a function of temperature was measured for MgFe_2O_4 samples. From $\log \rho$ V/s $1/T$ plots the activation energies for conduction were calculated.

2.2.11 Dielectric constant.

The dielectric constant, ϵ' , measurements were made using the two-probe method. The pellets of 1.5 cm diameter and 2-3 mm thickness were used for the dielectric measurements which were carried out from 27 to 327°C at 1KHz, on

MIC 4060-D LCR meter. The capacitance 'c' was measured as a function of temperature and was used in the calculation of dielectric constant, ϵ' using the relation

$$\epsilon' = cd/\epsilon_0 A$$

where 'd' is the thickness of the pellet, A is the cross-sectional area of the flat surface of the pellet and ϵ_0 is the free-space permittivity.

CHAPTER III

STUDY OF γ -Fe₂O₃

Part I

Studies on the synthesis, characterisation and decomposition of iron oxyhydroxides

Part II

Studies on the synthesis of γ -Fe₂O₃ from iron (II) carboxylato-hydrazinate

Gamma ferric oxide, $\gamma\text{-Fe}_2\text{O}_3$ (maghemite), a ferrimagnetic material, finds use as, a magnetic tape material in electronic industry, as well as, a catalyst in chemical industry. It is also reported to be used as a raw material in ferrite industry for the preparation of ferrites, in place of usual $\alpha\text{-Fe}_2\text{O}_3$ and found to increase the rate of spinelization. A systematic study of the synthesis of $\gamma\text{-Fe}_2\text{O}_3$ from precursor method can give additional information in optimising different properties of this industrially important material. So it was felt necessary to understand the formation of $\gamma\text{-Fe}_2\text{O}_3$ from the precursors.

As we are envisaging the utilisation of iron ore reject to synthesise active iron oxide useful in ferrites preparation, such information on the various

methods of preparation of $\gamma\text{-Fe}_2\text{O}_3$ may help us in adopting an easier method to prepare the oxide from chemically beneficiated iron ores (acid extracts).

3.1 Literature survey on $\gamma\text{-Fe}_2\text{O}_3$ preparation

A good recording material must possess a coercivity value in the range of 250 Oe to 1200 Oe to prevent accidental erasure but not so high that the magnetisation cannot be reversed. Particles having acicular shape with a length to width ratio of 3:1 to 10:1 and an average length of 0.6 μm act as a good recording material, since the shape anisotropy confers a coercivity of 250 - 400 Oe. $\gamma\text{-Fe}_2\text{O}_3$ is the most commonly used magnetic recording material. The acicular shaped particles with a length to width ratio of approximately equal to 6:1, an average length of 0.6 μm , saturation magnetization of 71 to 75 emu/g and coercivity of about 250 - 300 Oe are generally used.

The particle size distribution and shape, thus, play an important role in such applications. The literature survey reveals that a lot of stress is being given on these, during the synthesis of $\gamma\text{-Fe}_2\text{O}_3$. In our present investigation, our main aim was to prepare active iron oxide (mainly $\gamma\text{-Fe}_2\text{O}_3$) to be used as a raw material in the synthesis of ferrite (MgFe_2O_4) and, hence, an elaborate study of synthesis of $\gamma\text{-Fe}_2\text{O}_3$ was carried out.

$\alpha\text{-FeOOH}$ is commercially utilized in the synthesis of $\gamma\text{-Fe}_2\text{O}_3$, which is a multistage process (eqn. 7). The $\alpha\text{-FeOOH}$ is first dehydrated to $\alpha\text{-Fe}_2\text{O}_3$, then reduced to Fe_3O_4 and finally oxidised to $\gamma\text{-Fe}_2\text{O}_3$. Although this process is cumbersome, it is best suitable to obtain a needle shape $\gamma\text{-Fe}_2\text{O}_3$ from acicular $\alpha\text{-FeOOH}$.

This reduction oxidation method was first developed by Camras [311]. He further recommended another reduction of $\gamma\text{-Fe}_2\text{O}_3$ to Fe_3O_4 and reoxidation to $\gamma\text{-Fe}_2\text{O}_3$ to have improved magnetic properties. Dehydration and reduction at high temperature, however, may give a sintering effect.

Boronius et al [312] pointed out that the unwanted sintering of the particles that takes place during reduction and oxidation can be prevented by coating the particles of $\alpha\text{-FeOOH}$ by inorganic chemicals like, sodium silicate. Woditsch et al [313] used silicon oil instead of sodium silicate and claimed higher coercivity due to this treatment.

The thermal transformation of goethite in alkali-halide disks has been widely investigated [314-317]. These works have shown that in diluted alkali iodide disks (0.1 - 0.5%), spinel structures such as maghemite or magnetite are obtained by adequate treatment. But, when the initial concentration of $\alpha\text{-FeOOH}$ in the salt mixture is higher (~33%), the final products are protohematite and hematite.

Osmond [318] in 1951 studied the reduction - oxidation of $\alpha\text{-Fe}_2\text{O}_3$ to get $\gamma\text{-Fe}_2\text{O}_3$. Thereafter, this method was used by other researchers [247,267,319-335] to prepare $\gamma\text{-Fe}_2\text{O}_3$.

The $\gamma\text{-Fe}_2\text{O}_3$ particles formed by reduction - oxidation of $\alpha\text{-Fe}_2\text{O}_3$ usually show some cation ordering. [266,326], while those prepared by the decomposition of $\gamma\text{-FeOOH}$ have been reported to produce disordered structure [336-337].

The transformation of $\gamma\text{-FeOOH}$ to $\gamma\text{-Fe}_2\text{O}_3$ has been studied by many workers [335-356]. Many investigators [337,339-340] reported that those $\gamma\text{-Fe}_2\text{O}_3$ which are prepared by low-temperature calcination of $\gamma\text{-FeOOH}$ conserve the con-

figuration of cation atoms in the mother γ -FeOOH. This means that the dehydration reaction proceeds by shifting and re-stacking the structure already existing in the mother crystal.

The structure of oxides / oxyhydroxides of metals are built up of close-packed oxy / hydroxyl layers. When one form of oxide or oxyhydroxide transforms into another, the change may be effected simply by removing or adding close-packed oxy / hydroxyl layers from or to the original structures. Thus, one might expect to find an oriented relationship between the original and transformed products. Such a relationship which is not limited to any particular type of crystal, was observed by Galdsztanb [357-358] in the transformation of α -FeOOH to α -Fe₂O₃.

This sort of inter - relationship can be explained in terms of topotaxy, a term proposed by Gorter to denote the transformation from one crystalline phase to another, where there are definite oriented relationships between the axis of the original and transformed crystals.

The transformation of γ -FeOOH \rightarrow γ -Fe₂O₃ \rightarrow α -Fe₂O₃ was studied by Bernal et al [337] using single crystals of γ -FeOOH. The (100) of γ -FeOOH is parallel to one of the cubic axes (001) of γ -Fe₂O₃. The mechanism of the transformation of γ -FeOOH to γ -Fe₂O₃ involves the removal of half of the hydroxyl group together with the hydrogen in the adjoining hydroxyl sheet, water molecules. There is also a shift of an half oxygen ion in the (100) direction. The resulting strain due to the shift explains the disorder in the γ -Fe₂O₃ crystal. The transformation of γ -Fe₂O₃ to α -Fe₂O₃ does not involve any loss or gain of material but only a

restacking of close-packed oxygen atoms (cubic to hexagonal) on the (111) faces of $\gamma\text{-Fe}_2\text{O}_3$.

Although a simple elimination of water on dehydration of $\gamma\text{-FeOOH}$ topotactically transforms it easily into $\gamma\text{-Fe}_2\text{O}_3$, commercially $\gamma\text{-Fe}_2\text{O}_3$ is prepared from $\alpha\text{-FeOOH}$ by reduction - oxidation method (eqn 7). This is mainly because $\gamma\text{-Fe}_2\text{O}_3$ synthesized from $\gamma\text{-FeOOH}$ shows lower saturation magnetization values than that obtained from controlled oxidation of Fe_3O_4 . A plausible reason given for such superior properties for the $\gamma\text{-Fe}_2\text{O}_3$, obtained from Fe_3O_4 oxidation, is based on the consideration of easy diffusion of Fe^{3+} ion through the spinel frame work that already present in Fe_3O_4 to give a well ordered vacancies, on the so called 'Lithium sites' (Actually $\text{Fe}_{64}\text{O}_{96}, \{\text{Fe}_{24}^{\text{Tetrahedral}} [\text{Fe}_{36}^{\text{Octahedral}} (\text{Fe}_4^{\text{Li-sites}} \square_8^{\text{Li-sites}})]\text{O}_{96}\}$) of $\gamma\text{-Fe}_2\text{O}_3$ [342, 352].

On the other hand, defect spinel $\gamma\text{-Fe}_2\text{O}_3$, of frame work of $[\text{FeO}_6]$ octahedra with edge and corner sharing that formed from the corrugated layers of $[\text{FeO}_6]$ octahedra of $\gamma\text{-FeOOH}$, has no sufficient time and occasion for Fe^{3+} ions to diffuse through the developing framework of $\gamma\text{-Fe}_2\text{O}_3$, to occupy the lithium sites for giving well ordered $\gamma\text{-Fe}_2\text{O}_3$.

The thermal decomposition of $\gamma\text{-FeOOH}$ yields $\gamma\text{-Fe}_2\text{O}_3$. Alternative procedures of dehydrating $\gamma\text{-FeOOH}$ have been described, which include intercalation reactions [341] and mechanochemical processes. With regards to the mechanochemical dehydration, it is well known that dry grinding of lepidocrocite $\gamma\text{-FeOOH}$, leads to $\alpha\text{-Fe}_2\text{O}_3$ [359-361]. Such behaviour is also found in other phases of iron oxyhydroxide such as, goethite, $\alpha\text{-FeOOH}$, [362] or akaganeite, $\beta\text{-FeOOH}$, [363].

But the mechanochemical treatment of γ -FeOOH in wet medium [343,364-365] was shown to yield γ -Fe₂O₃.

It has been suggested [365] that in dry milling water released, due to the dehydration, reaches to such a high partial pressure of water vapour in the grinding vessel which is sufficient to accelerate the transformation of the formed γ -Fe₂O₃ into α -Fe₂O₃. On the otherhand, in wet grinding the non - aqueous medium helps in optimizing the water vapour partial pressure over the dehydrating particles of γ -FeOOH. This partial pressure is adequate in stabilizing the γ -Fe₂O₃.

Effect of the partial pressure of water vapour on the thermal decomposition of γ -FeOOH has been studied [350] and established that an increase in water vapour accelerates the transformation of γ -Fe₂O₃ to α -Fe₂O₃. The explanation given for this is that, the particles of the γ -Fe₂O₃ that formed in fine size get coalesced with the increasing partial pressure of water vapour, thereby, increasing the particle size. The larger particles influence the phase transformation.

A mild transformation of γ -FeOOH to γ -Fe₂O₃ is also achieved using organic reagents [341]. When γ -FeOOH is treated with organic bases (pyridine, n-hexylamine) at temperature of 120 - 140°C, it is quantitatively converted into the topotactically related γ -Fe₂O₃. Here, the first step is an intercalation of the organic base in the host lattice of γ -FeOOH. The second and relatively faster step is a sequential elimination of water from the interlayer where the base plays the role of a catalyst.

Slightly impure samples of γ -FeOOH that contain a small (5%) amount of α -FeOOH are transformed quantitatively into α -Fe₂O₃ under the above conditions

but, pure α -FeOOH is unaffected. The fact that α -FeOOH is unaffected by pyridine or n-hexylamine under these conditions shows that this base assisted transformation is strongly structure dependent. It is observed [343] that the mechanochemically prepared maghemite increases in its thermal stability due to the higher crystallinity of ground micro crystals, as revealed by the values of crystallite size and micro strains. It is also known that maghemite stores significant amounts of energy when submitted to dry milling [366-368] and, that, this fact causes alterations in its thermal behaviour, related with heat released processes and changes in the temperature of the thermally promoted phase transition of maghemite \rightarrow hematite.

Magnetic and electric fields are also tried to assist dehydration and dehydroxylation of inorganic hydroxy compounds [369]. Clarke and Hall [335] have studied the preparation and interconversion of iron (III) oxide, hydroxides and oxyhydroxides and their characterization, by X-ray diffraction and small angle neutron scattering (SANS). Thus, the studies on the decomposition of iron oxyhydroxides seems to be quite thoroughly investigated.

A reverse transformation of thermodynamically more stable α -Fe₂O₃ state to metastable γ -Fe₂O₃ state by grinding process is also reported [370]. Matsumoto et al [371] synthesized γ -Fe₂O₃ from amorphous Fe(OH)₃. Dovey et al [372] used iron oxalate and formate to prepare maghemite. First these precursors were decomposed in a mixture of steam, nitrogen and carbon - dioxide to obtain Fe₃O₄ which was then dampened and heated in an oven between 100-200^oC to convert it to γ -Fe₂O₃. Van Oosterhout et.al. [235] were able to prepare γ -Fe₂O₃ by decom-

posing ferrous oxalate dihydrate in an atmosphere of steam and nitrogen, followed by oxidation in a mixture of air and water. Anantharaman et al [57] too prepared $\gamma\text{-Fe}_2\text{O}_3$ from ferrous oxalate dihydrate. They first decomposed the precursor in moist nitrogen at 502°C to yield Fe_3O_4 which was then oxidised by dry air to acicular $\gamma\text{-Fe}_2\text{O}_3$ at 302°C . The resulting $\gamma\text{-Fe}_2\text{O}_3$ had saturation magnetization ~ 70 emu/g, coercive force $\sim 300^\circ\text{C}$ and squareness ratio $\sim 0.6-0.65$.

According to Venkatesh Rao et al [270], the ferrous oxalate dihydrate containing traces of moisture decomposes in air under the ambient of its own gaseous products at $\sim 300^\circ\text{C}$ to $\gamma\text{-Fe}_2\text{O}_3$. However, the decomposition is highly exothermic, so that, the local oxidative heating leads to unavoidable contamination with $\alpha\text{-Fe}_2\text{O}_3$. The final product had a saturation magnetization of 70emu/g, coercive force $\sim 250^\circ\text{C}$ and ratio of remanence to saturation ~ 0.6 . Tsyrnorchki et al [373-374] prepared $\gamma\text{-Fe}_2\text{O}_3$ by heating $\text{FeC}_2\text{O}_4 \cdot 2\text{H}_2\text{O}$ at 350°C for 24 h in an atmosphere containing 4 to 5% oxygen.

Rane et al [264] too prepared $\gamma\text{-Fe}_2\text{O}_3$ from ferrous oxalate dihydrate by adopting a procedure almost similar to the procedures mentioned above. The decomposition was done in a controlled atmosphere of water vapours with nitrogen as a carrier gas and air for oxidation. They found that water helps in suppressing the release of lattice water which later forms oxygen and hydrogen. The hydrogen enters the lattice to form $\gamma\text{-Fe}_2\text{O}_3$ having hydrogen ion H^+ , in the octahedral vacancies.

According to Aharoni et al [257], $\gamma\text{-Fe}_2\text{O}_3$ consists of solid solution of $(\text{Fe}^{3+})_8 [\text{Fe}^{3+}_{1\ 1/3} \square_{2\ 2/3} \text{Fe}^{3+}_{12}] \text{O}_{32}$ and $(\text{Fe}^{3+}) [\text{H}^{1+}_4 \text{Fe}^{3+}_{12}] \text{O}_{32}$. They showed that

when $\gamma\text{-Fe}_2\text{O}_3$ was heated, hydrogen was evolved, in amounts of about 70% of that required to give the formula $\text{Fe}_8[\text{H}_4\text{Fe}_{12}]\text{O}_{32}$. Nikumbh, Rane and Mukhedkar [280] in their studies of direct current electrical conductivity of $\gamma\text{-Fe}_2\text{O}_3$ observed a kink in $\log \sigma$ versus $1/T$ around 177°C , indicating the removal of hydrogen from the octahedral site.

A simple single step hydrazine method of preparation of $\gamma\text{-Fe}_2\text{O}_3$ has been studied by many researchers. Moye Rane and Kamat Dalal [278] autocatalytically decomposed ferrous oxalato-hydrazinates, $\text{FeC}_2\text{O}_4 \cdot \text{N}_2\text{H}_4$ and $\text{FeC}_2\text{O}_4 \cdot 2\text{N}_2\text{H}_4$, prepared both by solution and equilibration method, to synthesize $\gamma\text{-Fe}_2\text{O}_3$. Patil et al [375-376] prepared magnetic ferric oxide by thermally decomposing iron hydrazino carboxylate hydrazinate $[\text{Fe}(\text{N}_2\text{H}_3\text{COO})_2(\text{N}_2\text{H}_4)_2]$, as well as, hydrazinium iron hydrazino carboxylate $[\text{N}_2\text{H}_5\text{Fe}(\text{N}_2\text{H}_3\text{COO})_3 \cdot \text{H}_2\text{O}]$. These complexes exhibit autocatalytic decomposition, once ignited.

According to Patil et al [377-378], the decomposition / combustion of $\text{FeC}_2\text{O}_4(\text{N}_2\text{H}_4)_2$ in air at $\sim 200^\circ\text{C}$ yields a mixture of γ - and $\alpha\text{-Fe}_2\text{O}_3$, while $\text{Fe}(\text{N}_2\text{H}_3\text{COO})_2(\text{N}_2\text{H}_4)_2$ gives exclusively $\gamma\text{-Fe}_2\text{O}_3$. The crystallite sizes of $\gamma\text{-Fe}_2\text{O}_3$ were in the range of 170-250 Å and the surface area was $40\text{m}^2\text{g}^{-1}$. Temperature profile measurement of $\text{FeC}_2\text{O}_4(\text{N}_2\text{H}_4)_2$ [379] showed that the maximum temperature attained during the combustion is 600°C , although ignition occurs at $\sim 200^\circ\text{C}$. On the other hand, in the case of $\text{Fe}(\text{N}_2\text{H}_3\text{COO})_2(\text{N}_2\text{H}_4)_2$, the combustion releases heat amounting to the temperature $\sim 425^\circ\text{C}$. This difference in the exothermicity of the combustion of $\text{FeC}_2\text{O}_4(\text{N}_2\text{H}_4)_2$ and $\text{Fe}(\text{N}_2\text{H}_3\text{COO})_2(\text{N}_2\text{H}_4)_2$ is probably re-

sponsible for the formation of a mixture of γ - and α - Fe_2O_3 in the former and, exclusively γ - Fe_2O_3 in the latter.

Patil [185] reported the preparation of γ - Fe_2O_3 by the combustion of redox compound $[\text{N}_2\text{H}_3\text{Fe}(\text{N}_2\text{H}_3\text{COO})_3 \cdot \text{H}_2\text{O}]$ and redox mixtures such as $\text{Fe}(\text{NO}_3)_3$ and $\text{C}_3\text{H}_8\text{N}_4\text{O}_2$ (malonic dihydrazide, MDH). He compared the properties of γ - Fe_2O_3 prepared by both combustion processes and found that, the surface area of the oxide powder prepared by the combustion of redox compound is higher than that obtained by the combustion of redox mixture. This is because redox compounds undergo flameless (smouldering) combustion, whereas redox mixtures burn with a flame.

A mixture of α - and γ - Fe_2O_3 (mainly) was obtained by autocombustion of iron sulphite hydrazine hydrate [380].

Excepting iron, the hydrazine complexes of the other metals, such as, manganese, nickel, cobalt, zinc, have also been studied by many researchers. The different metal hydrazine complexes are metal acetate hydrazinate [381], metal formate hydrazinate [382-383], metal propionate hydrazinate [384], bis hydrazine metal maleates and fumarates [385] and bis hydrazine metal malonates and succinates [386]. Recently, the preparation, characteristics and thermal analysis of iron acetate hydrazinate have been reported [387].

Some researchers [371,388] used hydrothermal processes for the preparation of γ - Fe_2O_3 . Many have used spray pyrolysis / roasting for the preparation of γ - Fe_2O_3 [247,333,389-391]. Spherical γ - Fe_2O_3 particles of nanometer size can be directly obtained by spray pyrolysis of iron salt solution [391]. These particles have

different states of aggregation, depending on the precursor salt used and were found to be superparamagnetic. The iron salt solutions used, by Morales et al [333] for the preparation of $\gamma\text{-Fe}_2\text{O}_3$ by spray pyrolysis, were iron (III) nitrate which gave compact spherical aggregates of small crystallites ($\sim 6\text{nm}$), and iron (II) ammonium citrate which gave hollow spheres of crystallites size $\sim 4\text{nm}$.

Cabanas [392] reported the synthesis of spherical gamma iron-oxide particles by an aerosol technique.

A composite of polyaniline (PANI) containing iron oxides [393] with nanometer size was synthesized by a chemical method. Kroll et al [394] have reported *in-situ* preparation of nano crystalline gamma Fe_2O_3 in iron (II) cross-linked alginate gels. A microemulsion-mediated chemical reaction [395] was used to synthesize acicular particles of gamma Fe_2O_3 , with an equivalent spherical diameter (ESD) of 7-8 nm. It was observed that each microemulsion droplet gives birth to a single particle of $\gamma\text{-Fe}_2\text{O}_3$. Thus, it may be possible to control size and shape of $\gamma\text{-Fe}_2\text{O}_3$.

Many researchers [396-397] have studied the direct preparation of high coercivity $\gamma\text{-Fe}_2\text{O}_3$ thin films for magnetic recording, by chemical vapour pyrolysis technique. Deng et al [398] prepared $\gamma\text{-Fe}_2\text{O}_3$ by a low temperature flux method. Abe et al [399] prepared nanoparticles of Fe_2O_3 through encapsulation into the pores of MCM-41(molecular sieve). The bandgap of the resulting Fe_2O_3 particles is widened from 2.1 to 4.1 eV, owing to the quantum size effect. Nanoparticles of $\gamma\text{-Fe}_2\text{O}_3$ were prepared in silica matrix by sol-gel process [400]. Da Costa et al

[401] prepared $\gamma\text{-Fe}_2\text{O}_3$ by heating the product of a sol-gel reaction between iron (III) nitrate and ethylene glycol.

Ziolo et al [402] have reported the matrix-mediated synthesis of nanocrystalline $\gamma\text{-Fe}_2\text{O}_3$. A new magnetic material, with appreciable optical transmission in the visible region at room temperature, has been isolated as a $\gamma\text{-Fe}_2\text{O}_3$ /Polymer nanocomposite.

Batis - Landoulsi and Vergnon [403] prepared $\gamma\text{-Fe}_2\text{O}_3$ from vapours of ferric chloride by reaction in an oxygen-hydrogen flame (2727°C).

This chapter is divided into two parts : part I and part II. In part I of this chapter we are presenting our results of the studies on the synthesis, characterization and decomposition of iron oxyhydroxides: $\gamma\text{-FeOOH}$, $\alpha\text{-FeOOH}$ amorphous FeOOH and their hydrazinated complexes. The raw material (iron salts) used for the preparation of iron oxyhydroxide is obtained by chemical beneficiation of iron ore rejects. Part II deals with the study of the synthesis and characterization of novel iron (II) carboxylates: ferrous fumarato - hydrazinate, ferrous succinato - hydrazinate, ferrous malonato - hydrazinate, ferrous tartrato - hydrazinate, ferrous maleato - hydrazinate and ferrous malato - hydrazinate and their thermal decomposition.

Studies on the synthesis, characterisation and decomposition of iron oxyhydroxides

3.2 Experimental :Preparation characterisation and thermal de- composition

3.2.1 Chemical beneficiation of iron ore reject.

a) Direct precipitation of iron(III)hydroxides

In our present study we have chemically beneficiated an iron ore reject dump sample of Goan origin containing, 35.5 % Fe, 3.30 % Al_2O_3 , 40.28 % SiO_2

and, traces of oxides of manganese, calcium and magnesium. The moisture percentage in it was 9.86.

The sample was first crushed and brought to a size of -100 mesh. Each time 20g of this sample was taken in a conical flask and dissolved by adding 50 % HCl solution. First, 50 ml of 50 % HCl solution and 2-3 drops of Conc. HNO_3 was added to 20g of the sample and the mixture was boiled on a sand bath. Then, again 5ml of the HCl solution was added to the mixture and continued boiling. This was repeated till all the particles of the iron oxide are dissolved and only white coloured SiO_2 is seen at the bottom of the flask. This SiO_2 is then removed by filtration.

The filtrate which is called as acid extract contains chlorides of Fe, Al and trace elements. To this filtrate 20 % NaOH was added, drop by drop, with constant stirring. Iron (III) ions only start precipitating in the acidic pH as Iron (III) hydroxides. Since the solubility product (K_s) of $\text{Fe}(\text{OH})_3$ is less than that of $\text{Al}(\text{OH})_3$ and hydroxides of other trace elements [404], the $\text{Fe}(\text{OH})_3$ can be selectively precipitated out. The precipitated iron hydroxide was filtered and washed with hot, water repeatedly till it is free from alkali and chloride ions.

b) Synthesis of ferric nitrate and ferrous chloride from iron ore rejects

The iron hydroxide obtained from iron ore (section 3.2.1.a) was then converted into ferric nitrate and ferrous chloride.

Ferric nitrate : The iron hydroxide was first neutralised by adding nitric acid solution and then concentrated on the water bath. The ferric nitrate slowly crystallises,

as the solution cools to room temperature. These crystals were then removed and washed with alcohol, dried and stored in the desiccator.

Ferrous chloride : The iron hydroxide was converted to ferric chloride by adding hydrochloric acid solution. This solution was then reduced to ferrous state by adding pure iron metal powder and requisite quantity of conc. HCl and then boiling the mixture in an atmosphere of CO₂. These salts were then used in the synthesis of iron oxyhydroxides.

3.2.2 Synthesis of Iron oxyhydroxides from ferric nitrate and ferrous chloride prepared from ferric hydroxide of iron ore

Iron oxyhydroxides: γ -FeOOH, α -FeOOH and amorphous FeOOH are synthesised, as follows, by using ferric nitrate and ferrous chloride, prepared from ferric hydroxide of iron ore, as in section 3.2.1.b.

a) Synthesis of γ -FeOOH

γ -FeOOH was prepared as per the method of Fricke and Zerrweck [405]. A solution of freshly prepared ferrous chloride (0.15 M, 750ml) was added to the aqueous solution of (CH₂)₆ N₄ (42 g in 150ml), drop by drop. A blue green precipitate of Fe(OH)₂ is formed. To this then an aqueous NaNO₂ solution (10.5g in 150ml) was added slowly with stirring and the mixture was heated to about 60⁰C and allowed to stand 3 hours. The reddish orange precipitate formed was filtered and washed with warm water till free of chloride ions and dried.

b) Synthesis of α -FeOOH

α -FeOOH was synthesized following the method described by the Fricke and Ackermann [406]. A cold solution of 81g of ferric nitrate in 200ml of water was slowly poured with vigorous stirring into an ammonia solution. The hydroxide precipitated was washed repeatedly by decantation. The slurry was then stirred with sufficient concentrated KOH to give a mixture 2N approximately and allowed to stand for 3-4 h. Finally, steam was bubbled through the solution for 2 h. The precipitate was then washed with calculated amount of NH_4Cl which removed the excess KOH. The precipitate was filtered, washed with water and dried.

c) Synthesis of amorphous FeOOH

The method similar to Kung et al [407] is used here. 20.2g ferric nitrate in 500 ml of water was added to 0.1 M NH_3 solution. The pH of the solution was maintained at 10.5 by adding conc. NH_3 to obtain the precipitate which was then filtered and washed until the filtrate showed the pH of distilled water. The precipitate was dried in over at 60 °C.

3.2.3. Hydrazination of ferric hydroxide and iron oxyhydroxides

a) Equilibration method.

A requisite amount of the iron oxyhydroxide was taken in a petridish and kept in a desiccator containing hydrazine hydrate (99 - 100 %) for few days.

A specially designed reactor, however, enabled us to monitor the hydrazine uptake by titrimetric method using KIO_3 as titrant.

The set up for the hydrazine equilibration consists of a round bottom flask with two necks of standard joints. A separating funnel with a side arm is fitted to one of the necks of the round bottom flask.

A dry iron oxyhydroxide sample was placed in the separating funnel using glass wool as a plug. Through the second neck of the round bottom flask dry nitrogen was bubbled (10 bubbles/min.) into the hydrazine hydrate (99-100%), placed in the flask. Separating funnel was closed with stopper and the arm provided to it was used to flush out the nitrogen gas carrying unreacted hydrazine hydrate vapours by passing through an acidified water. When the hydrazine uptake of the sample reaches its saturation point (that is, just before sample turns black) the separating funnel was closed at the bottom. Then a known amount of conc. HCl was run down into it. The separating funnel was removed from the round bottom flask and the whole solution of the hydrazinated sample was run down in a reagent bottle and titration was carried out using KIO_3 and CCl_4 [299].

3.2.4 Characterization.

a) Chemical analysis.

i) Metal estimation

The estimation of iron content of iron oxyhydroxides and hydrazinated iron oxyhydroxides was carried out by standard potassium dichromate method [299].

ii) Hydrazine estimation

The hydrazine content was estimated titrimetrically using KIO_3 as titrant [299].

As the hydrazine equilibrated iron oxyhydroxides on exposure to air decompose spontaneously to oxides, the estimation of hydrazine uptake was difficult to monitor. Hence, a specially designed reactor, however, enabled us to follow up the hydrazine uptake titrimetrically.

b) Infrared analysis

Infrared spectra of the oxyhydroxides and their thermal products were obtained on Shimadzu FTIR instrument, model 8101.

c) Density measurements.

Pycnometric density of the oxyhydroxides and their thermal products was measured at room temperature using CCl_4 the reference liquid.

d) X-ray diffraction analysis

X-ray diffraction patterns of the decomposed products of iron oxyhydroxides were obtained by using Philips X-ray diffractometer model PW 1710 with $\text{Cu K}\alpha$ radiations and Nickel as a filter, as well as, by using Rigaku D Max II X-ray diffractometer with Cu and Fe targets. The inter planar spacings, d_{hkl} , values were compared with JCPDS files for metallic Fe [408] and the iron oxides such as $\alpha\text{-Fe}_2\text{O}_3$ [409], $\alpha\text{-Fe}_2\text{O}_3$ [410-411], Fe_3O_4 [412] and FeO [413].

e) Magnetic characterization

The saturation magnetization values of the thermal products of iron oxyhydroxides and autocatalytically decomposed hydrazinated oxyhydroxides were measured, using an alternating current hysteresis loop tracer described. The saturation magnetization values, σ_s , in emu/g were calculated using Ni as a standard.

f) Mössbauer Spectroscopy

The thermal products of amorphous FeOOH are studied by Mössbauer spectroscopy. The Mössbauer spectra were taken at ~~-183~~ and 27°C using a constant acceleration spectrometer and a $^{57}\text{Co/Rh}$ source. The isomer shifts are quoted with reference to $\alpha\text{-Fe}$.

3.2.5 Thermal analysis and decomposition

a) Thermogravimetric (TG) analysis and Isothermal weight loss studies

TG analysis of iron oxyhydroxides was done on Rigaku TAS 1000 instrument in N_2 atmosphere. Isothermal mass loss studies were carried out on the complexes at different predetermined temperature, in an oven by using platinum crucible.

b) Thermal decomposition in different atmosphere

The thermal decomposition of the iron oxyhydroxides was carried out in different atmospheres like, Air, dry N_2 , $\text{N}_2/\text{H}_2\text{O}/\text{Air}$, dry N_2 /Methanol, dry N_2 / Isopropyl alcohol and dry N_2 / cyclohexane at 300°C.

The assembly used for this purpose (Fig. 3.1) comprises of a hollow cylindrical glass tube of 5cm diameter with one end tapering into a small tube which is the inlet for the carrier gas, while the other end is fixed with a cork having an outlet for the carrier gas. Inside this glass tube another hollow glass tube is inserted, having diameter of 4cms and wound with a metallic wire. The one end of this wire is removed out through the cork which can be used to rotate the wound glass tube through 360° , for the uniform heating of the sample which is kept inside it. This assembly is inserted into a temperature controlled tubular furnace built in our laboratory. The assembly is kept in such a way that the sample to be decomposed lies exactly in the heating zone of the furnace. The heating rate of $5^{\circ}/\text{min}$. was maintained.

The carrier gas N_2 is first purified, by passing through the traps of conc. H_2SO_4 , pyrogallol and calcium chloride, to make it dry and free of oxygen. For maintaining the required partial pressure of vapours of methanol (MeOH), isopropyl alcohol (IPA) cyclohexane etc, a dry N_2 was bubbled through these liquids, contained in a flask kept on a heating mantle at the desired temperature. The carrier gas with the partial pressure of these vapours was made to pass through a pre-heater which, in turn is connected to the tapering end of the hollow cylindrical tube containing another tube with the sample. A pulse of air was also made to enter the reaction zone whenever required.

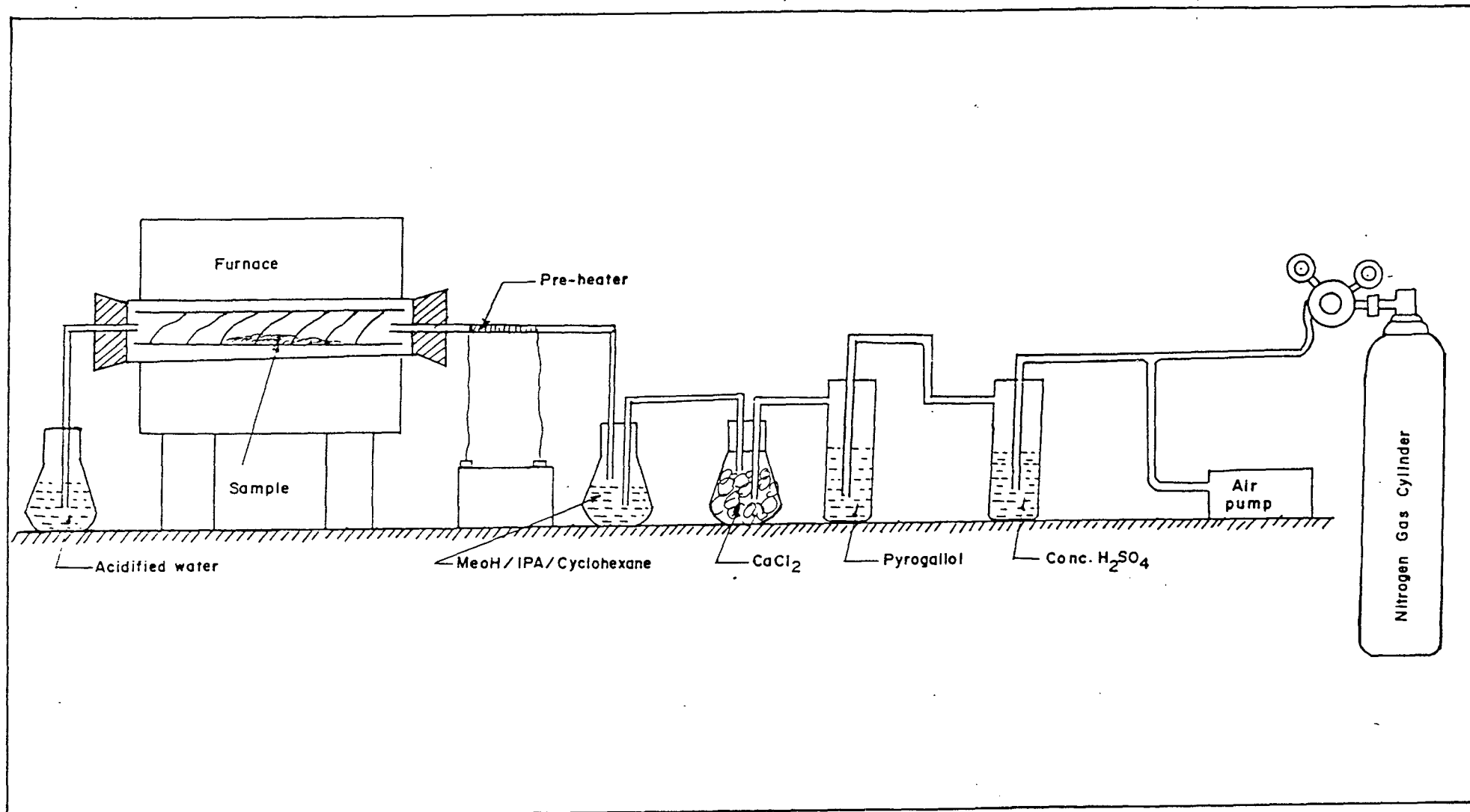


FIG. 3.1 Assembly for controlled atmospheric decomposition

i. Air decomposition

The iron oxyhydroxides : γ -FeOOH, α -FeOOH and amorphous FeOOH were decomposed in a tubular furnace at 300⁰C, in an ordinary atmosphere.

ii. N₂ atmosphere

The sample tube was inserted in the tubular furnace. The inlet was connected to the N₂ gas cylinder via the purification train. The decomposition was carried out at 300⁰C. The sample tube was rotated during decomposition, intermittently.

iii. N₂ + H₂O + Air atmosphere

The iron oxyhydroxide sample was taken in the sample tube and inserted in the furnace. N₂ as a carrier gas was bubbled in the hot water (kept at 60⁰C), at the rate of 15-20 bubbles/min. The water vapours with carrier gas was passed in the sample tube via preheater and the temperature of the furnace was raised at a rate of 5⁰C/min. till it reaches 270⁰C. At this stage, air is passed instead of N₂, till the temperature reaches to 300⁰C. The sample was rotated after every 5 minutes during decomposition. After the completion of the decomposition, the sample tube was cooled to room temperature, by passing only N₂ gas.

iv Dry N₂ + MeOH atmosphere

After placing the iron oxyhydroxide sample in the tubular furnace, the inlet of the sample tube was connected to the flask containing a pure and warm methyl alcohol (MeOH). Dry N₂ gas was bubbled at the rate of 15 -20 bubbles / min. in

MeOH solution. The MeOH vapours were carried through a preheater to the sample tube along with N₂ gas. The temperature of the furnace was increased to 300°C. The sample tube was rotated frequently during heating. The sample tube was cooled to room temperature in the N₂ atmosphere.

v. Dry N₂ + IPA atmosphere.

The IPA vapours formed by bubbling the dry N₂ gas through warm isopropyl alcohol (A.R. Grade) at the rate of 15 bubbles /min were carried by N₂ gas through the preheater into the glass tube containing sample, kept in a tubular furnace. The sample was heated slowly in this atmosphere upto 300°C and then cooled by passing N₂ gas. During heating, the sample tube was rotated after every 4-5 minutes, for the uniform heating of the sample.

vi. Dry N₂ + Cyclohexane atmosphere

The iron oxyhydroxide is placed in the sample tube which was then inserted into the tubular furnace. The dry N₂ gas was bubbled into the warm and pure cyclohexane. The cyclohexane fumes formed along with the N₂ gas were made to enter into the preheater which is connected to the sample tube. The furnace containing sample tube was heated at a rate of 5°C / min. till the temperature reaches to 300°C. The sample was rotated through 360°C during decomposition, after every 5 minutes. While cooling the decomposed sample, only N₂ gas was passed through it till the room temperature is attained.

c) Autocatalytic decomposition of hydrazinated iron hydroxides and iron oxyhydroxides.

Iron hydroxides and iron oxyhydroxides on equilibrating in hydrazine hydrate atmosphere, in a desiccator, change their colour indicating the hydrazine uptake by them. A reddish orange γ -FeOOH and reddish brown amorphous FeOOH turned black after seven days of the equilibration, while the yellow α -FeOOH shows no change in colour. On exposure to air the hydrazinated γ -FeOOH and amorphous FeOOH decomposed autocatalytically, while α -FeOOH only fumed.

3.2.6 Hydrazine equilibration studies of iron oxyhydroxides by electrical conductivity measurements

a) Variation of electrical conductivity on hydrazination as a function of time

Although the specially built reactor enabled us the estimation of the hydrazine uptake by iron oxyhydroxides titrimetrically, the colour change observed in the hydrazine equilibration of these and chemical analysis indicated that the products consists of oxides of Fe^{2+} and Fe^{3+} . Hence, along with the hydrazine content estimation, it was decided to measure electrical characteristic of these iron oxyhydroxides during the hydrazine uptake, as there occurs reduction of Fe^{3+} ions to Fe^{2+} on hydrazination and these ferric and ferrous ions may contribute to the enhanced electrical conductivity in the products that formed.

A specially built set up was used for the measurement of direct current electrical conductivity during the hydrazination of the iron oxyhydroxides. The iron oxyhydroxides in the pellet form were pressed between platinum electrodes in

a conductivity cell designed for such work. The conductivity cell was placed in the reactor containing hydrazine hydrate atmosphere and the leads were connected to a multimeter and the resistance measurements were done as a function of time. From the dimensions of the pellet, the resistance values were converted into resistivity and conductivity.

3.3 Results and Discussion

A chemical formulas for iron oxyhydroxides and hydrazinated iron oxyhydroxides were fixed based on chemical analysis, IR and thermal analysis. Decomposition of these precursors was carried out and the thermal products were X-ray characterized to establish the phase formation. The thermal products were then systematically studied to understand their magnetic characteristics. A plausible mechanism for the formation of the iron oxides was proposed.

3.3.1 Fixation of chemical formulas

a) Chemical formulas of iron oxyhydroxides.

i Chemical analysis

The iron contents of 59.0 % for γ -FeOOH, 60.0 % for α -FeOOH and 54.0 % for amorphous FeOOH are observed. The calculated percentage of Fe for all these iron oxyhydroxides, considering formula FeOOH is 62.86. The iron contents of all these iron oxyhydroxides are, thus, found to be lower than the calculated ones.

ii. Infra red analysis

Infra red band positions of O-H stretching, O-H bending and Fe-O stretching are given in Table 3.1 for these iron oxyhydroxides. The O-H stretching, O-H bending and Fe-O stretching are respectively found at 2890, 1020 and 747 cm^{-1} for γ -FeOOH and at 3100, 904 and 774 cm^{-1} for α -FeOOH. Amorphous FeOOH, however, shows two absorption peaks O-H stretching, 3100 cm^{-1} ; Fe-O stretching, 775 cm^{-1} . These band positions are agreeing well with the reported band positions for γ -FeOOH and α -FeOOH [356,414].

iii Pycnometric density

The densities of γ -FeOOH, amorphous FeOOH and α -FeOOH are 1.54, 1.73 and 2.66 respectively (Table 3.1).

iv TG and total mass loss

Iron oxyhydroxides decompose in air $\sim 300^{\circ}\text{C}$ giving iron oxide, Fe_2O_3 . The total mass loss observed $\sim 300^{\circ}\text{C}$ in air [Table 3.1] is 15.62 % for γ -FeOOH; 13.76 % for α -FeOOH and 22.9 % for amorphous FeOOH. Total mass loss observed on TG in nitrogen is, for γ -FeOOH -15 %; for α -FeOOH -15 % and amorphous FeOOH - 23 %. Considering formula FeOOH for all these oxyhydroxides, the calculated weight loss for Fe_2O_3 formation is 10.13 %. Thus, an increased weight loss is observed for all these iron oxyhydroxides. These observations indicate that these iron oxyhydroxides consist of an additional water which may be present as water of hydration.

Based on these observations in TG and total mass loss studies, the chemical formula for these iron oxyhydroxide are fixed as, $\gamma\text{-FeOOH} \cdot 0.3\text{H}_2\text{O}$, $\alpha\text{-FeOOH} \cdot 0.2\text{H}_2\text{O}$ and amorphous $\text{FeOOH} \cdot 0.8\text{H}_2\text{O}$. These formulas now agree well with the iron contents calculated with the observed values by chemical analysis (Table 3.1). The iron contents, thus, observed and calculated (in bracket) show closeness in the values, confirming the formulas fixed as given above.

b) Hydrazine equilibration of iron oxyhydroxides

i. Equilibration in 80% and 99-100% hydrazine hydrate

Powdered as well as the compact (pellets used in the electrical conductivity measurements) samples of reddish orange $\gamma\text{-FeOOH} \cdot 0.3\text{H}_2\text{O}$ and reddish brown amorphous $\text{FeOOH} \cdot 0.8\text{H}_2\text{O}$ when placed in a desiccator containing 99-100% hydrazine hydrate turned black on the hydrazine equilibration. The yellow $\alpha\text{-FeOOH} \cdot 0.2\text{H}_2\text{O}$, however, did not change its colour. On exposure to air these hydrazine equilibrated samples fumed with glow indicating intense decomposition taking place and the products obtained were now dull reddish brown in colour and magnetic in nature.

The equilibration when carried out in a desiccator containing 80% hydrazine hydrate also indicated the colour change, but they did not show spontaneous decomposition on exposure to air. The black products were magnetic in nature. The black coloured product of $\gamma\text{-FeOOH}$ indicated 41.0% FeO content in it, while the product of amorphous FeOOH showed to consist of just 1.2% FeO (Table 3.2).

TABLE 3.1 Chemical analysis, density, IR, total weight loss of iron - oxyhydroxides

Sr. No.	Sample	% Fe	Density	Infra Red Data, cm^{-1}			Total Weight Loss (%) in	
							Air (Isothermal)	N_2 (TG)
			g cm^{-3}	O-H stret.	O-H bend.	Fe-O stret.	Obs. (Calc.)	Obs. (Calc.)
1.	$\gamma\text{-FeOOH}\cdot 0.3 \text{H}_2\text{O}$	59.0 (59.25)	1.54	2890	1020	747	15.62 (15.28)	15 (15.28)
2.	Amorph. $\text{FeOOH}\cdot 0.8 \text{H}_2\text{O}$	54.0 (54.09)	1.73				22.9 (22.66)	23 (25.25)
3.	$\alpha\text{-FeOOH}\cdot 0.2\text{H}_2\text{O}$	60.0 (60.41)	2.66	3100	904	774	13.76 (13.63)	15 (13.63)

104

TABLE 3.2 Chemical analysis of iron oxyhydroxides on hydrazine equilibration in 80% $\text{N}_2\text{H}_4\cdot\text{H}_2\text{O}$

Sr. No.	Sample	% N_2H_4	Colour Change after Equilibration
1.	$\gamma\text{-FeOOH}\cdot 0.3 \text{H}_2\text{O}$ (Reddish Orange)	10.4	Black (FeO 41%)
2.	Amorph. $\text{FeOOH}\cdot 0.8 \text{H}_2\text{O}$ (Reddish Brown)	10.8	Black (FeO 1.2%)

Yellow coloured α -FeOOH did not show any change in colour on its exposure to hydrazine. On exposing to air hydrazinated α -FeOOH fumed.

ii. Hydrazine estimation

The hydrazine equilibration studies carried out both in 99-100% and 80% hydrazine hydrate did not allow us to estimate the hydrazine uptake by these iron oxyhydroxides. Hence, a special set up described in section 3.2.3 that used for such hydrazine uptake study enabled us to analyse the hydrazine (Fig. 3.2) by titrimetric method. And, about 10.4% of hydrazine uptake was observed in γ -FeOOH. 0.3H₂O (Table 3.2), while amorphous FeOOH.0.8H₂O showed 10.8% hydrazine in it. α -FeOOH.0.2H₂O, on the other hand, indicated just 1.5% hydrazine uptake. However, these results did not allow us to fix a chemical formula for these iron oxyhydroxide, as further studies like, ir, isothermal weight loss, DTA and TG analysis could not be carried out on these hydrazinated complexes due to their unstable nature.

As the black coloured product of hydrazine equilibrated γ -FeOOH is magnetic in nature and consist of 41% of FeO and the product of amorphous FeOOH is also magnetic in nature with 1.2% FeO (Table3.2), it was felt that the electrical conductivity measurements on these iron oxyhydroxides during the hydrazine uptake may throw some light on the process of hydrazination. Also, as the black coloured products on exposure to air gave a dull brown product characterized as gamma ferric oxide, γ -Fe₂O₃, by xrd, the continuation of the electrical conductivity measurements on exposure to air should, therefore, indicate the phase transforma-

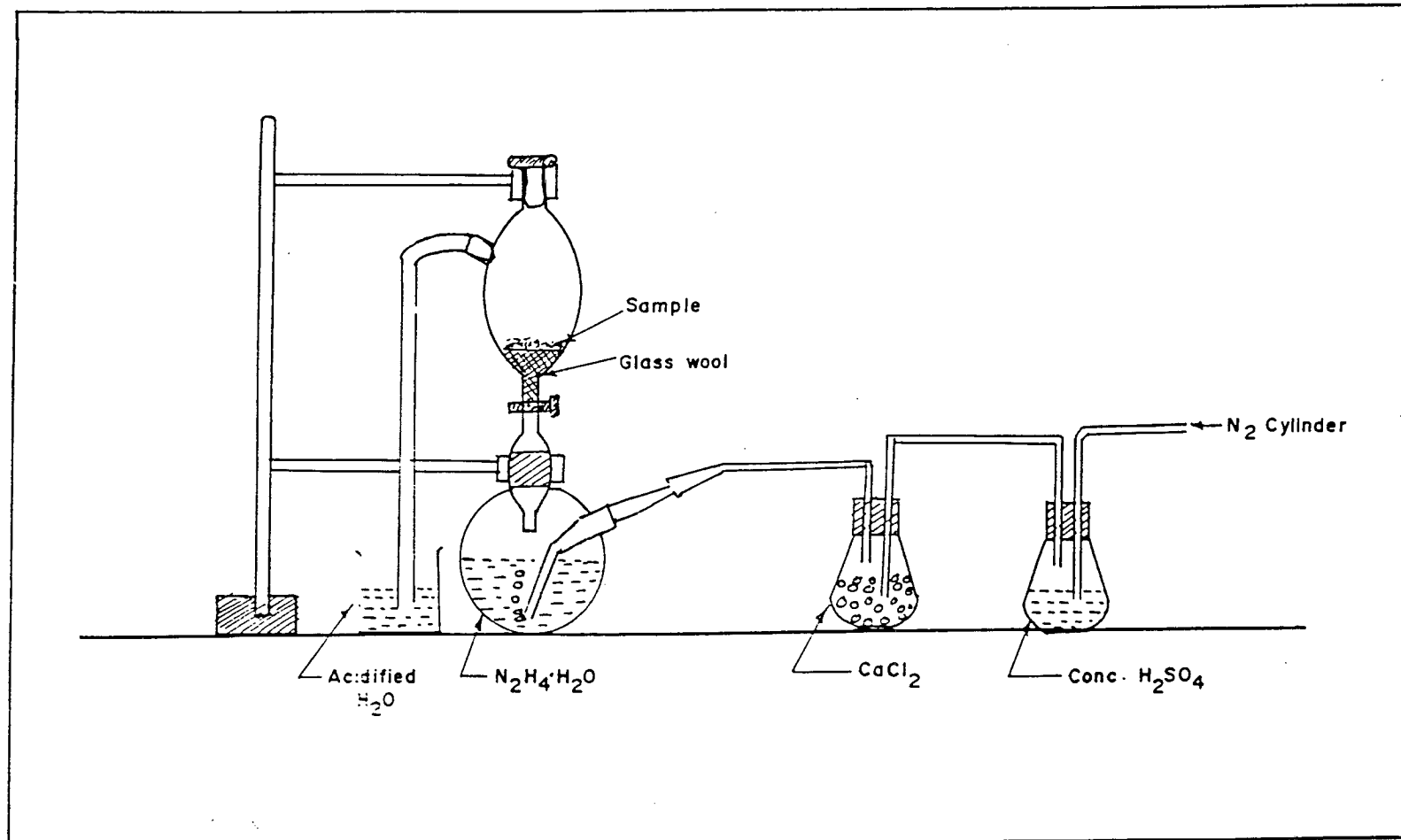


FIG. 3.2 Hydrazine estimation set up

tion of the black coloured magnetic product. Therefore, the electrical conductivity measurement were done on these iron oxyhydroxides during hydrazine equilibration.

iii. Variation of d.c. electrical conductivity during hydrazination as a function of time

The electrical conductivity of the iron oxyhydroxides in pellets form of 10 mm diameter and thickness of 2-3 mm were pressed between two circular platinum discs in a special conductivity cell built (section 3.2.6a) for such study. The whole assembly was then introduced in a desiccator containing hydrazine hydrate. The lead wires of the platinum electrodes were then connected to a multimeter. Resistance of the pellet was measured as a function of time. From the dimension of the pellet, the resistivity and then the conductivity values were plotted as log conductivity (σ) versus time in hours.

In Fig.3.3 the $\log \sigma$ vs. Time in hours plots of γ -FeOOH.0.3H₂O, amorphous FeOOH.0.8H₂O and α -FeOOH.0.2H₂O are shown. A room temperature conductivity value of $2.63 \times 10^{-7} \text{ ohm}^{-1} \text{ cm}^{-1}$ of γ -FeOOH (curve A), on introducing in the hydrazine hydrate atmosphere, shows initial dip in conductivity and then increase linearly in 20 hours to $6.96 \times 10^{-6} \text{ ohm}^{-1} \text{ cm}^{-1}$. After 20 hours of exposure to hydrazine atmosphere the conductivity increases slightly and then again steeply upto 50 hours. Thereafter, the conductivity remains constant at $6.86 \times 10^{-5} \text{ ohm}^{-1} \text{ cm}^{-1}$ indicating the equilibration of hydrazine is completed. On exposure to air, after keeping in the hydrazine atmosphere for 120 hours, the conductivity value showed a sudden increase to $2.13 \times 10^{-4} \text{ ohm}^{-1} \text{ cm}^{-1}$ and then started decreasing very fast

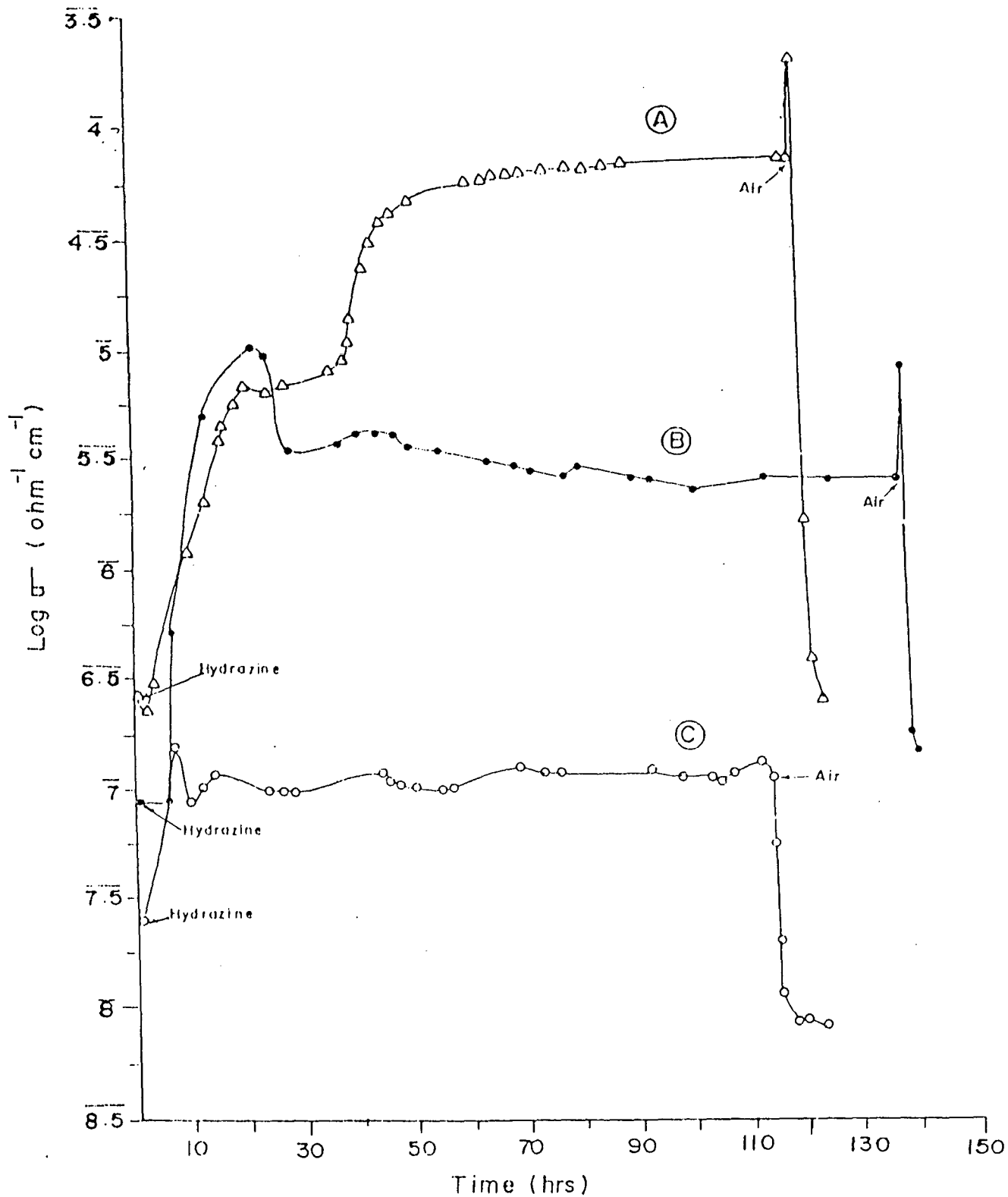


FIG. 3.3 Variations in electrical conductivity of iron oxyhydroxides in Hydrazine atmosphere as a function of time A) γ -FeOOH B) amorphous FeOOH and C) α -FeOOH

and remained constant at $2.56 \times 10^{-7} \text{ ohm}^{-1} \text{ cm}^{-1}$, a three order decrease in the conductivity value is thus observed.

A room temperature conductivity value of $6.1 \times 10^{-8} \text{ ohm}^{-1} \text{ cm}^{-1}$ of amorphous FeOOH, which is half an order less than that of γ -FeOOH, shows no change in the σ value for initial 5 hours in the hydrazine atmosphere (curve B) and then it increases, like γ -FeOOH, steeply in 20 hours to $1.05 \times 10^{-5} \text{ ohm}^{-1} \text{ cm}^{-1}$. But, after that, unlike in γ -FeOOH, the conductivity here shows a decrease and then remains constant at $\sim 3.53 \times 10^{-6} \text{ ohm}^{-1} \text{ cm}^{-1}$. When the hydrazine equilibrated sample was exposed to air the value increased to $8.92 \times 10^{-6} \text{ ohm}^{-1} \text{ cm}^{-1}$ and then it suddenly decreased to $1.7 \times 10^{-7} \text{ ohm}^{-1} \text{ cm}^{-1}$ and remained constant at this value.

Both γ -FeOOH amorphous FeOOH when exposed to air after the hydrazine equilibration fumed and the value of conductivity of the products remained at $\sim 10^{-7} \text{ ohm}^{-1} \text{ cm}^{-1}$. The product being γ -Fe₂O₃ in both these cases, the conductivity value is now of the oxide.

Thus, γ -FeOOH amorphous FeOOH undergo electrical conductivity changes on equilibrating with hydrazine. Since the value increase is of 2-3 order, and the oxyhydroxides convert into black coloured magnetic oxide consisting of 41% FeO and the rest Fe₂O₃ content in it, the increase in conductivity may be due to the presence of Fe²⁺ and Fe³⁺. A Fe₃O₄ type of black product is thus formed on hydrazine equilibration, which on exposure to air oxidizes into a dull brown coloured γ -Fe₂O₃ and since in this oxide only Fe³⁺ ions are present, the conductivity shows a decrease.

On the other hand, the α -FeOOH on exposure to hydrazine atmosphere (curve C) shows just a half order change from its room temperature conductivity value in air. Then, the value from $1.56 \times 10^{-7} \text{ ohm}^{-1} \text{ cm}^{-1}$ decreases to $8.93 \times 10^{-8} \text{ ohm}^{-1} \text{ cm}^{-1}$ and thereafter, remains constant till it was exposed to air. Unlike in γ -FeOOH and amorphous FeOOH, here there is no increase in conductivity initially after the exposure of the sample to air. However, the value goes down to $1.16 \times 10^{-8} \text{ ohm}^{-1} \text{ cm}^{-1}$ and remains constant. The hydrazine equilibration, although, did not show significant change in the conductivity, the sample did fume in air and the product was found to be mixture of γ -Fe₂O₃ and α -Fe₂O₃.

c) Analysis of thermal products of iron oxyhydroxides and hydrazinated iron oxyhydroxides

i. X-Ray Diffraction Analysis

The thermal products of iron oxyhydroxides in air and different controlled atmospheres and autocatalytic decomposition products of the hydrazinated iron oxyhydroxides were characterized by X-ray diffraction (Table 3.3). γ -Fe₂O₃ is the main thermal product of γ -FeOOH decomposed in all atmospheres. γ -FeOOH decomposed in atmospheres such as, N₂/MeOH and N₂/IPA at 300°C shows all peak intensities corresponding to those of γ -Fe₂O₃. The end product of γ -FeOOH decomposed in other atmospheres such as, dry N₂, N₂/cyclohexane, as well as, autocatalytically decomposed hydrazinated γ -FeOOH complex is γ -Fe₂O₃ with the traces of Fe₃O₄. The dehydration of γ -FeOOH in air gives γ -Fe₂O₃ with traces of α -Fe₂O₃, while decomposition in N₂/H₂O/air gives γ -Fe₂O₃ of better quality.

TABLE 3.3 XRD data of iron oxides obtained by decomposition of iron oxyhydroxides in different atmospheres

γ -Fe ₂ O ₃ (reported) tetragonal	d (l/l ₀)	2.95 (30)	-	-	2.51 (100)	2.086 (15)	-	1.7 (19)	1.60 (20)	1.47 (40)	1.2 (8)
γ -Fe ₂ O ₃ (reported) cubic	d (l/l ₀)	2.95 (34)	2.78 (19)	-	2.52 (100)	2.08 (24)	-	1.7 (12)	1.61 (33)	1.48 (53)	1.27 (11)
Fe ₃ O ₄	d (l/l ₀)	2.96 (30)	-	-	2.53 (100)	2.09 (20)	-	1.7 (10)	1.61 (30)	1.48 (40)	1.28 (10)
α -Fe ₂ O ₃ (reported) rhombohedral	d (l/l ₀)	3.66 (25)	-	2.69 (100)	2.51 (50)	2.20 (30)	1.838 (40)	1.690 (60)	-	1.452 (35)	-
γ -FeOOH (autocatal.)	d (l/l ₀)	2.96 (53)	-	-	2.523 (100)	2.09 (33)	-	1.70 (27)	1.61 (33)	1.48 (43)	1.27 (17)
γ -FeOOH in N ₂ +MeOH	d (l/l ₀)	2.95 (27)	-	-	2.51 (100)	-	-	-	1.60 (45)	1.46 (61)	-
γ -FeOOH in N ₂ +IPA	d (l/l ₀)	2.95 (44)	-	-	2.52 (99)	2.09 (43)	-	1.71 (34)	1.61 (41)	1.474 (33)	1.27 (18)
γ -FeOOH in N ₂ + cyclohexane	d (l/l ₀)	2.97 (38)	-	-	2.54 (100)	2.09 (23)	-	-	1.61 (27)	1.48 (54)	1.27 (15)
γ -FeOOH in N ₂ +H ₂ O+air	d (l/l ₀)	2.97 (34)	-	2.70 (65)	2.52 (100)	2.08 (22)	-	1.70 (31)	1.61 (24)	-	-
γ -FeOOH in N ₂	d (l/l ₀)	-	-	-	2.53 (100)	2.09 (39)	-	-	1.61 (47)	1.47 (79)	1.27 (58)
γ -FeOOH in air	d (l/l ₀)	2.943 (47)	2.78 (58)	2.70 (62)	2.52 (99)	2.08 (30)	1.83 (45)	1.70 (45)	1.60 (34)	1.47 (35)	-
α -FeOOH (autocatal)	d (l/l ₀)	-	-	2.7 (78)	2.52 (100)	-	1.83 (42)	1.69 (42)	1.60 (36)	1.48 (51)	1.27 (23)
α -FeOOH in N ₂ +MeOH	d (l/l ₀)	3.65 (27)	-	2.70 (94)	2.52 (99)	-	-	1.69 (36)	-	1.48 (31)	-
α -FeOOH in N ₂ +IPA	d (l/l ₀)	-	-	2.70 (71)	2.52 (87)	2.49 (99)	1.83 (46)	1.70 (53)	-	1.47 (60)	-
α -FeOOH in N ₂	d (l/l ₀)	-	-	2.69 (71)	2.51 (100)	-	1.79 (79)	-	-	1.45 (83)	-
Amp FeOOH (autocatal)	d (l/l ₀)	-	-	-	2.51 (99)	2.076 (58)	-	-	1.60 (74)	1.47 (81)	1.27 (71)
Amp FeOOH in N ₂ +MeOH	d (l/l ₀)	2.95 (58)	-	-	2.51 (99)	2.071 (51)	-	1.70 (43)	1.61 (58)	1.47 (72)	-
Amp FeOOH in N ₂ + IPA	d (l/l ₀)	-	-	-	2.52 (100)	2.09 (57)	-	1.70 (55)	1.61 (62)	1.48 (67)	-
Amp FeOOH in N ₂ + cyclohexane	d (l/l ₀)	-	-	-	2.53 (100)	2.1 (30)	-	1.70 (30)	1.60 (25)	1.48 (50)	-
Amp FeOOH in N ₂ +H ₂ O+air	d (l/l ₀)	2.947 (58)	-	-	2.513 (100)	-	-	-	-	1.47 (65)	-
Amp FeOOH in N ₂	d (l/l ₀)	-	2.78 (52)	-	2.516 (100)	2.086 (50)	-	1.71 (43)	1.605 (54)	1.478 (66)	1.27 (52)

Reported values [408-413]

The end product of amorphous FeOOH decomposed in N₂/H₂O/air, N₂/MeOH, N₂/IPA, and dry N₂ at atmospheres is γ -Fe₂O₃. All the peaks here corresponds to γ -Fe₂O₃, while the decomposition in N₂/cyclohexane gives γ -Fe₂O₃ with traces of Fe₃O₄. Autocatalytic decomposition of hydrazinated amorphous FeOOH complex exclusively gives γ -Fe₂O₃.

α -FeOOH decomposed in N₂/MeOH, N₂/IPA, dry N₂, as well as. autocatalytically decomposed hydrazinated α -FeOOH complex gives a mixture of α -Fe₂O₃ and γ -Fe₂O₃ as seen from their xrd data (Table 3.3).

ii Infra red analysis

Infrared bands at 558, 400, 395 and 370 cm⁻¹ observed in the thermal products γ -Fe₂O₃ of iron oxyhydroxides, hydrazinated iron oxyhydroxides and iron oxyhydroxides heated in different atmospheres such as N₂/MeOH, N₂/IPA N₂/Cyclohexane etc. are being compiled in Fig 3.4. These band positions agree well with the reported values for γ -Fe₂O₃ [280,333,350]. The thermal product α -Fe₂O₃ that formed from iron oxyhydroxides shows an ir band positions at 650, 525, 440, 390 and 382 cm⁻¹, are also shown in Fig 3.4 and these too agree closely with the reported bands for α -Fe₂O₃ [350,415]. These iron oxyhydroxides and hydrazinated iron oxyhydroxides which give a mixture of γ -Fe₂O₃ and α -Fe₂O₃ show ir bands (Fig 3.4) corresponding to both.

The iron oxyhydraxide and hydrazinated iron oxyhydroxides which gives γ -Fe₂O₃ or α -Fe₂O₃ or mixture of γ -Fe₂O₃ & α -Fe₂O₃ are clearly indicated in the Fig.3.4.

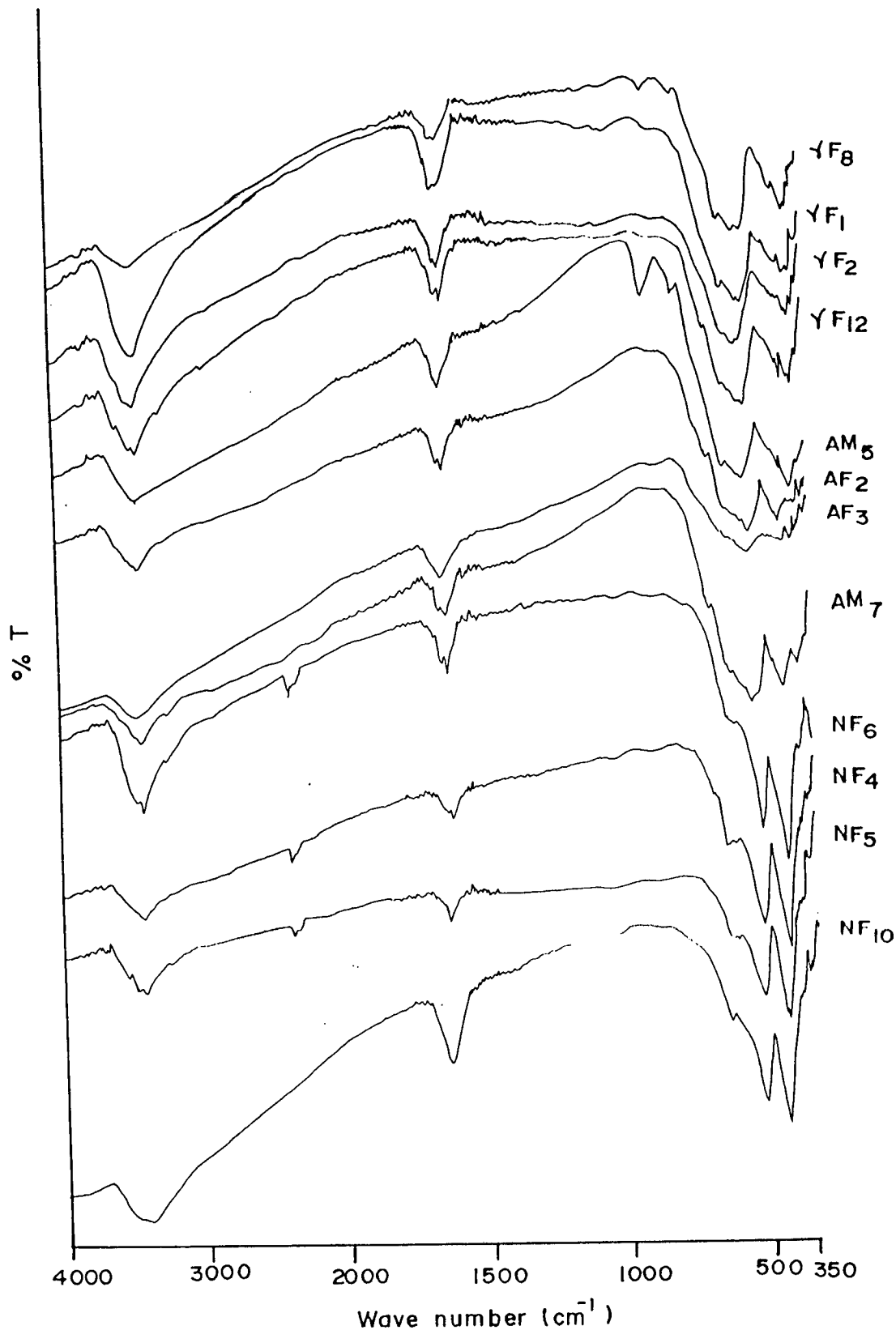


FIG. 3.4 Infra red spectra of the end products of iron oxyhydroxides decomposed in different atmospheres

	Auto cat,	N ₂ /MeOH,	N ₂ /IPA	N ₂ /cyclohexane
γ -FeOOH	γF_8	γF_1	γF_2	γF_{12}
α -FeOOH	NF ₆	NF ₄	NF ₅	NF ₁₀
Amp. FeOOH	AM ₅	AF ₂	AF ₃	AM ₇

These observations and also the phase identification done by XRD, allow us to confirm the formation of the oxides.

iii. Magnetic characterization

The saturation magnetization of the thermal products of iron oxyhydroxides in air and different controlled atmospheres and autocatalytic decomposition products of the hydrazinated iron oxyhydroxides were measured [417] by using a low field hysteresis loop tracer. In fig 3.5 the saturation magnetization value, σ_s , in emu/g, of the product is indicated at the end of the arrow, for each atmospheric decomposition.

A least value of 19.20 emu/g was observed for air decomposed product and a maximum of 71.65 emu/g for autocatalytically decomposed hydrazinated $\gamma\text{-FeOOH}\cdot 0.3\text{H}_2\text{O}$ which is close to the expected and reported value for $\gamma\text{-Fe}_2\text{O}_3$ of 71-74 emu/g [416]. $\gamma\text{-Fe}_2\text{O}_3$ obtained in dry N_2 atmospheric decomposition of $\gamma\text{-FeOOH}$ showed a σ_s of 43.69 emu/g. The dry nitrogen containing a known partial pressure of methanol when provided during the thermal decomposition of $\gamma\text{-FeOOH}$, the product $\gamma\text{-Fe}_2\text{O}_3$ showed an improvement in the σ_s value of 59.70 emu/g. The decomposition of the $\gamma\text{-FeOOH}$ in N_2/IPA and $\text{N}_2/\text{cyclohexane}$ did not improve further the σ_s value and remained at 58.5 and 56.11 emu/g, respectively. The $\text{N}_2/\text{H}_2\text{O}/\text{air}$ atmospheric decomposition of the $\gamma\text{-FeOOH}$ lead to the end product of smaller σ_s value of 26.6 emu/g.

The amorphous $\text{FeOOH}\cdot 0.8\text{H}_2\text{O}$ in air decompose to $\alpha\text{-Fe}_2\text{O}_3$ with lowest σ_s value of 2.46 emu/g. In dry N_2 the decomposition product is highly magnetic

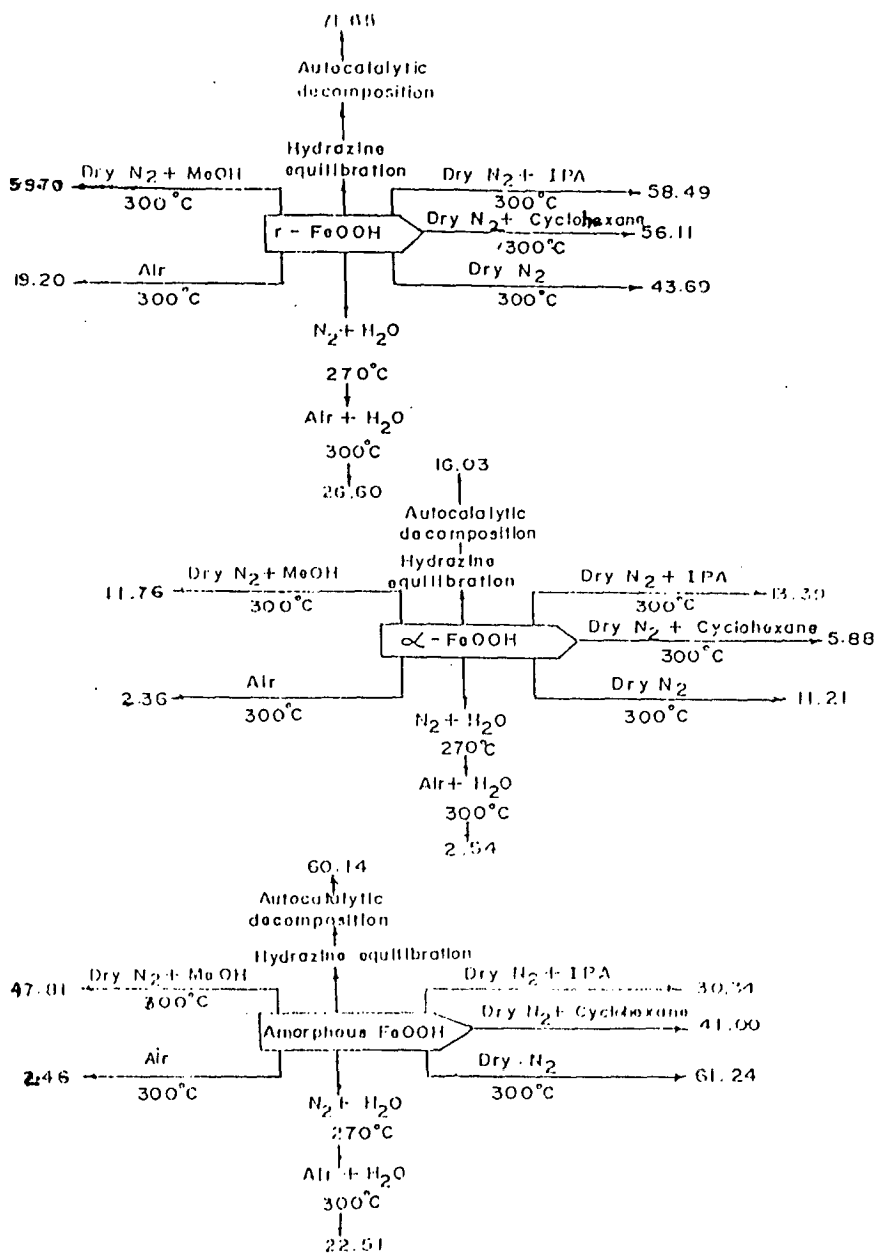


FIG.3.5 Saturation magnetization, σ_s , in emu/g of decomposed end products of iron oxyhydroxides and their hydrazinated complexes

with σ_s of 61.24 emu/g and found to be γ -Fe₂O₃. When the amorphous FeOOH was decomposed in N₂/Methanol, N₂/IPA and N₂/cyclohexane, the products obtained are mainly γ -Fe₂O₃ and the σ_s values are, respectively, 47.81, 30.34 and 41 emu/g. The hydrazine equilibrated sample of amorphous FeOOH on autocatalytic decomposition gave γ -Fe₂O₃ of σ_s value 60.14 emu/g. The least value of σ_s of 2.46 emu/g that observed in the air decomposed product of amorphous FeOOH improved to a value of 22.51 emu/g on decomposing it in N₂/H₂O/air, suggesting the influence of water in the decomposition.

In air and N₂/H₂O/air, the α -FeOOH.0.2H₂O decomposed to give α -Fe₂O₃ with a very small value of σ_s of ~ 2.45. In dry N₂, N₂/Methanol and N₂/IPA, the thermal products of α -FeOOH show σ_s values ~ 12.18 emu/g. This higher values of σ_s is due to the presence of γ -Fe₂O₃ along with α -Fe₂O₃ as the end product. Hydrazinated sample of α -FeOOH, however, on autocatalytic decomposition yielded fairly good magnetic material with σ_s value of 16.03 emu/g. The xrd revealed the presence of mixture of α -Fe₂O₃ and γ -Fe₂O₃ in the product.

iv. Mössbauer spectroscopy

The iron oxides synthesized by the thermal decomposition of amorphous FeOOH under different controlled atmospheres at 300°C were investigated by us[418], using ⁵⁷Fe Mössbauer spectroscopy. The Mössbauer spectra were taken at 90 and 300 K using a constant acceleration spectrometer and a ⁵⁷Co/Rh source. The isomer shifts are quoted with reference to α -Fe. Typical Mössbauer spectra recorded at 27 and -183 °C are shown in Fig. 3.6a,b&c.

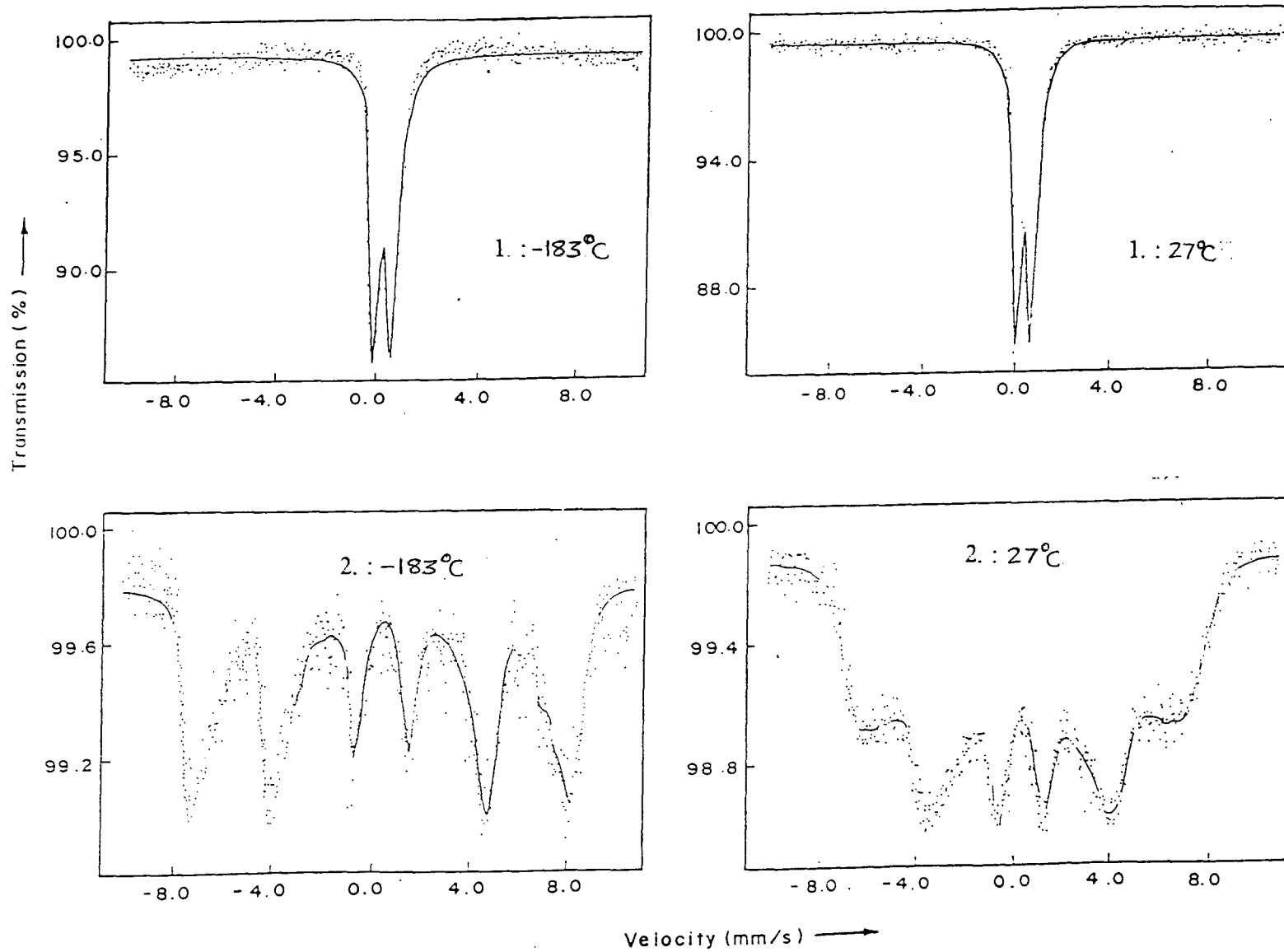
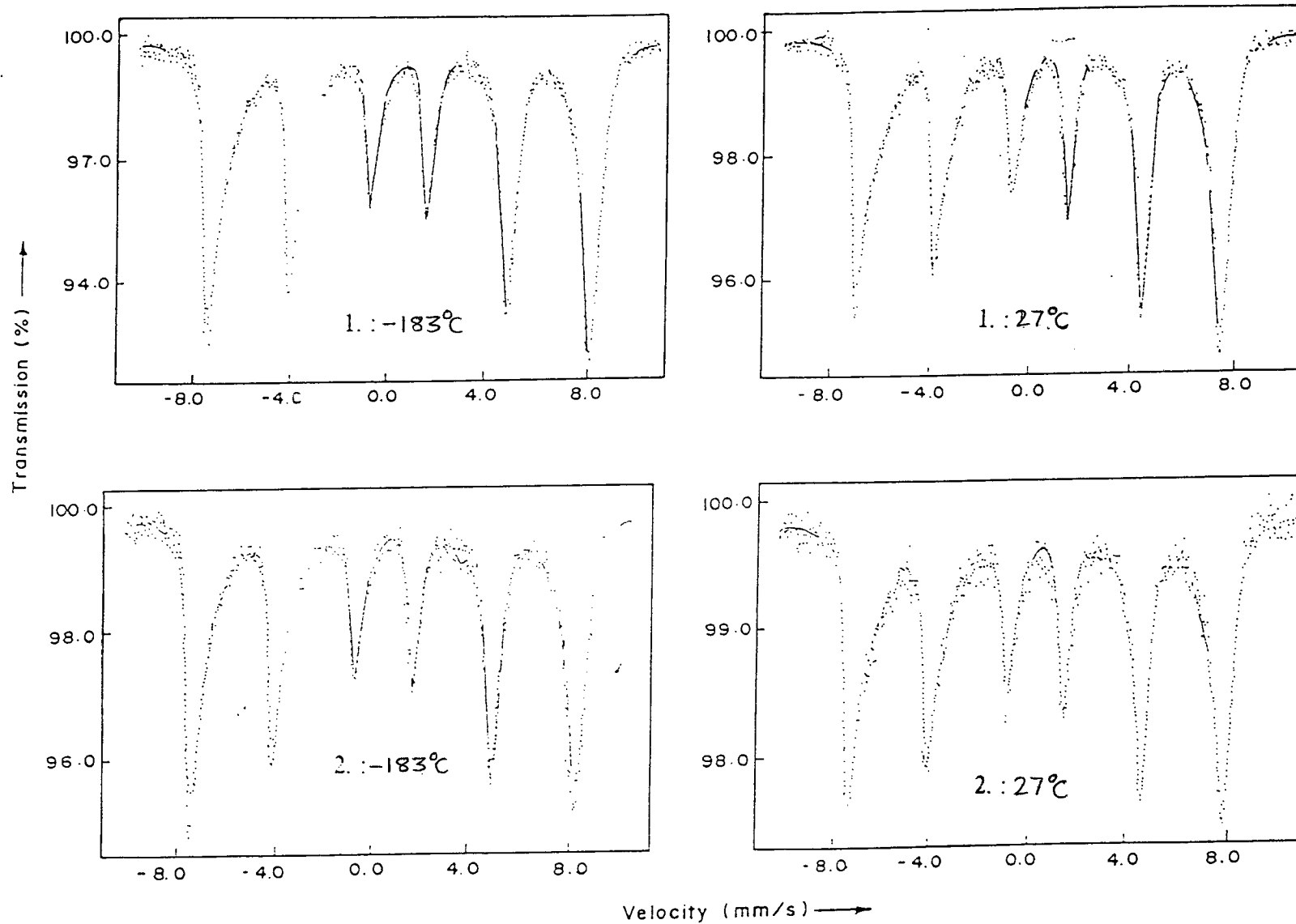
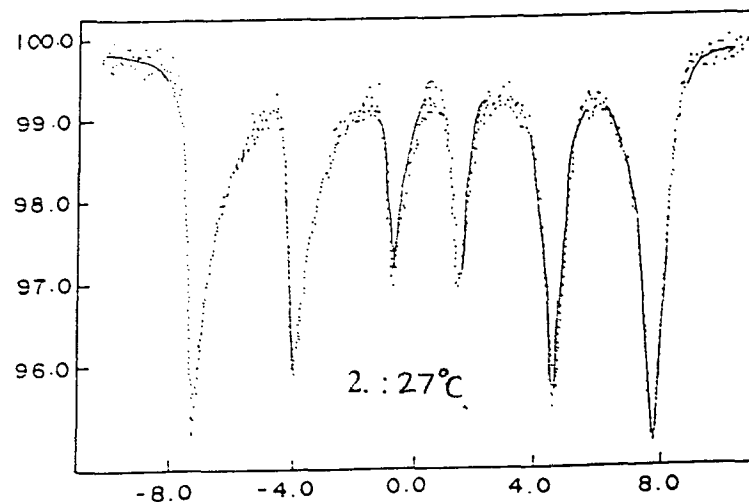
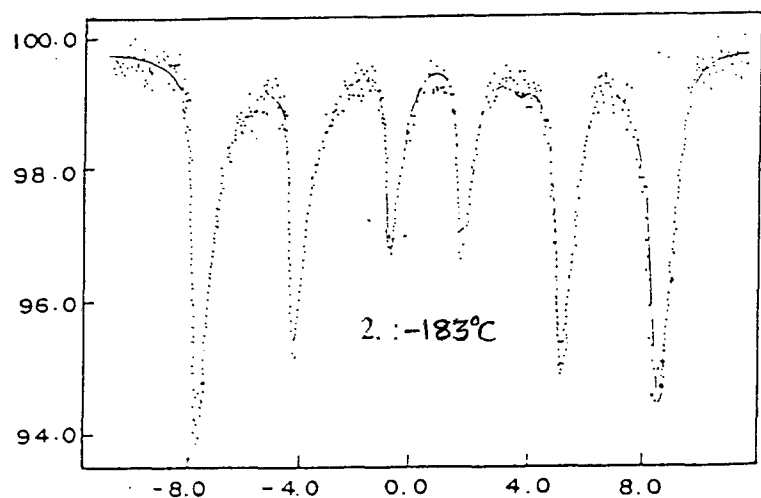
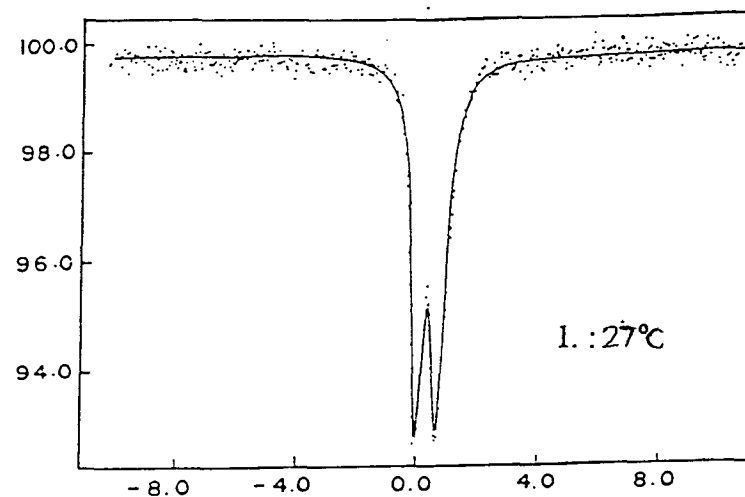
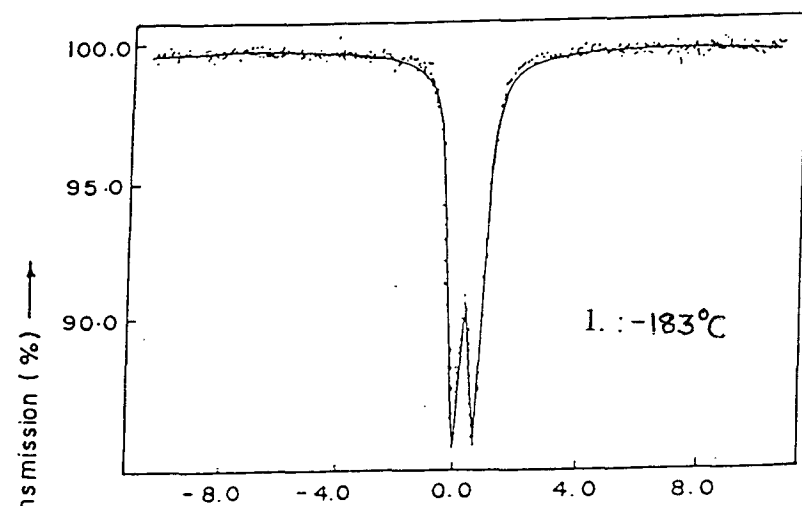


FIG.3.6a) Mossbauer spectra of 1) amorphous FeOOH and 2) amorphous FeOOH decomposed autocatalytically



3.6 b) Mossbauer spectra of decomposed end products of amorphous FeOOH at 300°C in 1) dry $\text{N}_2 + \text{MeOH}$ atmosphere and 2) dry $\text{N}_2 + \text{IPA}$ atmosphere

611

Velocity (mm/s) \longrightarrow

3.6 c) Mössbauer spectra of decomposed end products of amorphous FeOOH at 300°C in 1) $\text{N}_2 + \text{H}_2\text{O} + \text{air}$ atmosphere and 2) dry N_2 atmosphere

Amorphous FeOOH decomposes in air to non-magnetic α -Fe₂O₃. However, by heating this material under controlled atmosphere of N₂/H₂O/air at 300°C gives a mixture of magnetic and non magnetic iron oxide. The room temperature Mössbauer spectrum of this oxide consists of a paramagnetic doublet ($\delta = 0.33 \pm 0.02$ mm/s; $\Delta = 0.69 \pm 0.02$ mm/s). No further magnetic ordering was observed at -183°C. The relevant parameters are similar to those reported in the literature for super paramagnetic γ -Fe₂O₃.

A super paramagnetic doublet was also observed by Liaw et al [419] in their study of the products obtained from amorphous FeOOH, under the almost similar preparative conditions. They have attributed this to undecomposed FeOOH and consider it to be responsible for increasing activity in oxidative dehydrogenation of butene with steam. The fact that this end product is magnetic while the parent material is not, clearly indicates that the decomposition of the precursor has occurred. These results rule out the presence of any undecomposed FeOOH in our run. The increasing catalytic activity, as reported by Liaw and Coworkers probably arises from the *in situ* formation of active γ -Fe₂O₃.

The room temperature Mössbauer spectrum of autocatalytically decomposed hydrazinated amorphous FeOOH is characterized by asymmetrically broadened ($\Gamma = 0.83 \pm 0.02$ mm/s) lines, as well as, an intensity distribution, suggesting an uneven distribution of the particle sizes, and / or a poor crystallinity. As a result, the measured hyperfine field ($H_{av} = 31$ T, $H_{max} = 37$ T) are fairly low as compared to the values reported in the literature for γ -Fe₂O₃ [420]. No substantial

split was observed at -183°C apart from increasing average ($H_{av} = 41 \text{ T}$) and maximum ($H_{max} = 46 \text{ T}$) hyperfine fields.

The Mössbauer spectra recorded at 27°C , of the end product of decomposition of amorphous FeOOH at 300°C in dry N_2 , N_2/MeOH and N_2/IPA , are nearly symmetrical patterns, similar in appearance and typical for intermediate grain-sized ($\pm 60\text{nm}$) species. H_{av} falls in the range $41\text{-}43 \text{ T}$ and H_{max} in the range $45\text{-}47 \text{ T}$ [418] and no substantial changes are observed at -183°C , apart from increasing H_{av} and H_{max} to the range $45\text{-}47 \text{ T}$ and $48\text{-}50 \text{ T}$ respectively.

The distribution of hyperfine fields show a prevalent $\gamma\text{-Fe}_2\text{O}_3$ phase. The broadening of the line widths ($\Gamma = 0.57 \pm 0.02 \text{ mm/s}$) is ascribed to the overlapping of the hyperfine fields or / and a distribution of particle sizes. The slight difference observed in the parameters can be regarded as due to a gradual rearrangement in the Fe ions environment, or as a result of a mixture of structures (cubic and tetragonal) depending on the conditions of the preparation.

d) Decomposition of $\text{Fe}(\text{OH})_3$ and hydrazinated $\text{Fe}(\text{OH})_3$ of iron ore

The $\text{Fe}(\text{OH})_3$ precipitated from acid extract of iron ore (section 3.2.1.a) on thermal decomposition yielded oxide and x-ray characterization revealed $\alpha\text{-Fe}_2\text{O}_3$ formation. The hydrazinated $\text{Fe}(\text{OH})_3$, after equilibration in hydrazine hydrate, on exposure to air fumed to magnetic oxide. And the x-ray characterization indicated the presence of mainly $\gamma\text{-Fe}_2\text{O}_3$.

e) Mechanism of $\gamma\text{-Fe}_2\text{O}_3$ formation.

The results that have been discussed so far can be summed up as follows.

a) α -FeOOH decomposes in air to α -Fe₂O₃ but the hydrazine method yields a mixture of α -Fe₂O₃ and γ -Fe₂O₃.

b) γ -FeOOH thermally and the hydrazinated γ -FeOOH autocatalytically decompose giving mainly γ -Fe₂O₃. Hydrazine method, however, gives better quality oxide of σ_s 71.65 emu/g, while air decomposition product shows σ_s of mere 19.20 emu/g.

c) Amorphous FeOOH dehydrates in air to α -Fe₂O₃ but the hydrazine method produces γ -Fe₂O₃ of better quality.

d) Decomposition of these iron oxyhydroxides in different controlled atmospheres, however, gives some mixed results whose analyses require additional investigations to make any conclusion, as regarding the influence of water vapour in stabilizing the γ -Fe₂O₃. However, the different atmospheric decomposition of γ -FeOOH and amorphous FeOOH did indicate an improvement in the quality of γ -Fe₂O₃ that formed over that of simple air, as well as, N₂/H₂O/air atmospheres. The γ -Fe₂O₃ obtained in N₂/H₂O/air also found to show higher saturation magnetization value than that formed in ordinary air decomposition of γ -FeOOH and amorphous FeOOH.

Thus, the hydrazine method seems to be easily giving γ -Fe₂O₃ from iron hydroxides or oxyhydroxides.

γ -FeOOH consists of corrugated sheets of edge and corner shared octahedra of FeO₄X₂ (where X = OH). The layered structured γ -FeOOH with the hydrogen bonds in between the layers transform topotactically into γ -Fe₂O₃. Here,

the [100], [010] and [001] axes of γ -FeOOH become [001], [110] and [1 $\bar{1}$ 0] of γ -Fe₂O₃ [342].

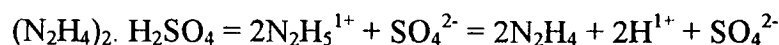
The topotactic change consists of two parts, geometrical and chemical. The geometrical part classifies the way in which one lattice can be transformed into another, while retaining the original network of the structure. The chemical part, on the other hand, accounts for the possibility of replacing one kind of atom by another and also the increase or lowering the total number of atoms per unit of lattice. Thus, in general, topotactic changes involving the loss or gain of atoms will leave the main symmetry directions of the crystals unchanged. But, it also seems possible that an asymmetrical crystals may, by loss of its atoms, transform into a form of higher symmetry.

γ -FeOOH on hydrazination, however, found to turn black in colour and the product is magnetic in nature containing 41.0 % of FeO in it (Table 3.2) and the rest being Fe₂O₃. A ferrous- ferric oxide is, thus, formed from γ -FeOOH in hydrazine atmosphere which on exposure to air fumed giving γ -Fe₂O₃. Thus, a ferrous- ferric oxide of Fe₃O₄ type is the intermediate phase in the hydrazine method of preparation of γ -Fe₂O₃ from γ -FeOOH.

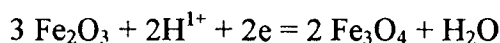
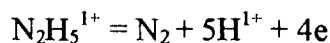
Amorphous FeOOH too turns black on hydrazine equilibration and fumes when exposed to air giving a dull brown γ -Fe₂O₃. But the intermediate powder had 1.2 % FeO. Here, Fe₃O₄ type of phase that formed might have transformed immediately into γ -Fe₂O₃. α -FeOOH, on the other hand, did not show any change in colour on hydrazination, but it too fumed when exposed to air forming a mixture of α -Fe₂O₃ and γ -Fe₂O₃.

Electrical conductivity studies too indicate the possibility of formation of Fe₃O₄ type of phase during hydrazine equilibration of the iron oxyhydroxide and the subsequent decomposition of it to γ-Fe₂O₃ on exposure to air.

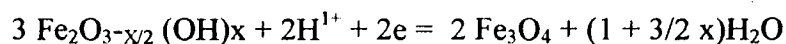
Hydrazine is a reducing agent and x-ray diffraction done on the product of hydrazine decomposition on Fe₂O₃ found [53] to convert it into magnetite, Fe₃O₄. Hydrazine sulphate decomposition in an alkaline medium on Fe₂O₃ also converted the oxide into magnetite and here the hydrazine sulphate first dissociates [421-422] into hydrazine,



The reduction of Fe₂O₃ is then a coupled reaction, as given below,



similarly a hydrous ferric oxide decomposes hydrazine sulphate and transforms the oxide into magnetite [423] as follows,



The ferrous-ferric intermediate that formed as intermediate in the decomposition of hydrazinated γ-FeOOH in the present studies finally transform into γ-Fe₂O₃. Thus, a Fe₃O₄ type of spinel is the intermediate product of hydrazination of γ-FeOOH and amorphous FeOOH which easily yields spinel γ-Fe₂O₃.

Thus, there are different mechanisms that occur in the transformation of γ-FeOOH and hydrazine modified γ-FeOOH into γ-Fe₂O₃. Simple topotactic thermal dehydration of γ-FeOOH directly yields γ-Fe₂O₃, while hydrazine method produces the oxide through an intermediate phase Fe₃O₄. However, the oxidation of

Fe_3O_4 is initiated just on exposure of the hydrazinated $\gamma\text{-FeOOH}$ in air. Commercial preparation of $\gamma\text{-Fe}_2\text{O}_3$ from $\alpha\text{-FeOOH}$ is a multistage process and every step requires a laborious control of atmosphere. In this regard, the hydrazine method of the synthesis of $\gamma\text{-Fe}_2\text{O}_3$ is simple and the quality of the oxide is also comparable with the oxide obtained by the cumbersome commercial process.

3.3.2 Conclusions

1. $\gamma\text{-FeOOH}$, $\alpha\text{-FeOOH}$ and amorphous FeOOH synthesized by solution method from reported procedures are found to contain water of hydration in their structure and accordingly formulas, $\gamma\text{-FeOOH}\cdot 0.3\text{H}_2\text{O}$, $\alpha\text{-FeOOH}\cdot 0.2\text{H}_2\text{O}$ and amorphous $\text{FeOOH}\cdot 0.8\text{H}_2\text{O}$ respectively, are fixed for these oxyhydroxides.
2. Both $\alpha\text{-FeOOH}$ and amorphous FeOOH dehydrate in air to $\alpha\text{-Fe}_2\text{O}_3$ at 300°C , while $\gamma\text{-FeOOH}$ topotactically transforms mainly into $\gamma\text{-Fe}_2\text{O}_3$.
3. Hydrazine equilibrated $\gamma\text{-FeOOH}$ and amorphous FeOOH found to uptake 10 % hydrazine and autocatalytically decompose to $\gamma\text{-Fe}_2\text{O}_3$. On the other hand, $\alpha\text{-FeOOH}$ take up just 1 % hydrazine when equilibrated in a desiccator containing hydrazine hydrate, but on exposure to air it fumes and yields a mixture of $\alpha\text{-Fe}_2\text{O}_3$ and $\gamma\text{-Fe}_2\text{O}_3$.
4. The topotactic dehydration of $\gamma\text{-FeOOH}$ directly yields $\gamma\text{-Fe}_2\text{O}_3$, while the hydrazine equilibrated $\gamma\text{-FeOOH}$ autocatalytically decomposes and forms $\gamma\text{-Fe}_2\text{O}_3$ through an intermediate phase Fe_3O_4 .

5. The saturation magnetization value of the $\gamma\text{-Fe}_2\text{O}_3$ obtained by hydrazine method from $\gamma\text{-FeOOH}$ is close to the reported value of σ_s , 71-74 emu/g. The simple dehydration of $\gamma\text{-FeOOH}$ yields the oxide of σ_s value of just 19.20 emu/g.
6. Commercial preparation of $\gamma\text{-Fe}_2\text{O}_3$ from $\alpha\text{-FeOOH}$ is a multistep reaction requiring a rigid control of atmosphere in every step, while hydrazine method to prepare the oxide is simple and single step from $\gamma\text{-FeOOH}$. Commercial method too adopts the formation of $\gamma\text{-Fe}_2\text{O}_3$ via Fe_3O_4 . An intermediate phase Fe_3O_4 is essential in the formation of better quality $\gamma\text{-Fe}_2\text{O}_3$.
7. Iron hydroxide, $\text{Fe}(\text{OH})_3$ precipitated by NaOH from acid extract of iron ore decomposes to $\alpha\text{-Fe}_2\text{O}_3$ in air, while the hydrazinated $\text{Fe}(\text{OH})_3$ yields mainly $\gamma\text{-Fe}_2\text{O}_3$ on autocatalytic decomposition in ordinary atmosphere.

**Synthesis of γ -Fe₂O₃ from iron (II) carboxylato-
hydrazinates**

Synthesis of γ -Fe₂O₃ from iron (II) carboxylato-hydrazinates

Metal carboxylates are widely studied precursors in the synthesis of metal oxides. Mixed metal carboxylates by controlling methods of synthesis are further giving scope for preparing, by simple thermal decomposition, a wide variety mixed metal oxides of different crystal structure such as, spinels of different magnetic properties and, perovskites with diversent properties like dielectric, semi conducting, magnetic and super conducting of technological importance. Simple iron oxalate, ferrous oxalate dihydrate, FeC₂O₄.2H₂O, has been investigated by many researchers and the results of this is taken as model in understanding the preparation, characterization and thermal decomposition of other iron carboxylates : Mono or dicarboxylates or higher carboxylates.

However, in our present investigations we are aiming at an easy synthesis of γ -Fe₂O₃. We have selected iron carboxylates which have been systematically synthesized by research group in our laboratory and others. During the very first attempt to prepare γ -Fe₂O₃ from, ferrous oxalate dihydrate, by Rane et al [264], they considered the various aspects in controlling the preparation of this oxide. Especially, a controlled atmosphere of water vapour transforms the FeC₂O₄.2H₂O to mainly γ -Fe₂O₃, while simple air decomposition yields the thermodynamically more stable iron oxide, α -Fe₂O₃. The control of water vapour during decomposition of other iron (II) carboxylates [272 - 277] such as, ferrous fumarate, ferrous succinate, ferrous malonate, ferrous tartrate, ferrous maleate and ferrous malate, also yielded γ -Fe₂O₃, on the other hand, air decomposition of all carboxylates ended into α -Fe₂O₃.

But, then, a simple modification of FeC₂O₄.2H₂O in our laboratory by Moye, Rane & Kamat Dalal [278] on hydrazination yielded FeC₂O₄.N₂H₄ and FeC₂O₄.2N₂H₄ and their decomposition in ordinary atmosphere easily produced γ -Fe₂O₃. Such hydrazine methods of synthesis of metal oxides and mixed metal oxides of technological importance [424,-430] are attracting attention of many researchers. As we were looking for a simple method to synthesize γ -Fe₂O₃ useful in ferrites synthesis, the hydrazine method seems to be a way out. Already we have used such method in easy synthesis of γ -Fe₂O₃ from iron hydroxides from iron ore rejects and iron oxyhydroxides again obtained from iron hydroxides from iron ore rejects in part I of this chapter.

To explore the importance of γ -Fe₂O₃ in ferrites synthesis it is better to consider different sources for γ -Fe₂O₃ and hence, we decided to prepare γ -Fe₂O₃ from iron (II) carboxylates, by hydrazine method. In this chapter we are presenting our results on the synthesis, characterization and decomposition of iron (II) carboxylato-hydrazinates: ferrous fumarato-hydrazinates, ferrous succinato-hydrazinates ferrous malonato-hydrazinates, ferrous tartrato-hydrazinate, ferrous maleato-hydrazinate and ferrous malato-hydrazinate. No such hydrazinate complexes of the iron (II) carboxylates are observed in the literature.

3.4 Experimental :Preparation, characterization and decomposition

3.4.1 Synthesis of Iron (II) Carboxylato-hydrazinates

Both solution and equilibration methods similar to the one used for ferrous oxalato-hydrazinates [268] have been adopted to synthesize iron (II) carboxylato-hydrazinates.

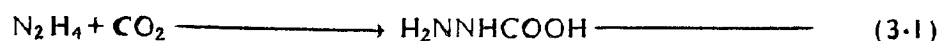
Ferrous fumarato-hydrazinate, ferrous succinato-hydrazinate, ferrous malonato-hydrazinate, ferrous maleato-hydrazinate and ferrous malato-hydrazinate were all prepared by taking the required quantities of the sodium salts of their respective carboxylic acids in hydrazine hydrate, N₂H₄.H₂O (99 - 100 %). The mixture were stirred well in an inert atmosphere for 2-3 hours. To the well stirred solution a freshly prepared ferrous chloride solution, obtained from pure iron (99.99%), was added slowly and the stirring was continued further for an hour.

Caution : Hydrazine and hydrazine derivatives are carcinogens. Handle them carefully.

a) Solution method

i. Ferrous fumarate - hydrazinate (FFH)

0.5 M Sodium fumarate was mixed with hydrazine hydrate (99-100 %) in the molar ratio of 1:4 and stirred on a magnetic stirrer for one and half hour in the presence of nitrogen atmosphere, bubbling at the rate of 10 -15 bubbles / min. The use of N₂ atmosphere was to avoid the atmospheric CO₂ from reacting with hydrazine and forming carbazic acid [279] as per the equation,



To this solution of sodium fumarate and hydrazine hydrate, a freshly prepared 0.5 M FeCl₂ solution was slowly added with vigorous stirring, in presence of N₂ atmosphere. Yellow coloured ferrous fumarate - hydrazinate slowly starts precipitating. The precipitate was then extracted with alcohol and carefully filtered on the suction pump and dried with ether.

It has been reported [170] that if a strong suction is applied for longer duration, precursors may catch fire. During the stirring of sodium fumarate and hydrazine hydrate, some fumes of hydrazine were present in the upper part of the container and on addition of FeCl₂ solution, it reacted directly with hydrazine fumes forming a dark blue coloured complex. This complex gets mixed with the yellow precipitate of FFH, thus, contaminating it. In order to avoid this contamination, N₂ gas was bubbled at a faster rate before chloride solution was added.

ii. Ferrous succinato - hydrazinate (FSH)

An aqueous solution of sodium succinate and hydrazine hydrate in the molar ratio of 1:4 was stirred for 1¹/₂ h. in N₂ atmosphere at room temperature and then a freshly prepared ferrous chloride solution was run down into the mixture and continued stirring in N₂ atmosphere for half an hour more. Pale yellow coloured precipitate obtained was filtered, washed with alcohol and dried with ether.

iii. Ferrous malonato - hydrazinate (FMH)

0.5 M Malonic acid was stirred with hydrazine hydrate in the molar ratio of 1:4, in N₂ atmosphere. Freshly prepared ferrous chloride solution was then added slowly to the mixture with constant stirring. The pale yellow coloured precipitate was extracted in alcohol, filtered, washed with alcohol and dried with ether.

iv. Ferrous maleato - hydrazinate (FEH)

Sodium maleate (0.5M) and hydrazine hydrate in the molar ratio of 1:4, were stirred for 1¹/₂ h. in N₂ atmosphere. To this, a freshly prepared 0.5M ferrous chloride solution was added, drop by drop, with constant stirring in N₂ atmosphere. The yellow coloured precipitate obtained was filtered, washed with alcohol and dried with ether.

v. Ferrous malato - hydrazinate (FLH)

Sodium malate solution was mixed with hydrazine hydrate in the molar ratio of 1:4 and stirred for 1¹/₂ h in an inert atmosphere of N₂. Freshly prepared solution of ferrous chloride was then run down into the mixture. The stirring was continued

in N_2 atmosphere for half an hour more. The yellow coloured precipitate formed, was extracted with alcohol, filtered and dried with ether.

b) Equilibration method

i. Ferrous tartrato - hydrazinate (FTH)

Ferrous tartrato - hydrazinate was prepared by hydrazine equilibration method. First ferrous tartrate one and half hydrate was prepared by adding sodium tartrate to an aqueous ferrous ammonium sulphate in an inert atmosphere, with constant stirring. Pale greenish yellow precipitate that formed was filtered, washed with little warm water and then dried.

The dry hydrated ferrous tartrate was then placed in a petridish and kept in a desiccator containing hydrazine hydrate (99-100%). Hydrazine hydrate vapours got equilibrated on the ferrous tartrate thus forming ferrous tartrato - hydrazinate complex.

All these iron carboxylato - hydrazinate complexes were filled in the air tight sample tubes and stored in a vacuum desiccator.

3.4.2 Characterization.

a) Chemical analysis

I. Hydrazine estimation

Hydrazine content of all the complexes was analyzed titrimetrically using KIO_3 as titrant [299].

ii. C, H, N analysis

The percentages of carbon and hydrogen was estimated by a standard technique.

iii. Analysis of iron content

The percentage of iron was determined by the standard potassium dichromate method [299].

b) Infra red analysis

The infra red spectra of all the complexes and their thermal products were taken soon after the preparation of the sample on Shimadzu FTIR, model 8101 A.

c) Density measurement

The density of the complexes and their final thermal products was determined at room temperature using carbon tetrachloride as the medium.

3.4.3 Thermal decomposition studies

a) Thermogravimetric analysis (TGA) and Differential thermal analysis (DTA)

Simultaneous TG and DTA in air was carried out on STA 1500 instrument from RT to 600⁰C of all the complexes. The heating rate of 10 -15⁰/min. was maintained.

b) Isothermal weight loss studies

Isothermal weight loss studies were carried out at various predetermined temperatures, based on TGA and DTA traces, by using a platinum crucible. The

isothermal products obtained at different interval of temperature were chemically analysed for the hydrazine content.

c) Autocatalytic decomposition

All these iron (II) carboxylato - hydrazinates decompose autocatalytically. Here, the dry samples were spread over a petridish and a burning splinter was brought near to it when the small portion of it caught fire. A red glow that formed immediately spreads over the entire bulk, completing the decomposition in an ordinary atmosphere.

3.4.4 Phase identification and magnetic studies of the thermal products

a) X - ray analysis

X - ray powder diffraction (XRD) studies were carried on Rigaku D MAX II, X - ray diffractometer, using Cu and Fe targets on all the iron (II) carboxylato - hydrazinate complexes. Autocatalytically decomposed products of the complexes were also studied by XRD and the phase identification was done by comparing the observed d-values with the JCPDS files [408-413].

b) Magnetic Characterization

Saturation magnetization values of the autocatalytically decomposed end products of the complexes were measured on a high field hysteresis loop tracer that described by Likhite et al [304], using Ni as the standard substance.

3.4.5 Microstructure analysis

Microstructure of the autocatalytically decomposed end product of the complexes were studied using scanning electron microscope (SEM). SEM micrographs were taken using a well polished pellet surface and were used to compute average grain size.

3.5 Results and Discussion

a) Fixation of chemical formulas of iron (II) carboxylato - hydrazinates

All the precursors were characterised by chemical analysis, IR analysis and density measurements. The characterisation was supported by thermal studies and the formula for each complex was identified.

i. Infra red analysis

The IR spectra of FFH, FSH, FEH and FLH are given in fig 3.7 a & b, while that of FMH and FTH are given in fig 3.7 c. The asymmetric and symmetric stretching frequencies of carboxylate ions [Table 3.4] in all the complexes are seen in the range of $1610-1624\text{ cm}^{-1}$ and $1377-1410\text{ cm}^{-1}$, respectively, with $\Delta\nu$ ($\nu_{\text{asy}}-\nu_{\text{sym}}$) separation of $\sim 210-240\text{ cm}^{-1}$, indicating the monodentate linkage of both carboxylate groups in the dianions [384-387]. Thus the fumarate, succinate, malonate, tartrate, maleate and malate dianions in these complexes coordinate to the metal as bidentate ligand via both the carboxylate groups.

The observed N-N stretching frequencies in the range of $960-980\text{ cm}^{-1}$ for all these complexes except ferrous tartrato-hydrazinate (FTH) reveal clearly that the

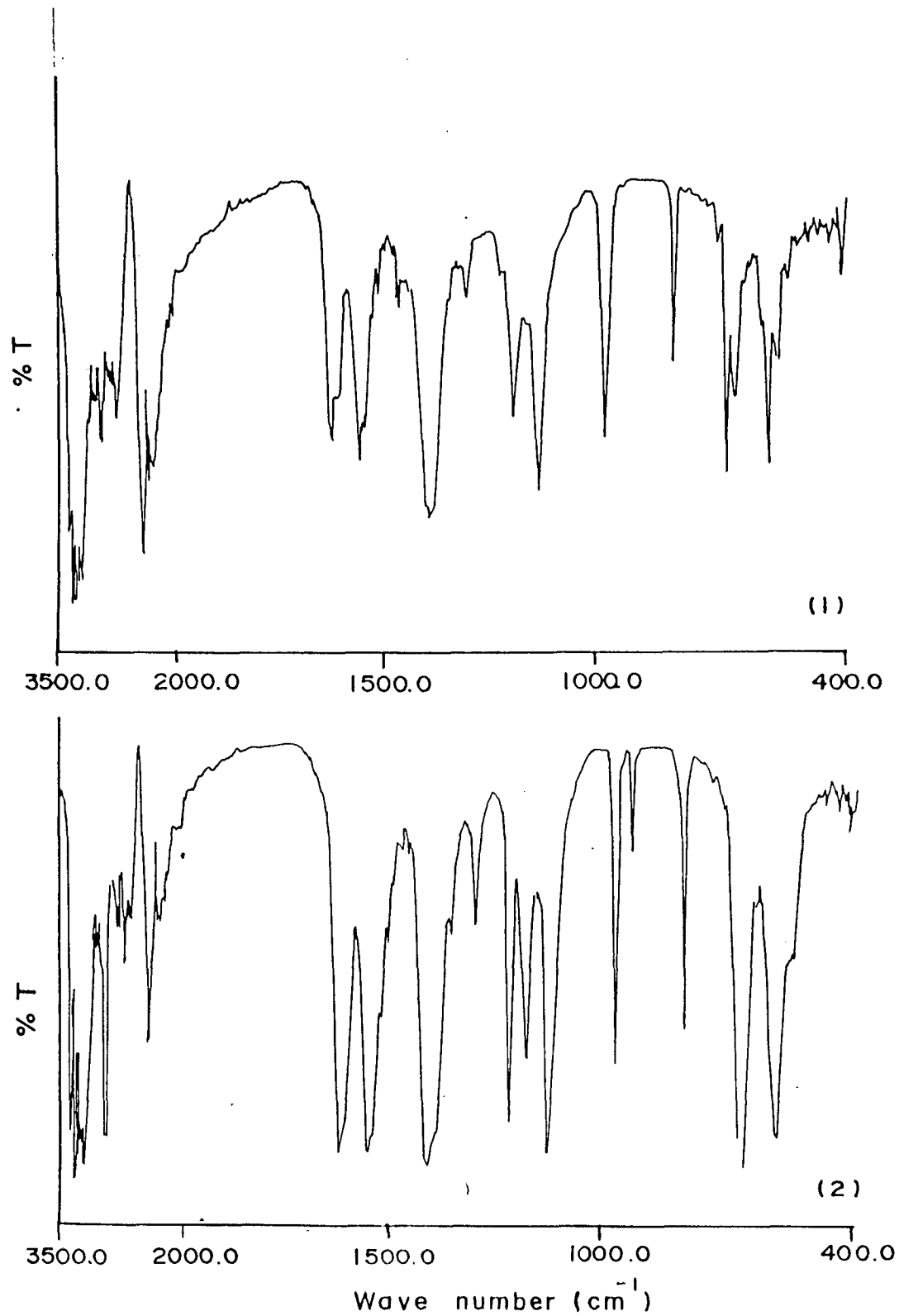


FIG. 3.7 a) Infra red spectra of 1) FFI and 2) FSH

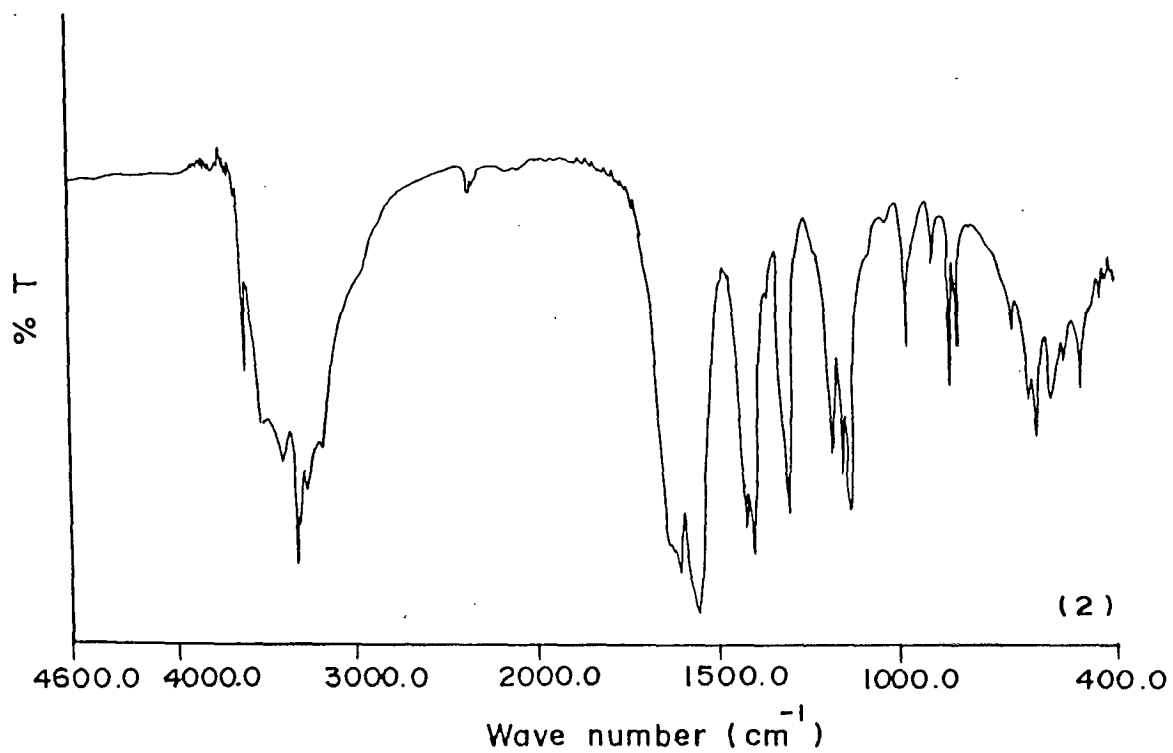
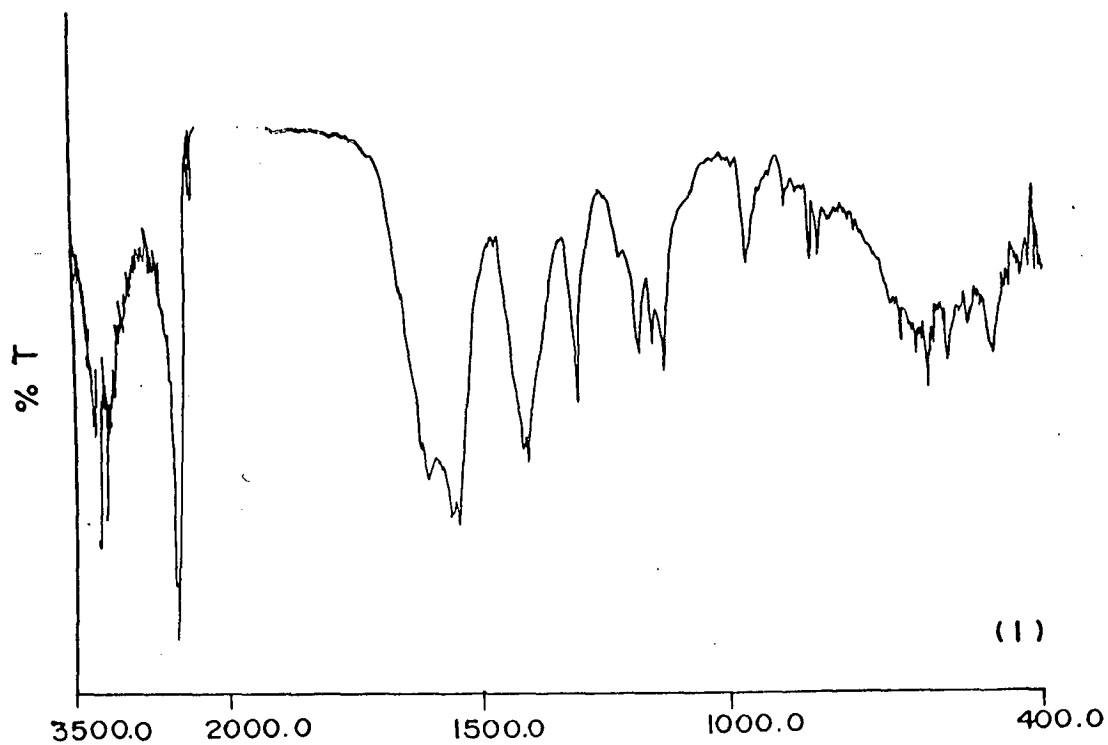


FIG. 3.7 b) Infra red spectra of 1) FEH and 2) FLH

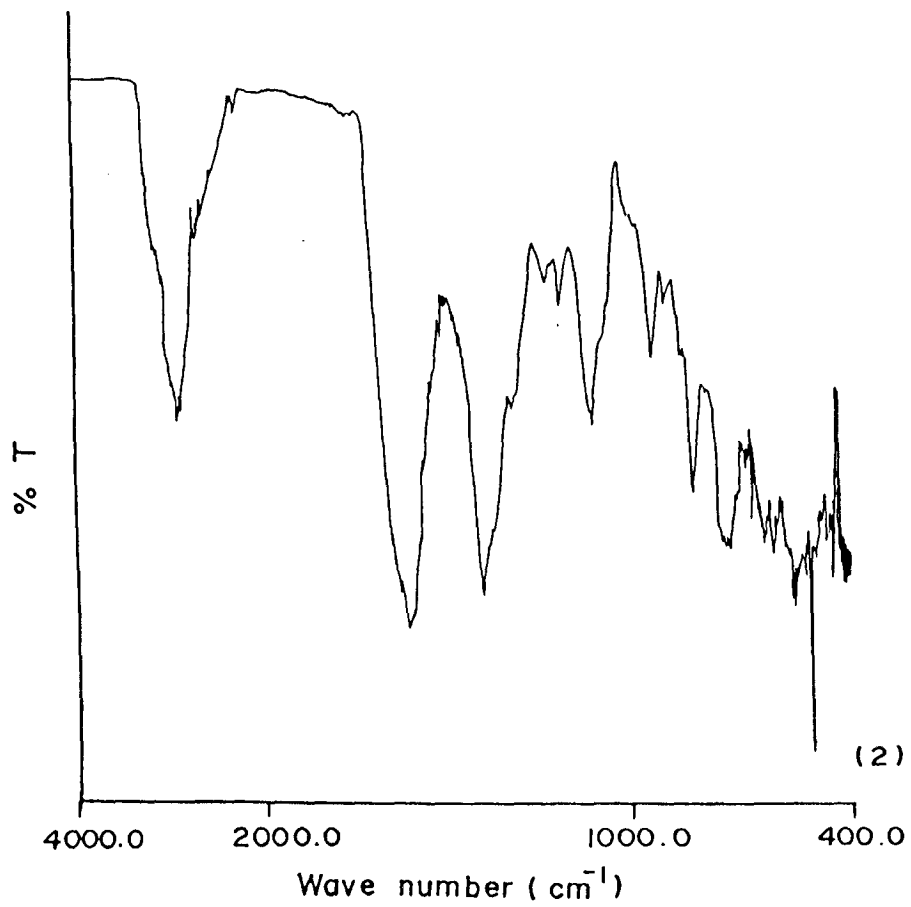
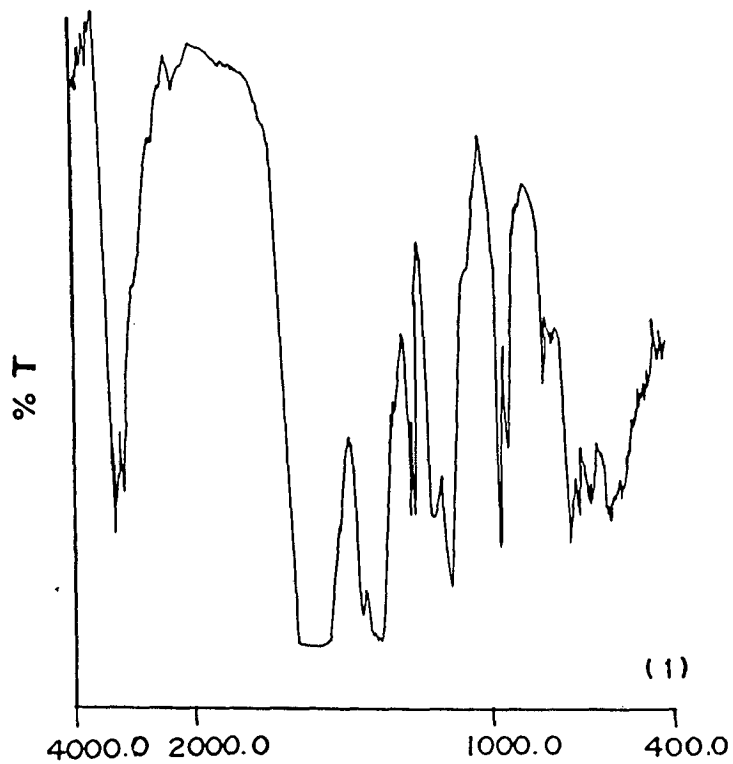


FIG. 3.7 c) Infra red spectra of 1)FMH and 2)FTH

hydrazine moieties are present as bridging bidentate ligands [278,384-386]. A monodentate link of hydrazine with iron is seen $\nu(\text{N-N}) \sim 930 \text{ cm}^{-1}$ for FTH. Ferrous malonato-hydrazinate (FMH), however, has both monodentate and bidentate linkage of hydrazine with the metal [Table 3.4]. These results suggest that the carboxylato-hydrazinate complexes of iron(II) carboxylato - hydrazinate complexes of iron(II) are formed.

ii. Chemical analysis

The percentages of hydrazine, iron, carbon and hydrogen of all the iron (II) carboxylato - hydrazinates are given in Table 3.4

The ferrous fumarato-hydrazinate was found to contain 27.16% hydrazine, 24.0% iron, 19.30% carbon and 3.96 % Hydrogen, while in ferrous succinato - hydrazinate the percentages of N_2H_4 , Fe, C and H are, 27.52, 23.87, 20.3 and 3.67, respectively. The percentage of N_2H_4 , Fe, C and H was found to be 20.43, 24.25, 17.90 and 3.73, respectively, in ferrous malonato-hydrazinate. The observed percentages of hydrazine, iron, carbon and Hydrogen in ferrous tartrato hydrazinate are, 12.41, 25.5, 17.22 and 3.53, respectively. Ferrous maleato-hydrazinate and ferrous malato-hydrazinate was found to contain 26.74 and 25.12 percent of N_2H_4 and 24.67 and 22.80 percent of Fe, respectively.

iii. Total weight loss

The observed total weight loss for FFH, FSH, FMH, FTH, FEH and FLH are 65.86, 65.94, 64.30, 68.54, 65.85 and 65.5 percent, respectively (Table 3.4). Thus, from the data of observed on the total weight loss and chemical analyses (section 3.8.1), the following chemical formula are fixed for the iron (II) carboxy-

TABLE 3.4 CHEMICAL ANALYSIS, DENSITY, I.R., TOTAL WEIGHT LOSS OF IRON (II) CARBOXYLATO-HYDRAZINATES

Hydrazinates	Chemical analysis in %		Density g cm ⁻³	Infrared data, cm ⁻¹							Total Weight Loss, %				
	Obsd.	Calcd.		$\delta(o-c-o)$	$\nu(N-N)$	$\delta(NH_2)$	$\nu_c(o-c-o)$	$\nu_{asv}(o-c-o)$	$\nu(NH)$	$\nu(H_2O)$	Obsd.	Calcd.			
FeC ₄ H ₂ O ₄ · 2N ₂ H ₄ (FFH)	N ₂ H ₄	27.16	27.35	1.38	800	960	1165	1377	1650	3273	--	65.86	65.81		
	Fe	24.00	23.88												
	C	19.30	20.52			980									
	H	3.96	4.27												
FeC ₄ H ₄ O ₄ · 2N ₂ H ₄ (FSH)	N ₂ H ₄	27.52	27.11	1.18	800	964	1126	1350	1624	3262	--	65.94	66.10		
	Fe	23.87	23.68												
	C	20.30	20.35			1176									
	H	3.67	5.00			3310 3350									
FeC ₃ H ₂ O ₄ · 1 1/2 N ₂ H ₄ ·H ₂ O (FMH)	N ₂ H ₄	20.43	21.46	1.51	795	962	1132	1370	1620	3306	3170	64.30	64.35		
	Fe	24.25	24.95												
	C	17.90	16.08			936									
	H	3.73	4.46												
FeC ₄ H ₄ O ₆ · N ₂ H ₄ ·H ₂ O (FTH)	N ₂ H ₄	12.41	12.61	1.22	820	931	1184	1320	1600	3150	--	68.54	68.56		
	Fe	25.50	25.17												
	C	17.22	18.90												
	H	3.53	3.94												
FeC ₄ H ₂ O ₄ · 2N ₂ H ₄ (FEH)	N ₂ H ₄	26.74	27.37	1.9	835	970	1130	1305	1620	3330	-	65.85	65.85		
	Fe	24.67	23.88												
						1150 1175								1395	3260
FeC ₄ H ₄ O ₅ · 2N ₂ H ₄ (FLH)	N ₂ H ₄	25.12	25.43	1.86	828	970	1128	1300	1611	3397	-	68.5	68.32		
	Fe	22.80	22.16												
						1150 1175								1390	3252

lato-hydrazinates.

(1) Ferrous fumarato-hydrazinate (FFH) - $\text{FeC}_4\text{H}_2\text{O}_4 \cdot 2\text{N}_2\text{H}_4$

A chemical formula, $\text{FeC}_4\text{H}_2\text{O}_4 \cdot 2\text{N}_2\text{H}_4$ is fixed for ferrous-fumarato-hydrazinate. The hydrazine content experimentally observed (Table 3.4) is 27.16% and the calculated value, based on the above formula, is 27.35%. The experimental iron, carbon and hydrogen percentages too match closely with the calculated ones, 24.00 (23.88), 19.30 (20.52) and 3.96 (4.27), respectively. The values in bracket are the calculated ones and, hereafter, the calculated values will be given in the bracket, soon after the experimentally observed values, for ready reference. The total mass loss of 65.86% observed is close to the calculated value of 65.81%, based on the above formula fixed for ferrous fumarato-hydrazinate (FFH).

(2) Ferrous succinato-hydrazinate (FSH)- $\text{FeC}_4\text{H}_4\text{O}_4 \cdot 2\text{N}_2\text{H}_4$

A formula of $\text{FeC}_4\text{H}_4\text{O}_4 \cdot 2\text{N}_2\text{H}_4$ for ferrous succinato-hydrazinate is arrived at from the percentage values of hydrazine, 27.52 (27.11), carbon 20.30 (20.35); hydrogen 3.67 (5.0), total mass loss, 65.94 (64.10).

(3) Ferrous malonato-hydrazinate (FMH) - $\text{FeC}_3\text{H}_2\text{O}_4 \cdot 1\frac{1}{2}\text{N}_2\text{H}_4 \cdot \text{H}_2\text{O}$

A chemical formula of $\text{FeC}_3\text{H}_2\text{O}_4 \cdot 1\frac{1}{2}\text{N}_2\text{H}_4 \cdot \text{H}_2\text{O}$ is assigned to ferrous malonato-hydrazinate, based on the different constituents, observed and calculated : hydrazine, 20.43 (21.46) ; iron, 24.25 (24.95) ; carbon, 17.90 (16.08); hydrogen, 3.73 (4.46) and total mass loss of 64.30 (64.35).

4. Ferrous tartrato-hydrazinate (FTH) - $\text{FeC}_4\text{H}_4\text{O}_6 \cdot \text{N}_2\text{H}_4 \cdot \text{H}_2\text{O}$

A chemical formula of $\text{FeC}_4\text{H}_4\text{O}_6 \cdot \text{N}_2\text{H}_4 \cdot \text{H}_2\text{O}$ is fixed for ferrous tartrato - hydrazinate. The observed and calculated percentages of the different constituents show a close values : hydrazine, 12.41 (12.61) ; iron, 25.5 (25.17) ; carbon, 17.22 (18.90); hydrogen, 3.53 (3.94). The total mass loss of 68.54% is also close to the calculated value of 68.56% suggesting that the formula is correct.

5. Ferrous maleato-hydrazinate (FEH) - $\text{FeC}_4\text{H}_2\text{O}_4 \cdot 2\text{N}_2\text{H}_4$

The observed contents of N_2H_4 - 26.74%, Fe - 24.67% and a total mass loss of 65.85%, match well with the calculated values of 27.88% for N_2H_4 , 23.88% for Fe and total weight loss 65.85%, using the formula for ferrous maleato-hydrazinate as $\text{FeC}_4\text{H}_2\text{O}_4 \cdot 2\text{N}_2\text{H}_4$.

6. Ferrous malato-hydrazinate (FLH) - $\text{FeC}_4\text{H}_4\text{O}_5 \cdot 2\text{N}_2\text{H}_4$

From the observed contents of N_2H_4 - 25.12%, Fe - 22.80% and a total mass loss of 68. a formula $\text{FeC}_4\text{H}_4\text{O}_5 \cdot 2\text{N}_2\text{H}_4$ is assigned to ferrous malato-hydrazinate. The calculated values for these constituents compare well (Table3.4) with the observed ones, indicating the correctness of the formula fixed by us.

Among all these complexes the FMH and FTH show a water of crystallization in them.

iv. Pycnometric Density

The densities of all the complexes are given in the table 3.4. The densities of FFH, FSH, FMH, FTH, FEH and FLH are 1.38, 1.18, 1.51, 1.22, 1.9 and 1.86, respectively.

b) Formation of γ -Fe₂O₃ from iron (II) carboxylato-hydrazinates

i. Thermal analysis and hydrazine estimation of thermal products

All iron (II) carboxylato-hydrazinates decompose in air, thermally and autocatalytically, to iron oxide of magnetic in nature. XRD patterns of these products match well with the pattern of the standard commercial γ -Fe₂O₃ and d_{hkl} values of these compare closely with the values of JCPDS files [410 - 411] for γ -Fe₂O₃.

All iron (II) carboxylato-hydrazinates lose weight continuously in air when heated from room temperature (RT) to 700^oC, showing no definite steps on the TG trace. DTA, however, indicates a few intense exothermic peaks in this temperature range, thereby, suggesting a step wise thermal decomposition. (Fig 3.8) In order to correspond these DTA peaks with the TG values, a rough weight loss steps were marked in certain temperature ranges and the results are compiled in Table 3.5. An electrothermal analysis (ETA) done on FFH, FSH, FMH and FTH too gave us [300,303] some information on the step wise thermal decomposition of these complexes. To investigate thoroughly the thermal path, isothermal weight loss measurements at different predetermined temperatures were carried out and hydrazine contents were also estimated on these thermal products. The results of such studies are tabulated in Table 3.5.

FFH, FSH, FEH and FLH

Ferrous fumarato-hydrazinate (FFH), FeC₄H₂O₄.2N₂H₄, on heating in air ~ 300^oC loses 65.86% of its weight yielding iron oxide, γ -Fe₂O₃. DTA shows exothermic peaks around 178^o, 217^o and 293^oC followed by a small exothermic hump ~ 353^oC.

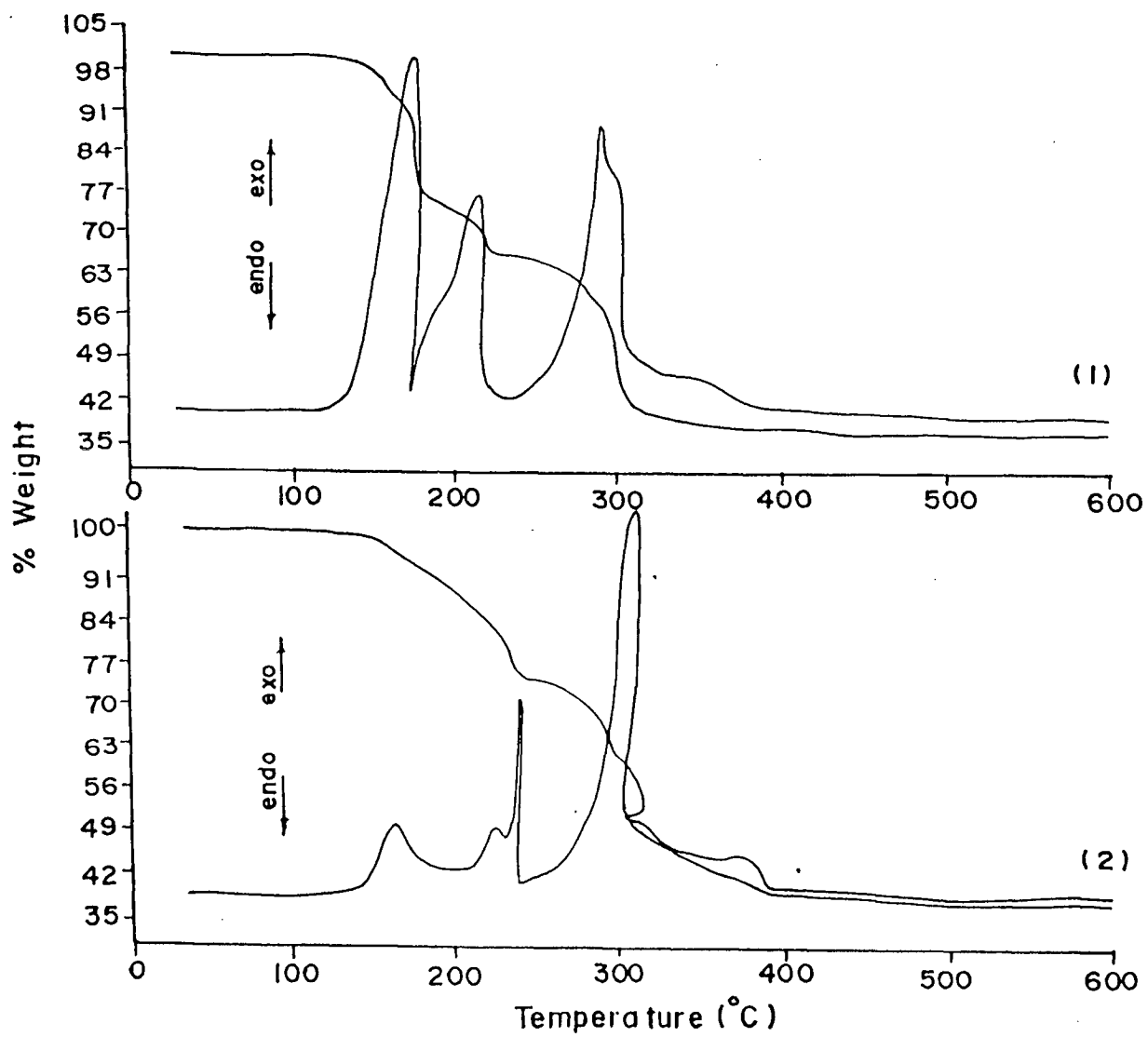


FIG. 3.8 a) TG/DTA traces of 1) FFH and 2) FSH

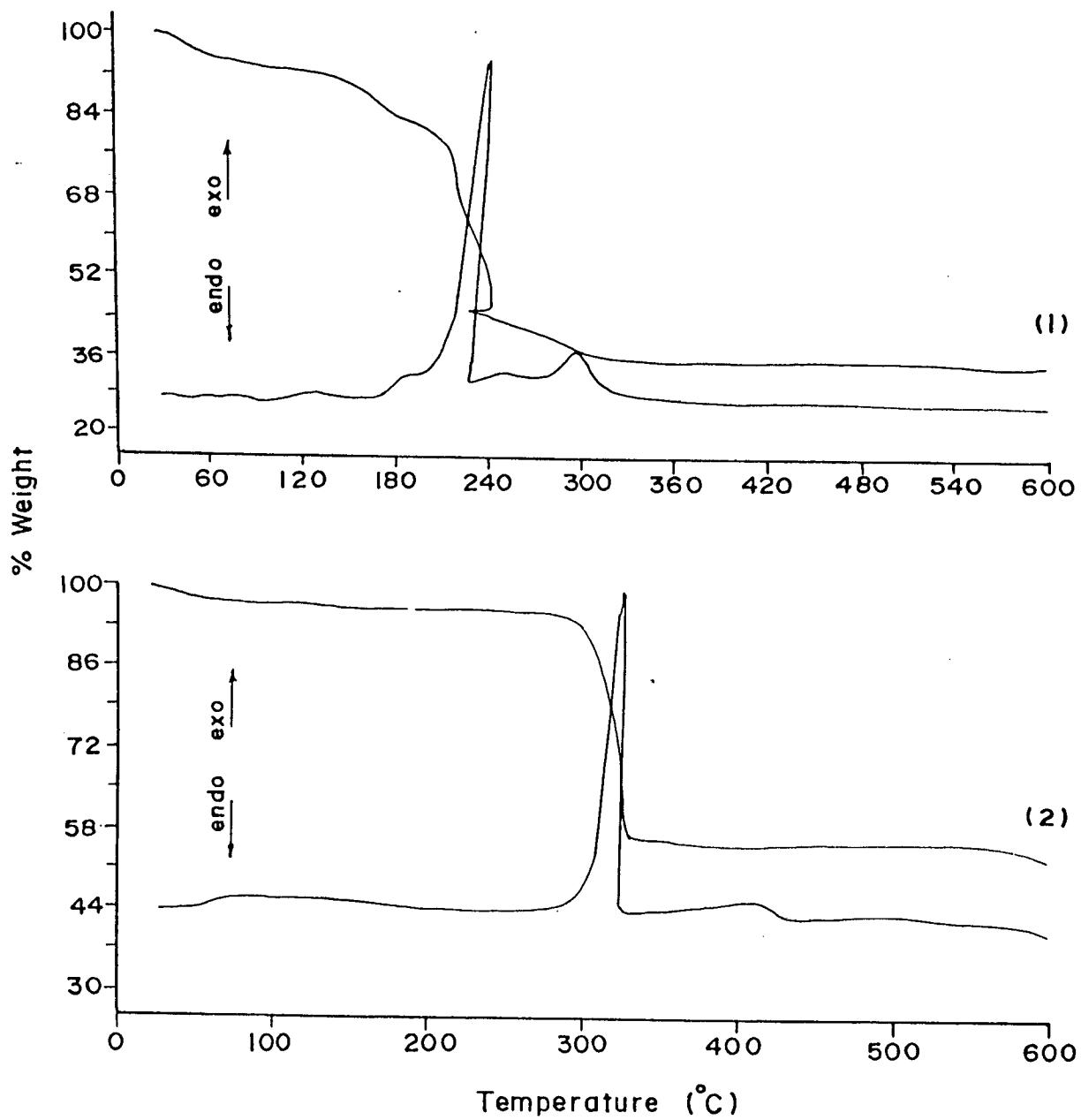


FIG. 3.8 b) TG/DTA traces of 1) FMH and 2) FTH

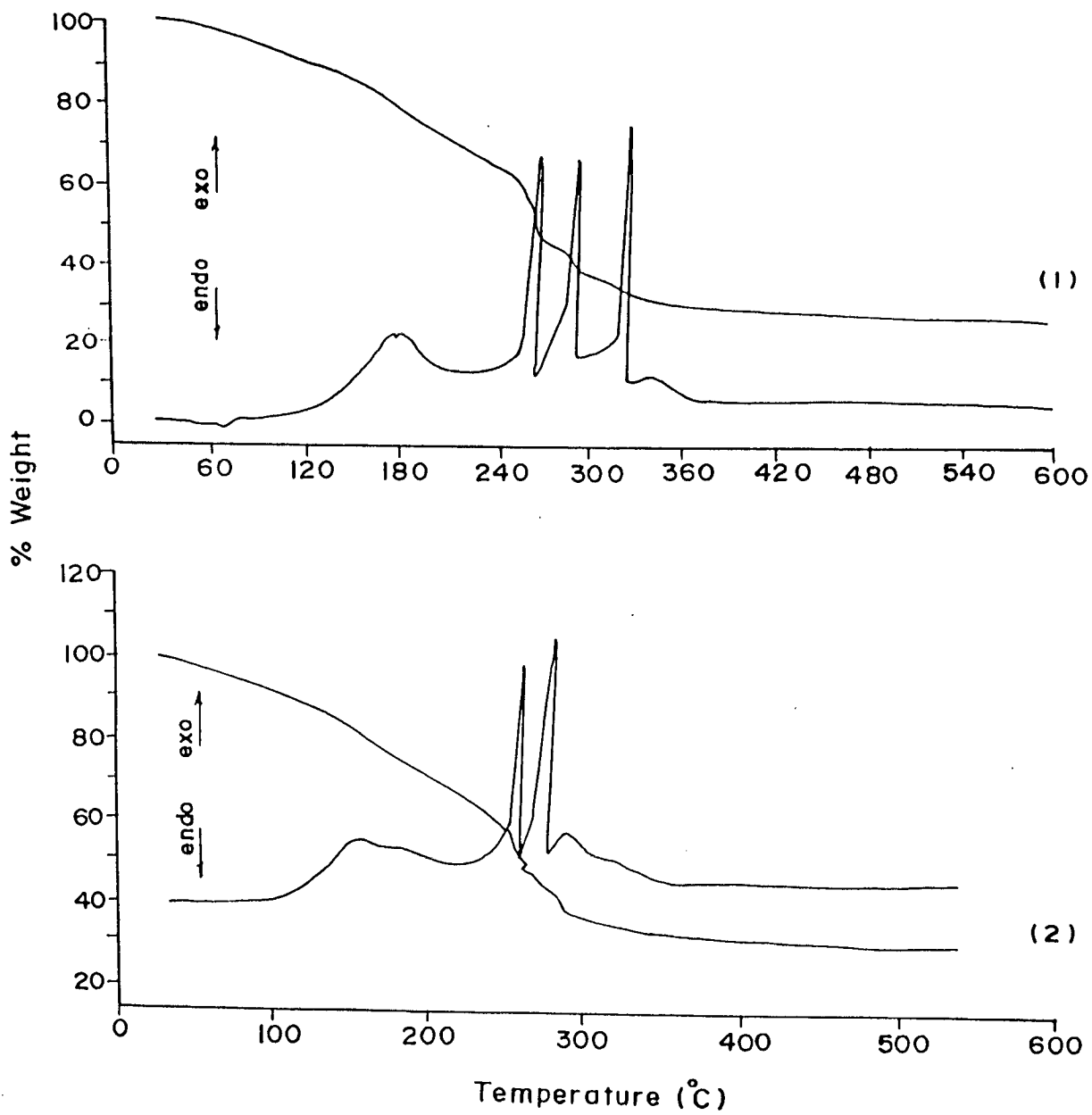


FIG. 3.8 c) TG/DTA traces of 1) FEH and 2) FLH

TABLE 3.5 Isothermal weight loss. DTA/TG analysis of iron (ii) carboxylato-hydrazinates

Hydrazinates	TG wt. loss/DTA peaks			Isothermal / Chemical analysis			Remarks	Saturation magnetization emu g ⁻¹
	Temperature range, °C	Wt. loss in %	Exo/Endo peaks at °C	Temp °C	Wt. loss %	% N ₂ H ₄		
Ferrous Fumarato-hydrazinate (FFH) FeC ₄ H ₂ O ₄ ·2N ₂ H ₄				RT	--	27.16		
				70	3.20	22.35		
	RT-182	23.63	178	90	15.35	5.44	dehydration	
			exo	110	19.50	2.40	followed by	
				200	37.65	--	decarboxylation	
	182-222	9.43	217					
			exo					
	222-308	24.83	293	310	64.15	--	γ - Fe ₂ O ₃ formation	24.44
			exo					
	308-368	4.38	353					
		exo hump						
Ferrous Succinato hydrazinate (FSH) FeC ₄ H ₄ O ₄ ·2N ₂ H ₄				RT	--	27.52		
	RT-194	9.3	161	50	1.2	27.52	dehydration	
			exo	90	21.02	3.36	followed by	
				140	25.20	--	decarboxylation	
				176	29.50	--		
	194-240	15.9	226	193	56.65	--		
			exo	248	66.25	--	γ - Fe ₂ O ₃ formation	40.02
	240-312	25.5	242					
		exo						
312-396	9.45	312	310	67.10	--			
		exo						

TABLE 3.5 (Continued)

Hydrazinates	TG wt. loss/DTA peaks			Isothermal / Chemical analysis			Remarks	Saturation magnetization emu g ⁻¹
	Temperature range, °C	Wt. loss in %	Exo/Endo peaks at °C	Temp °C	Wt. loss %	% N ₂ H ₄		
149 Ferrous malonato-hydrazinate (FMH) FeC ₃ H ₂ O ₄ 1½N ₂ H ₄ .H ₂ O	RT-148	9.87	99 endo	RT		20.43	dehydration preceded by dehydrazination which is followed by decarboxylation γ-Fe ₂ O ₃ formation	37.83
				50	7.85	16.42		
				70	9.50	16.18		
	148-178	5.80		95	12.25	17.38		
				120	18.00	13.62		
	178-216	6.52	210 exo	140	21.40	9.77		
				150	24.90	9.61		
				170	32.00	5.68		
	182	63.10						
	216-246	34.12	242 exo					
246-312	7.04	298 exo						
Ferrous Tartrato hydrazinate (FTH) FeC ₄ H ₄ O ₆ . N ₂ H ₄ .H ₂ O	RT-158	3.08		RT		12.41	dehydration preceded by dehydrazination which is followed by decarboxylation γ-Fe ₂ O ₃ formation	42.96
				62	6.00	12.41		
				80	12.35	10.73		
				102	16.00	7.13		
	278-334	56	329 exo	140	19.85	4.85		
				160	22.50	2.40		
	225	68.20	--					
	334-555		broad exo					

TABLE 3.5 (Continued)

Complex	TG wt. loss/DTA peaks			Isothermal / Chemical analysis			Remarks	Saturation magnetization emu g ⁻¹
	Temperature range, °C	Wt. loss in %	Exo/Endo peaks at °C	Temp °C	Wt. loss %	% N ₂ H ₄		
Ferrous Maleato Hydrazinate (FEH) FeC ₄ H ₂ O ₄ ·2N ₂ H ₄	RT-162	15.4		RT	--	26.74	dehydrazination followed by decarboxylation γ - Fe ₂ O ₃ formation	18.52
				58	2.5	25.44		
				96	12.05	17.66		
				156	30.05	3.73		
				172	34.00	--		
				182	55.55	--		
				225	65.40	--		
				271-293	7.52	272 exo		
				293-331	7.98	297 exo		
						331 exo		
			341 exo hump					

TABLE 3.5 (Continued)

Complex	TG wt. loss/DTA peaks			Isothermal / Chemical analysis			Remarks	Saturation magnetization emu g ⁻¹
	Temperature range, °C	Wt. loss in %	Exo/Endo peaks at °C	Temp °C	Wt. loss %	% N ₂ H ₄		
Ferrous Malato Hydrazinate (FLH) FeC ₄ H ₄ O ₅ ·2N ₂ H ₄				RT	--	25.12		
				50	6.4	21.95	dehydrazination	
	RT-151	16.42		100	17.05	10.17	followed by	
				150	30.45	2.4	decarboxylation	
	151-267	35.46	154	175	31.65	--		
			exo	200	35.70	--		
			184	225	55.15	--		
			exo	250	64.05	--		
			hump					27.22
			264				γ-Fe ₂ O ₃ formation	
	267-360	15.14	285	300	66.55			
	360-500	1.57	289					
		exo						
		324						
		exo						
		hump						

Ferrous succinato-hydrazinate (FSH), $\text{FeC}_4\text{H}_4\text{O}_4 \cdot 2\text{N}_2\text{H}_4$, decomposes to $\gamma\text{-Fe}_2\text{O}_3$ $\sim 300^\circ\text{C}$ losing 65.94% of its weight. DTA indicates exothermic peaks around 161° , 226° and 242°C followed by an exothermic hump $\sim 312^\circ\text{C}$.

Ferrous maleato-hydrazinate (FEH), $\text{FeC}_4\text{H}_2\text{O}_4 \cdot 2\text{N}_2\text{H}_4$ decomposes to $\gamma\text{-Fe}_2\text{O}_3$ by losing 65.85% of its weight. Exothermic peaks around 175° , 272° , 297° , 331°C are followed by an exothermic hump $\sim 341^\circ\text{C}$.

Ferrous malato-hydrazinate (FLH), $\text{FeC}_4\text{H}_4\text{O}_5 \cdot 2\text{N}_2\text{H}_4$, yields $\gamma\text{-Fe}_2\text{O}_3$ by losing 68.5% of its weight $\sim 300^\circ\text{C}$. An exothermic hump $\sim 324^\circ\text{C}$ is preceded by several exothermic peaks : 154° , 184° , 264° , 285° , and 289°C .

Hydrazine content estimation done on the thermal products of all these iron (II) carboxylato-hydrazinates indicated that the hydrazine present in them is found to be released $\sim 110^\circ$ in FFH, $\sim 90^\circ$ in FSH, $\sim 156^\circ$ in FEH, and $\sim 150^\circ\text{C}$ in FLH (Table 3.5). The total weight loss of all these unhydrazinated products then completed $\sim 300^\circ\text{C}$, yielding poorly magnetic Fe_2O_3 . Only FLH showed an exothermic peak $\sim 154^\circ\text{C}$ corresponding to the removal of hydrazine around this temperature. The other three, however, indicated the first exothermic reaction well above the dehydrazination temperatures. And, all these complexes undergo multistep exothermic reactions to give mainly $\gamma\text{-Fe}_2\text{O}_3$. The intense exothermic process $\sim 300^\circ\text{C}$ is then followed by an exothermic hump in all complexes. This event is considered here due to the crystallization of the oxide that formed in all these complexes, after the intense exotherm, $\sim 300^\circ\text{C}$.

FMH and FTH

Ferrous malonato-hydrazinate (FMH), $\text{FeC}_3\text{H}_2\text{O}_4 \cdot 1 \frac{1}{2}\text{N}_2\text{H}_4\cdot\text{H}_2\text{O}$, loses 64.30% of its weight to give mainly $\gamma\text{-Fe}_2\text{O}_3$. DTA trace shows one intense exothermic peak $\sim 242^\circ\text{C}$ followed by an exothermic hump $\sim 298^\circ\text{C}$.

Ferrous tartrato-hydrazinate (FTH), $\text{FeC}_4\text{H}_4\text{O}_6\cdot\text{N}_2\text{H}_4\cdot\text{H}_2\text{O}$, yields magnetic iron oxide by losing 68.54% of its mass. DTA here too indicates one intense exothermic peak $\sim 329^\circ\text{C}$ which is then followed by an exothermic hump.

The exothermic hump following the intense exothermic peak is due to the crystallization of the gamma ferric oxide that formed at the end of the intense exothermic reaction.

The hydrazine content estimation done on the thermal products of these complexes, however, shows some different behavior than that observed in FFH, FSH, FEH and FLH.

On heating FMH to 50°C , the hydrazine content of 20.43% that present in it goes down to 16.42%, but the weight loss observed at this temperature, however, is 7.85% (Table 3.5). At 70°C the product obtained retains the hydrazine percentage to 16.18, while the total mass amounts to 9.5%. Further heating to 95°C indicates weight loss of 12.25% and the hydrazine content in it now shows an increase to 17.38%. The thermal product at 170°C still shows 5.68% hydrazine in it and the total hydrazine loss and a almost total mass loss are found to occur $\sim 180^\circ\text{C}$. DTA shows one intense peak $\sim 242^\circ\text{C}$ yielding mainly $\gamma\text{-Fe}_2\text{O}_3$. Thus, these results indicate that the dehydrazination begins above 110°C and the weight loss observed below this temperature, hence, is due to the dehydration.

Similar observations were also made on the FTH (Table 3.5). Here, too the dehydration precedes the dehydrazination which is then followed by oxidative decomposition yielding mainly $\gamma\text{-Fe}_2\text{O}_3$.

The FMH and FTH are carboxylato-hydrazinate complexes of iron with water of crystallization, thus, undergo dehydration before dehydrazination, which is then followed by oxidative decomposition. The other complexes, FFH, FSH, FEH and FLH, on the other hand, have no water of hydration in them. Here dehydrazination is then immediately followed by oxidative decomposition. A single intense exothermic peak observed in FMH and FTH suggests that the total decomposition is reactive process, while the multistep reactions in the other four complexes indicate the decomposition process is less reactive. A bis-hydrazine malonate, succinate, and maleate and fumarate complexes of metals, Co, Ni and Zn [384-386] are also found to show single and multistep decomposition reactions, suggesting reactive and less reactive processes yielding the respective metal oxides as an end products.

ii. X-ray characterization

The XRD patterns of the autocatalytically decomposed end product of the iron (II) carboxylato-hydrazinates are shown in Fig. 3.9. The end products are found to be magnetic in nature. XRD patterns of these end products match with the pattern of the standard commercial $\gamma\text{-Fe}_2\text{O}_3$ and d_{hkl} values of these compare well with the values of JCPDS files [410-411] for $\gamma\text{-Fe}_2\text{O}_3$. An extra peak at $d = 2.7$ is found in these XRD spectra which corresponds to the strongest line of $\alpha\text{-Fe}_2\text{O}_3$.

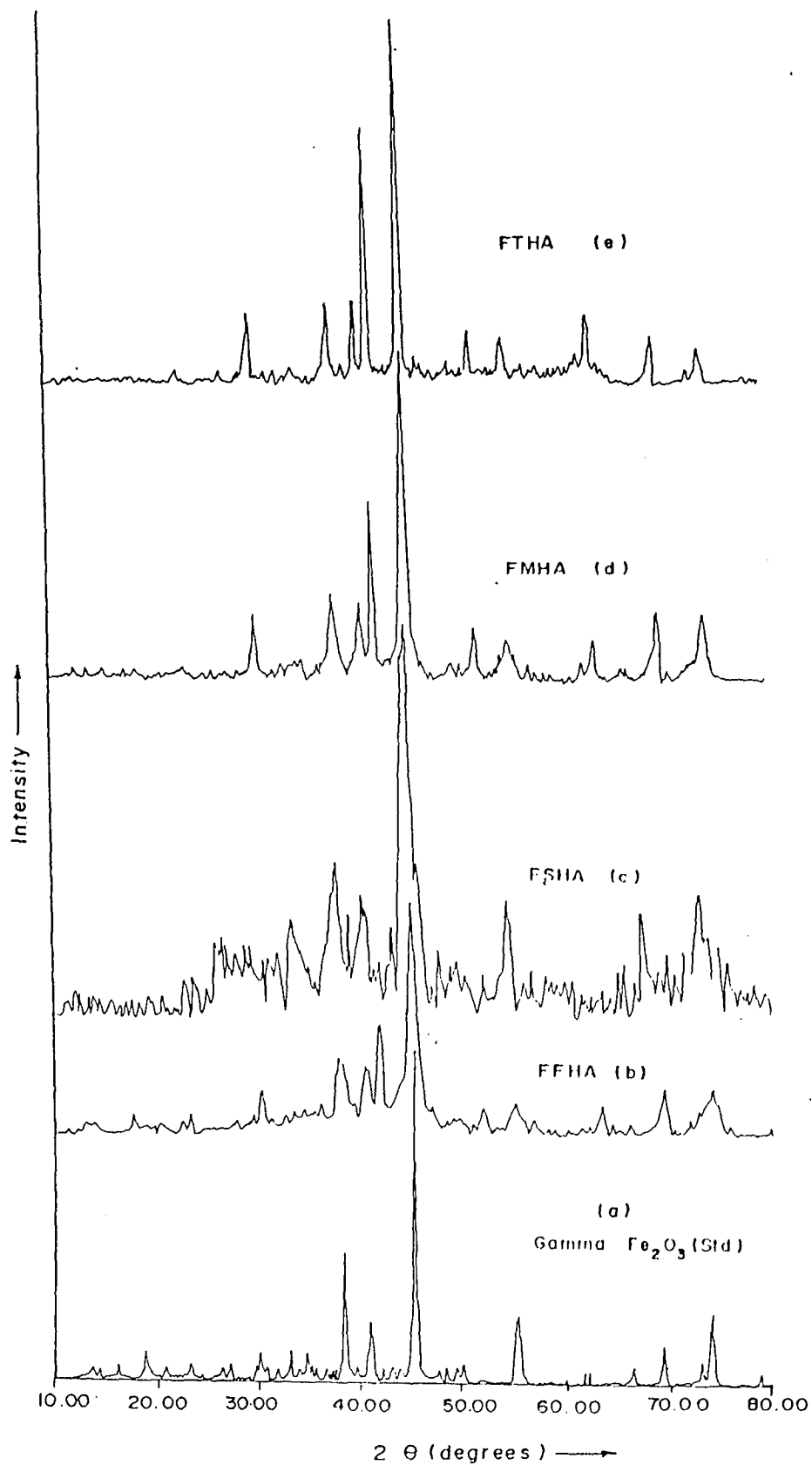


FIG. 3.9 XRD patterns of the autocatalytically decomposed end products of iron(II) carboxylato-hydrazinates

The traces of α -Fe₂O₃ that found are due to the intense heating taking place during the autocatalytic decomposition converting few particles of γ -Fe₂O₃ to α -Fe₂O₃.

iii. Infra red analysis

The IR spectra of autocatalytically decomposed end products of the iron (II) carboxylato-hydrazinates (Fig 3.7.d) reveal that the end products of all the complexes are mainly, γ -Fe₂O₃ with some admixture of α -Fe₂O₃. The band position observed for γ -Fe₂O₃ are 558, 463, 450 and that observed for α -Fe₂O₃ are 542, 440, 382 which match well with the reported values [280, 333, 350, 415] and these values are close to those γ -Fe₂O₃ synthesized from iron oxy hydroxides as described in part I of this chapter.

c) Magnetic characterization and microstructure analysis.

A saturation magnetization value, σ_s , in the range of 18 to 43 emu/g, (Table 3.5) is observed for γ -Fe₂O₃ obtained from autocatalytically decomposed products of all these iron (II) carboxylato-hydrazinates. A standard commercial sample of γ -Fe₂O₃ with a J_s value of 71 emu/g suggests that the values obtained for the oxide, synthesized in the present investigations, are not close to the reported values [416] of 71-74 emu/g. However, the values in the range of 35-60 emu/g are also observed in the literature [431] for γ -Fe₂O₃. One explanation for such low values in our gamma ferric oxide samples may be due to some admixture of α -Fe₂O₃. XRD and IR data reveals such admixture in our samples. This may be due to the fact that the hydrazinated complexes decompose almost explosively to gamma ferric oxide.

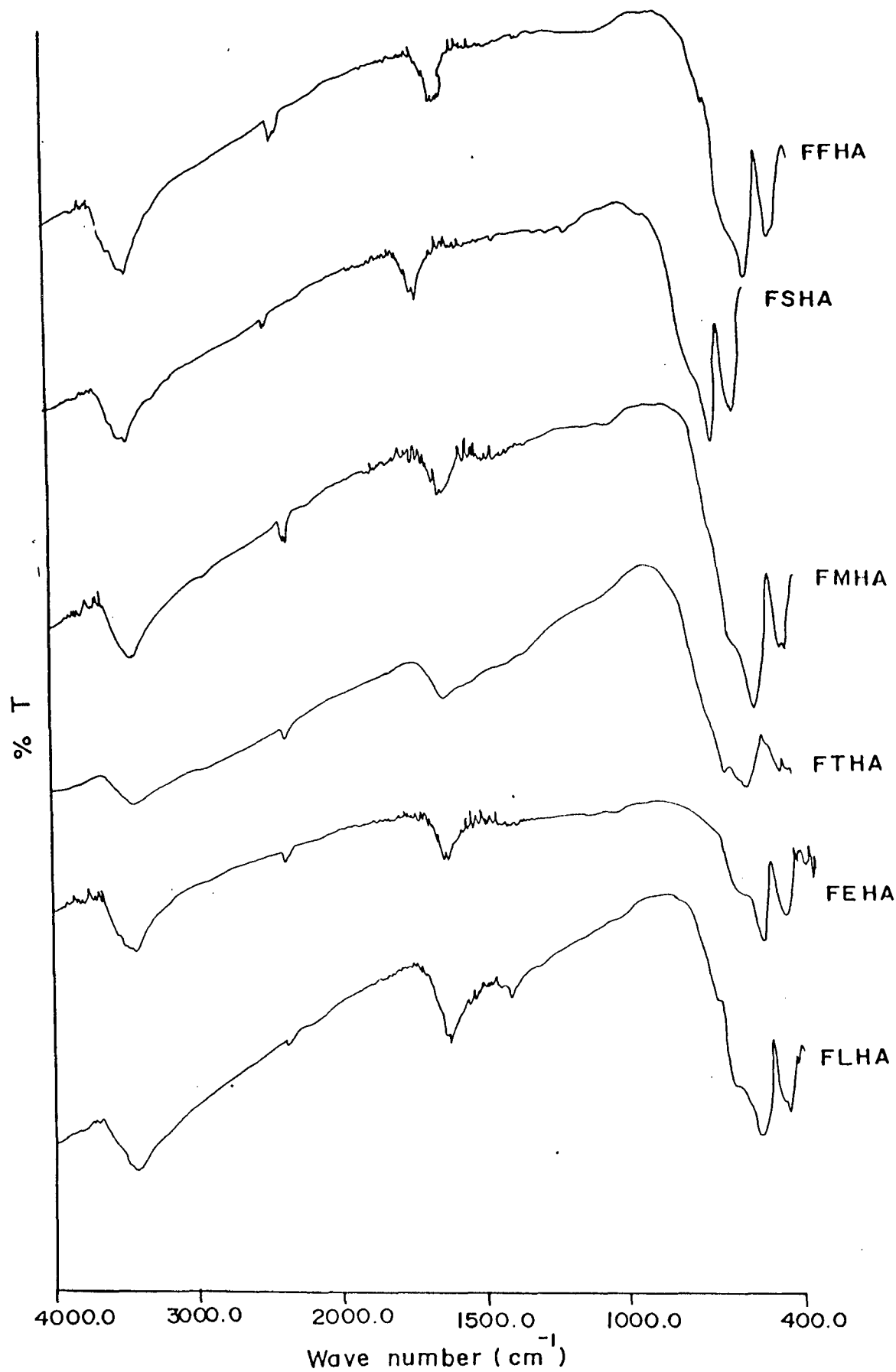


FIG. 3.7 d) Infra red spectra of the end products of iron(II) carboxylato-hydrazinates

And, the local temperature reaches to such a high temperature that the formed oxide transforms partially into a thermodynamically more stable α - Fe_2O_3 .

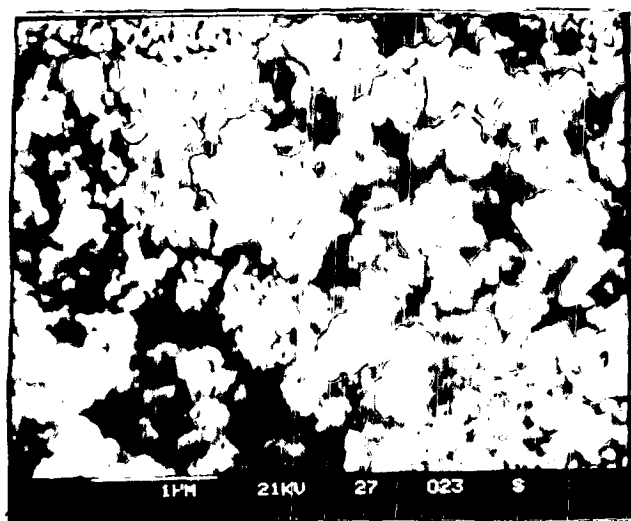
Another reason for the low saturation magnetization value is the small particle size and large surface area. The SEM micrographs reveals that the average particle size of the autocatalytically decomposed end products of iron (II) carboxylato-hydrazinate ranges from 0.1-0.3 μm . The Particles of the oxide end products are spherical in shape. All the SEM micrographs (Fig. 3.10) show the aggregation of the particles at some places, which is due to the excessive burning of some of the particles during decomposition of the complexes, which results in agglomeration.

3.6 CONCLUSIONS

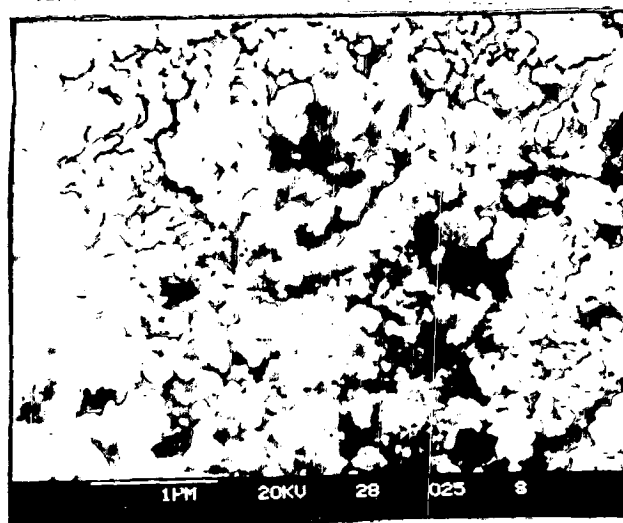
1. Iron (II) carboxylato-hydrazinates : Ferrous fumarato-hydrazinate, $\text{FeC}_4\text{H}_2\text{O}_4 \cdot 2\text{N}_2\text{H}_4$; ferrous succinato-hydrazinate, $\text{FeC}_4\text{H}_4\text{O}_4 \cdot 2\text{N}_2\text{H}_4$; ferrous malonato-hydrazinate, $\text{FeC}_3\text{H}_2\text{O}_4 \cdot 1 \frac{1}{2}\text{N}_2\text{H}_4 \cdot \text{H}_2\text{O}$; ferrous tartrato-hydrazinate, $\text{FeC}_4\text{H}_4\text{O}_6 \cdot \text{N}_2\text{H}_4 \cdot \text{H}_2\text{O}$; ferrous maleato-hydrazinate, $\text{FeC}_4\text{H}_2\text{O}_4 \cdot 2\text{N}_2\text{H}_4$ and ferrous malato-hydrazinate, $\text{FeC}_4\text{H}_4\text{O}_5 \cdot 2\text{N}_2\text{H}_4$, are being synthesized easily from the respective sodium salts of carboxylic acids, ferrous chloride and hydrazine hydrate in an inert atmosphere.

2. All iron (II) carboxylato-hydrazinates decompose autocatalytically in an ordinary atmosphere yielding mainly γ - Fe_2O_3 .

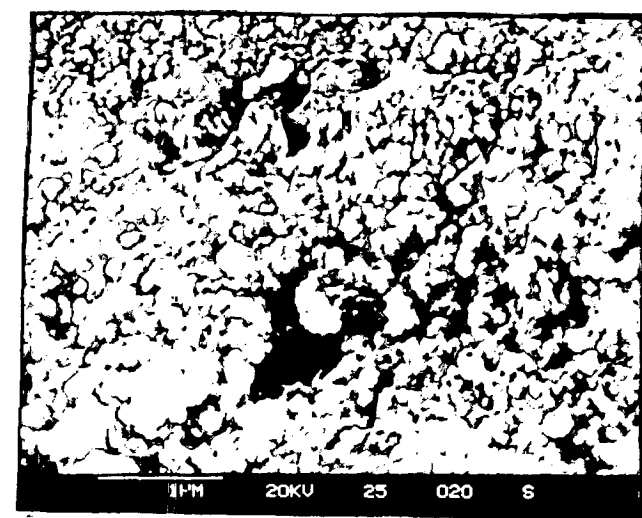
3. The easy synthesis of γ - Fe_2O_3 from iron (II) carboxylato-hydrazinates, thus, avoids a cumbersome control of water vapor partial pressure that required in arresting the thermal decomposition path of iron (II) carboxylates at γ - Fe_2O_3 step



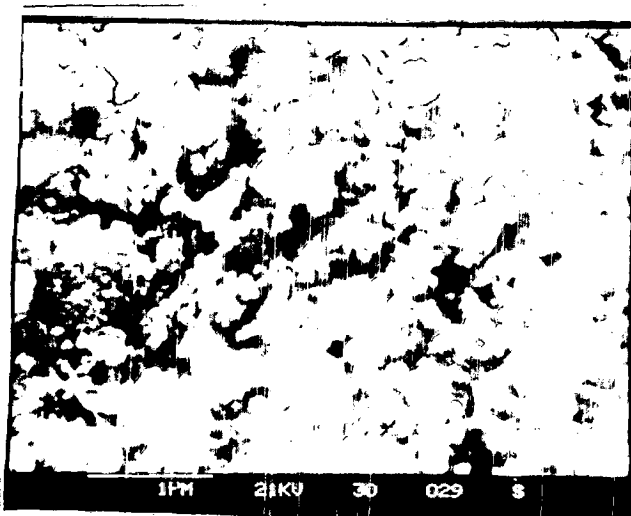
FFHA



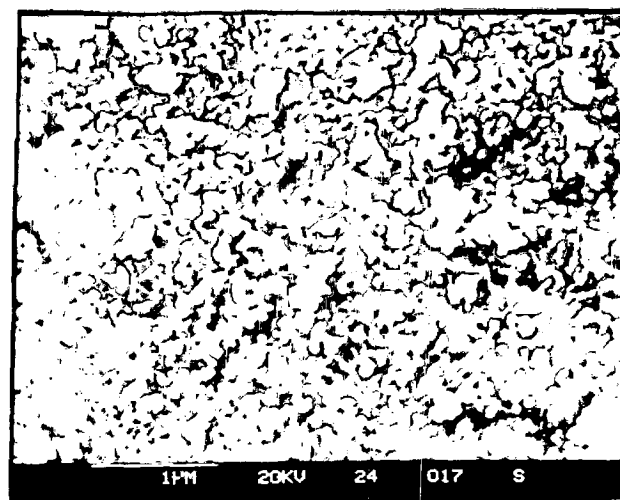
FSHA



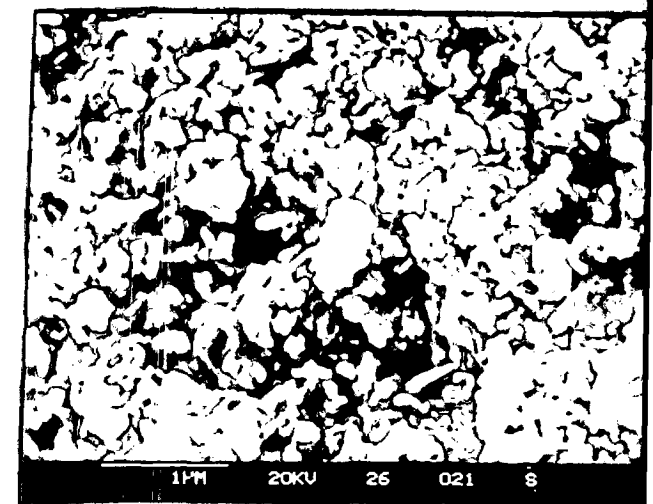
FMHA



FTHA



FEHA



FLHA

FIG. 3.10 SEM micrographs of the autocatalytically decomposed end products of iron (II) carboxylato-hydrazinates

CHAPTER IV

Study of ferrites

Study of ferrites

4.1 Introduction

The polycrystalline ferrites, which have high resistivity and low eddy current losses play an important role in many technological applications, ranging from radio-frequency to microwave frequencies. Their properties are very strongly dependent on the sample preparation methodology and the amount and type of substitution.

Magnesium ferrite, which is a mixed spinel, has been a subject of study for long time [432]. It may indeed be counted among the most versatile of the ferrites [433]. This is largely due to the comparatively low magnetic and dielectric losses

obtainable and, in particular, to the high resistivities which can be obtained by selection of suitable minor additives and use of appropriate firing procedures. High electrical resistivity and relatively easy preparation make these materials widely usable, for the cores of intermediate and high frequency electro magnetic devices [106,434].

$MgFe_2O_4$ is an ionic conductor which changes its impedance characteristics, as a function of the humidity. Thus, $MgFe_2O_4$ spinel finds use as a sensing element for humidity measurement devices [435-437]. Its electrical response, with impedance changes at different relative humidities, is due to physisorption and the capillary condensation of water molecules [436]. Therefore the microstructure of porous compacts is primarily responsible for their humidity - sensitive electrical properties [436,438].

The low rectangularity of the hysteresis loop, low coercive force and low microwave losses are the essential requirements of a microwave ferrite for latching applications. Magnesium ferrites are known to possess these characteristics [439].

Fine magnetic ferrite powders are critical to ferrofluid applications and have recently been proposed for the use in high temperature magnetic refrigeration [440]. Like $\gamma-Fe_2O_3$, $MgFe_2O_4$ has been known to be active and selective in the oxidative dehydrogenation of butene to butadiene [64-72]. It is also reported to be the major component of an industrial catalyst for the dehydrogenation of ethylbenzene to styrene [73].

The spinel oxide materials synthesized by two different methods exhibit differences in their magnetic properties [432-433]. This has generated a considerable

interest in the comparative study of magnetic and structural properties of spinel ferrites, such as, MgFe_2O_4 [147].

Many researchers prepared MgFe_2O_4 by ceramic method [143-151]. Guillaud [441] and Bertaut [442] have shown that magnesium ferrite is partially inverted to an extent which is qualitatively in accord with the saturation moment measurements. The saturation magnetization of MgFe_2O_4 has been studied by Pauthenet et al [115], by Guillaud [116] in connection with a study of MgZn ferrite system and by Jones et al [117], as part of a study of magnesium ferrite aluminate. They found that the magnetization depends rather sensitively, on the heating schedule.

Pauthenet and Bochirol [115] were able to vary the magnetic moment per molecule by 250 percent of MgFe_2O_4 by rapidly quenching the material from temperatures ranging from 200 to 1200°C . Neel [443] attributed this phenomenon to the fact that magnesium ferrite is only partially inverted and that the degree of inversion can be varied, by adjusting the quench temperature. This explanation was verified directly by Bertaut [442] through the use of x-ray diffraction. A closely related variation with heat treatment is observed in the curie temperature, T_c . Guillaud [116] found it possible to cause T_c to vary from 320°C to 440°C by adjusting the quenching temperature.

The saturation magnetization and the curie temperature of the quenched and furnace cooled MgFe_2O_4 was studied by many researchers [144,444-445]. They observed that the curie temperature for the furnace cooled samples were higher than the quenched ones. According to them, a lower concentration of Fe^{3+} ions at A

site can be expected in the quenched samples that will cause a decrease in the Fe^{3+}_A - Fe^{3+}_B magnetic interaction, thereby, lowering Tc. These researchers also found that the magnetization of the quenched samples was much higher than that of the corresponding furnace cooled samples. This difference, according to them, obviously arises from the difference in the cation distribution. The quenched samples having a more normal cation distribution than the furnace cooled samples, will have higher magnetization. The saturation magnetization in emu /g of MgFe_2O_4 reported by many researchers [147, 446, 447], ranges from 22-28 emu/g. It depends on the method of preparation, as well as, heat treatment. The lattice constant (a) reported for MgFe_2O_4 in the literature [170,448] ranges from 8.36 - 8.42 Å.

The literature survey reveals the synthesis of MgFe_2O_4 , by different methods and, from different precursors. The age old ceramic method was used by many investigators [115-116,143-151] for the preparation of MgFe_2O_4 . The raw materials used here are generally oxides or carbonates of metals. The different precursors used in the synthesis of MgFe_2O_4 are mainly coprecipitated hydroxide precursors [147,150,159-161], carboxylate precursors [166-167], Hydrazine precursors [170-171, 173, 179-180]. The MgFe_2O_4 is also prepared by super critical drying process by some researchers [207-209]. Wold [133] prepared magnesium ferrite by ignition of pyridinates.

Gajapathy et al[171] prepared MgFe_2O_4 from oxalate hydrazinate precursor which autocatalytically decomposes, between 100 -230°C, to form the ferrite. The

resistivity of this sample was of the order of 10^9 ohm.cm., but the saturation magnetization value was only 22.7 emu/g.

Seshan et al [449] prepared $MgFe_2O_4$ as a part of their magnesium nickel ferrite studies. They reported the saturation magnetization ($4\pi Ms$) for furnace cooled and quenched samples, at $-273^\circ C$ and $27^\circ C$. The saturation magnetization for the furnace cooled sample was 1335 Gauss, while for the quenched one it was 3005 Gauss.

In $MgFe_2O_4$, the site preference lead to a predominantly inverse structure, with Mg^{2+} ions mainly on B-sites and, Fe^{3+} ions distributed almost equally between A and B sites. Thus, the cation distribution suggested [450] for this ferrite is given by :



Joshi et al [451] prepared $MgFe_2O_4$ as part of a study of magnesium zinc ferrite. Lattice parameter (a), bond length (R_A and R_B), cation distribution and curie temperature were evaluated for the ferrite system. The lattice parameter and curie temperature reported here are 8.38\AA and $360^\circ C$, respectively. Rao and Murthy [149] measured the electrical conductivity of $MgFe_2O_4$, prepared by conventional double sintering method. The electrical conductivity at RT was $3.52 \times 10^{-8} \text{ ohm}^{-1} \text{ cm}^{-1}$, while the curie temperature was $395^\circ C$. The activation energy for the ferri and para regions were, 0.44eV and 0.61eV, respectively. From the sign of the seebeck coefficient, they found out that the magnesium ferrite is n-type semiconductor.

Yang et al [63] prepared MgFe_2O_4 from coprecipitated hydroxide precursor. The hydroxide precursor was prepared by spraying 0.1 methanolic solution of nitrates into the ethanol (95%) saturated with ammonia (by continuous bubbling) and kept at -30°C . The fine hydroxide precipitate formed was filtered, dried at 100°C and then calcined at 700°C to get MgFe_2O_4 . This MgFe_2O_4 sample was used by them as a catalyst in oxidative dehydrogenation of butene to butadiene. They found that butadiene and its precursors are not degraded by gaseous oxygen over MgFe_2O_4 , as well as, on $\gamma\text{-Fe}_2\text{O}_3$ due to their inverse spinel structure, but, are easily degraded over corundum $\alpha\text{-Fe}_2\text{O}_3$ and normal spinel ZnFe_2O_4 .

Traversa et al [160] synthesized MgFe_2O_4 by the thermal decomposition of coprecipitated hydroxide mixtures, at temperatures as low as 380°C .

Patil et al [452] prepared MgFe_2O_4 from standard ceramic technique by sintering the samples at 1100°C for 15 and 30 h. They observed that the saturation magnetization and the magnetic moment values for samples sintered for longer duration are higher than those samples sintered for shorter duration.

Patil et al [453] prepared MgFe_2O_4 by conventional ceramic technique. The final sintering was carried out at 1000°C for 40 h, after pelletization. The lattice constant, $4\pi M_s$, n_B and T_c reported by them for MgFe_2O_4 are 8.374\AA , 1149G , $1.02\mu_B$ and 372°C , respectively. Kadam et al [454], on the other hand, used ceramic technique and sintering temperature of 1250°C . The curie temperature, saturation magnetization and magneton number obtained by them for MgFe_2O_4 are, 437°C , 27.9 emu/g and $1.00\mu_B$, respectively.

Suresh et al [455] synthesized and characterized $MgFe_2O_4$ as a part of a study on $Mg_x Zn_{1-x} Fe_2O_4$ (where $x = 0 - 1.0$). The $MgFe_2O_4$ is prepared by the combustion of magnesium nitrate, iron (III) nitrate, ammonium nitrate and oxalyl dihydrazide (ODH) at $350^\circ C$ in less than 5 min. The Brunauer - Emmett - Teller (BET) surface area of $MgFe_2O_4$ is found to be $110m^2g^{-1}$, indicating the fine particle nature. The other properties of $MgFe_2O_4$ studied by them are particle size $\sim 0.017\mu m$, saturation magnetization ~ 25.2 emu/g and curie temperature $\sim 337^\circ C$.

Some researchers [207] synthesized fine powders of $MgFe_2O_4$, through the sol-gel, super critical drying method. A 1:2 mixture of magnesium acetate tetrahydrate and ferric acetyl acetonate powders was dissolved in methanol and hydrolyzed with water. This mixture was then heated upto $251^\circ C$ in an autoclave under a pressure of 82.5 bar. The pressure was then slowly relieved and then autoclave was cooled, with a low flow of nitrogen gas passing through it, to obtain a fine powder, which was then heated in air at $500^\circ C$ and $800^\circ C$ for 3 h. The average particle diameter of the $MgFe_2O_4$ was 11 nm and the $4\pi Ms$ of sample heated at $800^\circ C$ was 1530 G. Ho et al [208] prepared magnesium ferrite nanoparticles from an aerogel process and measured their low temperature heat capacities.

This chapter is centered around the synthesis and characterization of magnesium ferrite. In the present studies, the ferrite is prepared by conventional ceramic technique, using raw materials $MgCO_3$ and active iron oxide (mainly $\gamma-Fe_2O_3$) obtained from autocatalytic decomposition of iron(II) carboxylato hydrazinate and hydrazinated iron oxyhydroxides precursors, as described in chapter III. The properties of these ferrites samples were compared with the

chapter III. The properties of these ferrites samples were compared with the ferrites sample prepared by using α -Fe₂O₃ (commercial) and MgCO₃ under the same conditions of preparations

4.2 Experimental: Preparation and characterization

4.2.1 Preparation of ferrites: Ceramic technique

Magnesium ferrite of formula, MgFe₂O₄, was synthesized by using standard ceramic technique. Iron(III) oxide and magnesium carbonate, MgCO₃, in the required stoichiometric composition were mixed and heated to a high temperatures. The MgCO₃ of commercial grade (LOBA, India, AR Grade) was used. The iron oxide used was in γ -Fe₂O₃ form, from (as described in chapter III)

i) Autocatalytic decomposition of iron (II) carboxylates.

- a) Ferrous fumarato-hydrazinate (FFHA)
- b) Ferrous succinato-hydrazinate (FSHA)
- c) Ferrous malonato-hydrazinate (FMHA)
- d) Ferrous tartrato-hydrazinate (FTHA)

ii) Autocatalytic decomposition of hydrazinated iron oxyhydroxides (from iron ore)

- a) Gamma FeOOH (γ FA)
- b) Alpha FeOOH (α FA)
- c) Amorphous FeOOH (AmpFA)

These iron oxyhydroxides were prepared from iron hydroxide Fe(OH)₃, obtained on chemical beneficiation of low grade iron ore (as described in 3.2.1 and 3.2.2) and then hydrazinated, as in 3.2.3.

For the comparison of the ferrites prepared from the above γ - Fe_2O_3 samples, a commercial grade α - Fe_2O_3 (Baker Analyzed, 99.9% Fe_2O_3) was used for MgFe_2O_4 preparation.

iii) α - Fe_2O_3 (BAKER ANALYZED Reagent 99.9 % Fe_2O_3)

a) Preheating of raw meal (Fe_2O_3 and MgCO_3)

The stoichiometric quantities of iron oxide (mentioned above) and MgCO_3 (AR Grade) were weighed on a single pan balance (Sartorius) having least count of 0.0001 g and mixed thoroughly in the agate-mortar, in acetone medium for 2 h. The dried mixture was transferred to a platinum crucible and heated slowly to 800°C and then maintained at that temperature for 5 h. The crucible was furnace cooled and then the preheated sample was ground in agate-mortar in acetone medium for two hours. The preheating temperature 800°C was selected to completely decompose MgCO_3 to MgO . The preheating also initiate a preliminary reaction of MgO with Fe_2O_3 .

b) High temperature heating of preheated samples

The preheated samples, after grinding, were further heated to high temperatures to complete the reaction. This was done by first pelleting the preheated mixtures.

i) Pellet formation

Two grams of the pre-sintered ferrite sample was mixed in agate mortar using P.V.A. as binder in acetone medium. After mixing, acetone was allowed to evaporate and the dry powder was transferred to a die having 1.5 cm diameter, and

cold pressed it in a hydraulic press, with a load of about 10 tonnes for 3 minutes to form the pellet.

The pellets were placed on a platinum lid base and heated slowly to 200-300°C to remove the binder and, then increased the temperature to 800°C and kept at that temperature for 12 h. The samples were then furnace cooled.

The furnace cooled samples were broken and reground in a agate mortar. Using PVA as a binder pellets as above and torroids as below, were prepared for final sintering.

c) Final sintering

i. Preparation of pellets / torroids

Three grams of the pre-sintered ferrite sample was pressed with a load of 10 tonnes for five minutes to form the toroid, with internal diameter of 1cm and outer diameter of 2cm and the height of 3mm. Pellets of the presintered samples were prepared as above.

Both pellets and torroids were introduced in a muffle furnace whose temperature could be controlled to $\pm 5^{\circ}\text{C}$ and the temperature was measured using Chromel- Alumel thermocouple.

A slow heating upto 400°C was undertaken so that binder leaves slowly, the samples, without creating undue cracks in the pellets and torroids. After maintaining temperature $\sim 400^{\circ}\text{C}$ for 5 hours, the temperature of the furnace was slowly increased to 1000°C and maintained at that temperature for 24 hours. Furnace cooled samples were then stored in a vacuum desiccator .

d) Coding of samples

The samples prepared as above were coded as below, depending upon their iron oxide sources:

Iron oxide source		code name of magnesium ferrite
(1) FFHA	$(\gamma\text{-Fe}_2\text{O}_3 + \text{MgCO}_3)$	MGFFHA
(2) FSHA	„	MGFSHA
(3) FMHA	„	MGFMHA
(4) FTHA	„	MGFTHA
(5) γ FA	„	MG γ FA
(6) α FA	$(\gamma\text{-}\&\alpha\text{-Fe}_2\text{O}_3 + \text{MgCO}_3)$	MG α FA
(7) AmpFA	$(\gamma\text{-Fe}_2\text{O}_3 + \text{MgCO}_3)$	MGAmpFA
(8) Commercial	$\alpha\text{-Fe}_2\text{O}_3 + \text{MgCO}_3$	MGHEM

4.2.2 Characterization.

a) X-ray diffraction (XRD) studies

The x-ray analysis of the magnesium ferrite samples was done on Philips X-ray diffractometer, model PW 1710, with Cu K α radiations and Nickel as a filter. In the present study X-ray diffraction is used to (1) confirm the completion of solid state reactions, (2) observe the impurity phases and, (3) determine the lattice constants, interplaner distances, octahedral and tetrahedral site radii, bond length, X-ray density etc. As the crystallites are randomly oriented, a reflection at the particular position is due to a set of atomic planes satisfying Bragg's condition. The

Bragg's law is given as,

$$n \lambda = 2 d_{hkl} \sin \theta \quad \text{-----} \quad 4.11$$

where d_{hkl} is the interplanar spacing of crystal planes of miller indices (hkl), θ is glancing angle, λ is the wavelength of x-ray radiation and 'n' is the order of diffraction

For a cubic lattice, the interplaner distance, d_{hkl} , lattice parameter 'a' and the miller indices (hkl) are related by relation,

$$d_{hkl} = \frac{a}{\sqrt{h^2 + k^2 + l^2}} \quad \text{-----} \quad 4.12$$

The planes that diffract x-rays in inverse cubic spinel systems are (220), (311), (400), (422), (440), (533), etc. The lattice parameter 'a' is calculated from the observed 'd' value of (311) plane which is the most first intense one. The interplaner distance (d) for each diffraction angle was calculated by the relation 4.12 and then the lattice parameter 'a' was calculated. Finally the values of 'a' for all $MgFe_2O_4$ samples were computed by the least square method.

The values of bond lengths (R_A and R_B) and site radii (r_A and r_B) were calculated by using the relations given below,

$$R_A = a \sqrt{3} (\delta + 1/8) \quad \text{-----} \quad 4.13$$

$$R_B = a \sqrt{1/16 - \delta/2 + 3\delta^2} \quad \text{-----} \quad 4.14$$

$$r_A = (u - 1/4) a \sqrt{3} - R_O \quad \text{-----} \quad 4.15$$

$$r_B = (5/8 - u) a - R_O \quad \text{-----} \quad 4.16$$

where R_A is the shortest distance between A-site (tetrahedral) cation and oxygen ion

R_B is the shortest distance between B-site (octahedral) cation and oxygen ion

r_A is the tetrahedral site radius

r_B is the octahedral site radius

R_o is the Radius of oxygen ion (1.35 Å)

δ is the Deviation from oxygen ion parameter (u)

$$\delta = u - u_{\text{ideal}} \quad [u_{\text{ideal}} = 0.375 \text{ \AA}]$$

The u value used for calculations are from the data already reported for magnesium ferrite [456].

The x-ray density (dx), actual density (da) and porosity (p) of the ferrite samples was calculated from the relations

$$dx = 8M/N a^3 \quad \text{-----} \quad 4.17$$

$$da = m/\pi r^2 \cdot t \quad \text{-----} \quad 4.18$$

and

$$P(\%) = ((dx-da)/dx) \cdot 100 \quad \text{-----} \quad 4.19$$

Where M is the molecular weight of the sample

N is the avagadro's number

a is the lattice parameter.

m is the mass of the pellet.

r is the radius of the pellet.

t is the thickness of the pellet.

b) Infra - Red Analysis

The IR spectra of all the magnesium ferrite samples were recorded on Shimadzu FTIR, model 8101 A. The pellets used for recording spectra were prepared by mixing small amount of ferrite powder in KBr. The IR spectra in the frequency range of 400 - 4600 cm^{-1} were recorded at room temperature.

c) Magnetic characterisation

i. Saturation magnetisation

The saturation magnetisation, σ_s , values in emu/g of all the MgFe_2O_4 samples were determined at room temperature with the help of high field hysteresis loop tracer, described by Likhite et al [304].

The saturation magnetisation in Gauss (G) is determined by formula $4\pi M_s$.

M_s is calculated as,

$$M_s = (1-P) d_x \cdot \sigma_s \quad \text{-----} \quad 4.20$$

Where P is the Porosity

d_x is the X-ray density

σ_s is saturation magnetisation in emu/g

The magnetone number, that is, the magnetic moment per formula unit (n_B)

in Bohr magnetons, is given by

$$n_B = M \cdot \sigma_s / 5585 \quad \text{-----} \quad 4.21$$

Where M is the molecular weight of the sample.

ii. A.C.Susceptibility

The domain structure and the curie temperature were determined by a.c.susceptibility method, developed by Likhite et al [305] and described in section 2.2.7.b. The powdered ferrite was taken in a quartz sample tube and placed at the centre of the pick up coil. Pt-Rh thermocouple was used to read the temperature of the sample. The pick-up coil was placed in a mini furnace. The furnace was built by winding platinum coils. A d.c. current was used to energise the coil to get required temperature. The magnetic moment and temperature were recorded till this moment becomes zero. The relative susceptibility, that is ratio of magnetic moment at higher temperature to the moment at room temperature, was plotted against temperature. The curves are called χ - T curves.

iii. Initial Permeability

The initial permeability as a function of temperature was measured at 1000 Hz over the temperature range from 27 °C to 527 °C using MIC 4060 - D LCR meter. The initial permeability was calculated from the low field inductance measurements with a torroidal core of 50 turns using the formula,

$$L = 0.0046 \mu_i N^2 h \log d_1/d_2 \quad \text{-----} \quad 4.22$$

where L is the inductance in Hz

d_1 is the outside diameter of a torroid

d_2 is the inside diameter of a torroid

μ_i is the initial permeability of the core

h is the height of the core in inches.

d) Electrical characteristics

i. Resistivity

The electrical resistivity measurements of the MgFe_2O_4 samples were carried out using the two terminal d.c. method, in a range of temperature from 27 to 527°C . The experimental set up was similar to that described in section 2.2.10.b. The pellets of dimensions 15 mm diameter and 2-3 mm thickness were pressed between two platinum electrodes and then measurements were taken. The resistivity [457] was determined by the relation.

$$\rho = \pi r^2 / t \cdot R \quad \text{-----} \quad 4.23$$

Where r is the radius of pellet

t is the thickness of pellet

R is the resistance

The activation energies in the ferrimagnetic and paramagnetic regions were calculated from the plot $\log \rho$ against $1/T$.

ii. Dielectric constant

The dielectric measurements were made using the two - probe method. The pellets of 15 mm diameter and 2-3 mm thickness were used for the dielectric measurements which were carried out from 27 to 327°C at 1KHz on MIC 4060 - D LCR meter. The capacitance, c , was measured and was used in the calculation of dielectric constant, ϵ' , using the relation

$$\epsilon' = cd / \epsilon_0 A \quad \text{---} \quad 4.24$$

where d is the thickness of the pellet

A is the cross-sectional area of the flat surface of the pellet and ϵ_0 is the free - space permittivity

4.3 Results and discussion

a) phase identification by XRD

X-ray diffraction method is used to confirm the formation of single phase spinel structure. The x-ray diffraction patterns of $MgFe_2O_4$, obtained from different iron oxide sources, are presented in Fig. 4.1(a&b), which show well defined peaks. The lattice parameter and d-values are calculated for each sample. The calculated d-values agree with the observed d-values, as well as, with the reported ones [458], which confirms the formation of spinel ferrites. The observed, calculated and reported d-values are tabulated in Table 4.1(a,b,c&d).

From the diffraction patterns of the samples, it is observed that there are no extra peaks, the fact which can be regarded as the confirmation of single phase ferrite formation, excepting for MGHEM sample, that is, the sample prepared from commercial $\alpha-Fe_2O_3$. In MGHEM sample one additional peak $d=2.7$ appears. The d-spacing of this peak does not match with the spinel lattice. The JCPDS table shows that the observed additional peak belongs to $\alpha-Fe_2O_3$ phase which is 100% peak of pure $\alpha-Fe_2O_3$.

The lattice parameters of all the magnesium ferrite samples are given in table [4.1a,b,c&d]. They are calculated by using the relation 4.12. The values of the lattice parameter are found in the range of 8.3877 to 8.4147 Å which agrees well with the reported values [133, 170, 444, 451, 459-560] for magnesium ferrite. The values of bond lengths (R_A and R_B) and site radii (r_A and r_B) are presented in

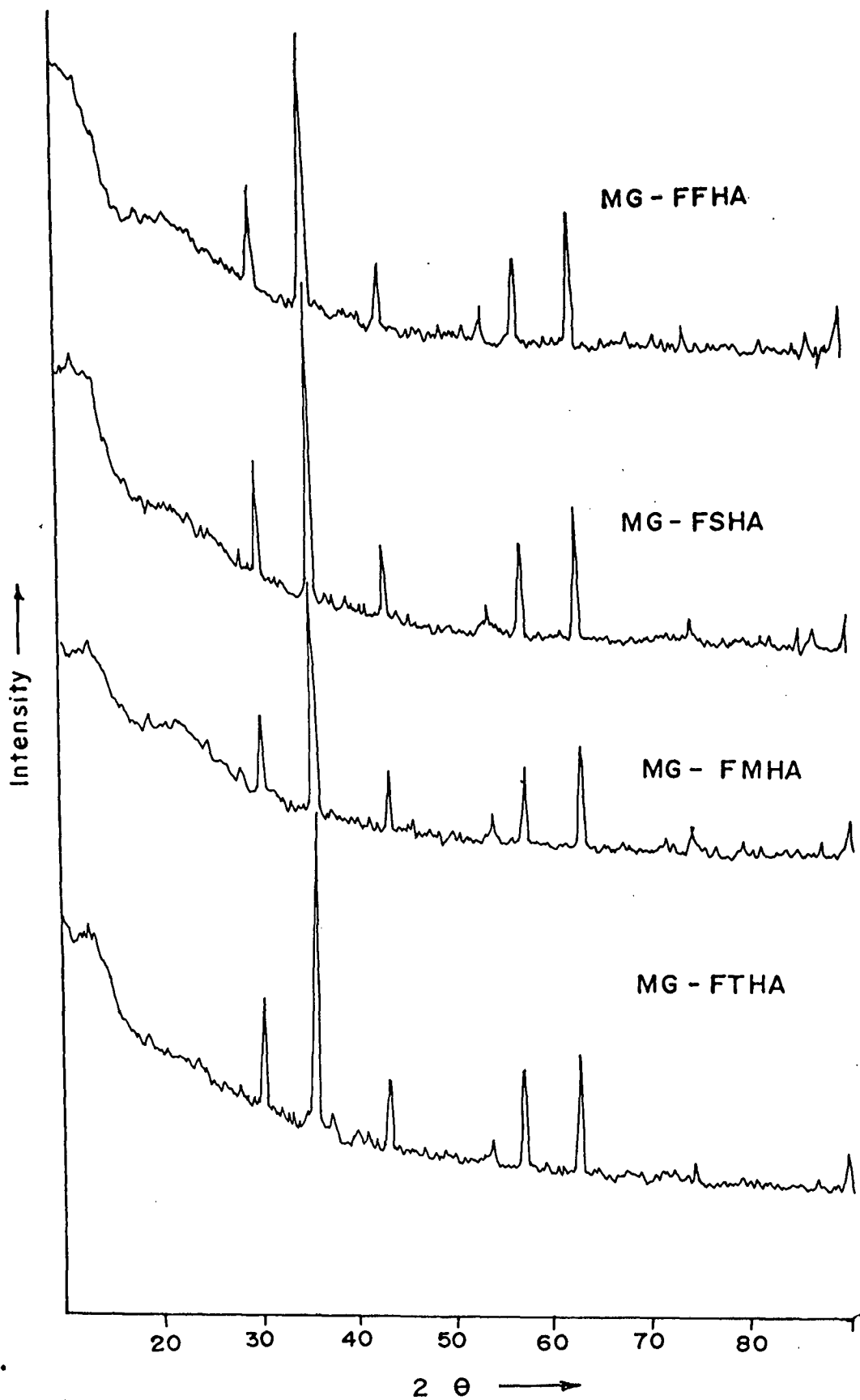


FIG. 4.1a) XRD patterns of MgFe₂O₄ ferrites 1) MgFFHA 2) MgFSHA 3) MgFMHA and MgFTHA

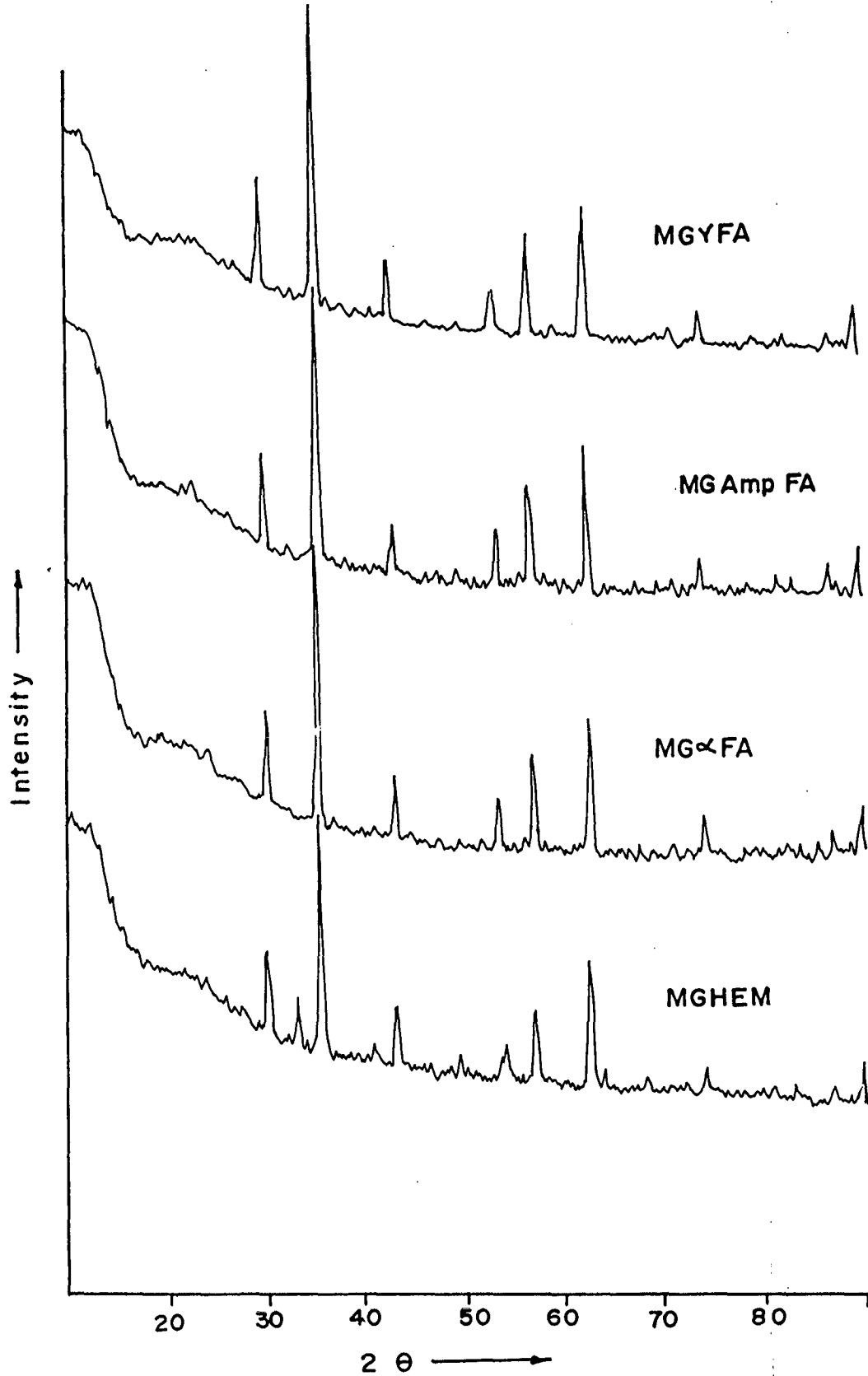


FIG. 4.1b) XRD patterns of MgFe₂O₄ ferrite 1) MgyFA 2) MgaFA 3) MgAmpFA and 4) MgHEM

TABLE 4.1 a) XRD data of MgFe_2O_4 ferrite 1) MgFFHA and 2) MgFSHA

X-ray diffraction data of MGFFHA
 Lattice parameter $a=8.3927$
 structure - cubic

Sr.No.	2θ , deg.	d_{cal} , Å	d_{obs} , Å	(hkl)
1	30.060	2.9666	2.9704	220
2	35.405	2.5299	2.5333	311
3	43.040	2.0977	2.0999	400
4	53.420	1.7128	1.7138	422
5	57.040	1.6148	1.6133	511/333
6	62.580	1.4833	1.4831	440
7	74.040	1.2796	1.2794	620
8	86.820	1.1212	1.1209	533

X-ray diffraction data of MGFSHA
 Lattice parameter $a=8.3912$
 structure - cubic

Sr.No.	2θ , deg.	d_{cal} , Å	d_{obs} , Å	(hkl)
1	30.080	2.9685	2.9685	220
2	35.429	2.5315	2.5316	311
3	43.100	2.0990	2.0971	400
4	53.480	1.7138	1.7120	422
5	57.020	1.6158	1.6138	511/333
6	62.620	1.4842	1.4823	440
7	71.060	1.3275	1.3255	620
8	74.100	1.2804	1.2785	533
9	89.820	1.0931	1.0911	731/553

TABLE 4.1 b) XRD data of MgFe₂O₄ ferrite 1) MgFMHA and 2) MgFTHA

X-ray diffraction data of MGFMA
Lattice parameter a=8.3877
structure - cubic

Sr.No.	2θ, deg.	d _{cal} , Å	d _{obs} , Å	(hkl)
1	30.100	2.9665	2.9665	220
2	35.454	2.5298	2.5299	311
3	43.100	2.0976	2.0971	400
4	53.500	1.7127	1.7114	422
5	57.020	1.6147	1.6138	511/333
6	62.600	1.4832	1.4827	440
7	74.080	1.2795	1.2788	533
8	87.100	1.1212	1.1180	642

X-ray diffraction data of MGFTA
Lattice parameter a=8.3999
structure - cubic

Sr.No.	2θ, deg.	d _{cal} , Å	d _{obs} , Å	(hkl)
1	29.960	2.9771	2.9801	220
2	35.324	2.5290	2.5389	311
3	37.020	2.4222	2.4264	222
4	42.940	2.0977	2.1046	400
5	53.360	1.7128	1.7156	422
6	56.880	1.6148	1.6175	511/333
7	62.480	1.4833	1.4853	440
8	73.960	1.2796	1.2806	533
9	86.780	1.1230	1.1213	642

TABLE 4.1 c) XRD data of $MgFe_2O_4$ ferrite 1) $Mg\gamma FA$ and 2) $MG\alpha FA$

X-ray diffraction data of $MG\gamma FA$
Lattice parameter $a=8.4147$
structure - cubic

Sr.No.	2θ , deg.	d_{cal} , Å	d_{obs} , Å	(hkl)
1	29.940	2.9784	2.9820	220
2	35.297	2.5399	2.5408	311
3	37.040	2.4284	2.4251	222
4	42.960	2.1060	2.1036	400
5	53.340	1.7195	1.7162	422
6	56.880	1.6212	1.6175	511/333
7	62.480	1.4892	1.4853	440
8	70.920	1.3319	1.3278	620
9	73.960	1.2846	1.2806	533
10	89.700	1.0967	1.0922	731/553

X-ray diffraction data of $MG\alpha FA$
Lattice parameter $a=8.4103$
structure - cubic

Sr.No.	2θ , deg.	d_{cal} , Å	d_{obs} , Å	(hkl)
1	29.960	2.9763	2.9801	220
2	35.333	2.5381	2.5382	311
3	36.980	2.4301	2.4289	222
4	42.980	2.1027	2.1045	400
5	53.380	1.7183	1.7150	422
6	56.920	1.6200	1.6164	511/333
7	62.540	1.4881	1.4840	440
8	74.040	1.2837	1.2794	533
9	86.780	1.1249	1.1213	642
10	89.720	1.0959	1.0920	731/553

TABLE 4.1d) XRD data of $MgFe_2O_4$ ferrite 1) MgAmpFA and 2) MgHEM

X-ray diffraction data of MGampFA
Lattice parameter a=8.4143
structure - cubic

Sr.No.	2 θ , deg.	d _{cal} , Å	d _{obs} , Å	(hkl)
1	29.960	2.9779	2.9801	220
2	35.314	2.5396	2.5395	311
3	42.960	2.1057	2.1036	400
4	53.360	1.793	1.7156	422
5	56.900	1.6209	1.6169	511/333
6	62.500	1.4889	1.4848	440
7	70.920	1.3317	1.3278	620
8	73.980	1.2844	1.2803	533
9	89.700	1.0965	1.0922	731/553

X-ray diffraction data of MGHEM
Lattice parameter a=8.4172
structure - cubic

Sr.No.	2 θ , deg.	d _{cal} , Å	d _{obs} , Å	(hkl)
1	29.960	2.9759	2.9801	220
2	35.338	2.5378	2.5379	311
3	42.960	2.1043	2.1036	400
4	53.360	1.7181	1.7156	422
5	56.920	1.6198	1.6164	511/333
6	62.500	1.4879	1.4848	440
7	71.060	1.3308	1.3255	620
8	73.980	1.2836	1.2803	533
9	86.740	1.1247	1.1217	642

Table 4.2 and they compare well with the values reported in literature [451]. The bond length R_B is greater than R_A , as expected. The average bond length, R_A , varies with the variation in lattice constant 'a'.

The data on x-ray density, actual density and porosity are given in Table 4.3. The x-ray density obtained in the present studies ranges between 4.45 and 4.49, while the reported is 4.52 [448]. The ferrite samples are about 25% porous except MGHEM sample (from α - Fe_2O_3 source) whose porosity is very high (42.19%). The porosities of 31% [452] and 27% [461] are reported for $MgFe_2O_4$ samples sintered at $1100^\circ C$ where as all our samples were sintered at $1000^\circ C$.

The literature survey reveals that the sintering temperature used by researchers for the preparation of $MgFe_2O_4$, by ceramic method, is $1100^\circ C$ and above [145, 150, 449, 451 - 452]. In the present study, the sintering temperature of $1000^\circ C$ was used for the preparation of impurity free $MgFe_2O_4$ samples. This was possible as the raw material, iron oxide used here was mainly γ - Fe_2O_3 with or without traces of α - Fe_2O_3 , which was found to increase the rate of ferritization at lower temperatures [7,9]. However, the $MgFe_2O_4$ sample prepared from commercial α - Fe_2O_3 (MGHEM) shows an impurity peak of α - Fe_2O_3 , suggesting that the sintering temperature is not sufficient to form single phase $MgFe_2O_4$.

b) Infra - Red Analysis

The IR spectra of all the magnesium ferrite samples are shown in Fig 4.2. The infra red absorption spectroscopy is an important technique to describe the

TABLE 4.2 Data on lattice parameter, bond length(R_A and R_B) and site radii (r_A and r_B) for magnesium ferrite

Sample	Lattice parameters 'a'	Bond length (°A)		Site radii (°A)	
		R_A-O	R_B-O	r_A	r_B
1. MGFFHA	8.3927	1.9042	2.0490	0.5542	0.6978
2. MGFSHA	8.3912	1.9039	2.0486	0.5539	0.6975
3. MGFMHA	8.3877	1.9031	2.0478	0.5531	0.6965
4. MGFTHA	8.3999	1.9056	2.0506	0.5556	0.6993
5. MG γ FA	8.4147	1.9092	2.0544	0.5592	0.7031
6. MG α FA	8.4103	1.9082	2.0532	0.5582	0.7021
7. MGamp.FA	8.4143	1.9051	2.0542	0.5591	0.7030
8.MGHEM	8.4063	1.9073	2.0523	0.5573	0.7011

TABLE 4.3 X-ray density, Physical density and porosity data for Magnesium ferrites

Sample	X-ray density (dx)	Physical density (da)	Porosity (P) %
1. MGFFHA	4.4868	3.3183	26.04
2. MGFSHA	4.4892	3.1614	29.58
3. MGFMHA	4.4948	3.3156	26.24
4. MGFTHA	4.4767	3.5228	21.31
5. MG γ FA	4.4517	3.2758	26.41
6. MG α FA	4.4586	3.4050	23.63
7. MGamp.FA	4.4530	3.2977	25.92
8.MGHEM	4.8804	2.8210	42.19

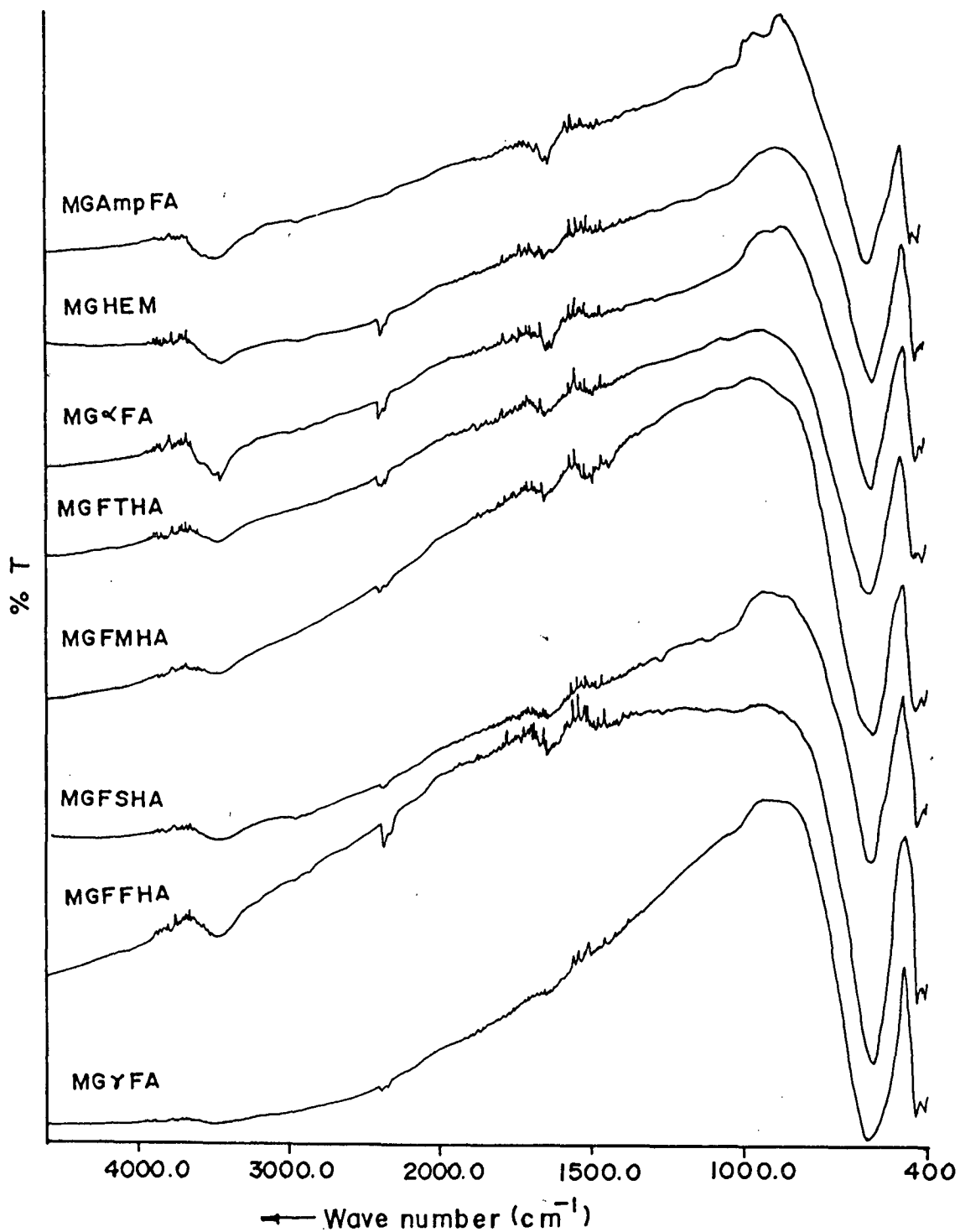


FIG. 4.2 Infra red spectra of MgFe_2O_4 ferrites 1) MgFFHA 2) MgFSHA 3) MgFMHA 4) MgFTHA 5) MgyFA 6) Mg α FA 7) MgAmpFA and 8) MgHEM

local symmetries in crystalline [461] and non - crystalline solids [462] and, various ordering phenomenon in spinels [463-464].

In the present IR studies (Fig 4.2), for all the $MgFe_2O_4$ samples, the high frequency band, ν_1 , is observed between $565 - 580 \text{ cm}^{-1}$ and low frequency band ν_2 , at 410 cm^{-1} and between $425 - 440 \text{ cm}^{-1}$, match closely with the ν_1 and ν_2 bands reported for $MgFe_2O_4$ by Waldron [465]. This confirms the formation of $MgFe_2O_4$. Since magnesium ferrite is highly sensitive to humidity the absorption bands are also observed at around 3400 cm^{-1} and 1620 cm^{-1} , in the IR spectra of all the samples. These bands are due to stretching and bending vibrations of water molecule [466].

The lattice vibrations of oxide ions with cations give rise to absorption bands in spinel ferrites, producing various frequencies for the unit cell. Generally the spinel ferrites show four IR active bands, ν_1 , ν_2 , ν_3 and ν_4 , in the range of 100cm^{-1} to 1000cm^{-1} . The occurrence of these four bands has been computed on the basis of group theoretical calculations, using space groups and point symmetries.

Tarte and Preudhomme [467] have reported that the first three infrared fundamentals are due to tetrahedral and octahedral complexes, whereas the other is due to some type of lattice vibrations. It has been pointed out that vibrational frequencies depends on the mass of cations, bonding force and unit cell dimensions [468].

According to Braber [469], for inverse spinel and partly inverse spinels, the four IR active modes which are triply degenerate may split into three vibrations. If the splitting is not too large and, there is certain statistical distribution of various

cations over the tetrahedral and octahedral sites, one cannot observe the splitting but only broadening of the absorption band. The broadening of the spectral lines in the IR spectra, in the present studies, may be due to this reason.

Waldron [465] and Hafner [470] assigned the high frequency ν_1 band to the intrinsic vibrations of the tetrahedral groups and the low frequency ν_2 band to the octahedral group. Absorption ν_1 is caused by stretching of tetrahedral metal oxygen and ν_2 is caused by the oxygen vibrations in the direction perpendicular to the tetrahedral ion oxygen axis. The two absorptions, ν_2 and ν_1 , have been associated with the vibrations of the metal ion in the isotropic force fields to their octahedral and tetrahedral environments. The bands ν_3 and ν_4 are not observed in the spinel ferrites [471].

Siratori [472], Grimes et al [473] and Kanturek et al [474] have studied the influence, exerted by cubic lattice distortion or Jahn - Teller effect, on the IR spectra of spinels. Further, Patakova et al [475] have shown that, the presence of Fe^{2+} ions in ferrite can cause splitting of absorption bands, which is said to be due to Jahn - Teller distortion, produced by Fe^{2+} ions, which locally create deformation in the lattice. The absence of such split or a double band near 600 cm^{-1} (ν_1 band) in the IR spectra of all the ferrite samples indicates that excessive Fe^{2+} ions are not present in the MgFe_2O_4 samples. The presence of Fe^{2+} ions in the ferrite causes a shoulder or splitting of the absorption band.

c) Magnetic characterisation

i) saturation magnetization

The magnetic properties of the ferrites are strongly dependent on chemical composition, sintering temperature, sintering atmosphere, crystal structure, cation distribution, porosity, grain size etc. [476-477]. The saturation magnetization is studied with the help of hysteresis behaviour. The value of saturation magnetization depends on the nature of cations and cation distribution. The magnetization of ferrites results from the distribution and alignment of magnetic ions on the octahedral and tetrahedral sites. Spontaneous magnetization arises if the magnetic atoms are sufficiently close to each other. The electrons can undergo an exchange interaction between neighbouring magnetic atoms.

The exchange interaction between the neighbouring atoms may be indirect or may take place via an intermediate non-magnetic atom like oxygen [478]. The coupling between magnetic atoms in a substance may lead to parallel or antiparallel alignment of the spins of neighbouring atoms. When the alignment is parallel, the exchange interaction is positive and it is ferro magnetic. The alignment when antiparallel, the exchange interaction is negative and, it is either antiferromagnetic or ferrimagnetic, depending upon the complete or incomplete cancellation of magnetic moment within the crystal.

A demagnetized ferromagnetic material exhibits a state of zero magnetization. When sufficiently large magnetic field is applied to a ferro or ferrimagnetic substances, the magnetization changes from zero to saturation value. This was explained first by Weiss [479], on the basis of his domain theory. The process of magnetization of the specimen to saturation involves its conversion

to a single domain state, so that the magnetization vector lies parallel to the applied field.

From the hysteresis loops obtained in our studies, on all the MgFe_2O_4 samples, the saturation magnetization, σ_s , $4\pi M_s$ and magnetone number are calculated and tabulated in Table 4.4. The saturation magnetization, σ_s , values, are found to be in the range of 22.15 to 28.2 emu/g, for all MgFe_2O_4 synthesized from $\gamma\text{-Fe}_2\text{O}_3$ sources. A low σ_s value of 17.2 emu/g is observed for the ferrite MGHEM, prepared from $\alpha\text{-Fe}_2\text{O}_3$. These values are in comparable range of 22-28 emu/g, reported for the ferrite [147, 446-447, 454].

The $4\pi M_s$ values for all samples of MgFe_2O_4 , in the present studies, from $\gamma\text{-Fe}_2\text{O}_3$ source (Table 4.4), are in the range 922-1168 G and their value compare well with the reported values of 1140-1530 G, for the ferrite prepared by Sol gel super critical drying method [207] and other methods [449, 453]. Again, the MgFe_2O_4 (MGHEM) from $\alpha\text{-Fe}_2\text{O}_3$ source shows a low value of 609.5 G

The magnetone number (n_B) ranges from 0.79 to 1.01, in all MgFe_2O_4 preparations from $\gamma\text{-Fe}_2\text{O}_3$ (Table 4.4), while the reported have values between 0.93 - 1.2 [143,147]. The MgFe_2O_4 synthesized from $\alpha\text{-Fe}_2\text{O}_3$ (MGHEM), however, shows a lowest magnetone number of 0.62.

In general, the MgFe_2O_4 samples, in the present investigations, show slightly lower values of saturation magnetization ($4\pi M_s$) and magnetone number. This is due to, the lower temperature, as well as, comparatively shorter duration used for sintering the MgFe_2O_4 samples, which results in the higher porosity (Table 4.3) thus, decreasing the magnetic properties. It has been observed, generally, that

TABLE 4.4 Data on saturation magnetisation (σ_s), $4\pi M_s$ and magnetone number (n_B) for magnesium ferrites

Sample	Saturation Magnetisation		Magnetone number
	σ_s (emu/g)	$4\pi M_s$ (Gauss)	(n_B)
1. MGFFHA	25.96	1082	0.93
2. MGFSHA	24.36	967.2345	0.87
3. MGFMHA	22.15	922.3476	0.79
4. MGFTHA	24.79	1096.8411	0.89
5. MG γ FA	25.34	1042.656	0.91
6. MG α FA	25.96	1110.237	0.93
7. MGamp.FA	28.2	1168.4023	1.01
8.MGHEM	17.2	609.5038	0.62

TABLE 4.5 Data on curie temperatures by different methods for Magnesium ferrites

Sample	Curie temperature ($^{\circ}\text{C}$) from		
	Magnetic Susceptibility	Initial Permeability	Resistivity
1. MGFFHA	385	416	399
2. MGFSHA	397	—	399
3. MGFMHA	369	394	385
4. MGFTHA	387	409	412
5. MG γ FA	407	439	426
6. MG α FA	427	452	439
7. MGampFA	407	444	425
8.MGHEM	457	469	466

the magnetization values for samples sintered for longer duration and at higher temperatures are higher than samples sintered for shorter duration and also at lower temperature [452]. According to Rodrigue [480], the magnetic properties of ferrites depend greatly on the intrinsic parameters like grain size and porosity.

Higher sintering temperature and longer duration usually increases in grain size and decreases porosity [452, 481]. As a result, saturation magnetization increases for samples sintered for longer durations. Apart from the increase in grain size, the rise in magnetization may be attributed to a number of other micro structural changes that take place during sintering.

Each grain possesses a certain resultant magnetic moment. And, since the rate of grain growth depends on sintering time [482], the porosity is high for specimens sintered for lower sintering times. A pore is a sort of void or a gap and, this will break up the magnetic circuit between grain to grain. If the number of pores is large, this may lead to the net reduction of magnetization, in the bulk. The grain boundary acts as an obstacle for the domain wall motion or rotation. Due to the large number of grains per cc, the net area of the grain boundary increases and, thus, greater resistance for the process of magnetization is observed. But, when the material is sintered for longer sintering time, the net area decreases due to densification of grains and the magnetization gets intensified more easily.

Besides this, when there are more pores, the probability of occurrence of closed pore chains increases, leading to reduction of magnetization. This view is supported by the work of Rikukawa [483]. According to the model proposed by him, the demagnetizing field is caused by closed pores and closed grain boundaries.

But, at a high sintering temperature, the pores are reduced and the effect of formation of closed chains decreases, thereby, increasing the magnetization.

ii. A.C.Susceptibility

A.C.Susceptibility studies explore the existence of multidomain (MD), single domain (SD) and super paramagnetic (SP) particles in the material. For ferrimagnetic materials, the variations of normalized a.c. susceptibility versus temperature have been reported by many workers [119-121]. From these curves the curie temperature and domain structure have been estimated. It has also been found that at curie temperature the curve drops almost to zero.

Below curie temperature, ferrites have ferri magnetic nature. Above curie temperature, magnetic transition occurs from ferrimagnetic to paramagnetic. It is generally believed that the susceptibility of a magnetic material always increases on heating and shows a peak just, before the curie temperature, as was first observed for iron by Hopkinson [484]. Generally, when magnetic materials, such as, ferrites, are prepared by ceramic method, mixed domain states tend to be formed, resulting in bulk magnetic properties, appropriate to such mixtures [485]. The magnetic state of SD particles and SP particles are interchangeable with temperature.

In the present study, the measurement of low field a.c.susceptibility with temperature for all the MgFe_2O_4 samples are carried out. The plots of the variation of normalized susceptibility (χ_T/χ_{RT}) with temperature (T) are shown in

figs. 4.3 (a, b, c). It has been suggested [486] that, humps or cusps in χ_{ac} -T curves indicate the presence of a single domain (SD) in a sample and lack of such features imply that the sample consists predominantly of multidomain (MD) grains. The shape of the χ_{ac} -T curves for MGFTHA (Fig. 4.3) indicates that the sample contains a predominantly multidomain grains (MD), while the curves for MGFFHA, MGFMHA, MG γ FA, MGAmPFA and MGHEM show the single domain-superparamagnetic (SD-SP) transition. The χ_{ac} -T curve for MGFSHA and MG α FA shows a sharp fall, immediately after the Hopkinson peak.

From the present study, it can therefore be concluded that, the normalized susceptibility versus temperature curves indicate ferrimagnetic behaviour. From these curves the curie temperatures of all the $MgFe_2O_4$ samples are determined and given in table 4.5. The lowest T_c of $369^\circ C$ and the highest T_c of $457^\circ C$ was obtained for MGFMHA and MGHEM respectively. Except for MGHEM, the T_c of all the $MgFe_2O_4$ samples fall in the reported range of $320-440^\circ C$ [94].

Thus, $MgFe_2O_4$ from γ - Fe_2O_3 and α - Fe_2O_3 source show single domain-super paramagnetic (SD-SP) transition. The T_c values are, however, highest in $MgFe_2O_4$, prepared from α - Fe_2O_3 .

iii. Initial Permeability

The temperature variation of the initial permeability, μ_i , is measured for all

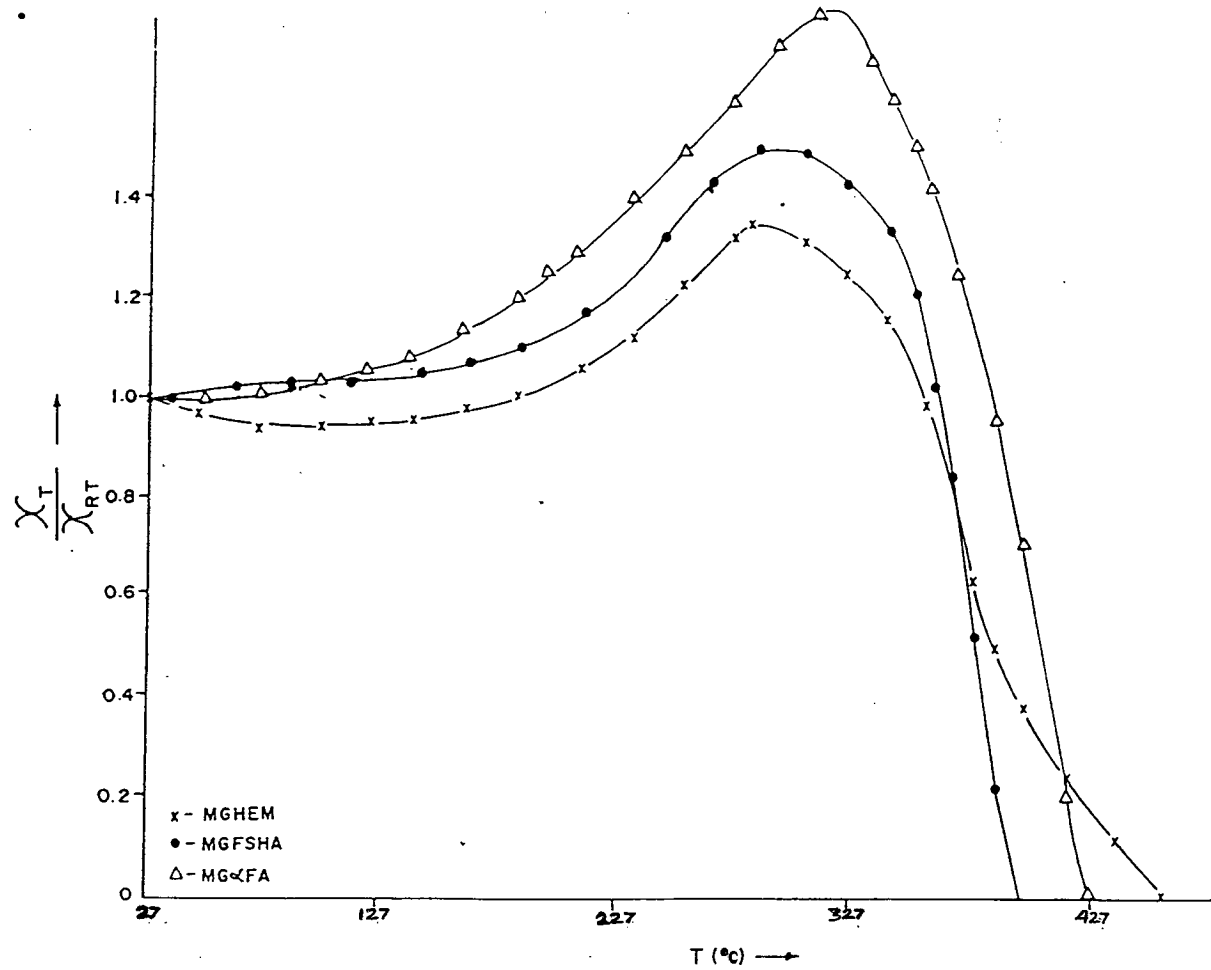


FIG. 4.3a) Temperature dependence of low field a.c. susceptibility of MgFe_2O_4 ferrites 1) $\text{Mg}\alpha\text{FA}$ 2) MgFSHA and 3) MgHEM

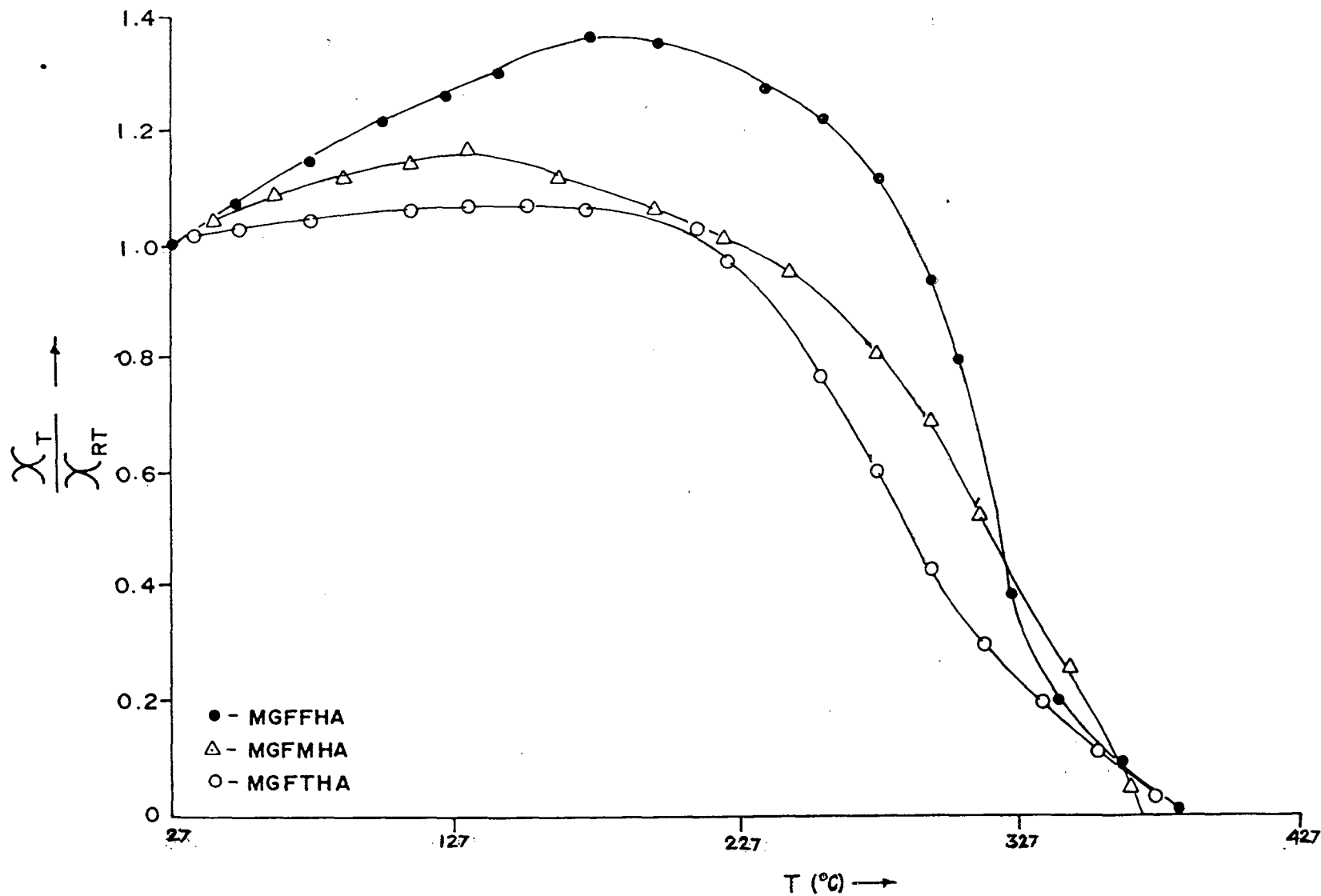


FIG. 4.3 b) Temperature dependence of low field a.c. susceptibility of MgFe_2O_4 ferrites 1) MgFFHA 2) MgFMHA and 3) MgFTHA

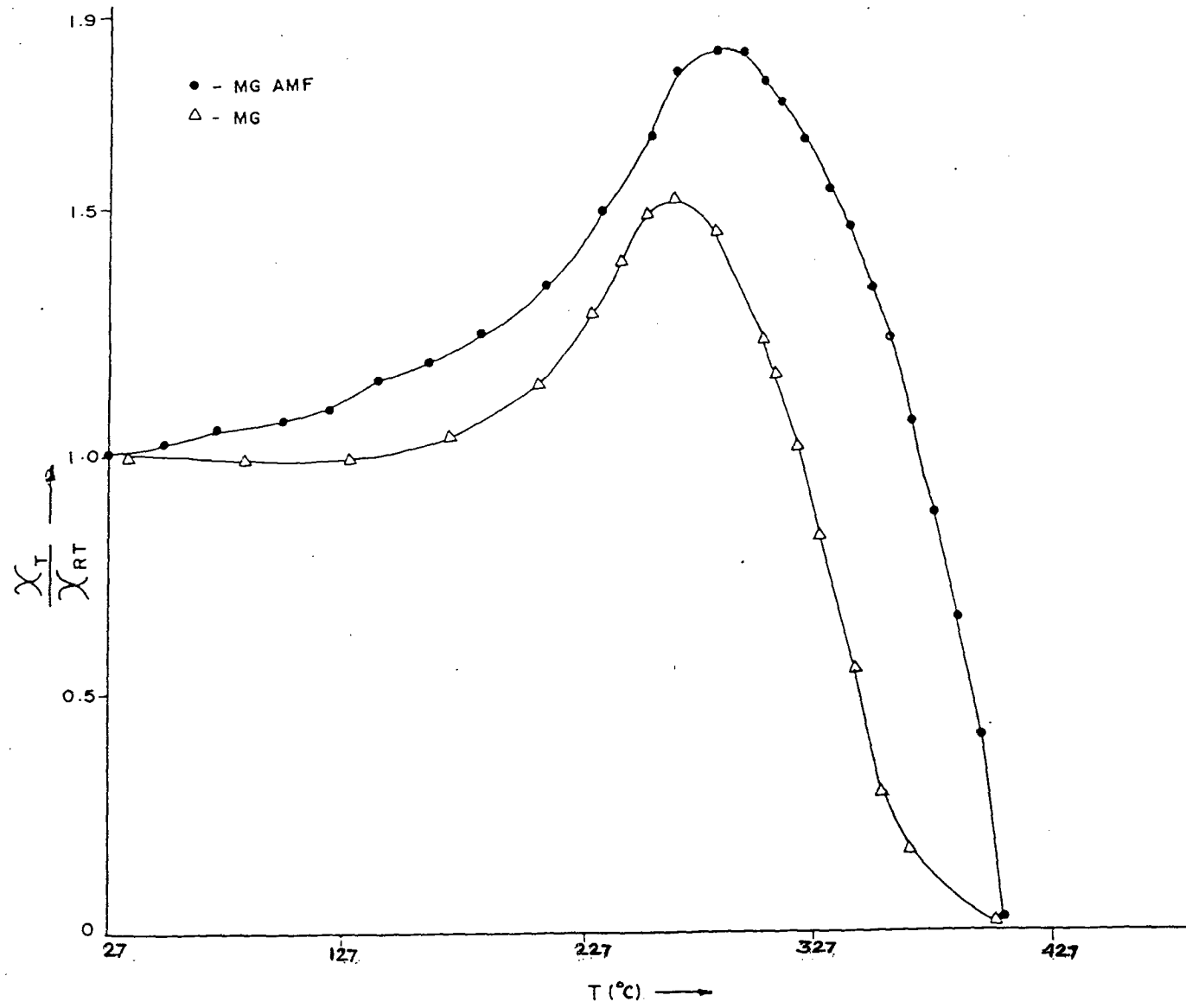


FIG. 4.3 c) Temperature dependence of low field a.c. susceptibility of MgFe_2O_4 ferrites 1) MgAmpFA and 2) MgyFA

the MgFe_2O_4 samples and is shown in Fig 4.4 (a & b). With the increase in temperature, μ_i initially increases gradually and, afterwards rapidly as it approaches near T_c . At the curie temperature of the samples, μ_i drops off sharply.

The sharp decrease in the samples of the ferrites prepared from $\gamma\text{-Fe}_2\text{O}_3$ excepting the one from $\alpha\text{-Fe}_2\text{O}_3$ (MGHEM) suggests a single phase MgFe_2O_4 presence. The MGHEM which had indicated an impurity phase of $\alpha\text{-Fe}_2\text{O}_3$ (in XRD) shows no sharp decrease in $\mu_i - T$ curve.

A variety of $\mu_i - T$ curves have been obtained for ferrites [448], but the domain state of the samples was not considered by these authors in accounting for the shapes, possibly, because of the traditional treatment of the peaks as simply due to the Hopkinson effect. However, it is quite easy to demonstrate that $\mu_i - T$ or $\chi - T$ curves will be different for MD and SD samples of the same material, as has been shown in the case of magnetite.

All the samples, in the present investigations, exhibit a peak called Hopkinson peak, in $\mu_i - T$ variations. From the $\mu_i - T$ curves of all the MgFe_2O_4 samples the curie temperatures are determined and given in Table 4.5. The lowest T_c recorded is 394°C for MGFMA while the highest for MGHEM, is 469°C . All the curie temperatures obtained for the samples (except MGHEM) match well with the reported one.

Many researchers [487-490] have investigated permeability in the samples of the same composition with different porosity and grain size. When pores occurred

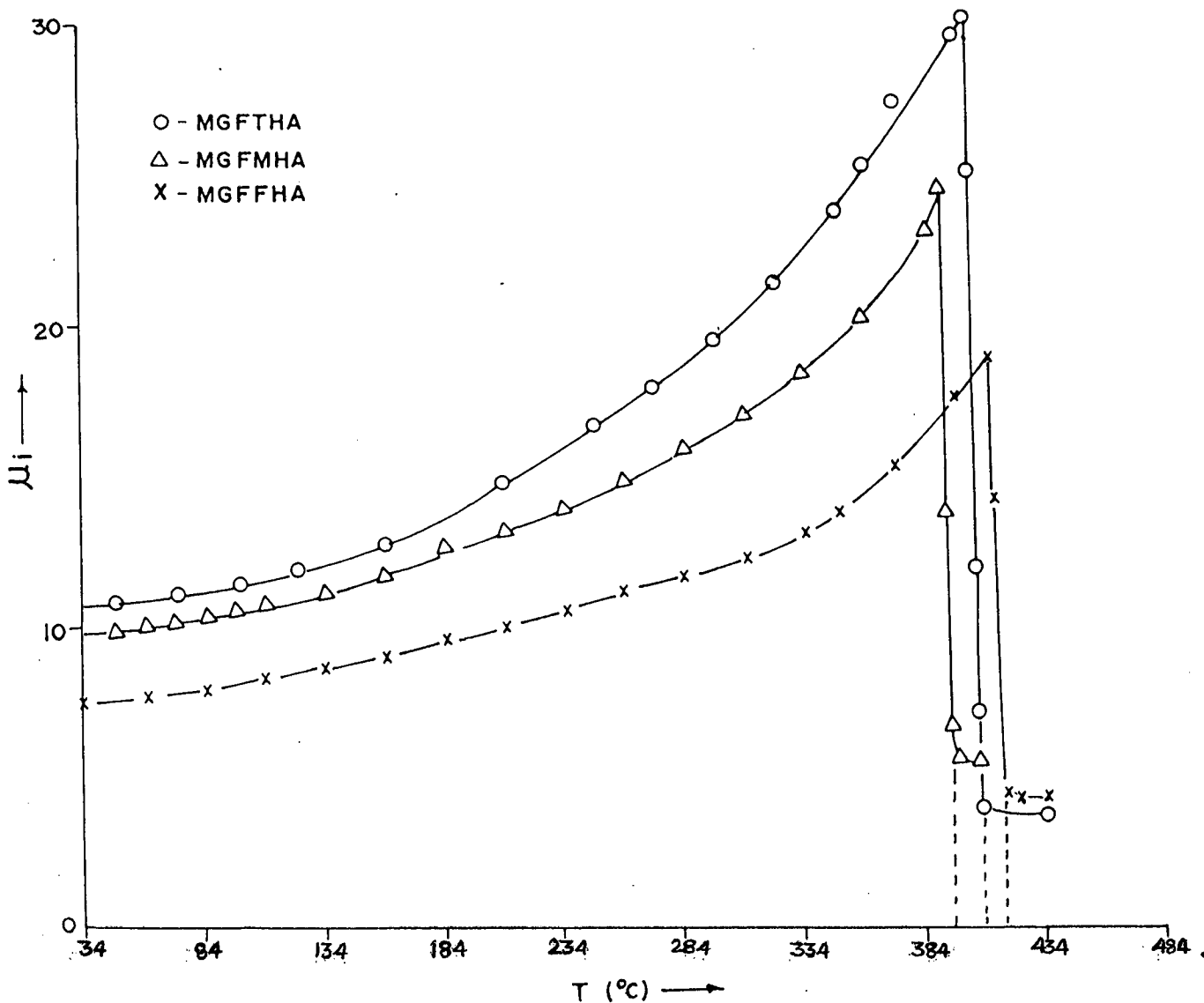


FIG. 4.4a) Temperature variation of initial permeability of $MgFe_2O_4$ ferrites 1) MgFTHA 2) MgFMHA and 3) MgFFHA

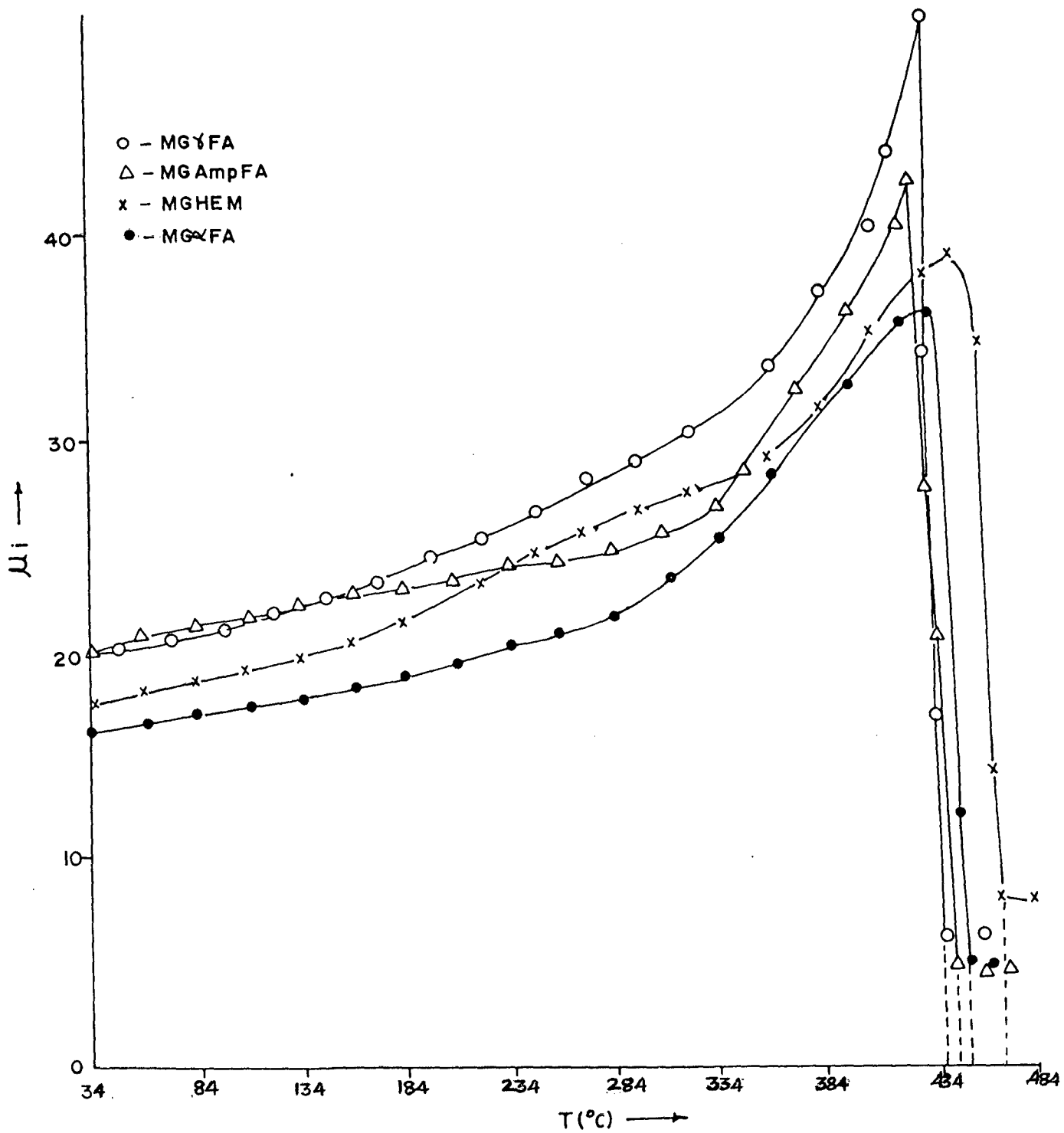


FIG. 4.4b) Temperature variation of initial permeability of MgFe₂O₄ ferrites 1) Mg γ FA 2) MgAmpFA 3) MgHEM and 4) Mg α FA

only between the grains, μ_i was found to vary as $1-P$, where P is the volume fraction of the pores. Large differences in μ_i were found with variation of the mean grain size D_m ; in fact μ_i proved to be almost proportional to D_m for grain size between 1 and 10 μm .

The contribution to μ_i comes from (i) domain wall motion and, (ii) spin rotation. The contribution due to spin rotation is smaller. In most of the magnetic materials μ_i increases with the temperature, upto the curie temperature T_c . This is because the anisotropy field usually decreases with the temperature much faster than M_s . In an ideal homogeneous ferrite, however, there is only one temperature at which the crystal anisotropy is exactly zero. When crystal anisotropy, K , passes through zero at a temperature T_k , the permeability rises to a high peak at this point. This has been observed in the present study.

In μ_i - T curves an appearance of second peak is observed in the case of samples containing excess Fe^{2+} ions, and the absence of such peak in the present samples indicate an absence of Fe^{2+} . This aspect of absence of excessive Fe^{2+} ions has also been confirmed by infra red studies done on these samples.

Initial permeability is one of the properties which can be very dependent upon the method of preparation ; its magnitude often varies markedly with firing temperature, as firing schedule alters the porosity of the sintered product. In a sintered ferrite if there are pores then they would form barriers to prevent or at least hinder the movement of the domain wall. In addition, the pores give rise to local

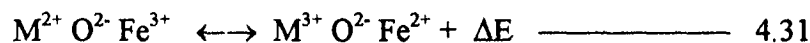
demagnetizing fields which are expressed to modify the domain pattern near to a boundary. The variation of initial permeability with grain size has been studied by many workers [456]. In general, μ_i increases with the increase in grain size. The initial permeability of a ferrite is also reported [491] to be affected by stress either internal stress or external applied stress.

d) Electrical properties

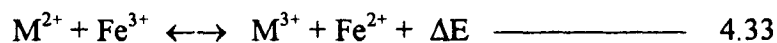
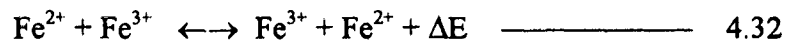
i. Resistivity

Ferrites have very wide range of resistivities from 10^{-3} to 10^{11} Ωcm , at room temperature [100]. This low and high resistivities of ferrites are mainly explained on the basis of actual location of cations in the spinel structure and hopping mechanism. Their high conductivity is due to simultaneous presence of ferrous and ferric ions in the crystallographically equivalent sites. The high resistivity in ferrites is associated with the occupation of B-sites by other divalent metal ions and trivalent iron ions. Such an arrangement requires higher activation energy for hopping of electrons.

The mechanism of transport phenomenon in ferrites can be represented as [492],



The two mechanism of conductivity can be represented as



where ΔE is the activation energy, the energy required for transfer of electron from M^{2+} to Fe^{3+} and vice versa. The valence states of the two ions get inter changed.

Under the influence of an electric field these extra electrons can be regarded to constitute the current, by jumping or hopping process [493].

The free electron model cannot explain the electrical conductivity of ferrites because of the fact that the electrons in ferrites are not free and, energy band model is not suitable to explain the electrical conductivity for the lack of Bloch type wave functions for electrons in ferrites. The conductivity of ferrites can be, however, explained in terms of electronic charge carriers, like electrons and holes, by the relation

$$\sigma = e [n_e \mu_e + n_h \mu_h] \text{ ————— } 4.34$$

where n and μ are the concentration and mobility of electrons and holes respectively.

In ferrite lattice, the electrostatic interaction between electron and the neighbouring ions results into the polarization field called polaron. When such association is weak, it constitutes large polaron. Such polarons are found in ionic crystals. When electron plus lattice deformation have a linear dimension smaller than lattice constant, they constitute small polarons. Such polarons are found in covalent crystals.

The electrical resistivity, the change in activation energy at Curie temperature and the relation of activation energies with composition can be explained and discussed in the light of the mechanism of the hopping of polarons, which has been successfully employed to explain the electrical properties of ferrites, [494-495]. These polarons have low activation energy in magnetic region, while more activation energy in non - magnetic region.

The electrostatic interaction between a conduction electron or hole and nearby ions may result in a displacement of the latter and hence in polarization of the surrounding region. So the carrier becomes situated at the centre of the polarization potential well. If this well is deep enough, a carrier may be trapped at a lattice site and its transition to a neighbouring site may be determined by thermal activation. If this activation is sufficient, the conduction can take place by hopping of electrons, from one lattice site to another.

In ferrites, having spinel structure, the B-B distances are smaller than A-A and A-B distances. Even then, the B-B distance is much larger than the sum of ionic radii of the cations involved, indicating a little or no overlap between d-d wave functions of ions on adjacent octahedral sites. This gives rise to a situation in which the electrons are not free to move through the crystal but remain fixed on B-sites, necessitating a hopping process. However, in the ferrite samples, like the one in the present study, conductivity is decided mainly by the availability of a pair of cations [496] that facilitate the hopping. Thus, in magnesium ferrites, non-availability of Fe^{2+} ions on the B-site due to occupancy by Mg^{2+} ions, would give rise to lower conductivity, as was reported [497] and is also observed in the present study.

The plots of $\log \rho$ Vs $1/T$ (Fig 4.5 a, b & c) for all MgFe_2O_4 prepared from $\gamma\text{-Fe}_2\text{O}_3$, in the present investigations, show a linear decrease in resistivity with the increase in temperature from room temperature to 525°C . At room temperature, $\log \rho$ values are $\sim 10^7 \Omega\text{cm}$ which decreases to $\sim 10^4 \Omega\text{cm}$ at $\sim 525^\circ\text{C}$. A straight line plots for all these samples show a change in inclination. A

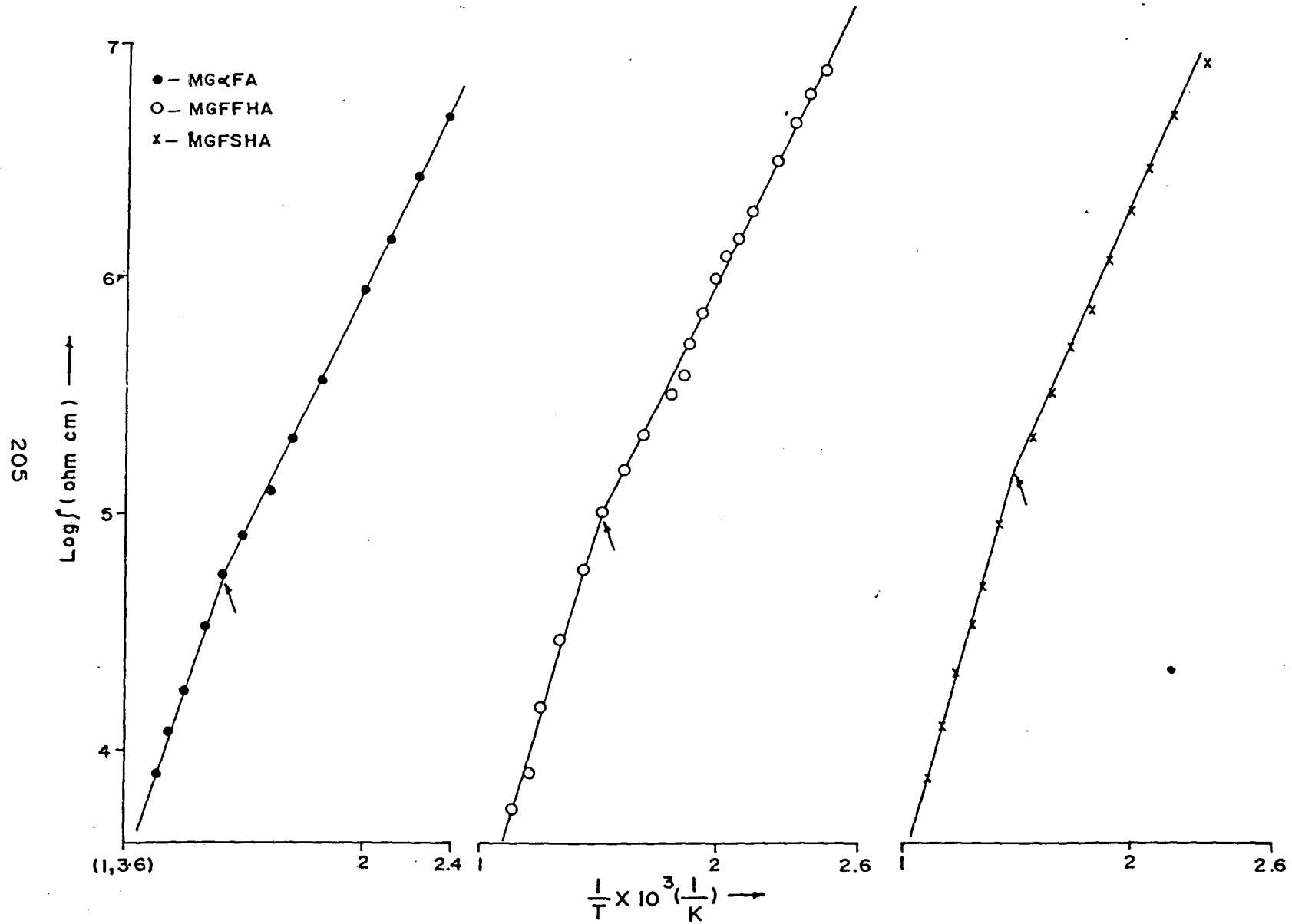


FIG. 4.5 a) Plot of $\text{Log } \rho$ versus $10^3/T$ of MgFe_2O_4 ferrites 1) MgαFA
2) MgFFHA and 3) MgFSHA

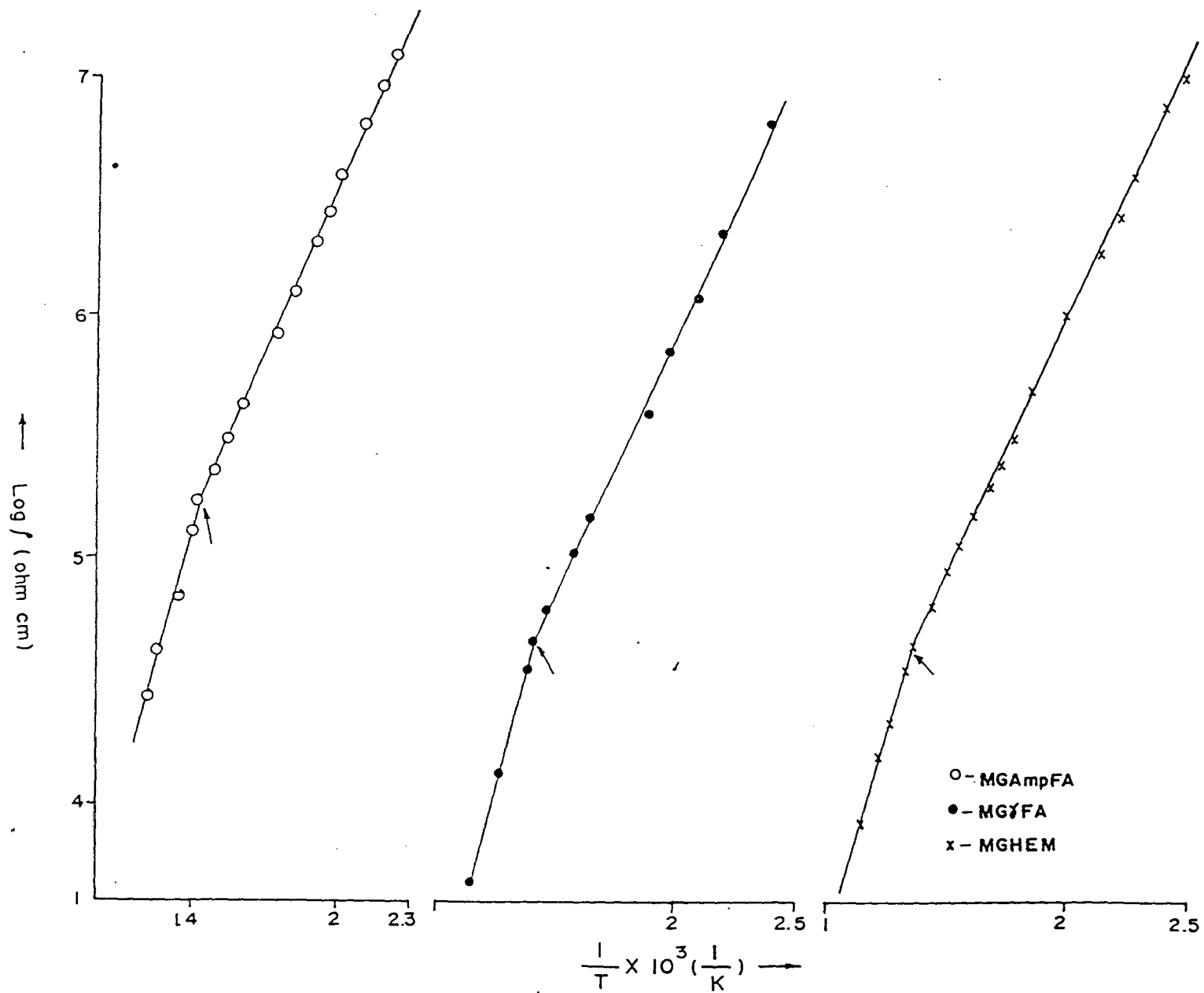


FIG. 4.5 b) Plot of $\text{Log } \rho$ versus $10^3/T$ of MgFe_2O_4 ferrites 1) MgampFA
2) MgγFA and 3) MGHEM

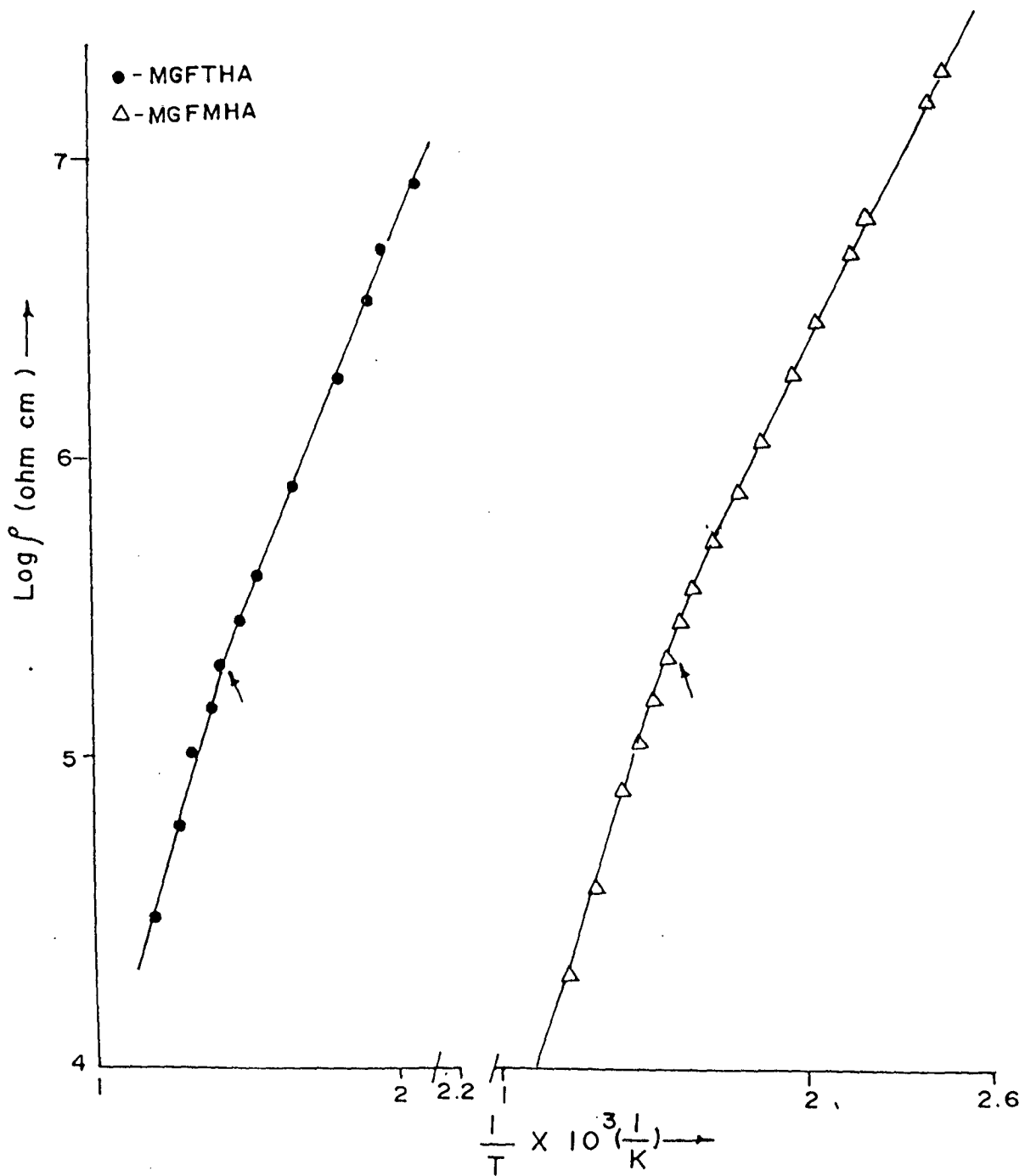


FIG. 4.5 c) Plot of $\text{Log } \rho$ versus $10^3/T$ of MgFe_2O_4 ferrites 1) MgFTHA and MgFMHA

clear two regions of the straight line plots of different slopes are observed for all. In general, the change in inclination is found $\sim 412^{\circ}\text{C}$. The MgFe_2O_4 synthesized from $\alpha\text{-Fe}_2\text{O}_3$ (MGHEM) however, shows a change in inclination $\sim 466^{\circ}\text{C}$. The region between RT and 412°C (low temperature region) gives an activation energy ~ 0.44 eV, measured from the slope (Ferri region, Table 4.6). The region above 412°C (Para region) in the straight line plot indicates an activation energy ~ 0.68 eV. A difference of 0.24 eV (ΔE) in activation energy is observed in going from low temperature region (ferri) to high temperature region (para). These observations match well with the reported values [149, 498].

The activation energy in the paramagnetic region is found to be higher with the theory developed by Irkin and Turov [499]. Similar results were also observed for many ferrites [492, 500].

It was shown [499, 501] theoretically that on passing through the curie point a change must occur in the gradient of the straight line and that the magnitude of this effect depends on the exchange interaction between outer and inner electrons which alters at the curie point. The experimental observation of the transition near the curie point, in all the magnesium ferrite samples, is in agreement with the theory.

The temperature at which the low temperature region switches to high temperature region, that is, ferri magnetic region to para magnetic region, in all these samples is considered to be curie temperatures of the samples and, these values resemble closely with the curie temperatures found in susceptibility and permeability measurements. A comparative table is given in Table 4.5.

TABLE 4.6 Data on activation energy and curie temperature for magnesium ferrites.

Sample	Activation Energy (ev)			Curie temperature (°C)
	Ferri region	para region	ΔE	
1. MGFFHA	0.43	0.71	0.28	399
2. MGFSHA	0.45	0.71	0.26	399
3. MGFMHA	0.43	0.66	0.23	385
4. MGFTHA	0.48	0.71	0.23	412
5. MG γ FA	0.44	0.70	0.26	426
6. MG α FA	0.42	0.66	0.24	439
7. MGamp.FA	0.48	0.66	0.18	425
8. MGHEM	0.44	0.66	0.22	466

According to Otari et al [500] the change in activation energy at curie point can be attributed to the effect of magnetic ordering in the conduction process. In the present studies, the activation energy ~ 0.4 eV suggests that the conduction is due to polaron hopping model. According to Semary et. al. [502] if the activation energy is in the range of 0.4 to 0.7 eV, then the conductivity is of an intrinsic nature and governed by the Fe^{3+} concentration in the B-site. In the present studies too the activation energies in the intrinsic or high temperature range are ~ 0.68 eV.

The electrical resistivity values, for all the MgFe_2O_4 samples in the present study at room temperature, match well with the reported values [149, 503-504]. The high resistivity values of the order of $10^7 \Omega \text{ cm}$, at room temperature, rules out the presence of any appreciable amounts of Fe^{2+} ions in the ferrite samples. The similar observations are also reported in the literature [444].

ii. Dielectric constant

Ferrites act as dielectric materials in the low frequency regions. The dielectric constant of poly crystalline ferrites depends upon operating frequency. When alternating electric field is applied on the ferrite materials, there occurs dielectric displacement. They have abnormally high dielectric constant which shows the frequency dispersion. The dielectric constant of ferrites depends upon method of preparation [106], chemical composition and substitution [505] and, porosity and grain size[506]. Krammer [104] has explained the relation between grain size and dielectric constant.

- According to Koops [507], the dielectric constant is inversely proportional to square root of conductivity. The variation in dielectric constant, ϵ' , with

temperature for all the MgFe_2O_4 samples, from 27 to 327°C at 1 KHz, was measured and is shown in the Fig. 4.6 (a & b). It can be seen from the figures that dielectric constant increases slowly with temperature up to around 177°C in all the samples except MGFTHA, where it slowly increases upto 227°C and, above these temperatures the increase is more rapid. These results closely match with the observations of RadhaKrishna and Badarinath [508].

The dielectric properties versus frequency is desired to draw any further conclusion on the system.

4.4 Conclusion

- (1) Single phase magnesium ferrite, MgFe_2O_4 , is achieved ~ 1000°C for all the samples prepared from $\gamma\text{-Fe}_2\text{O}_3$ source, while $\alpha\text{-Fe}_2\text{O}_3$ source indicated an impurity phase, $\alpha\text{-Fe}_2\text{O}_3$, along with the MgFe_2O_4 suggesting no complete ferritization taken place ~ 1000°C.
- (2) MgFe_2O_4 prepared from $\gamma\text{-Fe}_2\text{O}_3$ showed porosity in the range of 21-29 %, while the ferrite from $\alpha\text{-Fe}_2\text{O}_3$ indicated higher porosity of ~ 42%.
- (3) Saturation magnetization ($4\pi M_s$ in Gauss) in the range 920 - 1168 G is observed for all MgFe_2O_4 prepared from $\gamma\text{-Fe}_2\text{O}_3$ sources, whereas the ferrite obtained from $\alpha\text{-Fe}_2\text{O}_3$ showed low value, of ~ 610 G.
- (4) Magnetone number (n_B) of 0.79 - 1.01 is found for MgFe_2O_4 from $\gamma\text{-Fe}_2\text{O}_3$ source, while MgFe_2O_4 from $\alpha\text{-Fe}_2\text{O}_3$ source achieved only 0.62 Bohr magnetone.
- (5) Curie temperatures T_c of $412 \pm 27^\circ\text{C}$ from resistivity measurements, 425

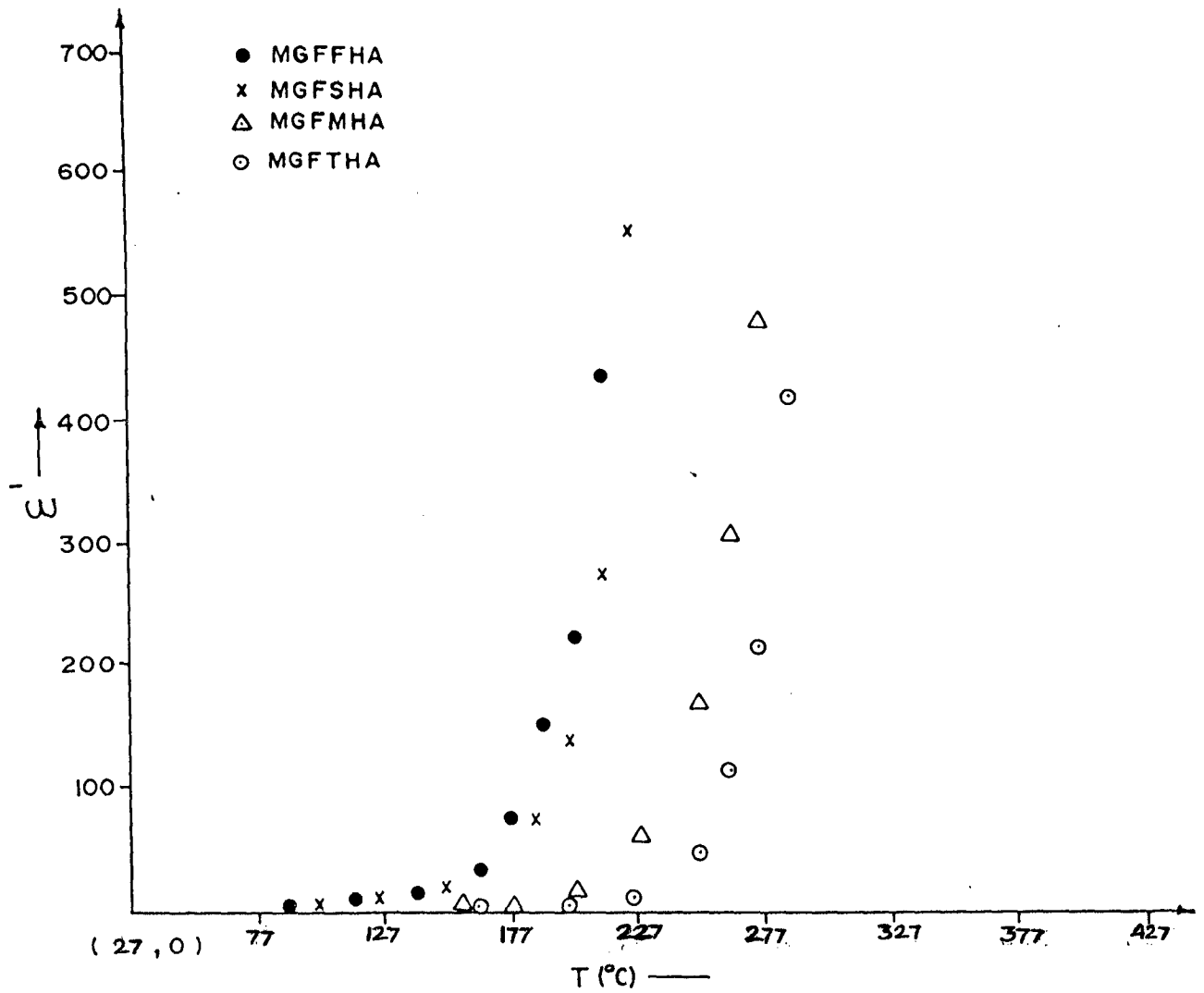


FIG. 4.6 a) Variation of dielectric constant with temperature of $MgFe_2O_4$ ferrites 1) MgFFHA 2) MgFSHA 3) MgFMHA and 4) MgFTHA

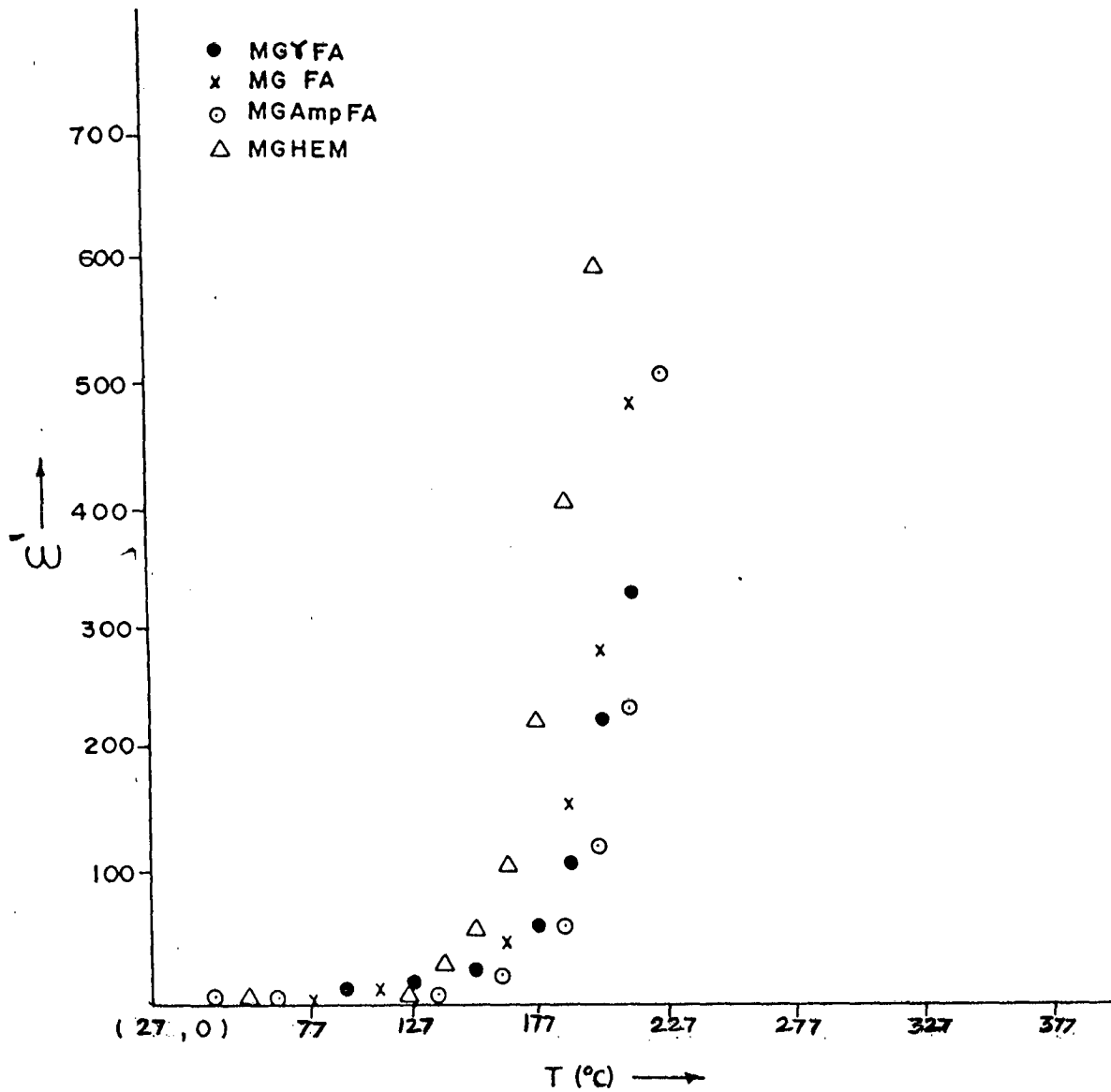


FIG. 4.6 b) Variation of dielectric constant with temperature of $MgFe_2O_4$ ferrites 1) $Mg\gamma$ FA 2) $Mg\alpha$ FA 3) $Mg\Delta$ mpFA and 4) MGHEM

$\pm 29^{\circ}\text{C}$ from permeability and, $397 \pm 29^{\circ}\text{C}$ from magnetic susceptibility measurement indicate not so large spread in the curie temperatures which usually observed (of $\sim \pm 60^{\circ}\text{C}$) in MgFe_2O_4 , depending on firing temperature. This suggests that, although $\gamma\text{-Fe}_2\text{O}_3$ sources are from different precursors, the present firing temperature does not allow the MgFe_2O_4 samples to have a wide range of curie temperatures.

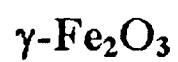
The MgFe_2O_4 prepared from $\alpha\text{-Fe}_2\text{O}_3$, however showed T_c , from all above measurements, of $\sim 464^{\circ}\text{C}$ which is higher than that observed in the ferrites prepared from $\gamma\text{-Fe}_2\text{O}_3$.

(6) MgFe_2O_4 synthesized from $\gamma\text{-Fe}_2\text{O}_3$ source suggests to be giving fairly optimum characteristics, in general, as compared to the ferrite obtained from $\alpha\text{-Fe}_2\text{O}_3$.

(7) Around 1000°C is sufficient to achieve single phase MgFe_2O_4 from $\gamma\text{-Fe}_2\text{O}_3$, while $>1000^{\circ}\text{C}$ is required for the $\alpha\text{-Fe}_2\text{O}_3$ to result into MgFe_2O_4 .

CHAPTER V

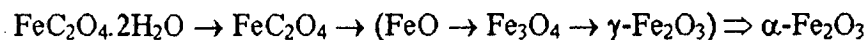
IMPORTANCE OF WATER IN STABILIZING



IMPORTANCE OF WATER IN STABILIZING

$\gamma\text{-Fe}_2\text{O}_3$

As our aim was to use $\gamma\text{-Fe}_2\text{O}_3$ for ferrites synthesis, a detailed literature survey on the preparation of ferric oxide, followed by different methods of preparation adopted by us, is described in chapter III. In the literature survey there we highlighted an importance of water in stabilising $\gamma\text{-Fe}_2\text{O}_3$. A simple thermal decomposition in air of ferrous oxalate dihydrate, $\text{FeC}_2\text{O}_4 \cdot 2\text{H}_2\text{O}$, yields thermodynamically more stable phase of iron oxide, hematite, $\alpha\text{-Fe}_2\text{O}_3$. But in a controlled atmosphere of water vapour, Rane et al [264] obtained mainly $\gamma\text{-Fe}_2\text{O}_3$ from the ferrous oxalate, in air $\sim 300^\circ\text{C}$. The water vapour partial pressure during the thermal decomposition of $\text{FeC}_2\text{O}_4 \cdot 2\text{H}_2\text{O}$ arrests the sequential reaction at $\gamma\text{-Fe}_2\text{O}_3$ stage.



Here the water vapours modify the Fe_3O_4 oxidation leading to $\gamma\text{-Fe}_2\text{O}_3$. It has been suggested that water is crucial in the oxidation of magnetite, Fe_3O_4 [261-271] and magnetite synthesised by dry method found to yield $\alpha\text{-Fe}_2\text{O}_3$, while the magnetite prepared from wet method on oxidation led to $\gamma\text{-Fe}_2\text{O}_3$ [262].

Ferrous oxalate dihydrate on hydrazination forms $\text{FeC}_2\text{O}_4 \cdot \text{N}_2\text{H}_4$ and $\text{FeC}_2\text{O}_4 \cdot 2\text{N}_2\text{H}_4$ and this on autocatalytic decomposition, Moye, Rane and Kamat Dalal [278] observed $\gamma\text{-Fe}_2\text{O}_3$ formation, in ordinary atmosphere. And, here, the hydrazine liberated during decomposition reacts, with atmospheric oxygen releasing enormous energy (eqn. 6) sufficient to oxidatively decompose the dehydrazinated complex. The hydrazine oxidation products ($\text{N}_2 + \text{H}_2\text{O}$) provide an adequate partial pressure of water vapour for stabilizing $\gamma\text{-Fe}_2\text{O}_3$.

Iron (II) carboxylates: ferrous fumarate, ferrous succinate, ferrous malonate, ferrous tartarate, ferrous maleate and ferrous malate [272-277] too decompose mainly to $\gamma\text{-Fe}_2\text{O}_3$, in a controlled atmosphere of water vapour, while in air they yield $\alpha\text{-Fe}_2\text{O}_3$.

In our present studies (chapter III) of the iron (II) carboxylate hydrazinates: ferrous fumarato-hydrazinate, ferrous succinato-hydrazinate, ferrous malonato-hydrazinate, ferrous tartrato-hydrazinate, ferrous maleato-hydrazinate and ferrous malato-hydrazinate, it is observed by us [300,303] that these autocatalytically decompose, in an ordinary atmosphere, mainly to $\gamma\text{-Fe}_2\text{O}_3$. And, here, too hydrazine oxidation products ($\text{N}_2 + \text{H}_2\text{O}$) provide the required partial pressure of water vapour for the stabilization of $\gamma\text{-Fe}_2\text{O}_3$.

The essential requirement of water vapour in the oxidation of Fe_3O_4 to $\gamma\text{-Fe}_2\text{O}_3$ [261-271] and the crystal structure similarity of such gamma ferric oxide with lithium ferrite, LiFe_5O_8 , $(\text{Fe}^{3+})_8[\text{Fe}^{3+}_{12}\text{Li}^{1+}_4]\text{O}_{32}$, are considered to be reflected as proton incorporation in the $\gamma\text{-Fe}_2\text{O}_3$, by such water vapour, during the oxidation. Based on this, protons, H^+ , are thought to be occupying the so called lithium sites [327, 336] of $\gamma\text{-Fe}_2\text{O}_3$ and a formula, HFe_5O_8 , $(\text{Fe}^{3+})_8[\text{Fe}^{3+}_{12}\text{H}^{1+}_4]\text{O}_{32}$, is given to the fully protonated $\gamma\text{-Fe}_2\text{O}_3$. Thus, a hydrogen iron oxide of formula $\text{H}_{1-x}\text{Fe}_{5+x/3}\text{O}_8$ has been proposed [266] with an upper limit of the proton presence is put at $\text{H}_{0.1}\text{Fe}_{5.1/3}\text{O}_8$

Such proton incorporated hydrogen ferrite type of phase was also identified by Nikumbh, Rane and Mukhedkar [280] on the thermal decomposition of $\text{FeC}_2\text{O}_4 \cdot 2\text{H}_2\text{O}$, in a controlled atmosphere of water vapour. Here, the presence of the low temperature phase of hydrogen ferrite type found to transform into usual vacancy ordered $\gamma\text{-Fe}_2\text{O}_3$, $(\text{Fe}^{3+})_8[\text{Fe}^{3+}_8\text{Fe}^{3+}_{5/3}\square_{8/3}]\text{O}_3$, at $\sim 200^\circ\text{C}$. And, such transformation studies were carried out by these authors, by making use of direct current electrical conductivity measurements in different atmospheres, on the $\gamma\text{-Fe}_2\text{O}_3$. Further, influence of divalent and trivalent dopants on these hydrogen iron oxide phase of $\gamma\text{-Fe}_2\text{O}_3$ was studied by Nikumbh, Rane and Mukhedkar [282] and confirmed that the dopants occupy the H^+ place in the $\gamma\text{-Fe}_2\text{O}_3$.

Considering the presence of H^+ in $\gamma\text{-Fe}_2\text{O}_3$ and its substitution by divalent/trivalent metal ions, a study was undertaken to synthesize nickel-zinc ferrite by Moye, Rane and Kamat Dalal [181] to see whether mixed metal ferrites can be easily synthesized. A coprecipitated nickel zinc oxalate, on decomposing in a con-

trolled atmosphere of water vapour gave $\gamma\text{-Fe}_2\text{O}_3$ type of phase $\sim 300^\circ\text{C}$, as an intermediate, incorporating nickel/zinc in the lattice in place of H^+ . This $\gamma\text{-Fe}_2\text{O}_3$ type of phase, consisting of divalent metals then easily form ferrite, MFe_2O_4 , by proper sites seeking, at higher temperature. Like ferrous oxalate in controlled water vapour decomposition leading to $\gamma\text{-Fe}_2\text{O}_3$, the mixed metal oxalates too lead to such $\gamma\text{-Fe}_2\text{O}_3$ type of phase. A $\gamma\text{-(Fe, Mn)}_2\text{O}_3$ type of phase was also observed [509] during the synthesis of catalyst based on iron and manganese oxides.

The hydrazinated nickel-zinc oxalates too decompose autocatalytically like $\text{FeC}_2\text{O}_4 \cdot 2\text{N}_2\text{H}_4$ [181] and $\gamma\text{-Fe}_2\text{O}_3$ type of phase was considered to be intermediate by Moye, Rane and Kamat Dalal [278] in the nickel-zinc ferrite formation. Here hydrazine oxidation products ($\text{N}_2 + \text{H}_2\text{O}$) provide the required partial pressure of water vapour.

Thus, water seems to be essential in $\gamma\text{-Fe}_2\text{O}_3$ formation as it gets incorporated as protons in the $\gamma\text{-Fe}_2\text{O}_3$ lattice.

If water is essential in $\gamma\text{-Fe}_2\text{O}_3$ synthesis then it should reflect as proton in the oxide. And, this aspect, although explored in $\gamma\text{-Fe}_2\text{O}_3$ formation from iron (II) carboxylates [180, 272-277], is considered to be worth while to study in our present investigations, as we have prepared $\gamma\text{-Fe}_2\text{O}_3$ from iron (II) carboxylato-hydrazinates and hydrazinated iron oxyhydroxides, useful for the synthesis of MgFe_2O_4 (chapter IV). These studies may throw some more light on easy ferrite preparation from $\gamma\text{-Fe}_2\text{O}_3$, as compared to usual raw material $\alpha\text{-Fe}_2\text{O}_3$ used in ferrite synthesis.

The present chapter deals with an electrical conductivity measurement of $\gamma\text{-Fe}_2\text{O}_3$, synthesized as in chapter III in various atmospheres. The results of such studies are presented here.

5.2 Experimental : Preparation and characterization

5.2.1 Preparation of $\gamma\text{-Fe}_2\text{O}_3$

A detailed experimental procedure for the synthesis of $\gamma\text{-Fe}_2\text{O}_3$ from different precursors are described in chapter III (part I and II)

FFHA, FSHA, FMHA, FTHA, FEHA and FLHA

$\gamma\text{-Fe}_2\text{O}_3$ is prepared by autocatalytically decomposing ferrous fumarato-hydrazinate (FFHA), ferrous succinato-hydrazinate (FSHA), ferrous malonato-hydrazinate (FMHA), ferrous tartrato-hydrazinate, (FTHA), ferrous maleato-hydrazinate (FEHA) and ferrous malato-hydrazinate (FLHA).

$\gamma\text{-FHA}$ and $\gamma\text{-FHHA}$

$\gamma\text{-Fe}_2\text{O}_3$ is prepared by decomposing $\gamma\text{-FeOOH}$ in air $\sim 300^\circ\text{C}$ ($\gamma\text{-FHA}$) and by autocatalytically decomposing $\gamma\text{-FeOOH}$ equilibrated in hydrazine ($\gamma\text{-FHHA}$).

5.2.2 Standard $\gamma\text{-Fe}_2\text{O}_3$

A standard $\gamma\text{-Fe}_2\text{O}_3$, on which several studies have been done to investigate influence of surface hydroxyl groups on aldol condensation, considering both Brønsted and Lewis acid sites [321], has been procured.

5.2.3 Characterization

a) X-ray diffraction

X-ray diffraction studies were carried out on Rigaku D-Max II x-ray diffractometer using Cu and Fe targets. The observed d-values of the samples were compared with JCPDS files [408-413] to identify the phases.

b) Infra red analysis

Infra red analysis of $\gamma\text{-Fe}_2\text{O}_3$ synthesized from different precursors was done on Shimadzu FTIR instrument, model 8101 A.

c) Magnetic characteristics

The measurements of magnetization of the samples were carried out using an alternating current hysteresis loop tracer described by Likhite et al [304] and supplied by M/s Arun electronics, Bombay, India. The saturation magnetisation values (σ_s) in emu/g of $\gamma\text{-Fe}_2\text{O}_3$ samples were determined.

5.2.4 Thermal analysis

DTA and TG analysis of $\gamma\text{-Fe}_2\text{O}_3$ was done on STA 1500 instrument in air. DSC analysis was carried on, TA instruments, 2000 Thermal analyser - DSC modulated.

5.2.5 Direct current (dc) electrical conductivity in Air, N_2 and $\text{N}_2/\text{H}_2\text{O}$ atmospheres.

Direct current electrical conductivity, σ , as a function of temperature in air, N_2 and again in air, after equilibrating samples with N_2 gas containing water va-

pours were measured for $\gamma\text{-Fe}_2\text{O}_3$, synthesized from different precursors, using a home built conductivity cell system as described in chapter II section 2.2.10.a.

All samples were in pellet form, 15 mm diameter x 2-3 mm thickness. They were pressed between two platinum electrodes in a conductivity cell. A sample of $\gamma\text{-Fe}_2\text{O}_3$ pressed between two platinum electrodes in the cell was introduced in a tubular furnace, where temperature and atmosphere could be monitored as required.

The measurement of resistivity as a function of temperature was carried out with the increase in temperature, from room temperature (RT) to 350°C . And, then, the measurements were continued, during cooling from 350° to RT. The measurements were done, in air and N_2 . Once, the measurements were completed in air and N_2 , the sample in N_2 was brought to 200°C and, then, a known water vapour was introduced over the samples, by bubbling the N_2 carrier gas through water, kept at 60°C . The sample in such a known partial pressure of water vapour in N_2 was kept at 200°C for 2-3 hours to get water equilibrated with the sample. Then, a dry N_2 was passed over the sample, after closing the $\text{N}_2 + \text{H}_2\text{O}$ (moisture) flow. And, in dry N_2 , the sample temperature was brought down to RT. Thereafter, the conductivity measurements were continued in air, during heating (RT - 350°C) and cooling (350°C - RT). The results are plotted as $\log \sigma$ Vs $1/T$ in air, N_2 and after equilibraing in moisture.

5.3 Results and discussion

5.3.1 Direct current (dc) electrical conductivity of $\gamma\text{-Fe}_2\text{O}_3$ in air, N_2 and in air after equilibrating in water vapour.

a) Hysteresis behaviour of conductivity

FFHA, FSHA, FMHA, FTHA, FEHA, and FLHA.

The $\gamma\text{-Fe}_2\text{O}_3$ synthesized by autocatalytic decomposition of ferrous fumarato-hydrazinate (FFHA), ferrous succinato-hydrazinate (FSHA), ferrous malonato-hydrazinate, ferrous-tartrato-hydrazinate (FTHA), ferrous maleato-hydrazinate (FEHA) and ferrous malato-hydrazinate (FLHA), all show similar conductivity behaviour during heating and cooling in air, N_2 and in air after equilibrating the samples with moisture

Results on a representative sample FTHA are shown in Fig. 5.1 (a,b,c).

Curve I and II are the $\log \sigma$ Vs $1/T$ plots during heating and cooling in air, respectively. Further heating in air (curve III), now instead of tracing curve I (Fig. 5a), follows curve II and then cooling (curve IV) too overlaps curve II. The second heating and cooling curves (III and IV) are given in Fig. 5.1b. The heating on this sample when continued in dry nitrogen, the heating and cooling curves (not shown here) also follow curve III and IV and, thus, overlap the cooling curve II.

The increase in σ from RT to 112°C (curve I, Fig. 5.1a) is followed by a decrease upto 198°C . The first increase in conductivity from RT is considered as region A and, the decrease in the conductivity that follows upto 198°C is taken as

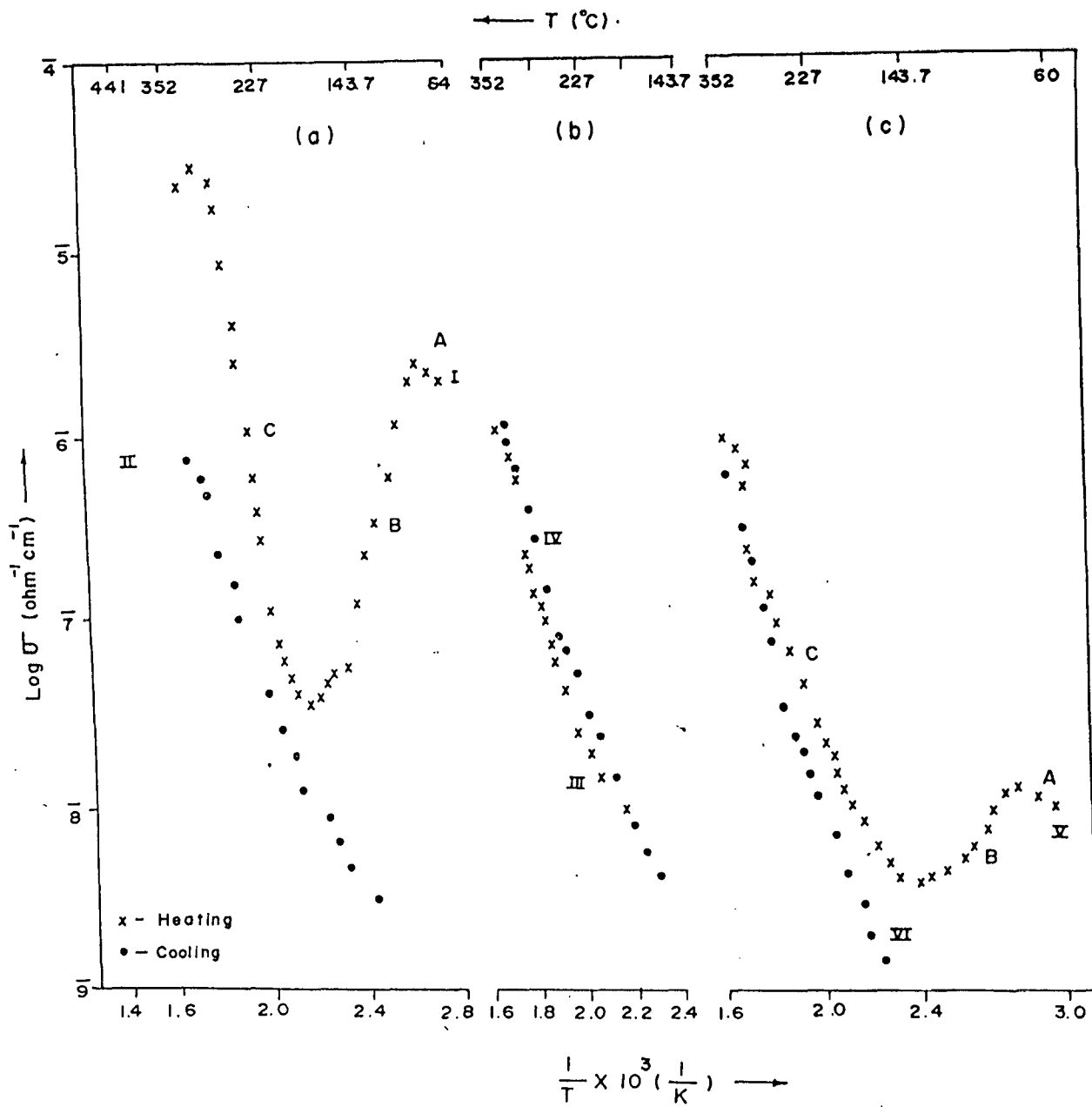


FIG. 5.1 Temperature variation of conductivity of γ -Fe₂O₃ synthesised from ferrous tartrato-hydrazinate (FTHA), in a) air b) Second run in air and c) in air after moisture equilibration ~ 200°C.

region B. From 198°C onwards, there is an increase in conductivity upto 350°C, showing change in inclinations in the otherwise straight line plot ($\log \sigma$ Vs $1/T$), ~ 227°, ~282° and a break ~ 322°C.

On cooling from 350°C (the maximum temperature of investigation in the present studies), the conductivity path does not retrace the heating curve I, instead it follows curve II. There is, thus, a hysteresis in conductivity behaviour which is observed during the first heating and first cooling. Second heating (curve III) now does not follow the path of the first curve I, but it almost overlaps curve II, suggesting that the once heated sample are different from that of as prepared $\gamma\text{-Fe}_2\text{O}_3$. The cooling, thereafter, also follows curve II. Continuing the measurements in dry N_2 atmosphere, too follow the curve II, during heating and cooling.

On equilibrating the sample, after completing the conductivity measurements in N_2 in a known partial pressure of water ~ 200°C for 2-4 h and then measuring conductivity during heating in air, the log plot (curve V, Fig. 5.1.c) shows an initial increase from RT upto ~ 90°C (region A) and then decrease upto 143°C (region B). Thereafter, there is a steep increase upto 350°C showing a change in inclination ~ 227°C and 282°C and a break around 329°C.

The increase in conductivity from 143°C upto 350°C (curve V, Fig. 5.1.c) and from 198 upto 350°C (curve I, Fig. 5.1a) are the region C. The conductivity then decreases from 350°C upto room temperature (curve VI, Fig. 5.1c) and this almost overlaps with curve II, III, IV of Fig. 5.1a & b. Thus the moisture equilibrated sample shows an almost similar behaviour in its conductivity during heating and cooling, to that of fresh samples of $\gamma\text{-Fe}_2\text{O}_3$. The hysteresis in conductivity be-

haviour is reappeared for $\gamma\text{-Fe}_2\text{O}_3$, after heating in air and N_2 and then moisture equilibrating.

These results on moisture treated samples suggests that the samples once heated in air and N_2 behave similar to the fresh one, after moisture equilibration.

Std. $\gamma\text{-Fe}_2\text{O}_3$

A sample of $\gamma\text{-Fe}_2\text{O}_3$ on which several studies have been done to investigate influence of surface hydroxyl groups on aldol condensation, considering both Brønsted and Lewis acid sites [321], has been procured by us.

The same sample of the $\gamma\text{-Fe}_2\text{O}_3$ is considered as standard and characterized by XRD, IR, density measurement. A detailed DTA, TG, DSC analysis were also done. The results of such studies are used to support the electrical characterizations of this and compare them with the results of FTHA.

DTA indicated (Fig.5.2a) $\gamma\text{-Fe}_2\text{O}_3$ to $\alpha\text{-Fe}_2\text{O}_3$ transformation $\sim 564^\circ\text{C}$, by an exothermic effect. A gradual mass loss of $\sim 1.5\%$ observed in TG upto this transformation suggests the loss of adsorbed water.

The temperature variation of conductivity of this as supplied Std. $\gamma\text{-Fe}_2\text{O}_3$ (Curve I, Fig.5.2a) shows an increase in σ from RT to 50°C (region A) followed by a decrease upto 98°C (region B). From 98°C onwards, there is a steep increase in σ upto 600°C . Thus, the temperature of 600°C was chosen to cover the transformation of $\gamma\text{-Fe}_2\text{O}_3$ to $\alpha\text{-Fe}_2\text{O}_3$. Between 400 and 550°C there are several conductivity breaks in the log plot. Then, there is again a steep increase in σ , after 550°C and, this behaviour above 550°C may be due to $\alpha\text{-Fe}_2\text{O}_3$, now formed. On cooling, the conduc-

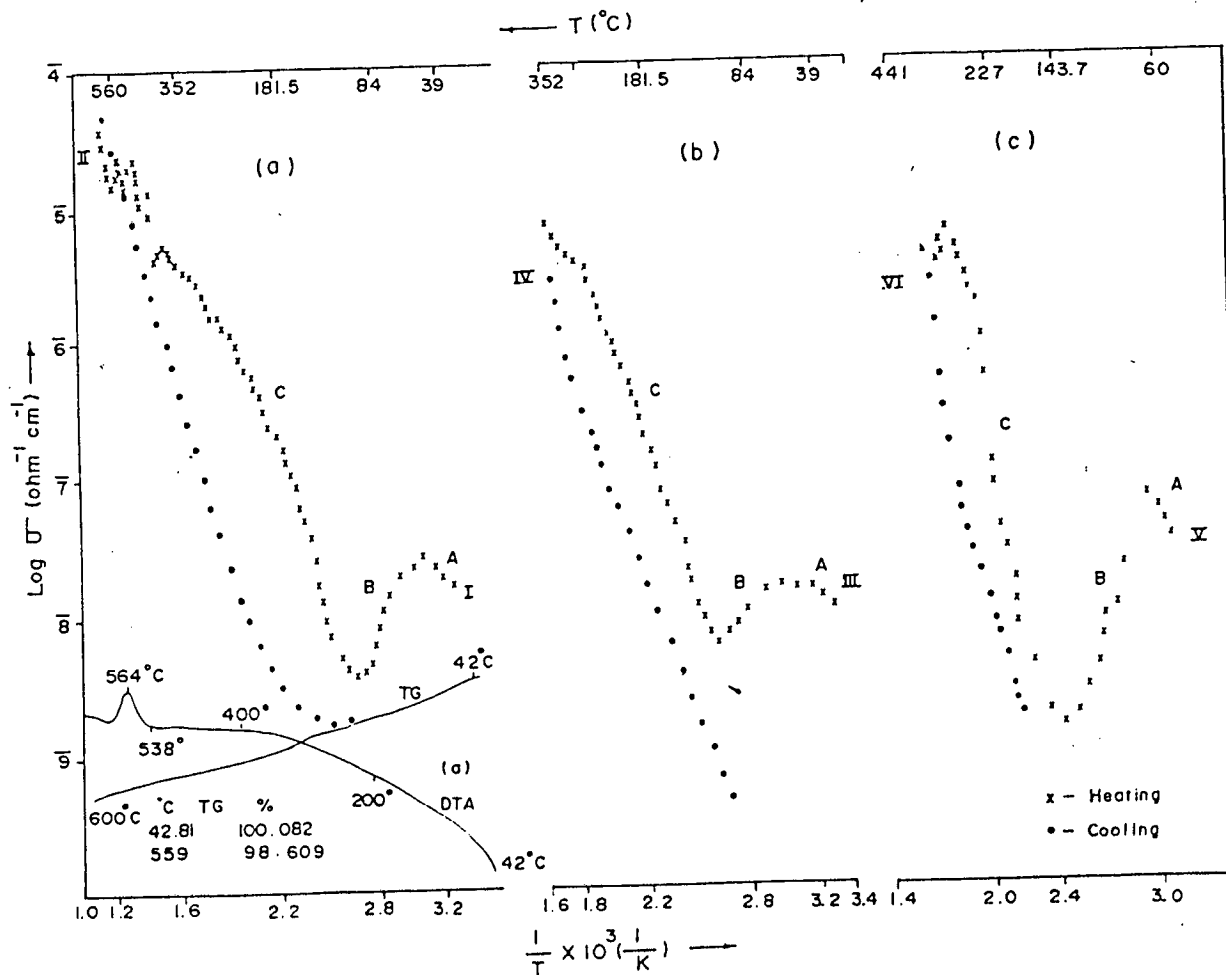


FIG. 5.2a) DTA/TG traces of $\gamma\text{-Fe}_2\text{O}_3$, RT-600°C and conductivity behaviour of $\gamma\text{-Fe}_2\text{O}_3$ transformation to $\alpha\text{-Fe}_2\text{O}_3$

FIG. 5.2 b) $\log \sigma$ v/s $1/T$ plot of standard $\gamma\text{-Fe}_2\text{O}_3$ upto 350°C during heating and cooling in air

FIG. 5.2 c) $\log \sigma$ v/s $1/T$ plot of standard $\gamma\text{-Fe}_2\text{O}_3$ in air after flushing in N_2 ~350°C and equilibration ~ 200°C

tivity values (curves II, Fig. 5.2a) do not overlap the curve I, as it is now the temperature variation of conductivity of α -Fe₂O₃.

Fig. 5.2b shows a conductivity behaviour of fresh Std. γ -Fe₂O₃ during heating (curve III) upto 350^o C, well below its transformation temperature. After regions A and B, the conductivity rise starts from 113^oC upto 350^oC. But \sim 270^oC there is a definite change in the linear behaviour of σ , as before in FTHA. The portion of log plot below 280^oC may be considered as region C. Cooling curve IV does not overlap the heating curve III and, thus, a hysteresis in conductivity is observed. As water is only lost in γ -Fe₂O₃ below its transformation, here the loss of absorbed water may lead to decrease in conductivity. Hence region B may be due to this removal of water. The increase in conductivity in the region C may now be due to water free γ -Fe₂O₃. If that is the case, the conductivity profile during heating from 113^oC (curve III, Fig.5.2b) should have been retraced during cooling too (curve IV, Fig.5.2b). Since there is no overlap in σ values of water free γ -Fe₂O₃ (curves III, region C) and curve IV, it seems that the phases which water free γ -Fe₂O₃ had, now been removed, once it was heated to 350^oC. Further heating in air, the log σ values follow curve IV, instead of curve III. The cooling curve too retraces curve IV. The sample, free of these unknown phases, when equilibrated in moisture \sim 200^oC, the log σ plots show, during heating (curveV, Fig.5.2c) and cooling curve VI, a hysteresis behaviour, as in fresh sample (Fig. 5.2b). And, again the water free γ -Fe₂O₃ \sim 143^oC (after region B) shows a region C, (Fig. 5.2b) not retraced by cooling curve

VI. From these observations it can be inferred that region C and cooling curves are of different nature.

Arrhenius plot

Direct current electrical conductivity, σ , of all $\gamma\text{-Fe}_2\text{O}_3$ samples measured here show, in general, an increase in conductivity with the elevation in temperature, in region C and obey Arrhenius equation, $\sigma_T = \sigma_0 e^{-\Delta E/kT}$ where σ_T is the conductivity value at a particular temperature T, σ_0 is a constant, ΔE is an activation energy of the conduction process and k is Boltzman constant. Log σ Vs $1/T$ plots, hence, will give a straight line plot of a negative slope. And, in all our samples studied here, the graphs of log σ Vs $10^3/T$ show such Arrhenius behaviour.

The Arrhenius plot of Std. $\gamma\text{-Fe}_2\text{O}_3$ during first cooling, after the first heating of fresh samples, and, subsequent heating and cooling in air and N_2 , overlap on each other. All these overlap curve IV. The similar behaviour is observed in all samples studied here. Two inclinations in the log σ plot indicate that there are two regions with different activation energies : $350 - 227^\circ\text{C}$ and $227^\circ\text{C} - \text{RT}$. This suggest that there are two different mechanisms of conduction possible in $\gamma\text{-Fe}_2\text{O}_3$. If $\gamma\text{-Fe}_2\text{O}_3$ is considered as a semiconductor, then the regions below 227°C and above 227°C , may be considered as extrinsic and intrinsic regions, respectively. But, then, different slopes found in the heating curves in fresh and moisture treated samples (region C) may account for some different mechanism of conduction.

A careful observation of curve III (Fig.5.2b) suggests that the Arrhenius plot between 113°C and 270°C (region C) indicates a change in inclination in three sub regions : $113 - 150^\circ\text{C}$, $150 - 215^\circ\text{C}$ and $215 - 270^\circ\text{C}$. A break in conductivity ~

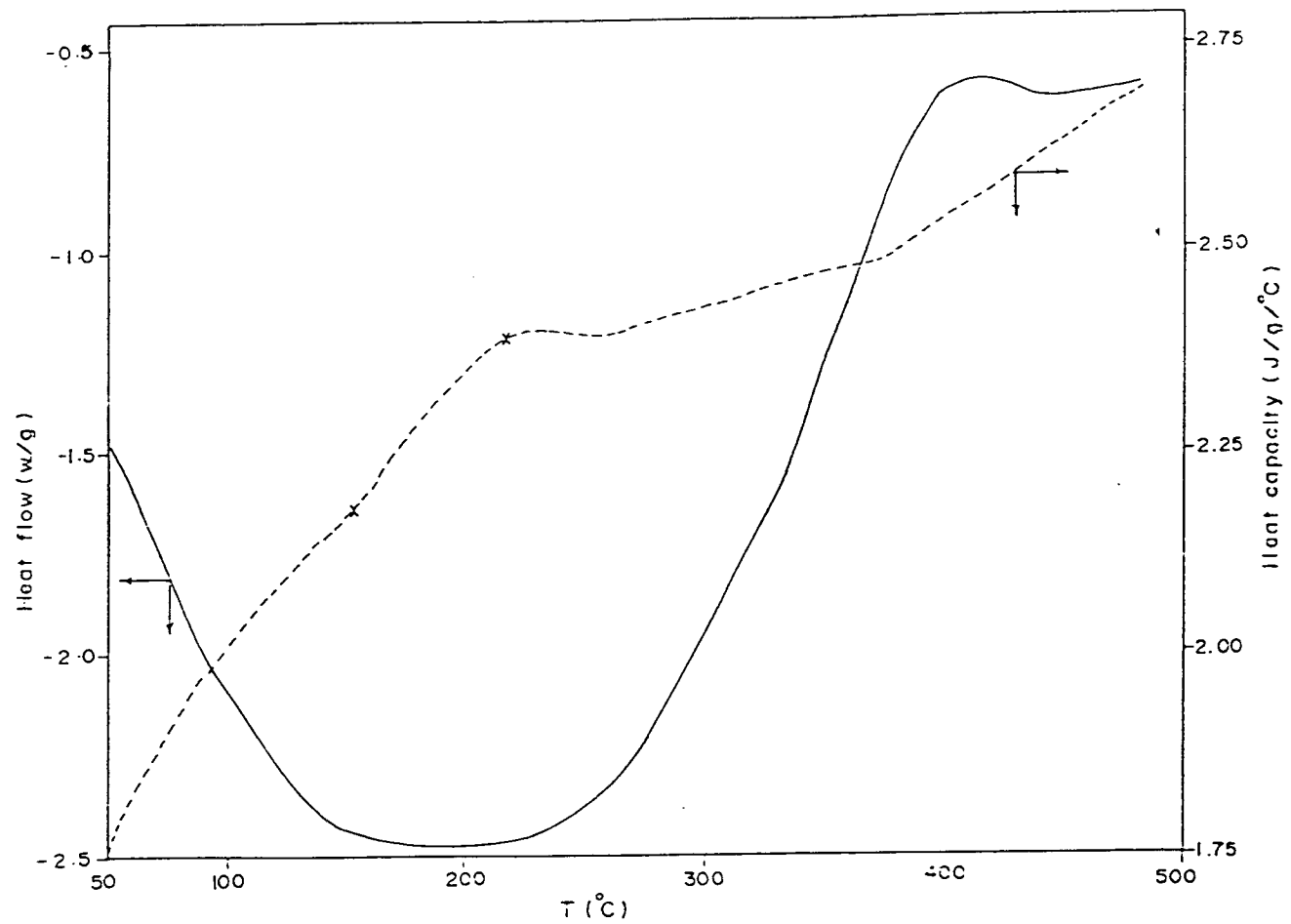
270°C with a definite change in slope is observed between 277-350°C. As major part of adsorbed water is lost below 113°C, and the water free γ -Fe₂O₃ seems to change its conductivity mechanism in these three sub regions of region C. In DTA / TG studies, upto temperature of 350°C, there are no any observable effects in fresh γ -Fe₂O₃, excepting less than 1.1% loss of water. Whereas, conductivity measurement indicates several changes in $\log \sigma$ Vs 1/T plot, in as prepared samples, in general.

As DTA / TG studies upto 350°C are unable to give any clue, DSC study was conducted on Std γ -Fe₂O₃. In Fig.5.3 it may be seen that the DSC trace of fresh γ -Fe₂O₃ shows some changes in heat capacity ~ 153°C and 218°C. The heat flow trace (Fig.5.3) too shows an increase in negative heat flow from RT to 150°C then between 150-225°C it remains constant which then followed by an increase in positive heat flow till 350°C. Although, the analysis of these studies are not complete, the elementary studies reveal that the fresh γ -Fe₂O₃ undergoes some changes ~ 150°C and 218°C. And, $\log \sigma$ plot (curve III, Fig. 5.2b) also indicates different inclinations : 113 - 150°C, 158 - 215°C and 215 - 270°C.

Electrical conductivity measurements, thus, give information about some changes occurring in γ -Fe₂O₃ below 280°C. However, the $\log \sigma$ plot of γ -Fe₂O₃ shows the conductivity increase in region C at ~ 140°C (curve V in Fig.5.1c) while in FTHA it is ~ 198°C (curve I, Fig.5.1a). Thus, region C seems to be at variance in these samples, as compared to Std. γ -Fe₂O₃, where the region starts ~ 113°C. But the inclination in the temperature region ~ 215 - 280°C is present in all these samples and this change that occurred in log plot ~ 215°C corresponds to heat content changes that occurred in DSC ~ 218°C. The change in heat content ~ 145°C found in

DSC (Fig.5.3) may also be connected to change in slope occurring in log plot $\sim 140^{\circ}\text{C}$ in FTHA (curve V, Fig 5.1c) and Std $\gamma\text{-Fe}_2\text{O}_3$ $\sim 150^{\circ}\text{C}$. Therefore, the log plot segment $\sim 140 - 227^{\circ}\text{C}$ also has resemblance with DSC change $\sim 145^{\circ}\text{C}$. Once samples are heated $\sim 280^{\circ}\text{C}$ a break in conductivity takes place and, thereafter, the σ increases upto 350°C . On cooling from that temperature, the log plot overlaps the heating segment, $350 - 280^{\circ}\text{C}$. Once cooled below 280°C , the curve IV follows entirely different path. The segments of log plot : $280 - 215^{\circ}\text{C}$ and $215 - 140^{\circ}\text{C}$ are not retracing first the heating curve showing, thus, a hysteresis behaviour. The segments are reappeared in moisture treated sample. The moisture treatment, thus, reintroduces the segments ($140\text{-}215^{\circ}\text{C}$; $215 - 280^{\circ}\text{C}$) that had vanished on heating above 280°C and this suggests that the phases that were present in fresh oxide have reappeared. Water vapour, hence, introduces these phases.

The fresh $\gamma\text{-Fe}_2\text{O}_3$, after heating to 350°C and cooling to RT, twice in air, and, once in nitrogen, is now freed of all adsorbed water / hydroxyl groups when equilibrated in a known partial pressure of water vapour $\sim 200^{\circ}\text{C}$, may be considered to reintroduce hydroxyl groups. On cooling in the same atmosphere to RT, water may also get adsorbed on it. Hence, the log σ plot of all moisture equilibrated samples look similar to the fresh samples. The adsorbed water is lost in region B and the region C may now be due to hydroxylated oxide. Water vapours $\sim 200^{\circ}\text{C}$ on $\gamma\text{-Fe}_2\text{O}_3$ get decomposed to H^+ on OH^- and same may be thought to be adsorbed by the oxides. David and Welch [262] in their detailed oxidation studies on wet and dry magnetite, prepared by different methods, considered the formation of $\gamma\text{-Fe}_2\text{O}_3$ having defect spinel structure, from wet magnetite. The composition of $\gamma\text{-Fe}_2\text{O}_3$ is in

FIG. 5.3 DSC traces of standard $\gamma\text{-Fe}_2\text{O}_3$

between $(\text{Fe}^{3+}_{20}\text{O}_4)(\text{OH})_4\text{O}_{28}$ (when the percentage of water is high) and $(\text{Fe}^{3+}_{211/3}\text{O}_{211/3})\text{O}_{32}$ and the oxide may be regarded as a solid solution between these two. And, the authors are of the view that a small proportion of combined water is essential for the stability of the oxide.

As our one of the objective was to look into this aspect of essential requirement of water in stabilizing $\gamma\text{-Fe}_2\text{O}_3$, we studied various methods of synthesis. And, the oxide synthesized from these methods have been investigated and their results are being presented here to get clue whether these oxides incorporate water as protons / hydroxyls in their structure. Protons were thought to be incorporated in Fe_3O_4 during topotactic transformation of $\text{Fe}_3\text{O}_4 \rightarrow \gamma\text{-Fe}_2\text{O}_3$, when the oxidation was carried out in the presence of trace quantities of water. Protons incorporated Fe_3O_4 now being defective, transforms into $\gamma\text{-Fe}_2\text{O}_3$, thereby making it proton defective $\gamma\text{-Fe}_2\text{O}_3$. These protons in $\gamma\text{-Fe}_2\text{O}_3$ occupy the lithium sites of lithium ferrite, LiFe_5O_8 , and, thus, a structural similarity is observed with this lithium ferrite. A formula HFe_5O_8 is suggested and based on maximum possible protons present, a structural formula $\text{H}_{1-x}\text{Fe}_{5+x/3}\text{O}_8$, with an upper limit at $\text{H}_{0.1}\text{Fe}_{5.3}\text{O}_8$, is considered to be likely phase of hydrogen iron oxide in $\gamma\text{-Fe}_2\text{O}_3$. The conductivity in region C (140 - 280°C) may now be considered to be due to hydroxyl or proton incorporated $\gamma\text{-Fe}_2\text{O}_3$. Around 280°C the $\gamma\text{-Fe}_2\text{O}_3$ loses all its protons / hydroxyls and the cooling curves does not retrace the heating curve due to $\gamma\text{-Fe}_2\text{O}_3$ free from protons/ hydroxyls.

$\gamma\text{-FHA}$ and $\gamma\text{-FHHA}$

$\gamma\text{-Fe}_2\text{O}_3$ synthesized from $\gamma\text{-FeOOH}$ in air ($\gamma\text{-FHA}$) and autocatalytically decomposed hydrazine equilibrated $\gamma\text{-FeOOH}$ ($\gamma\text{-FHHA}$) are studied by conductivity measurement.

$\gamma\text{-FHA}$

i. Electrothermal Analysis

The $\gamma\text{-FHA}$ required for the conductivity measurement was freshly prepared from $\gamma\text{-FeOOH}$. However, the decomposition of $\gamma\text{-FeOOH}$ was carried out on a pelletised sample of $\gamma\text{-FeOOH}$. Once the thermal decomposition is completed, then, the measurement of d.c. conductivity was carried out in air, N_2 and again in air, after moisture equilibration, as before. But, we considered it worthwhile to study the thermal decomposition of pelletized $\gamma\text{-FeOOH}$, by measuring d.c. electrical conductivity change, during the decomposition as a function of temperature - Electro thermal analysis (ETA). Such a thermo-analytical technique, ETA, has been utilized for many decomposable materials which change weight / enthalpy / electrical conductivity as a function of temperature, along with the usual techniques, like DTA / TG / DTG [301,510].

A freshly prepared $\gamma\text{-FeOOH}$ in a pellet form, on heating $\sim 300^\circ\text{C}$, forms $\gamma\text{-Fe}_2\text{O}_3$. The conductivity behaviour of $\gamma\text{-FeOOH}$ (curve I, Fig. 5.4) shows a marginal increase in conductivity from RT to 127°C , followed by a decrease upto 227°C . From 227°C , the σ steeply increases upto 282°C , then decreases till 290°C , followed immediately by an increase. The steep increase upto 280°C and then decrease till 290°C followed by again increase, thus indicates a formation of $\gamma\text{-Fe}_2\text{O}_3$.

~ 290°C. A separate isothermal weight loss ~ 290°C of γ -FeOOH also revealed the formation of γ -Fe₂O₃. The $\log \sigma$ Vs $1/T$ plot shows a steep increase in conductivity from 227°C, which may be considered due to the beginning of γ -Fe₂O₃ formation. The decrease in conductivity from 127°C to 227°C may be due to slow removal of hydroxyl of γ -FeOOH. Here, the thermal decomposition of γ -FeOOH is studied by the variations in electrical characteristics, an electro thermal analysis (ETA).

Measurement of conductivity during the thermal decomposition on iron hydroxide, cobalt hydroxide and mixed iron cobalt hydroxides also indicated [511] such a steep increase in conductivity, at the onset of thermal decomposition of the hydroxides leading to respective oxides.

The measurement of electrical conductivities during decomposition of FeC₂O₄ · 2H₂O, and, the continuing the measurement on the oxide, γ -Fe₂O₃ that formed, was studied by Rane et al [264] which gave them the information as regards the exact formation temperature of the oxide, in an controlled atmosphere of water vapour. However, usual DTA / TG did not reveal such formation of the oxide from ferrous oxalate dihydrate. The continuation of the conductivity measurements on γ -Fe₂O₃ further helped Nikumbh, Rane and Mukhedkar [282] to establish hydrogen ferrite type of phase. In our own studies of electro thermal analysis of iron (II) carboxylato-hydrazinate [300, 303], we made use of ETA technique to understand the thermal decomposition path of these complexes.

ii Study of electrical conductivity of γ -FHA.

The γ -Fe₂O₃ that formed γ -FeOOH from (curve I, Fig. 5.4) \sim 290^oC, which showed conductivity changes between 280 - 290^oC, by a kink \sim 290^oC, followed by an increase upto 350^oC. Further studies on this oxide were done as follows.

On cooling, (curve II, Fig.5.4) the log σ plot of γ -Fe₂O₃ shows a linear decrease in conductance. The σ values of the oxide on reheating and cooling in air, N₂, too found to overlap the values on curve II (not shown here). On moisture treatment \sim 200^oC and then continuing the measurement, the log σ plot (curve III) shows a decrease in conductivity from 80^oC to 180^oC (region B), after an initial increase from RT to 80^oC (region A), as observed before in other samples. Further heating, conductivity shows a linear increase (curve III). On cooling, the log σ plot (curve IV) runs parallel to the heating curve. However, subsequent heating and cooling makes these plots to almost overlap on each other. Thus, no hysteresis is observed during first heating and cooling, as well, heating after moisture treatment.

γ -FHHA

γ -Fe₂O₃ synthesized by hydrazine method shows regions A (RT - 94^oC) and B (94 - 190^oC) in log σ plot (curve I, Fig.5.5). From 190^oC onwards, there is an increase in conductivity upto 280^oC (region C). At 280^oC, there is a change in inclination, as before in γ -Fe₂O₃ samples. Cooling curve II now follows other than heating path, suggesting a hysteresis in conductivity in region C. Reheating and cooling in air and N₂, too now follow the curve II. Moisture equilibrated samples (curve III) shows region A (RT - 102^oC) and region B (102 - 168^oC). Region C starts at 168^oC. The increase in conductivity upto 350^oC shows a well pronounced regions,

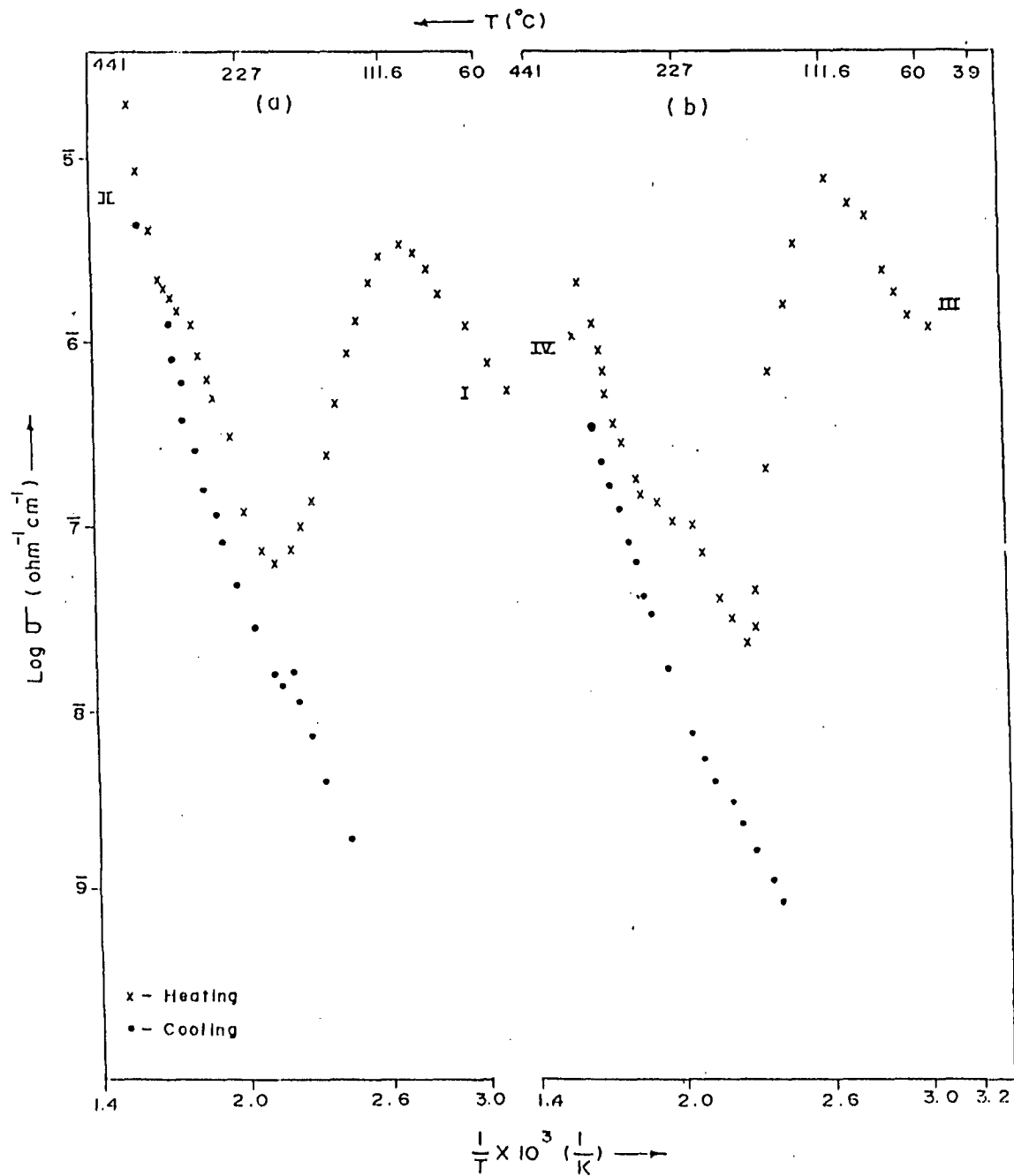
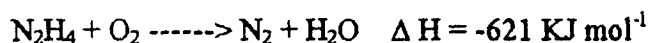


FIG. 5.5 Temperature variation of conductivity of $\gamma\text{-Fe}_2\text{O}_3$ synthesised by hydrazine method from $\gamma\text{-FeOOH}$ autocatalytically, a) in air and b) in air after moisture equilibration $\sim 200^\circ\text{C}$

between 168 - 225° C and 225 - 280° C. The change in inclination ~ 280° C is followed by an increase in conductivity upto 350° C. Cooling curve IV is not retracing heating curve III, indicating hysteresis behaviour. The cooling curve IV has two inclinations with two different slopes and, thus, are parallel to curve II. A hysteresis behaviour, thus, observed, in the γ -Fe₂O₃, synthesized by hydrazine method, suggests that the oxide contains protons in its structure.

Topotactic transformation of γ -FeOOH in air leads to γ -Fe₂O₃ while γ -Fe₂O₃ synthesized by hydrazine method follows different route and Fe₃O₄ is found to be an intermediate phase. Thus, γ -Fe₂O₃ formation from γ -FeOOH by hydrazine method yields Fe₃O₄ which then oxidises to γ -Fe₂O₃, in a atmosphere of its reaction products N₂ + H₂O. The hydrazine released reacts with atmospheric oxygen liberating heat energy.



The intermediate Fe₃O₄ will now have some percentage of water and further oxidation of it leads to γ -Fe₂O₃, thereby, retaining water in the γ -Fe₂O₃ as protons or hydroxyls.

As hysteresis behaviour in conductivity is observed in this sample, it may be inferred that protons are present in the oxide. The hydrogen iron oxide phase then loses its protons ~ 280° C and transforms into vacancy ordered γ -Fe₂O₃. Hence on cooling, the log σ plot do not trace the heating curve.

An absence of hysteresis behaviour in γ -Fe₂O₃ (γ -FHA), prepared from γ -FeOOH in air, suggests that there is no hydrogen iron oxide phase in it. It may be

simply vacancy ordered / disordered defect spinel.

Saturation magnetization value of 71.6 emu/g is observed only in the γ -Fe₂O₃, synthesized by hydrazine method from γ -FeOOH. While a low value of σ_s ~19 emu/g found in γ -Fe₂O₃ obtained from the decomposition of γ -FeOOH suggests that the intermediate phase Fe₃O₄ makes all that difference in proper ordering of Fe³⁺ on lithium sites, as there is spinel framework already present. In air decomposition of γ -FeOOH, no such Fe³⁺ ordering is possible, as there is a topotactic transformation, allowing no time and occasion for the Fe³⁺ diffusion.

Although the present investigations are thorough in probing the hydrogen iron oxide phase which has unit cell structural formula in between γ -Fe₂O₃, (Fe³⁺)₈ [Fe³⁺₁₂ Fe³⁺_{4/3} □_{8/3}]O₃₂ and fully protonated HFe₅O₈, (Fe³⁺)₈ [Fe³⁺₁₂ H¹⁺₄]O₃₂ which is similar to lithium ferrite LiFe₅O₈, (Fe³⁺)₈ [Fe³⁺₁₂ Li¹⁺₄]O₃₂, a preliminary studies done [512] on lithiation of γ -Fe₂O₃ has given us some indications as regarding the occupation of Li¹⁺ by replacing H⁺ from the so called lithium sites. The conductivity measurement on the lithiated samples showed an absence of hysteresis in conductivity behaviour. However, a detailed study is already being undertaken in our laboratory to probe the proton by neutron diffraction studies.

General Conclusion

- (1) Acid extract of iron ore is precipitated as Fe(OH)₃ which decomposes thermally in air, to α -Fe₂O₃.
- (2) Fe(OH)₃ equilibrated in hydrazine hydrate decomposes autocatalytically to γ -Fe₂O₃, when exposed to air..

(3) Iron oxyhydroxides : γ -FeOOH, α -FeOOH and amorphous FeOOH synthesized from $\text{Fe}(\text{OH})_3$, that obtained from iron ore, decompose in air $\sim 300^\circ\text{C}$ to γ - Fe_2O_3 , α - Fe_2O_3 and α - Fe_2O_3 with traces of γ - Fe_2O_3 respectively. However, the hydrazination of these iron oxyhydroxides results into γ - Fe_2O_3 on autocatalytic decomposition, after exposing to air.

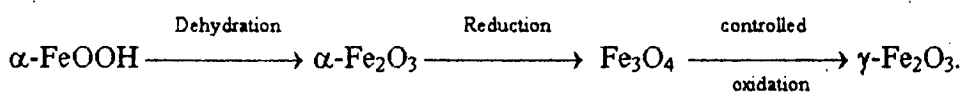
(4) The chemical formula for iron oxyhydroxides have been fixed based on TG, IR and isothermal weight loss as, γ -FeOOH.0.3H₂O, α -FeOOH.0.2H₂O and amorphous FeOOH.0.8H₂O

(5) Hydrazinated iron oxyhydroxides being unstable in air, no formula fixation is possible. However, a specially built reactor enabled to estimate the hydrazine uptake by these. And, both γ -FeOOH and amorphous FeOOH take up $\sim 10\%$ hydrazine while α -FeOOH takes up hydrazine $\sim 1\%$ of its weight.

(6) An intermediate phase Fe_3O_4 is observed during hydrazine uptake by iron oxyhydroxides.

γ -FeOOH on hydrazination decomposes autocatalytically to γ - Fe_2O_3 through an intermediate phase Fe_3O_4 , while thermal decomposition of the oxyhydroxide topotactically transforms into γ - Fe_2O_3 . However, hydrazine method yields γ - Fe_2O_3 of high saturation magnetization, σ_s , of 71.16 emu/g. The topotactic transformation of γ -FeOOH to γ - Fe_2O_3 , however yields low σ_s value of ~ 19.2 emu/g.

(7) Commercial preparation of γ - Fe_2O_3 from α -FeOOH is a multistage oxidation-reduction reaction requiring a rigid control of atmosphere.



while the hydrazine method of preparation of the oxide from γ -FeOOH is simple and single step

(8) Although a simple topotactic transformation involving removal of water from γ -FeOOH leads to γ -Fe₂O₃, the hydrazinated γ -FeOOH decompose to γ -Fe₂O₃ through an intermediate Fe₃O₄, with superior magnetic properties.

(9) Iron (II) carboxylato-hydrazinates : Ferrous fumarato-hydrazinate, FeC₄H₂O₄.2N₂H₄ ; ferrous succinato-hydrazinate, FeC₄H₄O₄.2N₂H₄, ferrous malonato-hydrazinate, FeC₃H₂O₄.1¹/₂ N₂H₄.H₂O ; ferrous tartrato-hydrazinate, FeC₄H₄O₆.N₂H₄.H₂O; ferrous maleato-hydrazinate, FeC₄H₂O₄.2N₂H₄ and ferrous malato-hydrazinate, FeC₄H₄O₅.2N₂H₄, are being synthesized easily and characterized.

(10) All iron (II) carboxylato-hydrazinates decompose autocatalytically in an ordinary atmosphere yielding mainly γ -Fe₂O₃.

(11) The easy synthesis of γ -Fe₂O₃ from iron (II) carboxylato-hydrazinates, thus, avoids a cumbersome control of water vapour partial pressure that required in arresting the thermal decomposition path of iron (II) carboxylates at γ -Fe₂O₃ step. The thermal decomposition of the unhydrazinated iron (II) carboxylates, however, in the absence of such controlled water vapour partial pressure in air, lead to thermodynamically more stable phase, α -Fe₂O₃.

(12) The γ -Fe₂O₃ synthesized from hydrazinated oxyhydroxides (prepared from Fe(OH)₃ obtained from iron ore) and iron (II) carboxylato-hydrazinates is mixed with MgCO₃ in the required stoichiometry and heated ~ 1000⁰C to yield single phase MgFe₂O₄.

Commercial α -Fe₂O₃ when used to synthesize MgFe₂O₄ showed an impurity phase due to α -Fe₂O₃. This suggests that single phase MgFe₂O₄ is difficult to obtain when α -Fe₂O₃ is a raw material.

(13) The magnesium ferrite prepared from commercial α -Fe₂O₃ source showed lower values of saturation magnetization and magnetone number as compared to the MgFe₂O₄, obtained from γ -Fe₂O₃ source.

(14) The Curie temperatures of MgFe₂O₄ (obtained from γ -Fe₂O₃ source) measured from susceptibility, permeability and resistivity studies compare well with the reported ones, but, the MgFe₂O₄ prepared from α -Fe₂O₃ showed higher T_c.

(15) Single phase MgFe₂O₄ was difficult to achieve with α -Fe₂O₃ + MgCO₃ at 1000°C, while single phase ferrite could be obtained from γ -Fe₂O₃ source, at the same temperature.

(16) Single phase MgFe₂O₄ from α -Fe₂O₃ source is possible only >1000°C.

(17) The Fe(OH)₃ precipitated from iron ore can thus be used to prepare γ -Fe₂O₃ useful in MgFe₂O₄ synthesis of superior magnetic characteristics.

References

1. M. Misono, K. Sakata, F. Ueda, Y. Nagawa, Y. Yoneda, *Bull. Chem. Jpn.* 53 (1980) 648.
2. H.H. Kung, B. Kundalkar, M.C. Kung and W.H. Chang, *J. Phys. Chem.* 84 (1980) 382.
3. B.L. Yang, M.C. Kung and H.H. Kung, *J. Catal.* 89 (1984) 172.
4. B.J. Liaw, D.S. Cheng and B.L. Yang, *J. Catal.* 118 (1989) 312.
5. H. Watanabe and J. Seto, *Bull Chem. Soc. Jpn.* 64 (1991) 2411.
6. B.L. Yang, D.S. Chang and S.B. Lee, *Appl. Catal.* 70 (1991) 161.
7. H.J. Hunh, *Z. Chem.* 27 (1987) 334.
8. P.A. Tuan, D.L. Minh, N. Chau, B.Thanhcong, in, *proc. VI Intern. conf.on Ferrites (Tokyo, Japan, 1992)* p.370.
9. J.J. Shrotri, A.G. Bagul, S.D. Kulkarni, C.E. Deshpande and S.K. Date, *ibid*, p. 404.
10. E.P.Wohlfarth, 'Ferromagnetic Materials' (North - Holland Publishing Co. 1980). Vol.1 and 2.
11. G. Economos, *Kirk Othmer Encyclopedia of chemical technology* 2nded. Vol.8.(Wiley, Newyork, 1965) p.881.
12. A.B.V.Groenou, P.F.Bongers and A.L.Stuijts, *Mat.Sci.Eng.* 3(1968-69) 317.

13. Y.Hoshino, S.Iida and M.Sugimoto, in, Proceedings of the first International Conference on ferrites, Kyoto, Japan. (Univ.of Tokyo Press,Japan 1971).p. 1870.
14. E.E.Riches, Ferrites - A Review of Materials and Applications (Mills and Boon, London, 1972).
15. W.H.Van Aulock, Encyclopedia Britannica, (Oxford university Press, Oxford, 1974) p. 248.
16. D.J.Craik (ed.), Magnetic Oxide Materials, Part 1,2 (Wiley,London, 1975).
17. Ferrites, in Proceedings of the second International Conference, Bullevue (France), J.Phys. c₁-38 (1977).
18. G.P.Rodrigue, Treatise on Material Science and Technology,Vol.II (R.K.MacCrone ed., Academic press, Newyork, 1977) p.383.
19. T.G.Reynold, Kirk Othmer Encyclopedia of chemical Technology, 3rd ed, Vol.9. (Wiley, New york, 1980) p.881.
20. B.K.Das, Preparation and Characterization of Materials (J.M.Honig and C.N.R.Rao eds., Academic Press, Newyork, 1981) p.75.
21. M.J. Ruthner, in 'Proceedings of the V international conference on ferrites'(Bombay, India, 1989) p.23.
22. S.G. Patil, Electronics, information and planning, 4 (1977) 979.
23. B. B. Ghate, in 'Proceedings of the V international conference on ferrites' Bombay, India, 1989.p.23.
24. S.M. Rege, in 'Earth Resources for Goa's development,' Goa, 1985 p. 89.

25. K.S. Mani and D. Subrahmanyam in 'Earth resources for Goa's Development, (Goa, India,1985) p. 98.
26. D.K. Pujari, in 'Earth resources for Goa's development', (Goa, India,1985) p.370.
27. Pradip, 'Metals, materials and processes' 6(3) (1994) 179.
28. K. Sreeramachandra Rao, P. Harinadha Babu and T.S.S. Murthy, in 'Proceedings of one day workshop on Integrated mineral exploration',. (Goa, India,6th Dec. 1996).
29. H. Wadhvani, A.G. Rao, N.C. Sahu and R.C. Mahanty, in 'Int. symp. on beneficiation and agglomeration' (1981).
30. S.P. Mahakud, P.K. panda and G.C. Das, in 'Earth resources for Goa's development', (Goa, India, 1985) p.370.
31. K.A. Natarajan, 'Trans. of the Indian Inst. of Metals' 31 (1978) 169.
32. K.A. Natarajan and R. Upadhyaya, 'Trans. of the Indian Inst. of Metals' 39 (1986) 627.
33. S.Subramanian and K.A. Natarajan, 'Trans. of the Indian Inst. of Metals' 40 (1987) 489.
34. S.Subramanian, K.A. Natarajan and D.N. Satyanarayana, ' Minerals & Metallurgical processing (Aug. 1989) p.152.
35. G.O.O.O. Uwadiale, Mineral & Metallurgical processing, (Aug. 1989) 1117.
36. K.A. Natarajan, in 'International symposium on recent advances in particulate Science and Technology, (I I T - Madras, India, Dec. 1982).

37. G.B.Raju, S. Prabhakar and C.Sankaran, 'Trans. Inst. Min. Metal section C Min. Proc. Ext. Metal'. 102 (1993) 132.
38. K. C. Sahu and R. P.Gurav, 'The Indian Mineralogist' 12 (1971) 63.
39. I.H. Warren, M.D. Bath, A.R. Prosser and J.T. Armstrong, 'Instt. of Min. and Met. Trans.' (1969) 21.
40. G.C. Kennedy, Econ. Geol. 4(1950) 629.
41. L.G.M. Bas Becking, I.R.Kaplan and D.Moore, J.Geol. 68 (1960) 243.
42. H.Wild and G.H. Wiltshire, Rhod. Cham. Mines. J. 11 (1971) 26.
43. A.L.Maclean and A.J. Dekker, Can. J. Soil. Sci. 56 (1976) 27.
44. M.H. Wong, W.M. Lau, S.W. Li and C.K. Tang, Environ. Res. 30 (1983) 26.
45. K.C. Sahu and R.P. Gurav, The Indian Mineralogist 12 (1971) 63.
46. M.A. Blesa et al, Mater. Sci. Forum., 29 (1988) 31.
47. R.Torres, M.A.Blesa and E. Matejevic, J colloid and Interface Sci, 134 (1990)475.
48. R.M. Garrels and C.L. Christ, solutions, minerals and Equilibria, Harper Row (1965) 450.
49. S.R.M. Ellis, Chem. Proc. Engg. (1975) 79.
50. R.Y. Aliev, Chem Abstr. 86 (1977) 199230.
51. D.H. Bowers, D.M. Littrel and B.J. Tatarchuk, Thin solid films 169 (1989) 143.
52. K.Wakai, Chem. Abstr. 87 (1977) 15202.
53. M.H. Tikkanen, Werkstoffe U. Korros. 13 (1961) 351.

54. G. Okamoto, R. Furuichi and N.Sato, *Electrochim. Acta* 12 (1967) 1289.
55. I. H. Warren and E.I. Devuyst, *Trans. Soc. Mining Engg. AIME* 252 (1972) 326.
56. J.L. Burba, *Chem. Abstr.*, 101 (1984) 134769.
57. M.R. Anantharaman, K.Seshan, D.K. Chakrabarty and H.V. Keer, *Bull Mater.Sci.* 3(3) (1981) 275.
58. M. Misono, K. Sakata, F. Ueda, Y. Nagawa, Y. Yoneda, *Bull. Chem. Jpn.* 53 (1980) 648.
59. H.H. Kung, B. Kundalkar, M.C. Kung and W.H. Chang, *J. Phys. Chem.* 84 (1980) 382.
60. B.L. Yang, M.C. Kung and H.H. Kung, *J. Catal.* 89 (1984) 172.
61. B.J. Liaw, D.S. Cheng and B.L. Yang, *J. Catal* 118 (1989) 312.
62. H. Watanabe and J. Seto, *Bull Chem. Soc. Jpn.* 64 (1991) 2411.
63. B.L. Yang, D.S. Chang and S.B. Lee, *Appl. Catal.* 70 (1991) 161.
64. R.J.Rennard and W.L. Kehl, *J. Catal.* 21 (1971) 282.
65. W.L.Kehl and R.J.Rennard, U.S.Patent 3450787, June 17, 1969.
66. M.A.Gibson and J.W.Hightower, *J.Catal.* 41(1976) 420.
67. E.N.Amirbekov, F.V.Aliev, L.I.Lafer, A.M.Rubinshtein and V.I.Yakerson, *IZV.Akad. Nauk. SSSR, Ser.Khim.* 7(1979) 1344.
68. E.N.Amirbekov, F.V.Aliev, L.I.Lafer, A.M.Rubinshtein and V.I.Yakerson, *IZV.Akad. Nauk. SSSR. Ser.Khim.* 11(1979) 2250.
69. G.Nedelcu and I.V.Nicolescu, *Rev Chimie*, 40 (1990) 881.
70. G.Nedelcu and I.V.Nicolescu, *Rev. Chimie* 42 (1991) 21.

71. G.Nedelcu and I.V.Nicoléscu, Rev. Chimie. 42(4-5)(1991) 177.
72. G.Nedelcu, I.V.Nicolescu and E.Angelescu, Rev. Chimie. 42(4-5)(1991) 182.
73. Nissan Girdler Catalyst Co., Japan Patent 59216634, Dec 6, 1984.
74. H.E. Du Bois, Phil. Mag. 29 (1890) 293.
75. P.J. Weiss, J. Phys. 6(4) (1907) 66.
76. S. Hilpert, Ber. Deut. Chem. Ges. 42 (1909) 2247.
77. J.A. Hedvall, Ber. Deut. Chem. 45 (1912) 2095.
78. G. Tammann, Z. Anorg. Allgem. Chem. 111 (1921) 78.
79. W. Jander, Z. Anorg. Allgem. Chem. 117 (1927) 1631.
80. J.L. Snoek, in 'New development in ferrimagnetic materials', (Elsevier press.Inc, New York. 1947).
81. Y. Kato and T. Takei, J. Of Institute of electrical Engineers, Jpn. 53 (1953) 408.
82. H. Forestéir, Ann. Chemie xe series Tome 9(1928) 353.
83. T.F. Barth and E. Posnjak, Z. Krist. 82 (1952) 325.
84. J.L. Snoek, Physica 3 (1936) 33.
85. E.J.W. Verwey and E.L. Heilman, J. Chem. Phys. 15 (1947) 174.
86. E.J.W. Verwey, P.W. Haayman and F.C. Romeijn, J. Chem. Phys. 15 (1947) 181.
87. E.J.W. Verwey, F.de Boer, and J.H. Van Santen, J. Chem. Phy. 16 (1948) 109.
88. L.Neel, Ann. Phys. 3 (1948) 137.

89. Y. Yafet and C. Kittel, Phys. Rev. 87 (1952) 290.
90. Guillaud, J. Phys. Radium. 12 (1957) 239.
91. E.W. Gorter, Phil. Res. Rept. 9 (1954) 295.
92. C. G. Koops, Phys. Rev. 83 (1951) 121.
93. M.A. Gilleo, J. Chem. Phys. 24 (1956) 306.
94. J.S. Smart, Phys. Rev. 94(1954) 847.
95. E.W. Gorter, Nature 173(1954) 123.
96. A.P.B.Sinha and P.G.Menon, in 'Solid State Chemistry' (Ed.C.N.R.Rao, Marcel Dekker, New York, 1974) p.385.
97. D.S. Maclure, J.Phys. Chem.Solids 3(1957)311.
98. J.D.Dunitz and L.E.Orgel, J.Phys.Chem.Solids 3(1957)20.
99. A.Miller, J.Appl.Phys. 30(4) (1959)245.
100. L.G.Van Uitert, Proc. I.R.E. 44(1956) 1294.
101. W.D.Kingeri in "Ceramic Fabrication Processes" (M.I.T.Technical Press, John Wiley, New York, 1958).
102. K.Kamiyoshi, Sci. Repts., Res.Inst., Tohoku Univ. A-3(1951)716.
103. F.W.Brockman, P.H.Dowling and Steneok, Phys.Rev. 77(1950)85.
104. G.P.Kramer, J.Ya Ponava and V.V.Passyukov., Phys. Stat. Sol.(a)86 (1993) 95.
105. S.Moltgen, Zh. Fur. Ang. Physik 4(1952)216.
106. K.Iwauchi, Jpn. J. Appl. Phys. 10(1971) 1520.
107. K.Iwauchi, S.Yemamoto and Y.Bando, Jpn. J. Appl. Phys. 10(1971)1513.
108. N.Rezlescu and E. Rezlescu, Phys. Stat. Sol. (a) 23 (1974) 575.

109. N.Rezlescu, E.Cuciuzeanu and V.Petrescu, Rev-Rom.Phys.Tome 15(1970) 965.
110. F.G.Brockman and K.E.Matteson, J.Amer. Ceram.Soc. 53(1970)517.
111. F.G.Brockman and K.E.Matteson, J.Amer. Ceram.Soc. 54 (1971) 180.
112. V.P.Avramenko and O.V.Sinyskov, Ukr.fiz.zh.(Ukr.Ed),13(1968)1174.
113. O.S.Joskyula and J.Sobhandri, Phys. Stat.Sol.(a) 59(1980)323.
114. A.K.Jonscher in 'Dielectric Relaxation Solids,(Chelsea Dielectric Press, London, 1983.)
115. R.Pauthenet and L.Bochirol, J.Phys.Radium 12(1951)249
116. C.Guillaud, C.R.Acad. Sci.232(1951)944.
117. G.O.Jones and F.F.Roberts, Proc. Phys. Soc.(London) B65(1952)390.
118. T.Okamura, T.Fujimara and M.Date, Sci. Rpts.Res.Inst.Tohoku Univ. A4 (1952)191.
119. C. Radhakrishnamurthy, J. Geol. Soc. India 26(9) (1985)640.
120. R.V. Upadhyay, G.J.Baldha and R.G.Kulkarni, Mater. Res. Bull. 21(1986) 1015.
121. G. J. Baldha and R. G. Kulkarni, Solid Stat.Commun. 53(1985) 11.
122. C. P. Bean, J. Appl. Phys. 26(1955) 1381.
123. L. Neel, Adv. Phys. 4(1955) 191.
124. G. C. Kucznski, in Proceedings of the International Conference on Ferrites, Kyoto, Japan, 1970 (University of Tokyo Press, 1971) p.87.
125. C. Wagner, 'Diffusion and High Temperature Oxidation of Metals, Atom Movements, (A.S.M. monograph, cleveland,1951), p.153.

126. H. Schmalzried, Z. Physik. Chem. 33 (1962) 111.
127. K. Hauffe and K. Pshera, Z. Anorg. Chem. 262 (1950) 147.
128. G. Economos, Kinetics of High Temperature Processes (ed. W.D. Kingery. M.I.T.Press, Cambridge 1959) p.243.
129. L.C.F. Blackman, J. Am. Ceram. Soc. 42(1959)143.
130. P.Reijnem, Sci. Ceram. 42(1959) 143.
131. M. Paulus, in Proceedings of the International Conference, Kyoto, Japan, 1970 (University of Tokyo Press, Tokyo, 1971).
132. R.E. Carter, J. Am.Ceram. Soc. 44 (1961) 116.
133. A.Wold, J. Chem. Educ. 57 (1980) 531.
134. E.P.Wohlfarth, 'Ferromagnetic Materials' (North - Holland Publishing Co. 1980). Vol.1 and 2.
135. R.G. Richards and J. White, Trans. Brit. Ceram. Soc. 53 (1954) 422.
136. G.Economos, J. Am. Ceram. Soc. 38 (8) (1955) 292.
137. G.Economos, J. Am. Ceram. Soc. 38 (1955) 335.
138. H.L.Turk, in Proceedings of the International Conference on Ferrites, Kyoto, Japan, 1970 (University of Tokyo press, Tokyo, Japan,1971)p.99.
139. C.Guilland, in Proc. Inst. Elect. Eng.Suppl. 104 B5 (1957) 165.
140. D.G.Wickham, in Proceedings of the International Conference on Ferrites Kyoto, Japan, 1970 (University of Tokyo press, Tokyo, 1971) p.105.
141. J.G.M.Delau, Proc. Brit. Cer. Soc. 10 (1968) 275.
142. R.J.Young, T.B.Wu and I.N.Lin, Mat. Res. Bull, 22 (1987) 1475.

143. L.M.Corliss, J.M.Hastings and F.G.Brockman, *Phys.Rev.* 90(6) (1953) 1013.
144. G.A.Sawatzky, F.VanDer Woude and A.H.Morrish, *Phys.Rev.*187(2) (1969) 747.
145. E.Wieser, H.Schroder and K. Kleinclück, *Phys.Stat.Sol. (a)* 1 (1970) 749.
146. H.Knoch and H.Dannheim, *Phys. Stat. Sol. (A)* 37 (1976) K 135.
147. R.G.Kulkarni and H.H.Joshi, *J.Solid State Chem.* 64 (1986) 141.
148. O.K.Samuilova, V.D.Yagodovskii and M.M.Kozlova, *Kinetics and Catalysis* 27(1) (1986) 208.
149. C.N.Rao and S.R.Murthy, *Cryst. Res. Technol.* 24(1989) K6.
150. G.Gusmano, P. Nunziante, E.Traversa and R. Montanari, *Mater.Chem. Phys.* 26(1990) 513.
151. G.Gusmano, G. Montesperelli, P.Nunzianante, and E. Traversa, *J. Mater. Sci.*, 28 (1993) 6195.
152. H.M.O'Bryan, P.K.Gallagher, F.R.Monforte and F.Schrey, *Am.Ceram.Soc. Bull.* 48(1969) 203.
153. A.C.C.Tseung and J.R.Goldstein, *J.Mater.Sci.* 7(1972) 1383.
154. R.M.Dell, 'Reactivity of Solids' (eds. J.S.Anderson, M.W.Roberts, and F.S.Stone, Chapman and Hall, London, 1972) p.553.
155. V.R.Palkar and M.S.Multani, *Mat. Res. Bull.*14(1979) 1353.
156. T.Iijima, M.Seiki, N.Inagaki and T.Sato, *Chem. Abstr.* 110 (1988) 127355.
157. T.T.Srinivasan, P.Ravindranathan, L.E.Cross, R.Roy, R.E.Newnham S.G.Sankar and K.C.Patil, *J.Appl. Phys.* 63(8)(1988) 3789.

158. T.Y.Tseng and J.C.Lin, *J.Mater. Sci.Lett.* 8(1989) 261.
159. G.Gusmano, P.Nunziante, E.Traversa, R.Montanari and G.Chiozzini, 'Advanced materials and Processes, vol.I: Advanced Processing and High Temperature Materials'. (eds.H.E.Exner and V.Schumacher) DGM Informationsgesellschaft, Oberursel, 1990, p.647.
160. E.Traversa, G.Montesperelli, P.Nunziante and G.Chiozzini, *J.Therm. Anal.* 38 (1992) 2583.
161. C.S.Narsimhan and C.S.Swamy, *Phys. Status Solidi (a)*59(1980) 817.
162. W. J.Schuele and V.D.Deetscreek, 'Ultrafine Particles' (ed. W. E. Kuhn, Wiley New York, 1963) p.218.
163. W.J.Schuele, *J. Phys. Chem.* 63(1959) 83.
164. D.G.Wickham, *Inorg. Synth.* 9(1967)152.
165. A.L.Stuijts, in *Proceedings of the Fifth International Conference on the Science of Ceramics, Ronneby Brunn, Sweden (1969)*.
166. J.M.Paris, thesis, University de Lyon (1963).
167. R.Glenn Rupard and P.K.Gallagher, *Thermochim. Acta.* 272(1996)11.
168. P.S.Bassi, B.S.Randhawa and S.Kaur, in *Proceedings ICF-5, 1989, India.* p.67.
169. N.S.Gajbhiye and S.Prasad, in '*Proc.10th Nat. Symp.Therm. Anal.*' 1995, Kanpur, India, p.136.
170. K.C.Patil, D.Gajapathy and V.R.Pai Verneker, *Mat. Res.Bull.* 17(1982)29.
171. D.Gajapathy and K.C.Patil, *Mater.Chem. Phys.* 9(1983)423.

172. V.A.Sharov, V.A.Zhilyaev, E.A.Nikonenko and T.M.Zhdanovskikh, *Koordinatsionnaya Khimiya* 6(3)(1980)431.
173. S.Sundar Manoharan and K.C.Patil, in *Advances in Ferrites*, (eds. C.M. Srivastava and M.J.Patni, Oxford and IBH Pub. Co. Pvt. Ltd., New Delhi) 1 (1989) 43.
174. P. Ravindranathan and K.C.Patil, *Am. Ceram. Soc.Bull.* 66(4)(1987)688.
175. P.Ravindranathan, T.T.Srinivasan, R.Roy, R.E.Newnham, S.G.Sankar and K.C.Patil, in 11th International Symposium on 'Reactivity of Solids' [Princeton U.S.A., 1988].
176. Martin - Marietta Corpn., *Chem. Abstr.* 108(1987)153102.
177. P.Ravindranathan, Ph.D.thesis, Indian Institute of Science, Bangalore, (1986) p.70.
178. P.Ravindranathan and K.C.Patil, *J.Mater. Sci.* 22 (1987) 3261.
179. J.S.Budkule and K.C.Patil, *Synth. React. Inorg. Met-Org. Chem.* 19(9) (1989) 909.
180. J.S.Budkule and K.C.Patil, *Synth. React. Inorg. Met-Org. Chem.* 21(4) (1991) 709.
181. V. Moye, K.S. Rane and V.N. Kamat Dalal, *J. Mater Sci. Mater. in Electronics*, 1(1990) 212.
182. B.N.Sivasankar and S.Govindarajan, *Ind.J.Chem.* 33A (1994) 329.
183. B.N.Sivasankar and S.Govindarajan, *Synth. React. Inorg. Met-Org. Chem.* 25(1) (1995) 127.
184. K.Suresh and K.C.Patil, *J. Solid State Chem.* 99(1992)12.

185. K.C.Patil, Bull. Mater. Sci. 16(6)(1993)533.
186. P.Pramanik and A.Pathak, Bull. Mater. Sci. 17(6)(1994) 967.
187. D.G.Wickham, E.R.Whipple and E.G.Larson, J. Inorg. Nucl. Chem. 14(1960) 217.
188. R.T.Richardson, J. Mat. Sci.15(1980)2569.
189. K.C.Patil, S.Sundar Manoharan and D.Gajapath, 'Handbook of Ceramics and Composites vol.1 (eds. Nicholas P. Cheremisinoff, Marcel Dekker, INC, New York) p.469.
190. J.F.Wenckus and W.Z.Leavitt, in Proceedings of the Conference on Magnetic Materials. AIEE special publication. T-91 (1956)526.
191. W.W.Malinosfsky and R.W.Babbit. J.Appl. Phys. 33 (1961) 2375.
192. J.E.Zneimer, B.Kaplan, K.Lehman and D.A.Lepore, J.Appl. Phys. 35 (1964) 1020.
193. M.J.Ruthner, H.G.Richter and I.L.Steiner, in Proceedings of the first International Conference on Ferrites, Kyoto, Japan,1970 (University of Tokyo Press, Tokyo, Japan, 1971)p.75.
194. P.Reijnen, G.P.Th, A.Aarts,R.M.Vande Heuvel and A.L.Stuijts, Ber. Deut. Keram. Ges. 47 (10) (1970) 669.
195. P.Peshev and M.Pecheva, Mat.Res.Bull. 15 (1980) 1055.
196. P.Peshev and M.Pecheva, Mat.Res.Bull. 13 (1978) 1167.
197. F.J.Schnettler and D.W.Johnson, in Proc. Internat.Conf. Ferrites, Kyoto, Japan1970 (Univ. of Tokyo press. Tokyo; 1971) p.121
198. T.Utsunomiya, Y. Hoshino and K.Show, Mat. Res.Bull. 20(1) (1985) 85.

199. T.Takada and M.Kiyama, in Proc.Internat. Conf. Ferrites Kyoto, Japan, 1970 (University of Tokyo press, Japan, 1971) p.69.
200. T.Akashi, I.Sugano, T.Okuda and T.Tsuji, in Proc. Internat. Conf. Ferrites, Kyoto,Japan. 1970 (Univ.OfTokyopress,Japan,1971) p.96.
201. T.Sato, C.Kuroda and M.Saito, in Proc.Internat.Conf. Ferrites Kyoto, Japan, 1970 (Univ. Of Tokyo Press, Japan, 1971)p.72.
202. Kh. M. Yakubov, V. A. Logvinenko, T.A.Zhemchuzhnikova , Sh. Kh. Abdullaev, G.V.Gavrilova and A.N.Mikheev, J.Therm. Anal. 30 (1985) 1095.
203. H.Langbein and P.Eichhorn, J.Therm.Anal. 37 (1991) 993.
204. H.Langbein, C.Michalk, K.Knese and P.Eichhorn, J. Eur. Ceram. Soc. 8(1991) 171.
205. S.Christen, H.Langbein and K.Jaenicke - Röppler, Thermochim. Acta., 209 (1992) 253.
206. Z.Gao, T.Wu and S.Peng, J. Mater. Sci. Lett. 13(1994)1715.
207. S.A.Oliver, R.J.Willey, H.H.Hamdeh, G.Oliveri and G.Busca, Scripta Metallurgica et. Materialia. 33(10/11)(1995)1695.
208. J.C.Ho, H.H.Handeh, S.H.Lin, Y.Y.Chen, Y.D.Yao and R.J.Willey, Chinese J.Phys. 33(6) (1995) 707.
209. R.J.Willey, P.Noirclere, G.Busca, Chem. Eng. Commun. 123 (1993)
210. R.M.Glaister, N.A.Allen and N.J.Hellicar, in Meeting of the Basic Science Section. British Ceramic Society, Brighton, England(1964).
211. H.B.Beer and G.V.Planer, Brit. Commun. Electron. 5(1958)939.
212. H.Sugaya IEEE Trans. Magn. Mag - 4 (1968) 295.

213. E.Hirota, T.Mihara, A.Ikeda and H.Chiba, *IEEE Trans. Magn. Mag.* 7(1971) 337.
214. H.Lubl, P.Neusser, M.Zenger and J.Frey, *J. Physique* 38(1977) C₁-345.
215. C.Buthker and T.Berben, *J. Physique* 38(1977) C₁-341.
216. L.S.Darken and R.W.Gurry, *J. Amer. Chem. Soc.* 67(1945) 1398.
217. A.E.Vol (ed), *Handbook of Binary Metallic Systems: Structure and Properties, Vol.III (English Transl.)*, Israel Program for Scientific translation, Jerusalem, 1967.
218. A.Muan, *Amer. J. Science*, 256(1958) 171.
219. D.S.Tannhauser, *J. Phys. Chem. Solids* 23(1962) 25.
220. C.C.Addison, B.F.G.Johnson and N.Logan, *J. Chem. Soc.* (1965) 4490.
221. R.Roy, *Bull. Soc. Chim. France.* 4 (1965) 1065.
222. R.Pauthenet, *C.R.Acad.Sci., Paris* 230(1950)1842.
223. T.Sato, M.Sugihara and M.Saito, *Rev.Elec.Commun.Lab.* 11(1963) 26.
224. R.Gerber, Z.Simsa and M.Vichr, *Czech. J.Phys.* 168(1966) 913.
225. C.A.Domenically, *Phys. Rev.* 78(1950) 458.
226. S.C.Abrahams and B.A.Calhoun, *Acta crystallogr.* 6(1953)105.
227. B.A.Calhoun, *Phys.Rev.* 94 (1954) 1577.
228. D.O.Smith, *Phys. Rev.* 102(1956) 959.
229. B.Klimaszewski and J.Pietrzak, *Bull. Acad. Pol., Sci. Ser., Math., Astron., Phys.*, 17(1)(1969)51.
230. Y.Imaoka, *J.Electrochem. Soc.Jpn.* 36(1) (1968) 15.
231. C.J.M.Rooymans, *Phil. Res. Rept., Suppl.* 1, (1968) 95.

232. M.Blackman and G.Kaye, Proc. Phys. Soc. 75(1960) 364.
233. V.Cirilli, Gazz. Chim. Ital. 80 (1950) 347.
234. A.Michael and M.Lensen, C.R.Acad. Sci., Paris, 243(1956) 1422.
235. G.W.Van Oosterhout and C.J.M.Rooymans, Nature 181(1958) 44.
236. N.Teijima, chem. Abstr. 69 (1968) 44935 n.
237. O.Glemser and E.Gwinner, Naturwissenschaftler 26(1938) 739.
238. O.Glemser and E.Gwinner, Z.Anorg. Allgem. Chem. 240(1939)161.
239. R.F.Conley, J.Amer.ceram.soc. 50(1967) 124.
240. S.Okamoto, J.Amer.ceram.soc.51(1968)54.
241. W.R.Cook, Jr., J.Amer. ceram. Soc. 51(1968) 408.
242. R.Schrader and G.Biithner, Z.Anorg. Allgem. Chem. 320(1963) 220.
243. S.P.Clark, 'Handbook of Physical constraints,' Geol. Soc. Amer. Mem., 97(1966) 153.
244. R.B.Sosman and E.Posnjak, J.Wash. Acad. Sci. 15(1925)329
245. B.Mason, Geol. Fören. i stockholm Förh. 65(2)(1943)97.
246. P.A.Wagner, Econ. Geol. 22(1927)845.
247. C.Pecharroman, T.González - Carreño and J.E.Iglesias, Phy. Chem. Minerals 22 (1995) 21.
248. J.Thewlis, Phil. Mag. 12(7) (1931) 1089.
249. E.J.W.Verwey, Z.Krist. 91 (1935) 65.
250. U.Colombo, G.Fagherazzi, F.Gazzarrini, G.Lanzavecchia and G.Sironi, Nature 202 (1964) 175.
251. G.A.Ferguson, Jr. and M.Hass, Phys. Rev. 112(1958)1130.

252. J.R.Armstrong, A.H.Morrish and G.A.Sawatzky, *Phys. Lett.* 23(1966)414.
253. H.Annersten and S.S.Hafner, *Z.Kristallog.* 137(1973) 321.
254. K.Haneda and A.M.Morrish, *Solid State Commun.* 22(1977) 779.
255. K.Egger and W.Feitknecht, *Helv. Chim. Acta.* XLV(1962)2042.
256. K.J.Gallagher, W.Feitknecht and U.Mann-Weiler, *Nature* 217(1968)1118.
257. Ö.Ozdemir, D.J.Dunlop and B.M.Moskowitz, *Geophys. Res. Lett.* 20(16) (1993)1671.
258. M.Iwatsuki and T.Fukasawa, *Taiki Osen Gakkaishi*, 27 (1992)220.
259. T.Fukasawa, M.Iwatsuki and M.Furukawa, *Anal. Chim. Acta.* 281 (1993) 413.
260. K.Kauffman and F.Hazel, *J.Inorg. nucl. Chem.* 37(1975)1139.
261. T.Elder, *J.Appl.Phys.* 36(1965)1012.
262. I.David and A.J.E.Welch, *Trans Faraday Soc.* 52(1956)1642
263. P.Ravindranathan and K.C. Patil, *J. Mater. Sci. Lett.* 5 (1986) 221.
264. K.S.Rane, A.K.Nikumbh and A.J. Mukhedkar, *J. Mater. Sci.* 16 (1981) 2387.
265. P.B.Braun, *Nature* 170(1952)1123.
266. C.Greaves, *J.Solid State Chem.* 49(1983) 325.
267. A.Aharoni, E.H.Frei and M.Schieber, *J.Phys. Chem.Solids* 23(1962) 545.
268. F.Gazzarini and G.Lanzavecchia, in *'Reactivity of Solids'* (Eds. J.W. Mitchell et.al., Wiley-Interscience, 1969) p.57.
269. G.D.Renshaw and C.Roscoe, *Nature* 224(1969) 263.
270. V.Rao, A.L.Shashimohan and A.B.Biswas., *J.Mater. Sci.* 9(1974)430.

271. F.E.Debock and P.W.Selwood, *J.Amer. Chem. Soc.* 76(1954) 3365.
272. A.Venkataraman, V.A.Mukhedkar, M.M.Rahman, A.K.Nikumbh and A. J. Mukhedkar, *Thermochim. Acta* 115(1987)215.
273. A.Venkataraman, V.A.Mukhedkar, M.M.Rahman, A.K.Nikumbh and A.J.Mukhedkar, *Thermochim. Acta* 112(1987)231.
274. M.M.Rahman, V.A.Mukhedkar, A.Venkataraman, A.K.Nikumbh, S.B. Kulkarni and A.J.Mukhedkar, *Thermochim.Acta.* 125(1988)173.
275. A.Venkataraman, V.A.Mukhedkar and A.J.Mukhedkar, *J.Therm. Anal.* 35(1989)2115.
276. A.Venkataraman and A.J.Mukhedkar, *J.Therm. Anal.* 36(1990) 1495..
277. A.K.Nikumbh, A.A.Latkar and M.M.Phadke, *Thermochim. Acta* 219 (1993) 269.
278. V.Moye, K.S.Rane, V.N.Kamat Dalal, *J. Mater. Sci. Mater. In Electronics* 4 (1993) 241.
279. E.W.Schmidt, in 'Hydrazine and its derivatives' (Wiley, 1984).
280. A.K. Nikumbh, K.S. Rane and A.J. Mukhedkar, *J. Mater. Sci.* 17 (1982) 2503.
281. A.Venkataraman and A. J. Mukhedkar, *J. Mater. Sci.* 23(1988) 3505.
282. A.K. Nikumbh, K.S. Rane and A.J. Mukhedkar, *J. Mater. Sci.* 18 (1983) 341
283. J.Preudhomme, *Seminaires chim. Et at sol.* 7(1974)31.
284. B.Gillot and F.Bouton, *J.Solid State Chem.* 32(1980) 303.
285. B.Gillot and R.M.Benloucif, *Mater. Chem.Phys.* 32(1992)37.

286. M.Boudeuille, H.Batis-Landoulsi C.H.Leclercq and P.Vergnon, *J.Solid State Chem.* 48(1983)21.
287. G.N.Kryukova, A.L.Chuvilin and V.S.Sadykov, *J.Solid State Chem.* 89(1990) 208.
288. N.N.Greenwood in 'Ionic crystals, Lattice defects and Non-Stoichiometry' (Butterworths, London, 1970)p.92.
289. H.D.Megaw in 'crystal structures' (W.B.Saunders company, Philadelphia) p. 221.
290. K. Sakata, F. Ueda, M. Misono and Y. Yoneda, *Bull. Chem. Soc. Jpn.* 53 (1980) 324.
291. S.V.Adhyapak, B.N.Wani, U.R.K.Rao and S.K.Kulshreshtha, *Synth. React. Inorg. Met.-Org. Chem.* 22(4) (1992)337.
292. M.Yamaguchi, *Jpn. Patent* 62216987; *chem. Abstr.* 108(1987) 141151.
293. B.Gillot, F.Jemmali, L.Clerc and A.Rousset, *React. Solids* 2(1986) 95.
294. H.Tzehoval and M.Steinberg, *Israel J.Chem.* 22(1982) 227.
295. D.Elwell, R.Parker and C.J.Tinsley, *J.Phys B* 17(1967)382.
296. A.Srivastava and P.Singh, V.G.Gujkar and A.P.B.Sinha, *Thermochim. Acta.* 86(1985)77.
297. Y. B. Voilkovskii, V.S. Pigulevskii, Y.S. Yusfin and T.N. Basilevskii, *Chem. Abstr.* 95 (1981) 136307.
298. A.L.Stuijts, in 'Proc. Intern. Conf. Ferrites' Kyoto, Japan. 1970 (University of Tokyo press, Tokyo, 1971)p.108.

299. I.A.Vogel, 'A Textbook of Quantitative Inorganic Analysis' (Longman ELBS, London, 1978).
300. V.M.S.Verenkar and K.S.Rane, in 'Proc.10th Nat. Symp. Therm. Anal.', Kanpur, India, 1995 (eds. S.R.Dharwadkar, S.R.Bharadwaj, S.K.Mukherjee and D.D.Sood, Ind. Therm. Anal. Soc., BARC, Mumbai, India, 1995) p.171.
301. C.B.Murphy, Anal.Chem. 36 (1964) 347 R.
302. L.G.Berg and N.P.Burmistrova, Russian J.Inorg.Chem.5 (1960) 326.
303. V.M.S.Verenkar and K.S.Rane, in 'Proc.10th Nat. Symp. Therm. Anal. Kanpur,India,1995 (eds. S. R.Dharwadkar, S. R.Bharadwaj,S.K.Mukherjee and D.D.Sood, Ind. Therm. Anal. Soc., BARC, Mumbai, India, 1995)p. 175.
304. S. D. Likhite and C. Radhakrishnamurthy, and P. W. Sahasrabudhe, Rev. Sci. Instr. 25 (1965) 302.
305. S. D. Likhite and C. Radhakrishnamurthy, curr. sci. 35 (1966) 534.
306. I. Smit, 'Magnetic properties of Materials' (Mc-Graw Hill, New York, 1971) p. 68-69, 93-94.
307. G. K. Wertheim, 'Mossbauer Effect: Principles and Applications' (academic Press, New York, 1964)
308. V. I. Goldanskii and R. H. Herber, 'Chemical Applications of the Mossbauer Effect' (academic Press, New York, 1968).
309. T. Postupolski, in 'Proc. ICF-5, (1989) p.639.
310. .S. Ishikawa, T.Mochizuki and I. Sasaki, in 'Proc. ICF-5, (1989) p.651.
311. M.Camras, U.S.Patent, 1954, No. 2694656.

312. W.Boronius, F.Henneberger and W.Geidel, East Ger. Patent, 1966 No. 48590.
313. P.Woditsch, P.Hund, G.Buxbaum and H.Hahnkamm, Ger.Patent, 1975 No.2339142.
314. S. Yariv, E. Mendelovici, R. Villaba and M. Cohen, Nature 279 (1979)519.
315. E.Mendelovici and S.Yariv, Thermochem. Acta. 36(1980)25.
316. S.Yariv and E.Mendelovici, Mater. Chem.5(1980)37.
317. S.Yariv, E.Mendelovici and R. Villalba, R. Trans. Far. Soc. 76(1980)1442.
318. W.P.Osmond, Proc.Phys. Soc. Lon, (GB) B-2 (1951) 121.
319. V.Prakash, V.Rao and S. Pramanik, Trans. of the PMAI. 6(1979) 40
320. V.Prakash, V.Rao and S.Pramanik, Trans. Ind. Inst.Metals 35(5) (1982) 513.
321. H.Watanabe and J.Seto, Bull. Chem. Soc. Jpn. 59(1986) 2683.
322. H.Watanabe and J.Seto, Bull. Chem. Soc. Jpn 61(1988) 3067.
323. H.Mehner, H.J.Koppe and W.Morke, Hyperfine Interaction 54(1990) 609.
324. H.Watanabe, and J.Seto, Bull. Chem. Soc. Jpn. 63(1990) 2916.
325. M.P.Morales, C.de.Julian, C.J.Serna and J.M.Gonzalez, IEEE Trans. Magnetics 30(2) (1994) 772.
326. E.Wolska and U.Schwertmann, Solid State Ionics 32-33 (1989) 214.
327. M.P.Morales, C.de Julian, C.J.Serna and J.M.Gonzalez, J.Solid State Chem. 108(1994)158.
328. M.P.Morales, C.de Julian, J.M.Gonzalez and C.J.Serna, J.Mater. Res. 9(1) (1994) 1.

329. E.J.Grootendorst, R.Pestman, R.M.Koster and V.Ponec, *J.Catal.* 148 (1994) 261.
330. W.P.Osmond, *Proc. Phys. Soc. Lon. (GB) B* 66(1953) 265.
331. E.Schmidbauer and R.Keller, *J.Mag. Mag. Mater.* 152(1996)99.
332. V.Chhbra, P.Ayyab, S.Chattopadhyay and A.N.Maitra, *Materials Lett.* 26 (1996)21.
333. M.P.Morales, M.Ocana, T.Gonzalez - carreno and C.J.Serna, in *Fine particles science and Technology* (ed. E.Pelizzetti, Kluwer Academic Publishers, Netherlands, 1996)p 197-208.
334. S.Music, S.Popovic and M.Gotic, *J.Mater. sci.*25(1990)3186.
335. N.S.Clarke and P.G.Hall, *Langmuir* 7(1991) 672.
336. R.Giovanoli and R.Briitsch, *Thermochim. Acta*, 13(1975)15.
337. J.D.Bernal, D.R.Dasgupta and A.L.Mackay, *Nature* 180(1957)645.
338. S.Music, M.Ristic and S.Popovic, *J.Radioanal. Nucl. Chem. Articles* 121(1) (1988) 61.
339. K.Iwase, K.Ogawa and T.Takada, *J.Inst. Metals(Jpn)* 17 (1953) 467.
340. T.Takada, *Sci. Powder.* 4(1958)120.
341. G.R.Desiraju and M.Rao, *Mat.Res.Bull.* 17(1982)443.
342. D.R.Dasgupta, *Ind. J. Phys.* 35(1961) 401.
343. R.Gomez - villacieros, L.Hernan, J.Morales and J.L.Tirado, *Mat. Res. Bull.* 25(4) (1987) 513.
344. R.Gomez - villacieros, L.Hernan, J.Morales and J.L.Tirado, *J.Colloid Interface sci.*, 101(1984)392.

345. H.Naono and K.Nakai, *J. Colloid Interface Sci.* 128(1989) 146.
346. J.Morales, J.L.Tirado and C.Valera, *J. Amer. Ceram. Soc.* 72(1989)1244.
347. C.Barriga, P.Lavela, J.Morales and J.L.Tirado, *J. Colloid Interface Sci.* 138(2) (1990) 565.
348. W.Lodding and L.Hammel, *Anal. Chem.* 32(1960)657.
349. T.Ishikawa and K.Inouye, *Bull. Chem. Soc. Jpn.* 45(8) (1972) 2350.
350. D.G.Klissurski, J.Subrt, V.N.Blaskov, J.Lipka, P.Hanousek and K.Bechine, *J. Mater. Sci.* 19(1984)183.
351. J.Subrt, F.Hanousek, V.Zapetal, J.Zapetal, J.Lipka and M.Hucl, *J. Thermal Anal.* 20(1981)61.
352. K.Bechine, J.Subrt, T.Hanslik, V.Zapetal, J.Tlaskal, J.Lipka, B.Sedlak and M.Rotter, *Z. Anorg. Allg. Chem.* 489(1982)186.
353. U.Schwertmann and R.M.Taylor, *Clay Miner.* 14(1979)285.
354. R.Gomez - villaceros, L.Hernan, J.Morales and J.L.Tirado *J. Colloid Interface Sci.* 101(2) (1984) 392.
355. R.Fricke and W.Zerrweck, *Ztschr. Elektrochem.* 43(1937)52.
356. N.Koga, S.Okada, T.Nakamura and H.Tanaka, *Thermochim. Acta* 267 (1995) 195.
357. S.Goldsztaub, *Compt. Rend.* 193(1931)533.
358. S.Goldsztaub, *Bull. Soc. Franc. Min.* 58(1935)6.
359. E. Mendelovici, A. Sagarzazu and R. Villaba *Mat. Res. Bull.* 17 (1982) 1017.
360. E. Mendelovici, S. Nativ and I. J. Lin, *J. Mater. Sci.*, 19(1983) 1556.

361. D. Klissurski and V. Blaskov, *J. Chem. Commun.*(1983)863.
362. E. Mendelovici, A. Sagarzazu and R. Villaba *Mat. Res. Bull.* 17(1982)241.
363. E.Barrios, L.Hernan, J.Morales and J.L.Tirado, *J.Colloid Interface Sci.* 113(1986)212.
364. R.Gomez - villacieros, J.Morales and J.L.Tirado, *J.Chem. Soc. Chem. Commun.* 566(1984).
365. R.Gomez - villacieros, J.Morales and J.L.Tirado, *J.Chem. Soc. Chem. Commun.*(1984)559.
366. M. Senna, S. Tojo and H. Kuno, *Keio Eng. Reports.* (1972)111.
367. H. Imai and M. Senna, *J. Appl. Phys.* 49(1978)4433.
368. Y Nakatani, M. Sakai, S. Nakatani and M. Matsukoa, *J. Mater. Sci. Lett.* 2(1983)129.
369. K.J.D.Mackenzie and M.E.Bowden, *J.Mater. Sci. Lett.* 2(1983)33.
370. S.Meillon, H.Dammak, E.Flavin and H.Pascard, *Phil. Mag. Lett.* 72(2) (1995) 105.
371. S. Matsumoto *Chem. Abstr.* 112(1989) 29679.
372. D.M.Dovey and W.R.Pitkin, US patent (1954) No. 2689168.
373. P. D. Peshwa and O.Tsyrnorchki, *Chem. Abstr.* 55(1961)9137h.
374. O.Tsyrnorchki, and I. V. Arshinkov, *ibid.* 55(1961)9138b.
375. K.C.Patil, R.Soundararajan and E.P.Goldberg, *Synth. React. Inorg. Met-Org. Chem.* 13(1) (1983) 29.
376. P.Ravindranathan and K.C.Patil, *Proc. Indian Acad.Sci (Chem. Sci)* 95(4) (1984) 345.

377. K.C.Patil, D. Gajapathi and K. Kishore, *Thermochim. Acta.* 52(1982)113.
378. K.C.Patil, *Proc.Indian Acad. Sci. (Chem. Sci.)* 96(6) (1986) 459.
379. K.Kishore, K.C.Patil and D.Gajapathy, *Explosives, propellants and pyro-techniques.* 10(1985)187.
380. J.S.Budkule and K.C.Patil, *J.Therm. Anal.* 36(1990) 2583.
381. G.V.Mahesh and K.C.Patil, *Thermochim. Acta.* 99(1986) 153.
382. P.Ravindranathan and K.C.Patil, *Thermochim. Acta.* 71(1983) 53.
383. F.J.Arnaiz Garcia, *An. Quim.* 73(1977) 1121.
384. B.N.Sivasankar and S.Govindarajan, *Zeitschrift Fur Naturforschung, Sect.B., J.Chem. Sci.* 49(7) (1994) 950.
385. S.Govindarajan, S.V.Nasrin Banu, N.Saravanan and B.N.Sivasankar, *Proc. Indian. Acad. Sci. (Chem. Sci.)* 107(5) (1995) 559.
386. B.N.Sivasankar and S.Govindarajan, *Synth. React. Inorg. Met.-Org. Chem.* 24(9) (1994) 1573.
387. E.R.Jiji and K.K.Aravindakshan, *J.Ind. Chem. Soc.* 70(1)(1993)67.
388. A.R.Corradi, S.J.Andress, J.E.French, G.Bottoni, D.Candolfo, A.Cecchetti and F.Masoli, *IEEE Trans. Magn.* 20(1984) 33.
389. T.Gonzalez - Carreno, A.Mifrud, C.J.Serna and J.M.Palacios, *Mater. Chem. Phys.* 27(1991) 287.
390. A.Lopez, F.J.Lazaro, T.Gonzalez - carreno, M.P.Morales and C.J.Serna, *J.Mag. Mag. Mater.* 140-144 (1995)383.
391. T.Gonzalez - carreno, M.P.Morales, M.Gracia and C.J.Serna, *Mater. Letters* 18(1993)151.

392. M.V.Cabanas, M.Valletregi, M.Labeau and J.M.Gonzalez calbet, *J.Mater. Res.* 8(10) (1993) 2694.
393. M.X.Wan, W.X.Zhou and J.C.Li, *Synthetic Metals* 78(1) (1996) 27.
394. E.Kroll, F.M.Winnik and R.F.Ziolo, *Chem. Mater.* 8(8) (1996) 1594.
395. V.Chhabra, P.Ayyub, S.Chattopadhyay and A.N.Maitra, *Materials Lett.* 26 (1996) 21.
396. S.Dhara, A.C.Rastogi and B.K.Das, *J.Appl. Phys.* 74(11) (1993) 7019.
397. S.Dhara, A.C.Rastogi and B.K.Das, *Thin Solid Films* 239(2) (1994) 240.
398. M.G.Deng, L.H.Chen, M.P.Hung, T.S.Chin and C.H.Lin, *IEEE Trans. Mag.* 25(5) (1989)3644.
399. T.Abe, Y.Tachibana, T.Uematsu and M.Iwamoto, *J.Chem. Soc. Chem.commun.* (1995) 1617.
400. D.Nizansky, J.L.Rehspringer and M.Drillon, *IEEE trans. Mag.* 30(2) (1994)821.
401. G.M.da Costa, E.De Grave, P.M.A.de Bakker and R.E.Vandenbergh, *J.Solid State chem.* 113(1994)405.
402. R.F.Ziolo, E.P.Giannelis, B.A.Weinstein, M.P.O'Horo, B.N.Ganguly, V.Mehrotra, M.W.Russell and D.R.Huffman, *Science* 257(1992)219.
403. H.Batis-Landoulsi and P.Vergnon, *J.Mater. sci.* 18(1983) 3399.
404. G. D. Chrisian, 'Analytical Chemistry' (John Wiley, New York, 1994).
405. R. Fricke and Zerrweck, 'Handbook of Preparative Inorganic Chemistry' (Eds. George Brauer, Academic Press, New York, 1965) Vol.2, p.1500.
406. R. Fricke and P. Ackermann, *ibid* p.1499.

407. M. C. Kung, W.H. Cheng and H.H. Kung, *J. Phys. Chem.* 83(1979)1737.
408. JCPDS, Powder diffraction file, (Int. centre for diff. data, swarthmore) PA no. 6-696.
409. JCPDS, file no. 13-534.
410. JCPDS, file no. 25-1402.
411. JCPDS, file no. 24-81.
412. JCPDS, file no. 19-629.
413. JCPDS, file no. 6-615.
414. N. Koga, S. Takemato, S. Okada and H. Tanaka, *Thermochim. Acta.* 254 (1995)193.
415. J. E. Iglesias and C. J. Serna, *Miner. Petrogr. Acta.* 29-A(1985)363.
416. D. Khalafalla A. H. Morrish, *J. Appl. Phys.* 43(1972)624.
417. V.M.S. Verenkar and K.S. Rane, in 'Proc. 82nd Session of Indian Sci. Cong.' (Calcutta, India, 1995) Part IV, p 31.
418. J. A. Lodya, H. Pollak, K. S. Rane and V. M. S. Verenkar, in 'Proc. 10th Intern. Conf. Hyperfine Interactions (eds. M. Rots, A. Vantomme, J. Dekoster, R. Coussement and G. Langouche, Leuven, Belgium, 1995); *Hyperfine Interaction* 1(1996)480.
419. B. J. Liaw, D. S. Chang and B. L. Yang, *J. Catal.* 118(1989)312.
420. P. M. A. de Bekker, E. De Grave, R. E. Vandenberghe, L.H. Bowen, R.J. Pollard R.M. Persoons, *Physics Chem. Minerals* 18(1991)131.
421. M. Fukuda, *Nat. Tech. Rep.* 3(1957)1.
422. M. Fukuda, *J. Electrochem. Soc. Jpn.* 28(1960) 67.

423. R. Furuichi, N. Sato and G. Okamoto, *Separatum of Chimia* 23(1969)455.
424. S. Ekambaram and K.C.Patil, *J. Mater.Chem.* 5(1995)905.
425. K.C.Patil, S.T.Aruna and S. Ekambaram, in 'current opinion in solid state and material science'(eds. A.K.Cheetam, H.Inokuchi and J.M.Thomas) 2(2)(1997)1.
426. T. Kikkawa, M. Yoshinaka, K. Hirota and O. Yamaguchi, *J. Mater. Sci.Lett.* 14(1995) 1071.
427. K. Ishida, K. Hirota, O.Yamaguchi, H. Kume, S. Inamura and H. Miyamoto, *J. Am. Ceram. Soc.* 77 (1994) 1391.
428. S.Kimoto, K. Hirota, O.Yamaguchi, H. Kume, S. Inamura and H. Miyamoto, *ibid.* 77 (1994) 1694.
429. K. Yamakata, K. Hirota, O.Yamaguchi, H. Kume, S. Inamura and H. Miyamoto, *ibid.* 77 (1994) 2207.
430. K. Goto, K. Hirota, O.Yamaguchi, H. Kume, S. Inamura and H. Miyamoto, *J. Mater.Sci.* 31 (1996) 204.
431. J.M.D.Coey and D. Khalafalla, *Phys. Stat. Sol. (a)* 11(1972)229.
432. D.R.Sagar, C.Prakash and P.Kishan, *solid state communications* 68(2) (1988)193.
433. W.H. Von Aulock, 'Handbook of Microwave Ferrite Materials' (Academic Press, New York,1965)p. 273.
434. H.H. Voge and C.R. Adams, *Adv. Catal. Relat. Subj.* 17(1967)151.
435. T. Seiyama, N. Yamazoe and H. Arai, *Sensors and Actuators* 4 (1983) 85.
436. Y. Shimizy, H. Arai and T. Seiyama, *Sensors and Actuators* 7 (1985) 11.

437. N. Yamazoe and Y. Shimizee, *Sensors and Actuators* 10 (1986)379.
438. K. Katayama, K Hasegawa, T.Takahashi, T. Akiba and H. Yanagida, *Sens. Actuators. A.24* (1990) 55.
439. N.Kumar and P.Kishan, *J.Mater. Sci. Lett.* 10(1991) 217.
440. L. H.Bennett.,R.D. Mc Michael, L.J. Schwantzendruber, R. D. Shull and R. E. Watson, *J. Magn. Mat.* 104-107 (1992) 1094.
441. C.Guillaud, *J.Phys. et. Radium* 12(1951)239.
442. E.F.Bertaut, *J.Phys. et. Radium* 12(1951)252.
443. L.Neel, *C.R. Acad. Sci.* 230(1950)190.
444. K. Sheshan, A.L. Shashimohan, D.K. Chakrabarty, and A.B. Biswas, *Phys. Stat.Sol. (a)*68(1981)97.
445. S.Unnikrishnan and D.K.Chakrabarty, *Phys. Stat. Sol. (a)*121(1990)265.
446. H.H.Joshi and R.G.Kulkarni, *J.Mater. Sci.* 21(1986)2138.
447. K.B.Modi, H.H.Joshi and R.G.Kulkarni, *J.Mater. Sci.* 31(1996)1311.
448. J.Smit and H.P.J.Wijn, 'Ferrites' (John Wiley and sons, New York, 1959), p.369.
449. K.Sheshan, M.J.Patni and D.K.Chakrabary, *J. Solid State Chemistry* 42 (1982)206.
450. C.J.Kriessman and S.E.Harrison, *Phys. Rev.* 103(1956)857.
451. G.K.Joshi, S.A.Deshpande, A.Y.Khot and S.R.Sawant, *Ind. J. Phys.* 61A (1987)251.
452. S.H.Patil, S.I.Patil, S.M.Kadam, S.R.Patil and B.K.Chougule, *Bull. Mater. Sci.* 14(5) (1991)1225.

453. S.H.Patil, S.I.Patil, S.M.Kadam, S.R.Patil and B.K.Chougule, *J. Mag. Mag. Mater.* 110(1992)147.
454. S.H.Patil, S.I.Patil, S.M.Kadam, S.R.Patil and B.K.Chougule, *Bull. Mater. Sci.* 15(20) (1992)127.
455. K.Suresh and K.C.Patil, *J. Mater. Sci. Lett.* 13(1994)1712.
456. K.J.Standley, 'Oxide magnetic materials' (Oxford : claredon Press, 1972).
457. B.Lorentz and D.Ihle, *Phys. Stat. Solidi* 69(1975) 451.
458. JCPDS, file no. 17-465
459. C.M.Srivastava, S.N.Shringi and M.Vijaybabu, *Bull. Mater. Sci.* 6(1) (1984) 27
460. M.D.Sundararajan, A.Narayanaswamy, T.Nagarajan, L.Häggström, C.S.Swamy and K.V.Ramanujachary, *J.Phys. C:Solid state Phys.* 17 (1984) 2953
461. S.A.Chim, *Ann. Chim (Fr.)* 9 (1974) 31.
462. W.L.Konijnendijk, *Philips, Res. Repts.* 30 (1975).
463. W.B.White and B.A.De Angelis, *spectro chim. Acta.* 23-A (1967) 985.
464. J.Preudhomme, *spectro chim. Acta.* 26-A (1970) 985
465. R.D.Waldron, *Phys. Rev.* 99 (1955) 1727.
466. K.Nakamoto, 'Infrared and Raman Spectra of Inorganic and Coordination Compounds' (Wiley-Interscience, 1976) p.142.
467. P.Tarte and J.Preudhomme, *J.Acta. Cryst.* 16(1963)227.
468. V.R.K.Murthy, S.Chitrasankar, K.V.Reddy and J.Sobhanadri, *Ind. J.Pure and Appl. Phys.* 36(1978)79.

486. R.S.Chaughule, C.Radhakrishnamurty, E.V.Sampathkumaran, S.K.Malik, and R. Vijayaraghavan, *Mat. Res. Bull.* 18 (1983) 817.
487. A.Globus, D.Paul, *J. Appl. Phys.* 39(2) (1968) 727.
488. A.Globus, D.Paul and M.Guyot, *IEEE Trans. Mag.* 7 (1971) 617.
489. B.Gloria, R.Valenzuela, M.A.Escobar and L.F.Magana, *J. Appl. Phys.* 51(1) (1985) 4183.
490. M.Guyot and A.Globus, *Phys. Stat. Sol. (b)* 52 (1972) 427.
491. C.T.Rado and A.Terris, *Phys. Rev.* 83 (1951) 177.
492. G.H.Jonkar, *J. Phys. Chem. Solids* 9 (1959) 195.
493. E.J.W.Verwey and J.H.de Boer, *Reuil Ches Travaux chimques des Phys. Bas(Czeckh)*. 55 (1936) 531.
494. N.Rezlescu and E.Rezlescu, *Solid-State commun.* 14 (1974) 69.
495. Z.Sisma, J.Simsova and V.A.M.Borabers, in *Proc 11th Int. Conf. on progr. of semiconductors (warsaw, Poland)* 2 (1972)1294.
496. E.J.W.Verwey, P.W.Haayman, F.C.Romeijn and G.W.Van Oosterhout, *Philips Res. Rep.* 5 (1950) 173.
497. L.G.Van Uitert, *J.Chem. Phys.* 24 (1956) 306.
498. J.I.Powar, Ph.D. Thesis, Shivaji university, Kolhapur (1980).
499. Y.P.Irkhin, E.A.Turov, *sov. Phys. JETP* 33 (1957) 673.
500. S.M.Otari, V.B.Kadam, S.R.Sawant and S.A.Patil, *Ind.J.Pure and Appl. Phys.* 28 (1990) 248.
501. A.P.Komar and V.V.Klivshin, *Bull.Acad. Sci.USSR Phys.* 18 (1954) 403.
502. M.A.Semary, M.A.Ahmed and Y.Abbas, *J.Mater.Sci.* 18 (1983) 2890.

503. J.I.Powar, S.A.Patil. and R.N.karekar, *Ind.J.Pure and Appl.Phys.* 20 (1982) 267.
504. C.S.Narasimham and C.S.Swamy, *Phys. Stat. Sol. (a)* 59 (1983) 817.
505. C.Prakash and J.S.Baijal, *J.Less common Met.* 107 (1985) 51, 169.
506. V.P.miroshkin, Y.I.Panovaand, V.V.Passynrov, *Phys. Stat.Sol.(a)* 66 (1981) 779.
507. C.G.Koops, *Phys. Rev.* 83(1951)121.
508. S.Radhakrishna and K.V.S.Badarinath, *J.Mater. Sci.Lett.* 3 (1984) 867.
509. G.R.Hearne and H.Pollak, *Hyperfine Interactions* 67(1991)559.
510. J.Chiu, *Anal. Chem.* 39(1967)861.
511. A.A.Said, k.M.Abd El - Salaam, E.A.Hassan, A.M.Mohamed, *J.Therm. Anal.* 39(1993)309.
512. unpublished data.